The role of biliverdin reductase A in cardiovascular and metabolic diseases.

Author:
Chen, Weiyu

Publication Date:
2019

DOI:
https://doi.org/10.26190/unsworks/2109

The role of biliverdin reductase A in cardiovascular and metabolic diseases

Weiyu Chen

A thesis in fulfilment of the requirements for the degree of Doctor of Philosophy

May 2019

Faculty of Medicine
UNSW Sydney

&

Division of Vascular Biology
Victor Chang Cardiac Research Institute

Victor Chang
Cardiac Research Institute

UNSW
SYDNEY

Thesis/Dissertation Sheet

Surname/Family Name	:	**Chen**
Given Name/s	:	**Weiyu**
Abbreviation for degree as give in the University calendar	:	**PhD**
Faculty	:	**Faculty of Medicine**
School	:	**St Vincent's Clinical School**
Thesis Title	:	**The role of biliverdin reductase A in cardiovascular and metabolic diseases**

Abstract 350 words maximum: (PLEASE TYPE)

Epidemiological studies show plasma concentrations of bilirubin, formed by biliverdin reductase A (BVRA), to inversely associate with the risk of cardiovascular and metabolic diseases. However, a causative link between bilirubin and these diseases remains to be established.

Global *Bvra* gene knockout (*Bvra*$^{-/-}$) mice were generated to assess the role of bilirubin in cardiometabolic diseases. *Bvra*$^{-/-}$ mice were healthy and fecund, had ~100-fold lower plasma bilirubin, ~25-fold higher plasma biliverdin and phenotypic green-coloured bile compared with their wild-type counterpart. BVRA deficiency had no measurable effect on plasma lipids and antioxidants. However, *Bvra*$^{-/-}$ mice had higher concentrations of plasma lipid hydroperoxides and their erythrocyte peroxiredoxin 2 was more oxidized, indicative of the presence of systemic oxidative stress.

To assess the role of bilirubin in cardiovascular disease, *Bvra*$^{-/-}$ mice were crossed with hyperlipidemic *apolipoprotein-E* gene knockout (*Apoe*$^{-/-}$) mice and subjected to tandem stenosis (TS) of the right carotid artery, a model of plaque instability. Compared with *Bvra*$^{+/+}$*Apoe*$^{-/-}$, *Bvra*$^{-/-}$*Apoe*$^{-/-}$ TS mice lacked bilirubin, were hyperlipidemic and had enhanced endothelial dysfunction and atherosclerosis. Unstable plaque in *Bvra*$^{-/-}$*Apoe*$^{-/-}$ TS mice had increased positive remodeling and decreased fibrous cap thickness compared with unstable plaque in *Bvra*$^{+/+}$*Apoe*$^{-/-}$ TS mice that contained BVRA activity, indicating that BVRA/bilirubin attenuates atherogenesis and plaque destabilization.

BVRA has been proposed to regulate insulin signaling and lipid metabolism. Contrary to this, *Bvra*$^{+/+}$ and *Bvra*$^{-/-}$ mice fed high fat diet had similar plasma lipids, glucose, and insulin signaling and tolerance. However, BVRA deficiency in combination with a high fat diet increased hepatic concentrations of cholesterol and triglycerides, indicating that BVRA/bilirubin deficiency enhances hepatic steatosis, but not insulin resistance.

Overall, our data show that while *Bvra* is not an essential gene, its absence increases systemic oxidative stress in naïve mice. In combination with a fat-rich diet, the absence of BVRA and bilirubin causes a pro-atherogenic phenotype, characterized by increased hyperlipidemia, endothelial dysfunction and atherogenesis, as well as plaque destabilization, compensatory arterial remodeling and hepatic steatosis. This phenotype is consistent with bilirubin decreasing cardiovascular and metabolic diseases.

FOR OFFICE USE ONLY Date of completion of requirements for Award:

INCLUSION OF PUBLICATIONS STATEMENT

UNSW is supportive of candidates publishing their research results during their candidature as detailed in the UNSW Thesis Examination Procedure.

Publications can be used in their thesis in lieu of a Chapter if:

- The student contributed greater than 50% of the content in the publication and is the "primary author", i.e. the student was responsible primarily for the planning, execution and preparation of the work for publication
- The student has approval to include the publication in their thesis in lieu of a Chapter from their supervisor and Postgraduate Coordinator.
- The publication is not subject to any obligations or contractual agreements with a third party that would constrain its inclusion in the thesis

Please indicate whether this thesis contains published material or not.

☐ *This thesis contains no publications, either published or submitted for publication*

☒ *Some of the work described in this thesis has been published and it has been documented in the relevant Chapters with acknowledgement*

☐ *This thesis has publications (either published or submitted for publication) incorporated into it in lieu of a chapter and the details are presented below*

CANDIDATE'S DECLARATION

I declare that:

- I have complied with the Thesis Examination Procedure
- where I have used a publication in lieu of a Chapter, the listed publication(s) below meet(s) the requirements to be included in the thesis.

Name	Signature	Date (dd/mm/yy)

Acknowledgements

I would like to extend my gratitude to the following people, who helped make this research possible:

My supervisor, Professor Roland Stocker, who encouraged me to take on the project of investigating the role of bilirubin *in vivo*. I am ever grateful for his patience, wisdom and unconditional support throughout my PhD study. His continuous inspiration and experienced mentorship not only made this project possible, but further inspired me to explore the dynamic nature of the academic world.

My co-supervisor, Louise Dunn, whose endless support and thoughtful attitude guided me through every point of my academic and personal life. Her advice helped me overcome various academic and cultural barriers, as well as make the most of my time in Australia.

Chris Stanley, Cacang Suarna, Darren Newington, Anita Ayer, Sergey Tumanov, Raphael Queiroz, Kathryn Wolhuter, Ghassan Maghzal, Stephanie Kong, David Cheng, Jihan Talib, Ragul Rajivan and other members of the Stocker Laboratory, who aided me with both experimental procedures and academic presentations.

Maree Stenglin who provided the detailed guideline for the writing of scientific manuscript. Michael Swift, Pietro Ridone, Celine Santiago and Andrew Kim, who provided advice and feedback as part of the UNSW Thesis Writing Support Program.

The University of New South Wales and the Victor Chang Cardiac Research Institute, whose facilities and staff provided me with invaluable support throughout this project.

My mother, father and sister, whose endless support throughout my life allowed me to pursue my career. A special thank you to my wife, Yu Gao, whose love changed my life's trajectory and also inspired me to start my scientific adventure in Australia.

I would like to thank the University of New South Wales, the Victor Chang Cardiac Research Institute, China Scholarship Council, and MacDonald Jones Homes Foundation for providing me with scholarships to overcome financial difficulties during my PhD.

Originality statement

'I hereby declare that this submission is my own work and to the best of my knowledge it contains no materials previously published or written by another person, or substantial proportions of material which have been accepted for the award of any other degree or diploma at UNSW or any other educational institution, except where due acknowledgement is made in the thesis. Any contribution made to the research by others, with whom I have worked at UNSW or elsewhere, is explicitly acknowledged in the thesis. I also declare that the intellectual content of this thesis is the product of my own work, except to the extent that assistance from others in the project's design and conception or in style, presentation and linguistic expression is acknowledged.'

Signed .....

Date .....

Copyright statement

Signed .....

Date .....

Authenticity statement

'I certify that the Library deposit digital copy is a direct equivalent of the final officially approved version of my thesis.'

Signed .....

Date .....

Abstract

Epidemiological studies show plasma concentrations of bilirubin, formed by biliverdin reductase A (BVRA), to inversely associate with the risk of cardiovascular and metabolic diseases. However, a causative link between bilirubin and these diseases remains to be established.

Global *Bvra* gene knockout ($Bvra^{-/-}$) mice were generated to assess the role of bilirubin in cardiometabolic diseases. $Bvra^{-/-}$ mice were healthy and fecund, had ~100-fold lower plasma bilirubin, ~25-fold higher plasma biliverdin and phenotypic green-colored bile compared with their wild-type counterpart. BVRA deficiency had no measurable effect on plasma lipids and antioxidants. However, $Bvra^{-/-}$ mice had higher concentrations of plasma lipid hydroperoxides and their erythrocyte peroxiredoxin 2 was more oxidized, indicative of the presence of systemic oxidative stress.

To assess the role of bilirubin in cardiovascular disease, $Bvra^{-/-}$ mice were crossed with *apolipoprotein-E* gene knockout ($Apoe^{-/-}$) mice and subjected to tandem stenosis (TS) of the right carotid artery, as a model of plaque instability. Compared with $Bvra^{+/+}Apoe^{-/-}$, $Bvra^{-/-}Apoe^{-/-}$ TS mice lacked bilirubin, were hyperlipidemic and had enhanced endothelial dysfunction and atherosclerosis. Unstable plaque in $Bvra^{-/-}Apoe^{-/-}$ TS mice had increased positive remodeling and decreased fibrous cap thickness compared with unstable atherosclerotic plaque in $Bvra^{+/+}Apoe^{-/-}$ TS mice that contained BVRA activity, indicating that BVRA/bilirubin attenuates atherogenesis and plaque destabilization.

BVRA has been proposed to regulate insulin signaling and lipid metabolism. Contrary to this, $Bvra^{+/+}$ and $Bvra^{-/-}$ mice fed high fat diet had similar plasma lipids, glucose, and insulin signaling and tolerance. However, BVRA deficiency in combination with a high fat diet increased hepatic concentrations of cholesterol and triglycerides, indicating that BVRA/bilirubin deficiency enhances hepatic steatosis, but not insulin resistance.

Overall, our data show that while *Bvra* is not an essential gene, its absence increases systemic oxidative stress in naïve mice. In combination with a fat-rich diet, the absence of BVRA and bilirubin causes a pro-atherogenic phenotype, characterized by increased hyperlipidemia, endothelial dysfunction and atherogenesis, as well as plaque destabilization, compensatory arterial remodeling and hepatic steatosis. This phenotype is consistent with bilirubin protecting against cardiovascular and metabolic diseases.

Abbreviations

Acaca	Acetyl-CoA carboxylase gene
ALT	Alanine aminotransferase
ALP	Alkaline phosphatase
Apoe$^{-/-}$	*Apolipoprotein E* gene-deficient
AAC	Area above curve
AST	Aspartate aminotransferase
BCA	Bicinchoninic acid
BVRA	Biliverdin reductase A
Bvra$^{-/-}$	*Biliverdin reductase a* gene-deficient
BSA	Bovine serum albumin
CO	Carbon monoxide
CVD	Cardiovascular disease
Cpt1a	Carnitine palmitoyltransferase 1A gene
CE-OOH	Cholesterylester hydroperoxides
CE	Cholesterylesters
Cyp4a12	Cytochrome P450 family 4 gene
Cyp2j6	Cytochrome P450 family 2 gene
2-DOG	[^{3}H] 2-Deoxy-D-glucose
DMT	Danish Myo Technology
DTPA	Diethylenetriaminepentaacetic acid
Cd36	Differentiation 36 gene
DMEM	Dulbecco's Modified Eagle Medium
ES	Embryonic stem
ER	Endoplasmic reticulum
ERK	Extracellular signal-regulated kinases
Fasn	Fatty acid synthase gene
Fe^{3+}	Ferric iron
Fe^{2+}	Ferrous iron
FRT	Flippase recognition target
FLECT	Fluorescence emission computed tomography
G6pase	Glucose 6-phosphatase gene
GTT	Glucose tolerance test
GLUT4	Glucose transporter type 4
H&E	Hematoxylin and eosin
Hmox1	Heme oxygenase-1

Hmox2	Heme oxygenase-2
HF	High fat
HFHS	High fat high sucrose
HDL	High-density lipoproteins
iAUC	Incremental area under curve
IRS-1	Insulin receptor substrate-1
ITT	Insulin tolerance test
ICAM-1	Intercellular adhesion molecule-1
IL	Interleukin
JNK	c-Jun N-terminal kinases
KRP	Krebs-Ringer phosphate
ANOVA	One-way analysis of variance
LPS	Lipopolysaccharide
LDL	Low-density lipoproteins
Ldlr$^{-/-}$	*Low-density lipoprotein receptor* gene-deficient
MCH	Mean corpuscular hemoglobin
MCHC	Mean corpuscular hemoglobin concentration
MCV	Mean corpuscular volume
MAPK	Mitogen-activated protein kinase
MRP2	Multidrug resistant protein 2
MPO	Myeloperoxidase
NHANES	National Health and Nutrition Examination Survey
NIRAF	Near infrared autofluorescence
NADH	Nicotinamide adenine dinucleotide
NADPH	Nicotinamide adenine dinucleotide phosphate hydrogen
NAFLD	Non-alcoholic fatty liver disease
oxLDL	Oxidized low-density lipoproteins
Prx2	Peroxiredoxin 2
PPARα	Peroxisome proliferator-activated receptor-α
PBS	Phosphate buffered saline
PDK1	Phosphatidylinositol-dependent kinase 1
PKG_*neo*	Phosphoglycerine kinase promoter driving a neomycin resistance gene cassette
PI3K	Phosphoinositide 3-kinase
PSR	Picrosirius red
PGE2	Prostaglandin E2
RIPA	Radioimmune precipitation assay

RBC	Red blood cell
SEM	Standard error of the mean
Srebf1	Sterol regulatory element-binding transcription factor 1 gene
TS	Tandem stenosis
TCFA	Thin-cap fibroatheroma
TLR4	Toll-like receptor 4
TG	Triglycerides
TBS	Tris-buffered saline
TNF-α	Tumor necrosis factor-α
α-TOH	α-Tocopherol
α-TO•	α-Tocopheroxyl radicals
UGT1A1	UDP glucuronosyltransferase family 1 member A1
VCAM-1	Vascular cell adhesion molecule-1
VEGF	Vascular endothelial growth factor
VSMC	Vascular smooth muscle cell
WD	Western diet

Publications in support of this thesis

Abstracts:

1. Chen W, Dunn L, Suarna C, Maghzal G, Stocker R. The effect of deletion of biliverdin reductase on oxidative stress in mouse models. The Society for Free Radical Research (Australasia) Conference, Gold Coast, Australia, 2016
2. Chen W, Maghzal G, Ayer A, Suarna C, Dunn L, Stocker R. Does bilirubin protect against oxidative stress and cardiovascular disease? Sydney Cardiovascular Symposium, Sydney, Australia, 2017
3. Chen W, Maghzal G, Ayer A, Suarna C, Dunn L, Stocker R. Generation of *biliverdin reductase a* gene knockout mice to study the *in vivo* activities of bilirubin. The Society for Free Radical Research (International) Conference, Lisbon, Portugal, 2018
4. Chen W, Maghzal G, Ayer A, Suarna C, Dunn L, Stocker R. A bilirubin-deficient mouse model: evidence the tetrapyrrole protects against oxidative stress. The Gordon Research Conference on Chemistry and Biology of Tetrapyrroles, Newport, USA, 2018
5. Chen W, Stanley C, Fazakerley D, Ayer A, Suarna C, Cheng D, Talib J, Dunn L, Stocker R Absence of bilirubin promotes atherosclerosis and metabolic disease in the mouse. Sydney Cardiovascular Symposium, Sydney, Australia, 2018

Full papers:

1. Chen W, Maghzal G, Ayer A, Suarna C, Dunn L, Stocker R. Absence of the *biliverdin reductase a* gene is associated with increased endogenous oxidative stress. *Free Radic Biol Med*. 2018; 115: 156-165
2. Chen W and Stocker R. Absence of bilirubin increases oxidative stress *in vivo*. *Atlas of Science*. 2018; November 22

Table of contents

List of Figures

List of Tables

Chapter 1

General introduction

1.1 Introduction

Cardiovascular disease (CVD) annually takes the lives of 17.9 million people, accounting for approximating 31% of all global deaths (World Health Organization reports) (1). Atherosclerosis is a major cause of CVD, with atherosclerotic plaque rupture and ensuing thrombosis representing a major contributor to death caused by CVD. Metabolic disease can exacerbate atherosclerosis and CVD. Despite advances in the prevention and treatment of CVD, our understanding of endogenous protective mechanisms of the body remains incompletely understood.

Bilirubin has shown potential cardiovascular protective properties, including antioxidant (2, 3) and anti-inflammatory activities (4), inhibition of vascular smooth muscle cell (VSMC) proliferation (5), promotion of endothelial function (6), and regulation of lipid metabolism (7, 8), which could underpin the epidemiologic observation that plasma concentrations of bilirubin inversely associate with the risk of atherosclerosis and CVD (9-11). Bilirubin is a product of heme catabolism. Heme is degraded by heme oxygenases to carbon monoxide (CO), ferrous iron (Fe^{2+}) and biliverdin, and the latter is then reduced to bilirubin by biliverdin reductase (BVR). Plasma concentrations of bilirubin are regulated primarily via hepatic conjugation of the pigment mediated by UDP glucuronosyltransferase family 1 member A1 (UGT1A1) (12, 13). Decreased UGT1A1 activity (*e.g.,* Gilbert Syndrome) leads to moderate hyperbilirubinemia and decreased CVD risk (9, 14-18). However, a direct causative link between bilirubin and CVD remains to be established, just as it remains unclear whether cardiovascular benefits are provided by bilirubin or other products formed during heme degradation, *i.e.*, CO, Fe^{2+} and biliverdin.

More recently bilirubin has been postulated to play role in glucose metabolism and insulin signaling (19, 20). Additionally, clinical evidence indicates that bilirubin is associated with metabolic disease (21, 22), which is an independent risk factor for diabetes, atherosclerosis and CVD. BVR, the enzyme that forms bilirubin, has been reported to be evolutionary conserved and to possess dual-specificity kinase activity and the ability to modulate glucose metabolism via phosphorylation of proteins in the insulin/ insulin-like growth factor-1 (IGF-1) signaling pathway (23). However, here too it remains unclear whether BVR itself or its reaction product, bilirubin, provides such putative protection.

The prevalence of CVD is projected to increase in the coming decades due to an ageing population and increased incidence of metabolic disease (24). A clearer understanding of whether bilirubin itself protects against cardiovascular and/or metabolic diseases is therefore of importance. Gaining such knowledge will be instrumental in devising novel strategies aimed at protecting against these diseases.

1.2 Heme metabolism

Heme is an important compound of hemoglobin in the red blood cells, which carry oxygen and transports carbon dioxide through the circulation. Heme also serves as the prosthetic group for

other heme proteins, such as myoglobin, cytochromes, peroxidases, catalases, guanylate cyclase, and nitric oxide synthase (25). Although heme is involved in a remarkable array of diverse biological processes, such as gas exchange, protein synthesis and cell differentiation, heme can also be toxic and cause oxidative damage to lipids, protein and DNA. For example, heme derived from hemolysis is an *in vivo* oxidant for low-density lipoproteins (LDL) and promotes atherogenesis in hypercholesterolemic rabbits (26). Heme also causes endothelial cell (EC) injury that can lead to vascular inflammatory disorders (27). It acts as a pro-inflammatory molecule to enhance arteriosclerosis, vasodilation disorder and other CVD related pathological conditions.

Bilirubin is the terminal product of heme metabolism. The single major source of bilirubin in mammals is the degradation of hemoglobin in aged red blood cells undergoing turnover. In mammals, senescent or damaged red blood cells in the circulation are captured and ingested by macrophages in the spleen and liver. In this process, globin is proteolytically degraded, while heme is released. Heme (Fe^{2+} protoporphyrin) is decyclized by heme oxygenase in a reaction requiring three molecules of oxygen and seven electrons donated from reduced nicotinamide adenine dinucleotide (phosphate) (NAD(P)H) (28), and producing CO, Fe^{2+} and biliverdin as products (Fig. 1.1). Released Fe^{2+} is stored commonly in the iron-binding protein ferritin (29). Upon formation, the blue-green biliverdin is immediately reduced by biliverdin reductase and eventually turns to orange-yellow bilirubin, with consumption of NAD(P)H (30). As a result of heme degradation, adult humans produce ~300 mg bilirubin daily. Due to intramolecular hydrogen bonds, bilirubin is poorly soluble in water and tightly bound to albumin for its transport in the blood. Once the albumin-binding capacity is exceeded, bilirubin may accumulate in biological tissues where it can potentially cause toxicity. However, the toxicity is avoided if bilirubin is removed from the circulation by hepatic glucuronyl transferase-mediated conjugation with glucuronic acid. The resulting water-soluble conjugated bilirubin is secreted into bile, and responsible for the typical yellow appearance of the gall bladder. Hepatic conjugation mediated by glucuronyl transferase, UGT1A1, is the primary regulator of plasma bilirubin concentration (12, 13).

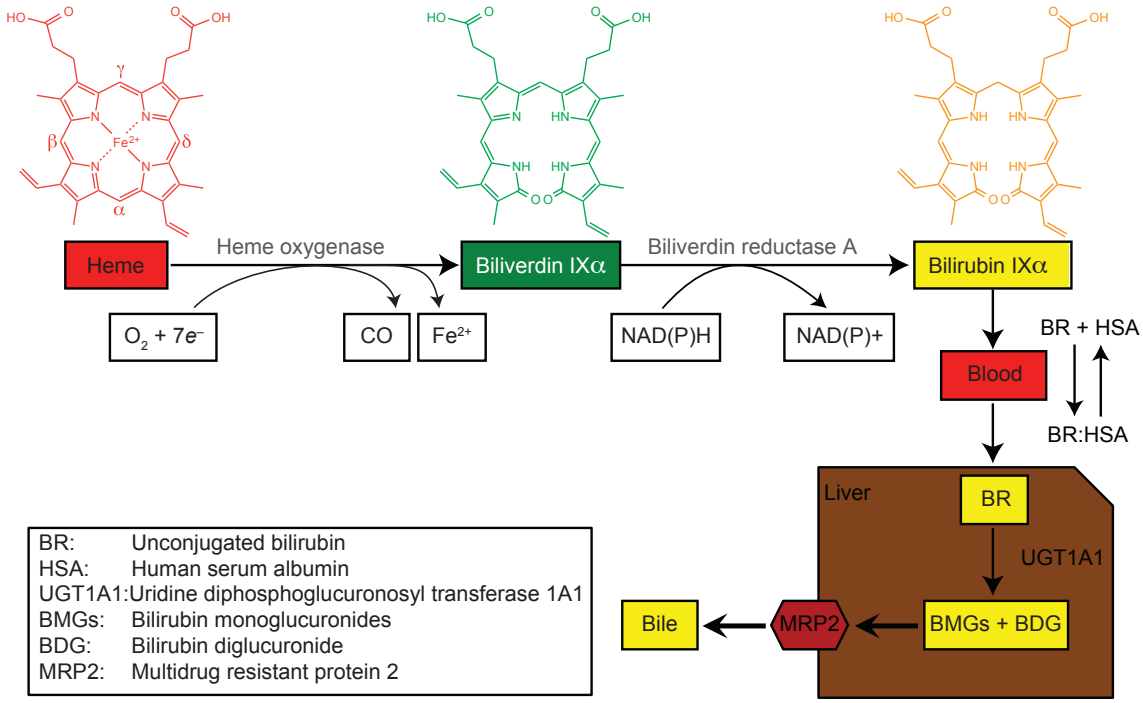

Figure 1.1 Heme metabolism in normal physiology

1.2.1 Heme oxygenase

Heme oxygenase (EC:1.14.14.18) is the initial and rate-limiting enzyme for heme degradation as well as the subsequent bilirubin production. Two isoforms of heme oxygenase exist in mammals and have been extensively investigated: the inducible heme oxygenase-1 (Hmox1) and the constitutive heme oxygenase-2 (Hmox2). Hmox1 and Hmox2 have similar amino sequences and catalyze heme degradation, however the two enzymes also show differences in their physiological properties and regulation.

Hmox1 is an inducible enzyme of 32 kDa molecular weight. It has long been known as a "stress protein" that becomes expressed when the body experiences stress, such as exposure to heat, hemin, cytokines, lipopolysaccharide, growth factors, hydrogen peroxide, hypoxia and CO (31). Various stimuli can activate Hmox1 via the transcription factor nuclear factor erythroid 2-related factor (Nrf2), which plays a role in resistance to oxidative stress (32).Under quiescent conditions, Nrf2 resides in the cytoplasm through binding to its inhibitor, Kelch-like enoyl-CoA-hydratase-associated protein1 (Keap1). Under conditions of stimulation, *e.g.,* oxidative and nucleophilic stress, Nrf2 is released from Keap1-Nrf2 complex and rapidly translocates into the nucleus, where it activates transcription of *Hmox1* and other genes by binding to antioxidant response element (ARE) motifs in the promoter region of *Hmox1*, thereby culminating in Hmox1 expression (33, 34). Hmox1 induction by Nrf2 has been reported to require inactivation of the transcriptional repressor BTB and CNC homology 1 (Bach1) (35). Hmox1 activation can also be induced via other transcription factors, including activator protein-1 (AP-1), hypoxia inducible

factor-1α (HIF-1α), signal transducer and activator of transcription 3 (STAT3) and Yin Yang 1 (YY1).

It is now well established that Hmox1 expression consistently associates with benefits in a number of pathologic conditions, including cardiovascular and metabolic diseases. The protection against CVD is ascribed to a range of biological consequences associated with increased Hmox1 expression, such as induction of ferritin expression to store redox-active iron, increased antioxidant activity, the regulation of vascular tone, promotion of endothelial cell growth and re-endothelialization, inhibition of vascular inflammation, protection against endothelial cell apoptosis, and regulation of lipid metabolism (34, 36, 37). Overexpression of Hmox1, or induction of Hmox1 expression by heme, increases endothelial progenitor cells (38), protects endothelial cells from apoptosis via its gaseous metabolic product CO, (39) and attenuates the proliferation of smooth muscle cells as a regulator of guanylate cyclase activation and cyclic guanosine monophosphate (cGMP) formation (40). Hmox1 is strongly implicated in atherosclerosis, the major cause of CVD. Early studies documented the presence of Hmox1 protein in atherosclerotic lesions in both animals and humans (41, 42), and increasing Hmox1 activity in arteries has been reported to protect against atherosclerosis and related vascular diseases (43, 44). Of particular note, studies showed that induction of Hmox1 enhances the stability of vulnerable atherosclerotic plaque (45, 46). Hmox1 expression correlates positively with features of plaque instability in human carotid endarterectomy specimens. In a mouse model of plaque instability (*apolipoprotein-E* deficient mice with carotid cast), induction of Hmox1 expression increases cap thickness (46). Work from our group has shown previously that pharmacological induction of Hmox1 protects against different forms of vascular disease, such as vascular remodeling and endothelial function (47). These protective activities of the enzyme may be cell-type specific in different vascular (48) and bone marrow cells (38). Additionally, Hmox1 shows an increasingly appreciated interplay with transcription factors and associated regulation of gene transcription (49, 50), which may underpin its beneficial properties.

Evidence for a role of Hmox1 in metabolic disease has also been reported. Induction of Hmox1 by hemin or cobalt protoporphyrin IX has been shown to increase insulin sensitivity, enhance glucose metabolism, and improve adipose remodeling in a range of diabetic animal models (51-54). Moreover, in line with these properties of Hmox1 in pre-clinical models, analysis of microsatellite polymorphisms indicates that Hmox1 may protect against diabetes in humans (55). Type 2 diabetes patients carrying short $(GT)_n$ repeats in the promoter region of the *Hmox1* gene, who have greater Hmox1 activity, also show greater susceptibility to diabetes than those with long $(GT)_n$ repeats polymorphism and weaker Hmox1 activity (56). However, the role of Hmox1 in cardiovascular protection and metabolic regulation is still controversial and needs further study, since inconsistent results has been observed in human studies (55, 57, 58) and it has also been reported that Hmox1 drives metaflammation and insulin resistance in mouse and

human (59).

Hmox2 is a constitutively expressed protein of 36 kDa molecular weight but may also be induced by corticoids (60). This isoform of heme oxygenase, highly expressed particularly in the brain and testis, has been reported to be involved in the oxygen sensing and the regulation of vascular tone (61), although a later study did not find an oxygen sensing phenotype in Hmox2 deficient mice (62). In addition, Hmox2 has also been reported to be involved in the regulation of redox sensing (63, 64), inflammatory response (65), cell proliferation (64), and neovascularization (65, 66), suggestive of a role in CVD.

The multiple lines of evidence reviewed in this section strongly infer a role for heme oxygenase in protection against cardiovascular and metabolic diseases. Nevertheless, it remains unclear whether the cardiovascular benefit of heme oxygenase is achieved via detoxification (elimination) of heme, or formation of CO, biliverdin and bilirubin. It is also important to remember that these products of heme catabolism have important biological activities under normal physiological conditions rather than being the waste products of heme degradation. Keeping these potentially important considerations in mind, this thesis will now review the evidence in support of cardiovascular protective properties of the products of heme degradation, with particular emphasis on bilirubin.

1.2.2 Carbon monoxide

CO is the first product released during heme degradation by heme oxygenase. It is a colorless, odorless, non-irritating but highly toxic gas at high concentrations. At low non-toxic concentrations (~250 p.p.m) (31, 67), however, CO has been reported to have antioxidant, anti-inflammatory, anti-apoptotic and anti-proliferative properties, and to regulate arterial tone (31, 68). CO protects against ischemic injury via scavenging of superoxide anion and regulation of mitochondrial respiration (69, 70). CO inhibits inflammation via selective suppression of pro-inflammatory cytokines (tumor necrosis factor-α (TNF-α), interleukin (IL)-1β (67) and macrophage inhibitory protein-β) and induction of the anti-inflammatory cytokine IL-10 (71). CO may also regulate vascular tone via modulation of nitric oxide synthase (72), and inhibit leukocyte infiltration/activation and smooth muscle cell proliferation in the context of neointimal hyperplasia following balloon-injury of rat carotid arteries (73). In addition, CO inhibits platelet aggregation and adhesion (74), thereby potentially affecting thrombosis.

Of note, several of the beneficial activities of CO mentioned here may help explain the cardiovascular protection attributed to heme oxygenase. The biological properties of CO are routinely investigated by administering CO gas or chemical CO donors, and it is argued that this mimics the endogenous formation of CO and hence may explain the biological consequence of induction of heme oxygenase. Indeed, studies have shown that CO derived from Hmox1 suppresses endothelial cell apoptosis (39), and promotes the survival of cardiac transplants (75).

As a positive feedback loop, CO also induces Nrf2-dependent Hmox1 expression and protects vasculature against apoptosis triggered by endoplasmic reticulum (ER) stress (76). Taken together, the beneficial effects of the Hmox1/CO pathway may provide dual protection against CVD (77). However, it remains unclear whether, and if so to what extent, endogenously produced CO reflects the tissue concentrations of CO achieved by exogenously administered CO, and what the sources of heme are that serve as substrate for heme oxygenase to provide the biological protection reported.

1.2.3 Iron

Iron serves as a metal cofactor for hemoproteins, and involves in a broad spectrum of crucial biologic functions including oxygen transport, DNA synthesis, protein synthesis and electron transfer via its redox ability of transferring between ferrous (Fe^{2+}) iron to ferric (Fe^{3+}) iron (78). In addition to heme, iron also plays important biological roles as part of iron-sulfur proteins which are widespread electron transfer agents regulating oxidation-reduction reaction in almost all organisms, and also in the form of non-heme, non-iron-sulfur proteins which have the major function as transportation and storage of iron.

Heme-derived Fe^{2+} iron is liberated from the protoporphyrin ring during heme degradation. Heme oxygenase plays an important role in recycling the body's iron by facilitating its release from heme (79). The released iron is then sequestered into storage proteins such as ferritin or released from cells via basolateral iron exporter ferroportin (80-82). Ferroportin-mediated release of iron requires its oxidation from the Fe^{2+} to Fe^{3+} form by ferroxidases hephaestin. Once released, Fe^{3+} is bound by the iron transport protein transferrin for circulation in the blood (83, 84). Transferrin has a very high affinity for iron, so that the concentrations of unbound iron in blood is very low, reflecting the tight control of iron metabolism. Most cells can take up iron and reuse it for synthesis of iron-containing proteins. Especially, erythroid progenitor cells in the bone marrow and spleen take up most of the transferrin-bound iron in the circulation for hemoglobin synthesis, and this process is part of the whole-body iron recycling process. If iron metabolism is left uncontrolled, iron can contribute to the cellular "labile iron pool" and act as a pro-oxidant (85). This can lead to increased production of reactive oxygen species that themselves may contribute to the oxidation of lipids, proteins and DNA, and ultimately cause cell damage.

There is convincing evidence that the pro-oxidant property of iron is related to many cardiovascular diseases. For instance, iron is increased in atherosclerotic plaque compared with the healthy arterial wall, consistent with arterial plaque iron contributing to, and being a risk factor for atherosclerosis (86). The higher iron storage in men and post-menopausal women is thought to contribute to the increased incidence of heart disease compared with premenopausal women who have slight deficiency of iron (87). There is also a large body of literature suggesting that

iron-mediated oxidation of LDL promotes atherogenesis (88, 89). In agreement with previous evidence, iron chelation eliminates pro-oxidant free iron and inhibits NF-κB-mediated endothelial adhesion molecule expression (90), may help attenuate inflammation and atherosclerosis. This treatment may be applied to atherosclerotic vascular diseases by suppressing oxidative stress and inflammation. Free iron is also a significant risk factor in ischemia/reperfusion injury. The main source of iron during ischemia/reperfusion injury is the release of heme proteins from the damaged cells, especially hemoglobin derived from red blood cells. Administration of iron chelators markedly protects myocardial and other tissue from necrosis after reperfusion (91, 92), which indicates the possible importance of lowering iron in anti-ischemia therapies. Epidemiologic observations and experimental studies also have shown iron to be associated with the pathogenesis of diabetes (93). Low iron diets or treatment with iron chelators increases insulin secretion and sensitivity of the leptin-deficient *ob/ob* mouse model of type 2 diabetes (94). However, studies in patients with hemochromatosis, who suffer from iron overload, showed that iron overload is not associated with an increased prevalence of CVD (95). Another study also showed no significant increase in the prevalence of diabetes in patients with hemochromatosis (96).

Therefore, many questions about the relationship between heme oxygenase and iron remain unanswered. For example, how does the elimination of heme-derived iron by heme oxygenase facilitate its protective property, and how can one separate the role of iron from the other products of heme oxygenase-mediated heme degradation?

1.2.4 Biliverdin

Biliverdin, the intermediate blue-green pigment of heme degradation, is the metabolic precursor of bilirubin. All natural biliverdins consist of an open chain tetrapyrrole derived from cleavage of the circular tetrapyrrole heme. Since the ring cleavage of heme can occur at any one of the four (α, β, γ and δ) methane bridges connecting the pyrrole moieties, four different structural isomers of biliverdin IXα, IXβ, IXγ and IXδ can be formed (with "IX" specifying the order of ring substituents and the Greek letter indicating the bridge that is cleaved, Fig. 1.2) (30, 97). Intriguingly, the currently known mammalian isoforms of heme oxygenases, *i.e.,* Hmox1 and Hmox2, only target the α methane bridge of heme and hence only produce biliverdin IXα (98). Indeed, the predominant bilirubin isomer detected in adult mammals is bilirubin IXα, indicating that the biliverdin, the precursor of bilirubin, is derived mainly from enzymatic heme degradation by heme oxygenase. In contrast, biliverdin IXβ is the major form of biliverdin in the fetus of mammals, just as 87% of bilirubin present in a 20 weeks old fetus is the β isomer. A very small amount of bilirubin IXγ and IXδ isomers have also been detected in fetal bile (99). The source of biliverdin IXβ, γ and δ remains unknown, although it is likely of enzymatic origin, as non-

enzymic oxidation of heme produces all four isomers of biliverdin IX *in vitro* (100). Further investigation is also needed to explain why IXβ, γ and δ isomers of biliverdin (and the resultant bilirubin isomers) are formed in the fetus.

Biliverdin is present in almost all the organisms ranging from archaea, bacteria, and eukaryote domains (30). In plants, cyanobacteria and algae, biliverdin has a vital role as a substrate for the biosynthesis of photoresponsive bilins (*e.g.,* phytochromes), which are essential elements in the physiology and development of these organisms (101). Biliverdin is accumulated in the skeleton of the blue coral *H. coerulea* via a mechanism that remains to be elucidated (102). In insects and other evolutionary older organism, biliverdin is found in the hemolymph and integument, and it is mainly used for camouflage or photoprotection. Similarly, birds apply biliverdin originated from shell gland, but not erythrocytes (103), to color their eggshells to assist in post-mating signaling, provide camouflage and/or crypsis, avoid predation, protect against tran-shell microbial contamination (104, 105), and strengthen the shell structure (106). Similar to birds, biliverdin was identified to be responsible for the coloration of the eggs of the dinosaur oviraptor (107).

However, the function of biliverdin, if any, in the blood of vertebrates, especially mammals, mostly remains unclear. Unlike some other vertebrates that directly excrete biliverdin into bile, mammals enzymatically reduce biliverdin to bilirubin before its secretion into bile. Accompanied by the fact that only a trace amount of biliverdin is present in most mammals and lacking solid evidence for its function, biliverdin was once proposed to be non-functional to human. By way of contrast, there is a growing body of current work reporting the potential protective role of biliverdin against pathological conditions. More specifically, biliverdin has potent antioxidant property, it scavenges peroxyl radicals more effectively than bilirubin in different forms (2, 3). Biliverdin is also able to react with hypochlorous acid and prevent protein inactivation mediated by hypochlorous acid oxidation (108). Biliverdin can act synergistically with α-tocopherol (α-TOH) to inhibit lipid peroxidation (109). In an *in vitro* study, biliverdin protected human erythrocytes and rat hepatocytes via its antioxidant activity (110). Biliverdin decreases oxidative injuries of brain cells and reduces cerebral infarction by suppressing superoxide production *in vivo* (111).

Biliverdin has also been recognized as a suppressor of inflammation. Thus, treatment of biliverdin suppresses T cells proliferation *in vitro* and promotes development of tolerance to cardiac allografts in mice (112). It is reported that biliverdin inhibits the inflammatory response either through regulation of BVR translocation into the nucleus (113) or by modulating the concentrations of IL-10 via the phosphoinositide 3-kinase (PI3K) signaling pathway (114). In models of lipopolysaccharide (LPS) induced endotoxemia or surgically induced sepsis, biliverdin has been reported to protect against injury to different organs (*e.g.,* liver, lung and intestine) (113, 115, 116).

In pre-clinical models, biliverdin has been studied in the context of preventing ischemia/reperfusion injury of the heart, lung, liver and other organs, which is partly dependent on the suppression of inflammatory response (117-119). The outcome of these studies indicates that biliverdin may be beneficial in organ transplantation.

In addition, studies have indicated that biliverdin is a potential modulator of vascular dysfunction. In a balloon injury model of intimal hyperplasia, biliverdin inhibited vascular stenosis via inhibition of smooth muscle cell migration (120, 121). In an arterialized vein graft model, biliverdin significantly suppressed the development of intimal hyperplasia via inhibition of endothelial cell apoptosis by reducing c-Jun N-terminal kinases (JNK) phosphorylation (121). Similarly, treatment with biliverdin greatly ameliorates excessive inflammatory and neovascular response in a murine corneal injury model (66).

In the context of a study related to metabolism, biliverdin administration was reported to enhance insulin sensitivity in a mouse model of type 2 diabetes, mainly via inhibition of oxidative stress and subsequent suppression of beta cell apoptosis (122). More recently, biliverdin was found to attenuate lipid accumulation *in vitro* via regulation of peroxisome proliferator-activated receptors-α (PPARα) (8).

The above body of literature suggests administration of biliverdin as a potential therapeutic approach to treat or prevent vascular and metabolic diseases. However, in most instances, biliverdin was applied *ex vivo* and as a precursor of bilirubin (111, 115, 118, 119, 122). There are currently only small number of studies addressing the questions of how biliverdin reaches its target tissue, what the effective concentration of biliverdin are, and how exogenously applied biliverdin becomes metabolized *in vivo*. In fact, in most mammals, biliverdin reductase is an evolutionarily conserved enzyme expressed in a broad range of tissues. As a result, biliverdin is readily and rapidly reduced to bilirubin, so that biliverdin is barely detectable even in bile (123). Therefore, it is reasonable to assume that neither exogenously added biliverdin (111), nor increasing endogenous formation of biliverdin by extreme hemolytic anemia (124) or partially mutating biliverdin reductase (125) will cause substantial accumulation of biliverdin *in vivo*. Therefore, the beneficial activities of biliverdin observed in mammalian system may in fact come from bilirubin, rather than biliverdin itself. To distinguish activities of biliverdin from bilirubin, some studies included bilirubin treatment for comparison, or examined biliverdin in *in vitro* systems (*e.g.,* erythrocytes) in the absence of biliverdin reductase (110, 115). However, these approaches have their own caveats (*e.g.,* differences in the solubility of biliverdin versus bilirubin) and they do not resolve the problem that biliverdin is effectively reduced to bilirubin *in vivo*. Given the potent enzymatic function of biliverdin reductase, an alternative approach to investigate the potential *in vivo* activity of bilirubin is the use of a global *biliverdin reductase a* gene knockout animal model (126).

It is also prudent to consider the possibility that administration of biliverdin may result

in mild toxicity, which is not as obvious and common as in the situation of bilirubin. In most cases, however, biliverdin appears safe and individuals with accumulation of biliverdin are healthy (126, 127). Of note, while the disorder may be safe for the adult (mother), the situation may be different for the fetus who may suffer premature births and stillbirths due to placental infarcts (127), since biliverdin is unable to cross the placenta and the fetus is therefore unable to excrete the pigment (128).

1.3 Biliverdin reductase

Biliverdin reductase (EC 1.3.1.24) is a highly efficient enzyme present in nearly all mammalian tissue (123, 129-131). As the name suggests, the major function of this cytosolic enzyme is the reduction of biliverdin to bilirubin, using NADH in pH range of 6.0-7.0, or NADPH in pH range of 8.5-8.7 as electron donors (123, 131). Therefore, NADH is the preferred cofactor for human biliverdin reductase under physiological intracellular pH.

Biliverdin reductase has two isozymes: BVRA and BVRB. In humans, BVRA (UniProtKB-P53004, $M_w \approx 33$ kDa) is encoded by *BLVRA* which is the located in the chromosome 7, while BVRB (UniProtKB-P30043, $M_w \approx 23$ kDa) is encoded by *BLVRB* that located in chromosome 19. The mouse homologs are located on chromosome 2 for *Blvra* and chromosome 7 for *Blvrb*, respectively. The *BLVRA* gene consists of 12 exons (NCBI GenBank accession number: NM_000712) that encode a protein of 296 amino acids in human. Exon 3 of *BLVRA* encodes the catalytic domain of the protein. On the other hand, the *BLVRB* gene consists of 5 exons (NCBI GenBank accession number: NM_000713) that encode a protein of 206 amino acids. Exon 3 of *BLVRB* encodes the active site of the protein (19, 132). Both the N terminus of BVRA and BVRB contain the catalytic domain and house a binding motif for their cofactors NAD(P)H. As eluded to earlier, cleavage of the heme ring template generates all four natural isomers of biliverdin (IXα, IXβ, IXγ and IXδ). BVRA can reduce all four biliverdin isomers to produce corresponding bilirubin isomers, while BVRB can only catalyze the reduction of the IXβ, IXγ and IXδ isomers (Fig. 1.2) (98).

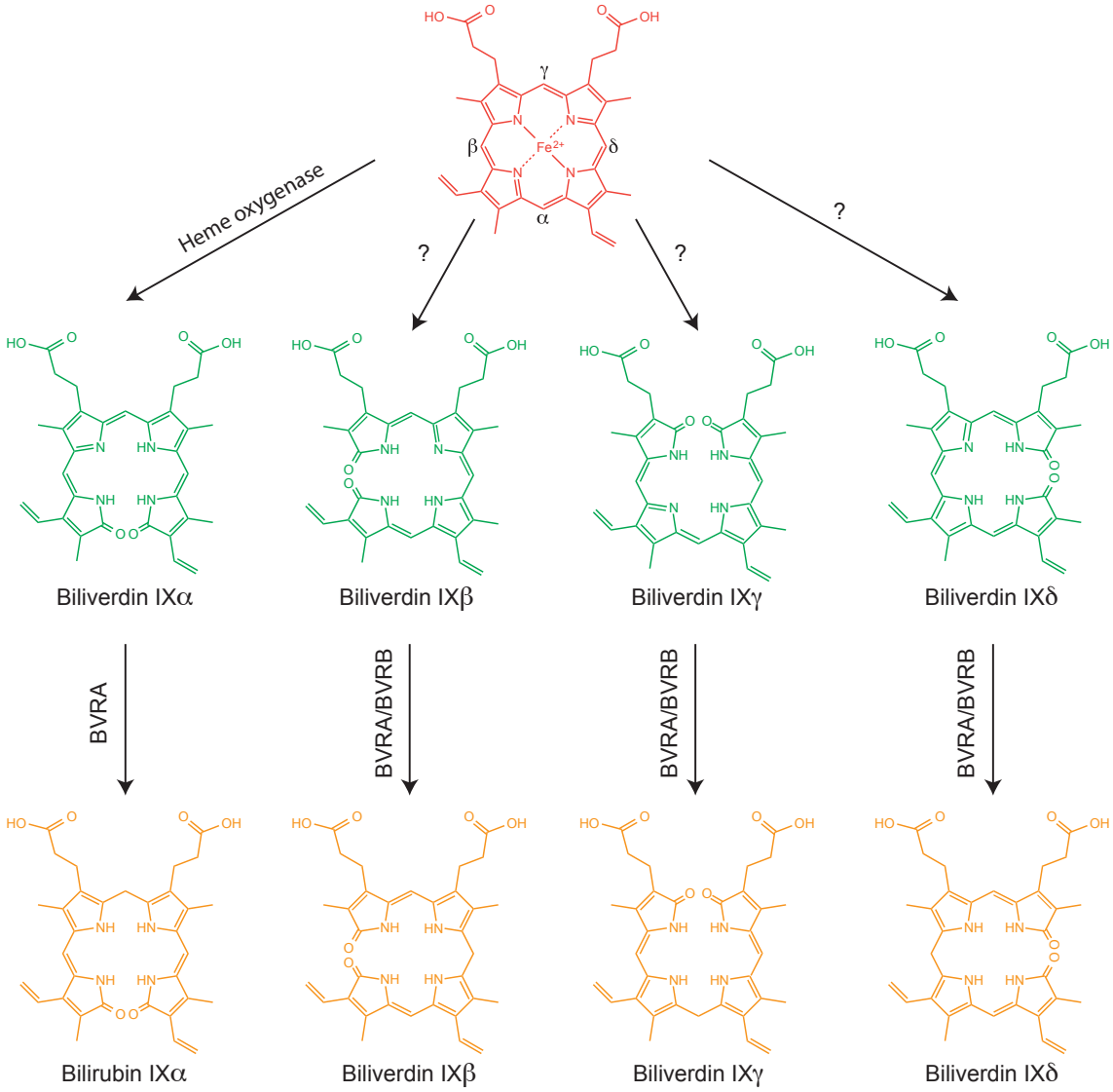

Figure 1.2 Generation of isomeric biliverdins (IXα, IXβ, IXγ and IXδ) and the corresponding isomeric bilirubins. This figure was reproduced from McDonagh AF. *Nat Struct Biol* 2001;8:198-200.

1.3.1 Biliverdin reductase A

BVRA reduces biliverdin IXα to bilirubin IXα, which is the predominant isomer of bilirubin in adult mammals (95-97%) (97). mRNA and protein of BVRA are detectable in almost all tissues, although the enzyme mainly functions in macrophages of the spleen where it participates in heme degradation associated with the turnover of senescent red blood cells. In addition to its enzymatic function as a reductase, the C-terminus of BVRA contains binding motifs that potentially allow for a broad range of interactions (19, 23). As such, BVRA is also proposed to act as a transcription factor and/or a kinase, and to modulate insulin signaling as well as to serve as a regulator of glucose metabolism.

The potential of BVRA to regulate *HMOX1* gene transcription via both antioxidant and hypoxia response elements is attributable to a number of similarities between its domain structure and other DNA-binding proteins with a leucine zipper motif (133, 134). However, to date, the evidence for such action is limited.

With regard to metabolic signaling it has been reported that BVRA contains two docking consensus sequences for mitogen-activated protein kinase (MAPK), enabling BVRA to act as a serine/threonine/tyrosine kinase, modulating phosphorylation of the insulin receptor substrate (IRS)-1 and other targets of both the insulin/IGF-1 and the IRK/IRS/MAPK/PI3K signaling pathways (20, 23, 135, 136). Studies also showed that human BVRA is a coactivator and substrate for protein kinase B (Akt), and can be a binding partner for phosphatidylinositol-dependent kinase 1 (PDK1)-Akt activation (137) which is important for in the insulin/IGF-1 signaling cascade and insulin sensitivity. It has also been reported that BVRA interacts at the crosstalk of MAPK and PI3K signaling pathways via protein kinase C (138). The duality (activation and inhibition) of BVRA in insulin signaling and glucose metabolism is highlighted in a recent study using peptide sequences of human BVRA in human cell lines. The terminal 290KYCCSRK peptide was found to increase glucose uptake and to potentiate insulin signaling, while a peptide (194KEDQYMKMTV) corresponding to BVRA's SH2-binding domain was a potent inhibitor of glucose uptake and insulin signaling (135). Additionally, BVRA can also diminish insulin signaling and act as a negative regulator of glucose uptake in cells through its kinase activity, by phosphorylating serine residues of IRS-1 (139).

The number of pathways in which BVRA is implicated continues to increase. A recent study using a liver specific *Bvra* deficient mouse fed a high fat diet reported that hepatic BVRA attenuated lipid accumulation in the liver via activation of the PPARα pathway (125). In these obese mice with hepatic *Bvra* deficiency, the observed dysregulation of lipid metabolism was accompanied by enhanced glucose intolerance and impaired insulin signaling. In addition, deficiency of BVRA in the proximal tubule cells of the kidney also promoted lipid accumulation and lipotoxicity in renal tissue via BCL-2-associated death promoter (140). Recent reports also suggest that impairment of BVRA is associated with increased β-amyloid peptide production and brain insulin resistance in aging dogs and in a transgenic mouse model of Alzheimer disease with 3 mutant human genes (APP_{Swe}, $PS1_{M146V}$, and tau_{P301L}) (141, 142). Moreover, it has been reported that BVRA is a critical regulator of innate immune responses. Thus, BVRA activates the PI3K-Akt-IL-10 axis and inhibits toll-like receptor 4 (TLR4) expression via direct binding to the TLR4 promoter in macrophages, thereby controlling the inflammatory response (113). To summarize, BVRA may be of benefit to metabolic diseases via its pleiotropic functions that include regulation of insulin signaling, glucose metabolism, lipid metabolism and inflammation. However, to date these studies were mostly conducted in *in vitro* or rodent models, and clinical evidence remains limited.

1.3.2 BVRA mediated redox cycle

A BVRA-mediated redox cycle has been proposed to explain the antioxidant activity of bilirubin (143, 144). Briefly, the anti-oxidative effect of bilirubin is proposed to be amplified by BVRA recycling of bilirubin from biliverdin formed as bilirubin becomes oxidized, *e.g.,* by peroxyl radicals, singlet oxygen or nitric oxide. According to this redox cycle, bilirubin may constitute the principal physiologic function. In these two studies, Snyder and colleagues reported 10 nM bilirubin to exert sufficient antioxidant activity via BVRA-mediated redox cycle to protect against almost 10,000-fold higher concentrations of H_2O_2 (143, 144). However, this observed benefit attributed to the biliverdin/bilirubin redox cycling by BVRA has been questioned ever since (145-147). The principal argument against the proposed cycle is that biliverdin is not a major product of bilirubin oxidation induced by biological oxidants including H_2O_2 *in vitro*, *ex vivo* and *in vivo*. The BVRA-mediated redox cycle also appears unlikely to explain our recent observations of increased oxidative stress in *Bvra*$^{-/-}$ mice (126), for two reasons. First, the BVRA-dependent redox cycle has been proposed for intracellular bilirubin/BVRA, whereas we observed that the absence of plasma bilirubin as a result of BVRA deficiency increases the circulating concentrations of cholesterylester hydroperoxides (CE-OOH), which are likely formed in the extracellular space. Second, bilirubin deficiency increased oxidative stress in red blood cells that are devoid of BVRA (126).

1.3.3 Biliverdin reductase B

BVRB is present in many tissues, with the highest expression in liver, particularly fetal liver (148, 149). BVRB reduces biliverdin IXβ to bilirubin IXβ, which is the predominant isomer of bilirubin (up to 87%) detected during fetal development (150). This suggests that BVRB plays a crucial enzymatic function in fetal heme catabolism since BVRB is the preferred enzyme for the reduction of biliverdin IXβ to bilirubin IXβ (151). However, the source of biliverdin IXβ in the fetus remains unknown. BVRB is identical to flavin reductase (152) and is a broad specificity oxidoreductase that catalyzes the NAD(P)H-dependent reduction of different flavins (152), methemoglobin and pyrroloquinoline quinone. In addition, BVRB also reduces complexed Fe^{3+} to Fe^{2+} in the presence of flavin mononucleotide and NADPH. Together, these findings suggest that BVRB may play a more general role in redox regulation, although current knowledge of BVRB is limited.

Similar to BVRA, BVRB also contains a range of binding motifs, some of which share similarity with the insulin receptor-interaction domain of BVRA. Yet, to date, no study has shown that BVRB can act as kinase and influence insulin signaling. The consensus sequences of the C-terminus of BVRB indicate that BVRB is unlikely act as a transcription factor (19).

BVRB has been found to associate with CVD. A recent study using a combination of proteomics and transcriptomics identified that enrichment of BVRB in atherosclerotic lesions and

plasma serves as a disease-related signature molecule for intra-plaque hemorrhage and plaque instability in carotid atherosclerosis (153). However, this study asserted that BVRB is functionally linked to heme metabolism by Hmox1, thereby playing a role in intra-plaque hemorrhage and plaque instability. Such assertion appears incorrect, however, as BVRB does not act on the product of Hmox1 enzymatic activity, *i.e.*, biliverdin IXα, as discussed earlier in Section 1.2.4. Interestingly, an earlier study of genetic association implied a physiological function of BVRB in governing terminal megakaryocytopoiesis, as a loss-of-function mutation of BVRB was associated with enhanced platelet production (149). Clearly, more research on this enzyme is warranted although that is outside the scope of this thesis.

1.4 Bilirubin

1.4.1 Bilirubin generation, metabolism and excretion

Daily production of bilirubin in human is approximately 300 to 400 mg. Based on theoretical calculations and existing reports, up to 80% of circulating bilirubin is derived from enzymatic degradation of hemoglobin-derived heme resulting from the turnover of senescent red blood cells in reticuloendothelial cells of spleen, liver and bone marrow. The remainder of bilirubin originates from the catabolism of other heme-containing proteins, including myoglobin, cytochromes, catalase, peroxidase and tryptophan oxygenase (154, 155). As heme catabolism is active in almost all types of cells, heme derived from these proteins is likely degraded locally, thereby generating bilirubin locally within various cells, such as skeletal muscle and endothelial cells (156, 157).

Bilirubin derived from the degradation of heme is commonly referred to as unconjugated bilirubin or indirect bilirubin. Unconjugated bilirubin is essentially water-insoluble due to its intramolecularly hydrogen-bonded ridge-tile conformation (158). The released unconjugated bilirubin is bound to albumin in the blood for transport throughout the body and eventually to the liver (159). As unconjugated bilirubin reaches the liver, it dissociates from albumin and enters the hepatocytes (160, 161), where it is converted to conjugated bilirubin (also called direct bilirubin). Bilirubin conjugation is catalyzed by UDP glucuronyl transferase (UGT), involves one or two molecules of glucuronic acid, and results in the formation of bilirubin mono- or diglucuronide (13, 162). The polar glucuronyl group(s) render(s) bilirubin, the yellow pigment, water-soluble for secretion into the biliary tree via multidrug resistant protein 2 (MRP2, a membrane transport protein), thereby contributes to the yellow color of bile (Fig. 1.1) (163). Biliary conjugated bilirubin then reaches the intestine, where bacteria degrade it to its breakdown products, such as stercobilin and urobilin that are ultimately excreted from the body (164).

Under physiological conditions, plasma concentrations of bilirubin in humans range from 5 to 17 μM, most of which is albumin-bound unconjugated bilirubin. The affinity of unconjugated bilirubin for albumin is extremely high, such that under normal conditions ‘free’ unconjugated bilirubin is essentially undetectable in plasma. However, when plasma concentrations of bilirubin

become elevated and surpass the binding capacity of albumin, unconjugated bilirubin can accumulate in biological tissue. Hyperbilirubinemia is responsible for the yellow discoloration in jaundice and characterized by yellow pigmentation as a result of bilirubin in plasma, skin, sclerae, mucous membranes, and other less visible tissues (165, 166). In principle, albumin-bound and conjugated bilirubin are not able to cross the blood-brain barrier and do not exhibit neurotoxicity (167). However, when the plasma concentration of bilirubin exceed 300 μM, free unconjugated bilirubin dissociates from albumin, crosses the blood-brain barrier and accumulates in certain regions of the brain where it causes toxicity and increases the risk of development of neurologic dysfunctions (*e.g.,* kernicterus) (168).

There are many reasons that can lead to bilirubin accumulation in our body. These include:

1) Increased bilirubin formation, *e.g.,* as a result of hemolysis caused by increased destruction of red blood cells. Increased expression and/or activity of heme oxygenase and/or biliverdin reductase could conceivably cause hyperbilirubinemia (169-171), although there is no clear *in vivo* evidence supporting this scenario;

2) Limited albumin binding capacity, *e.g.,* due to molecules that compete with bilirubin for albumin binding, such as sulfonamides, long-chain fatty acids from breast milk, salicylates and contrast media (172);

3) Impaired hepatic uptake of bilirubin by 1A and 1B members of the organic anion transporting polypeptide family (173);

4) Decrease in bilirubin conjugation, *e.g.,* in situations of glucuronyl transferase deficiency. For example, Gilbert's syndrome and type II Crigler-Najjar syndrome result in mild hyperbilirubinemia with plasma bilirubin concentrations in the range of 20 to 100 μM (174), while type I Crigler-Najjar syndrome results in severe hyperbilirubinemia with plasma bilirubin concentrations ranging from 300 to 700 μM (175). Further, physiological jaundice of the neonate is due to a transient insufficiency of glucuronyl transferase caused by liver immaturity (176) and overproduction of bilirubin caused by enhanced red blood cell destruction to replace fetal with adult hemoglobin;

5) Decreased secretion and excretion of conjugated bilirubin. Diseases that reduce the rate of secretion of conjugated bilirubin into the bile or the flow of bile into the intestine produce the conjugated hyperbilirubinemia due to 'reflux' of conjugated bilirubin back into the plasma. Conjugated hyperbilirubinemia usually indicates hepatobiliary disease, such as cholestasis and bacterial infection.

6) Finally, mutations in genes such as MRP2 can also lead to conjugated hyperbilirubinemia, such as in Dubin-Johnson syndrome (177, 178).

1.4.2 Bilirubin isomers

Same as biliverdin, natural bilirubin consists of an open chain of tetrapyrroles and may exist as one of the four different structural isomers, namely bilirubin IXα, IXβ, IXγ and IXδ. These isomers are derived from biliverdin IXα, IXβ, IXγ and IXδ by enzymatic reaction of biliverdin reductases, as described in the previous section (Fig. 1.2).

The IXα-isomer of bilirubin is the predominant form in most adults, while the IXβ isomer is the major form in fetus, with up to 87% of bilirubin as the β isomer in the 20-week-old fetus. A very small amount of bilirubin IXγ and IXδ have also been detected in fetal bile (99) and the proportion of the bilirubin isomers in bile is dynamic during fetal development. Bilirubin is not detected in the first 13 weeks of gestation, likely due to the lifetime of red blood cells (~60-90 days in the fetus) and the resulting absence of substantive turnover of hemoglobin during these early stages of development. From 14-week gestation, bilirubin IXβ is observed as the first and only detectable pigment in fetal bile. At 16-week gestation, unconjugated bilirubin IXα first appears, while IXβ isomer remains predominant. However, as bilirubin can be transported through the placenta (128, 179), whether unconjugated IXα is endogenously produced by the fetus during hemopoiesis or is exogenous transported from the mother via placental transfer is unknown. At 20-week, conjugated bilirubin IXα is first observed. Thereafter, the proportion of bilirubin present as the IXα isomer continually increases until it becomes the major bile pigment, with only trace amounts of other isomers detectable. The first appearance of conjugated bilirubin IXα may be the indication of the liver maturation (99, 180).

Photo-isomers of natural bilirubin IXα (4*Z*,15*Z* configuration) are also observed (181). When exposed to light or phototherapy treatment, used to treat neonatal jaundice or Crigler–Najjar disease, photo-isomers of bilirubin IXα (4*E*,15*Z*, 4*Z*,15*E* and 4*E*,15*E* configuration) are produced. Since these photo-isomers lack intramolecular hydrogen bonds, they are more hydrophilic and soluble in aqueous solution, and hence can be directly secreted into bile without the need for conjugation (182).

It is commonly known that unconjugated bilirubin IXα in its 4*Z*,15*Z* configuration needs to be bound to albumin for transportation and then conjugation with glucuronic acid for secretion. However, it remains unclear how the more water-soluble isomers are transported in the circulation and secreted into bile. In the absence of 'tight' intramolecular hydrogen bonding, all the biliverdin isomers, bilirubin IXα in 4*E*,15*Z* and the 4*Z*,15*E* and 4*E*,15*E* configuration, and bilirubin isomers of IXβ, IXγ and IXδ can be secreted into bile without the carboxylic acid chains glucuronidated, giving Crigler-Najjar patients and Gunn rats have the ability to eliminate bilirubin via an yet unknown pathways that does not involve glucuronidation (158, 183, 184). Trace amounts of the conjugated form of these water-soluble bile pigments are also detectable in normal population.

1.5 Bilirubin protective properties

For many years, bilirubin was considered to be a metabolic waste product. However, 30 years ago, in a series of publications, Stocker *et al*. demonstrated that bilirubin acts as a potent antioxidant (2, 3, 108, 185). In these studies, bilirubin was shown to efficiently protect linoleic acid from peroxyl radical-induced oxidation *in vitro*. Following this landmark observation and suggestion that bilirubin may provide benefits to the body rather than just being a potentially toxic waste product, numerous studies have shown that, in addition to antioxidant function, bilirubin has anti-inflammatory property, promotes endothelial function, inhibits VSMC proliferation, and positively regulates lipid metabolism. Despite this body of evidence, however, a clear role of bilirubin in the human body remains to be substantiated.

1.5.1 Antioxidant

Oxidative stress is caused by the imbalance between oxidants and antioxidant defenses. Oxidative stress is thought to contribute to a number of diseases, especially CVD and related metabolic syndrome. It is conceivable that modifying oxidative stress may attenuate the development and progression of these diseases, thereby improving the quality of human life. Bilirubin could potentially contribute to human health via its antioxidant property. As the antioxidant activity of bilirubin has been extensively reviewed in detail elsewhere (126, 186), only a summary will be provided here. Bilirubin is a potent antioxidant in its free (2), albumin-bound (185), and conjugated form (3). Each molecule of bilirubin scavenges 1.9 molecules of peroxyl radicals (2, 3). Bilirubin efficiently protects linoleic acid from peroxyl radical-induced oxidation *in vitro*, and suppresses the oxidation of peroxyl radicals better than α-TOH (48). Bilirubin also protects circulating lipids from oxidation by interaction with α-TOH (187). In addition to scavenging lipid peroxyl and α-tocopheroxyl radicals (α-TO$^{\bullet}$), bilirubin can attenuate oxidative damage to proteins (188, 189); scavenge hypochlorous acid (108), nitric oxide and reactive nitrogen species (190); and inhibit chloramine formation and myeloperoxidase-mediated protein oxidation (191).

Suggestions that bilirubin is an important antioxidant *in vivo* were initially based on experiments showing protective effects in cultured cells. Albumin-bound bilirubin was firstly observed to protect rat hepatocyte and human erythrocytes against different oxidants (162). Bilirubin induced by hemin treatment protects VSMC against oxidative stress (192). Bilirubin can also attenuate vascular endothelial cell dysfunction in response to oxidized low-density lipoproteins (oxLDL) (6). In human cardiomyocytes, albumin-bound bilirubin is a powerful protector against oxidant-induced toxicity (193).

The antioxidant properties of bilirubin have also been reported in several animal studies. For example, bilirubin protects against oxidative stress in hyperbilirubinemic Gunn rats exposed to hyperoxia by decreasing thiobarbituric acid-reactive substances (194). Hemin-induced or exogenous bilirubin preserved myocardial function during cardiac ischemia/reperfusion injury in

rats (195). Moreover, *ex vivo* treatment of perfused rat hearts with bilirubin ditaurate (a model of conjugated bilirubin) improved post-ischemic functional outcomes and decreased myocardial oxidative damage (196). We recently reported (126) higher concentrations of CE-OOH in plasma and increased oxidized peroxiredoxin 2 in red blood cells of *Bvra* gene deficient ($Bvra^{-/-}$) mice compared with $Bvra^{+/+}$ mice, suggesting that bilirubin provides antioxidant benefit *in vivo* (see Chapter 3 for more details). These results are consistent with previous observations in human individuals with Gilbert's syndrome, who have moderately increased plasma bilirubin concentrations due to decreased activity of UGT1A1. Thus, compared with the normal population, markers of oxidative stress, including serum malondialdehyde, serum malondialdehyde-modified LDL, and urinary excretion of 8-hydroxy-2'-deoxyguanosine, are decreased in people with moderately increased bilirubin (197).

1.5.2 Anti-inflammatory activity

Inflammation is a driver of the initiation and progression of cardiovascular and metabolic diseases. There is a growing body of evidence indicating that bilirubin dampens inflammation via several mechanisms. Thus, increasing bilirubin via induction of heme oxygenase or administration of the pigment inhibits the expression of the pro-inflammatory cytokines IL-1β, IL-6, and TNF-α. Bilirubin also suppresses the production of inflammatory mediators, such as prostaglandin E2 (PGE2), thereby attenuating macrophage infiltration mediated by vascular cell adhesion molecule-1 (VCAM-1) and intercellular adhesion molecule-1 (ICAM-1) (4, 198, 199) as well as the ensuing inflammatory disorder.

Exogenously administered bilirubin significantly inhibits T cell-mediated autoimmune disorder via inhibition T cell proliferation, suppression of co-stimulatory molecules, inactivation of NF-κB, and induction of reactive T cell apoptosis in the mouse model of autoimmune encephalomyelitis (200). Bilirubin was also found to inhibit the chemotactic activity of human granulocytes *in vitro*, and to activate the phagocytic activity of both granulocytes and monocytes in mice *in vivo* (201, 202). Both *in vitro* and *in vivo* exposure of macrophages to bilirubin decreased the expression of several cell surface Fc receptors, indicating a potential immunosuppressive effect (203), although this study did not specify the concentration of bilirubin for treatment. Bilirubin also attenuates LPS-induced inflammation via increasing antioxidant enzyme generation and decreasing IL-8 production in activated neonatal neutrophil (204).

Bilirubin can modulate inflammation across a broad range of acute and chronic diseases. Administration of bilirubin to low-density lipoprotein receptor deficient mice impedes plaque formation and significantly reduces the infiltration of monocytes and lymphocytes into aortic root lesions via suppression of VCAM-1 and ICAM-1 (205). This result indicates that bilirubin has potential anti-atherosclerotic activity via its immune regulatory activity. An inverse association of serum total bilirubin concentration with severity of coronary atherosclerosis is also linked to

systemic inflammation, with the concentration of inflammatory markers (*e.g.,* C-reactive protein, neutrophil to lymphocyte ratio and red cell distribution width) increased in individuals with unstable coronary artery disease and accompanying low plasma bilirubin concentration (206). Bilirubin may also attenuate obesity-induced insulin resistance via regulation of inflammation (207), while a clinical study in patients with metabolic syndrome has shown that serum bilirubin concentrations are inversely correlated with inflammatory marker hs-CRP, which indicates the protective role of bilirubin against metabolic syndrome (208).

1.5.3 Endothelial cell function

Endothelial cells line the interior surface of blood vessels and are key to many aspects of vascular function. The viability of endothelial cells is a marker of vascular function under pathological conditions, such as noxious stimuli and vascular injury. Bilirubin derived from heme oxygenase can inhibit endothelial cell death induced by high glucose concentrations (209). Recruitment of circulating endothelial progenitor cells is an important contributor to re-endothelialization. Although heme oxygenase is well known to promote proliferation and migration of endothelial cells, the effect of bilirubin on proliferation and migration of endothelial cells is unknown. A recent study (210) has shown that hyperbilirubinemia can promote the pro-angiogenic secretory activity of circulating endothelial progenitor cells, thereby resulting in enhancement of their regenerative wound healing properties. This is associated with increased expression of vascular endothelial growth factor (VEGF), anti-inflammatory IL-10, phosphorylation of extracellular signal-regulated kinases (ERK), and decreased expression of TNF-α. Treatment with bilirubin also reduces the pro-inflammatory factors such as VCAM-1 and ICAM-1, and it attenuates trans-endothelial migration of leukocytes *in vitro* and *in vivo*, thereby preserving endothelial function (205, 210).

1.5.4 Vascular smooth muscle cell function

In response to pathological condition and injury to the vasculature, migration and proliferation of VSMC is triggered and contributes to arterial remodeling. However, contrary to bilirubin's effect on endothelial cells, the pigment is a negative regulator of VSMC proliferation and migration. Bilirubin arrests cell cycle progression of VSMC by inhibition of retinoblastoma protein phosphorylation and the subsequent activation of p38 mitogen-activated protein kinase (MAPK) pathway (5). Bilirubin also suppresses the transcription factor YY1, which is known to regulate the expression of genes important for VSMC cycle control (5, 211). By blocking proliferation and migration of VSMC, bilirubin ameliorates neointimal hyperplasia in balloon injury models and has been applied to drug-coated stents, showing great potential in treating occlusive vascular disease (212).

1.6 Plasma concentrations of bilirubin inversely associate with cardiovascular and metabolic diseases

Cardiovascular and metabolic diseases are now the world's leading causes of death. Referring to the Fact Sheet of Cardiovascular Diseases by the World Health Organization (1), approximately 31% of all deaths globally are attributed to CVD. CVD is often grouped with metabolic disorders, because metabolic disorders including diabetes and dyslipidemia increase the risk of vascular diseases (213, 214). Notably, epidemiological studies consistently show that increased plasma bilirubin concentrations, especially in Gilbert's syndrome, are associated with decreased risk of cardiovascular and metabolic diseases, including coronary artery disease, stroke, peripheral artery diseases, diabetes and dyslipidemia. An increasing effort has been devoted to understanding the underlying molecular mechanism, however, a direct causative link between bilirubin and cardiovascular and metabolic diseases remains to be established.

1.6.1 Bilirubin and atherosclerosis

Atherosclerosis remains a major cause of CVD and death in Australia. Atherosclerosis is a lipid- and inflammation-driven disease that leads to plaque formation at specific sites of the arterial tree through intimal lipid-accumulation, inflammation, necrosis, fibrosis, and calcification. Once an atherosclerotic plaque is present in an artery, it causes the problems of coronary artery disease, myocardial infarction, stroke and peripheral artery disease.

There are two types of plaques - stable and unstable - which can affect people in different ways. Stable plaques are fibrous plaques composed of solid fibrous or fibrous cellular tissue with only a small amount of extracellular lipids. With the thick fibrous cap, stable plaques have lower risk of plaque rupture, however, can significantly narrow the arteries due to building up of plaques, thereby reducing the delivery of oxygen via the blood to the tissues. In coronary arteries, most stable plaques remain clinically silent, or in the long term, may result in stable angina pectoris (215). Unstable plaques are potentially more dangerous than stable plaques as there are no clear symptoms for the former and unstable plaques are also more difficult to diagnose. Unstable plaques are generally characterized as those having a thin fibrous cap overlaying a large lipid-rich necrotic core and high content of inflammatory cells. Unstable plaques can rupture and cause acute events such as acute coronary syndrome, myocardial infarction, stroke or death without substantial restrictions of blood flow (216, 217).

Plasma bilirubin concentration was first demonstrated to inversely correlated with lower risk of atherosclerosis in the carotid artery (14). In this study, individuals with serum bilirubin concentration higher than 15 μM have a statistically significant reduction in risk of carotid artery plaques, compared to those who have bilirubin concentration lower than 12 μM. A later study also showed that serum bilirubin concentration was negatively associated with carotid atherosclerosis (15). The inverse association between plasma bilirubin and atherosclerosis has

also been confirmed for coronary artery (206, 218). Furthermore, a study by Canpolet *et al.* demonstrated that serum bilirubin concentration was significantly associated with the presence, severity and morphology of the atherosclerotic plaque in coronary artery detected by CT angiography (219).

Oxidative stress, inflammation, endothelial dysfunction and dyslipidemia are considered major risk factors for atherosclerosis (220-223). Serum bilirubin concentrations have also been reported to be inversely associated with markers of oxidant damage (lipid hydroperoxides, fluorescent products of lipid peroxidation) in human atherosclerotic endarterectomy specimens and the severity of atherosclerosis (224). However, there is a limitation with the methodology used in this study as it is inaccurate to include fluorescent products of lipid peroxidation as an oxidative damage parameter. In this instance, lipid peroxidation was measured by production of thiobarbituric acid reactants and by the development of fluorescence in high-temperature conditions, which can generate up to 98% artefactual lipid oxidation (225). Akboga *et al.* also surmised that lower serum bilirubin concentrations negatively correlate with the severity of coronary atherosclerosis (206). Specifically, this study also showed serum bilirubin inversely associated with higher serum C-reactive protein, neutrophil to lymphocyte ratio, and red blood cell distribution width in patients with coronary atherosclerosis, linking bilirubin and atherosclerosis to systemic inflammation. In addition, the link between bilirubin, atherosclerosis and dyslipidemia, was demonstrated by bilirubin being inversely associated with carotid and femoral atherosclerosis in familial and non-familial dyslipidemia (226). Overall, clinical reports demonstrated the inverse association between plasma bilirubin concentration and atherosclerosis and the link to oxidative stress, inflammation, dyslipidemia, is consistent with the biochemical properties of bilirubin.

However, experimental evidence derived from animal models supporting these clinical observations is limited. Only a single study has shown elevated plasma bilirubin concentration protects against the formation of atheromatous lesions in *low-density lipoprotein receptor* deficient ($Ldlr^{-/-}$) mice (205). In that study, intraperitoneal administration of bilirubin (30 mg/kg/day) for 8 weeks decreased the size of stable atherosclerotic lesions in the aortic root as well as the lesion content of macrophages and markers of oxidative stress (nitrotyrosine and chlorotyrosine), without affecting the expression of VCAM-1 or ICAM-1 in lesions and serum cholesterol and TG. The dose of administered bilirubin used in this study corresponds to about six times the daily production of bilirubin in an adult human (~5 mg/kg/day). Also, the plasma bilirubin concentrations observed in treated mice (~30 μM), while in the range of that present in Gilbert syndrome (*i.e.*, 20 - 90 μM), was approximately 15 times higher than the normal concentration.

Rupture of an unstable atherosclerotic plaque can trigger acute coronary syndrome, myocardial infarction and death. More recently, a number of studies have reported that serum

bilirubin concentration negatively correlates with plaque vulnerability. In the study by Zhu *et al*. serum concentration of total bilirubin in patients with acute coronary syndrome was significantly lower than in those with stable angina pectoris and healthy subjects (227). Moreover, serum bilirubin concentrations positively associated with fibrous plaque, whereas they negatively associated with plaque burden, lipid and remodeling index (227), suggesting a positive association between plasma bilirubin and plaque stability. In apparent contrast, the bilirubin content in human carotid endarterectomy specimens as assessed by 467 nm absorbance was reported to positively correlate with intra-plaque hemorrhage (45), which is a common unstable feature of atherosclerotic plaques. Also, in mouse models of plaque instability, plaques with unstable phenotype contain increased bilirubin compared with stable plaque and healthy arteries (45). It is possible that the observed increase in bilirubin in unstable plaque is a consequence of intra-plaque hemorrhage and associated increase in local hemoglobin and bilirubin formation, rather than bilirubin causing formation of unstable plaque.

Disruption of the atherosclerotic plaque exposes flowing blood to subendothelial collagen, tissue factor, and other procoagulant molecules, thereby initiating the activation of platelets and formation of fibrin within the vessel lumen, generating thrombi that narrow or occlude the artery, resulting in acute coronary syndrome (228). Clinical and experimental studies by Kundur *et al.* demonstrate that the activation of platelets is mildly inhibited in individuals with hyperbilirubinemia (229, 230). Therefore, plasma bilirubin may attenuate CVD by inhibition of thrombosis.

Bilirubin is also implicated in protection against endothelial dysfunction, an early manifestation of atherosclerosis. Yoshino *et al.* showed that in overweight patients higher serum bilirubin concentrations are associated with favorable endothelial function evaluated by flow-mediated dilatation (231). Moreover, the anti-retroviral drug atazanavir induced hyperbilirubinemia and improved endothelial function assessed by intra-arterial infusion of acetylcholine and nitroglycerin in the type 2 diabetes patients (232). Low serum bilirubin concentrations are independently and inversely related to impaired flow-mediated vasodilation of the brachial artery and coronary microvessels as well (233, 234). Plasma bilirubin concentrations also inversely associate with arterial stiffness of coronary arteries (235), an indicator of vessel function. Finally, in high-fat-fed *Ldlr*$^{-/-}$ mice, induction of Hmox1 by administration of heme arginate improved *ex vivo* endothelium-dependent dilation of thoracic aortic rings that was associated with decreased expression of VCAM-1 and MCP-1 (236). Unfortunately, circulating concentrations of bilirubin were not determined in the study.

With an understanding of how bilirubin may modulate atherosclerotic disease, the next section will elaborate on epidemiological and clinical evidence.

1.6.2 Bilirubin and atherosclerotic cardiovascular diseases in humans

1) Coronary artery disease. Coronary artery disease is the most common type of CVD and it is the single leading cause of death in Australia, accounting for 33% deaths, according to Australian Institute of Health and Welfare National Mortality Database. Coronary artery disease materializes when the coronary arteries that supply blood to heart muscle become hardened and narrowed, reducing the blood flow and oxygen supply to the heart. This is caused by the buildup of plaque within the inner walls of arteries during atherosclerosis. Rupture of the unstable atherosclerotic plaque and the subsequent thrombus formation are the main cause of myocardial infarctions.

In 1994, Schwertner *et al*. reported the inverse association between plasma bilirubin concentration and coronary artery disease (9). In that study, a 50% decrease in serum total bilirubin was associated with a 47% increase in the odds of having more severe coronary artery disease, assessed by coronary angiography. The same group also performed a retrospective study to investigate if serum bilirubin improved the ability to predict coronary artery disease (16). They reported serum bilirubin, when combined with various lipid and lipoprotein risk factors such as cholesterol, LDL cholesterol and HDL cholesterol to improve the prediction of coronary artery disease. In 1996, Hopkins *et al.* observed patients with familial coronary artery disease to have significantly lower serum bilirubin concentration (8.9 ± 6.1 μM) compared with control subjects (12.4 ± 8.1 μM) for both men and women (11). They concluded that bilirubin acts as an independent protective factor to decrease the risk of coronary artery disease, and that its protective effect of coronary artery disease to be comparable to that of HDL cholesterol. However, Endler *et al.* stated that the inverse association between serum bilirubin and coronary artery disease was evident in men only, not in women (237). Epidemiological studies show plasma bilirubin concentrations to inversely associate with the risk of myocardial infarct (238-240). In the Framingham Offspring Study, Djousse *et al.* also found a higher concentration of total bilirubin to be associated with a lower risk of myocardial infarction in males, but the association is not clear in females (240). Together, these studies suggest that the relationship between plasma bilirubin concentrations and coronary artery disease may be more complex and hence requires to be explored further.

Recent studies using multi-slice computer tomography have also shown that low serum bilirubin concentrations are associated with coronary artery calcification, a marker of coronary atherosclerosis (241-243). Serum total bilirubin also related to outcomes in patients with different subtypes of coronary artery disease (244). Arterial stiffness (245) and coronary plaque vulnerability (227) in patients with coronary artery disease are associated with serum total bilirubin. In addition, serum bilirubin was independently associated with lipid-rich plaques (219). Reports also showed that the effect of low serum total bilirubin levels on risk of coronary artery disease was increased in individuals with metabolic syndrome (246-248). Furthermore, in healthy patients, high plasma bilirubin concentrations are associated with preserved coronary flow reverse

and coronary microvascular function, as assessed by Doppler echocardiography examination (234).

Plasma concentrations of bilirubin are regulated primarily via hepatic conjugation mediated by UGT1A1 (12, 13). Individuals with Gilbert's syndrome have an insertion of a TA in the TATAA box in the promoter region of the *UGT1A1* gene, designated as *UGT1A1*28*, thereby decreasing UGT1A1 activity and leading to moderate hyperbilirubinemia (174). Wagner *et al.* showed subjects homozygous for *UGT1A1*28* to have a risk reduction of 70% for coronary artery diseases and CVD when compared to *UGT1A1*28* heterozygotes and *UGT1A1* homozygotes (10). Similarly, other genetic variants of *UGT1A1* that result in increased serum bilirubin concentration, also inversely associated with a lower risk of coronary artery disease (249). Intriguingly, the *UGT1A1* genotype itself appears to have little or no effect on coronary artery disease (250, 251), suggesting that the plasma concentration of bilirubin alone is insufficient to explain the observed inverse associated with CVD. Plasma bilirubin concentrations are affected by processes in addition to the activity of UGT1A1, such varying degree of heme oxygenase activity and/or consumption of bilirubin as a result of oxidative stress.

Not just being inversely associated with risk of coronary artery disease, once acute coronary syndromes happen, plasma bilirubin has also been found as a powerful prognostic marker for the outcome of the diseases. Thus, high plasma bilirubin concentrations are independently positively associated with increased severity of the diseases, and also correlated to increased risk of in-hospital adverse outcomes, and long term adverse outcomes of the patients with non-ST segment elevated or ST segment elevated acute coronary syndromes, with or without percutaneous coronary intervention (252-256).

2) Stroke. Interruption of blood supply to the brain can cause the medical condition known as stroke. There are two main etiologies for stroke. One type is an ischemic stroke. In an ischemic stroke a cerebral vessel is typically blocked via a thrombus, plaque or other material (causing an embolism). The other type of stroke is a hemorrhagic stroke, in which a blood vessel in the brain ruptures.

Increased total plasma bilirubin concentrations have been associated with reduced stroke prevalence and improved stroke outcomes (17). Thus, clinical data from the National Health and Nutrition Examination Survey (NHANES) 1999 to 2004 showed that a 1.71 μM increment in serum total bilirubin concentration was associated with a 9% decrease in the odds of experiencing a stroke, and a 10% reduced odds of adverse stroke outcome in patients with prior history of stroke (17). Similarly, Eiji *et al.* observed that higher serum total bilirubin concentrations are associated with lower stroke prevalence in a Japanese general health screening study (18). Although the association between plasma bilirubin and stroke has been reported, the subtypes of stroke were not clarified in the previous two studies. A prospective study of healthy Korean

individuals found lower serum total bilirubin concentration to be specifically associated with increased risk of ischemic but not hemorrhagic stroke (257). That study showed that a 1 μM increase in bilirubin concentration was associated with a 2% reduction in the hazard ratio for ischemic stroke in men but not women (257). Unfortunately, most investigations of the association between bilirubin and stroke excluded patients with Gilbert's syndrome, to avoid inclusion of subjects with elevated bilirubin due to liver disease. Therefore, there is currently insufficient evidence to unambiguously demonstrate an inverse association between stroke and Gilbert's syndrome as well as genetic variation in the *UGT1A1* gene.

Despite showing no association with the risk of hemorrhagic stroke, plasma bilirubin concentrations post-hemorrhagic stroke reflect oxidative stress, severity of stroke and related outcome (258). Moreover, higher serum bilirubin reflects greater severity of ischemic stroke and poorer discharge outcome compared with those with a lower concentration of bilirubin (259-261). Other studies reported that plasma bilirubin to independently, or together with other biomarkers, differentiate various types of ischemic stroke, such as non-lacunar (262) and cardioembolic stroke (263) that are related to atherosclerosis (264). However, the reason why plasma bilirubin serves as the marker to evaluate the severity of stroke is unknown. The knowledge that the nervous system influences liver metabolism and bile secretion (265) may partially explain that neurological damage by stroke impacting hepatic function and resultant hyperbilirubinemia. This explanation is consistent with a study reporting serum conjugated bilirubin, rather than total bilirubin, to be associated with stroke severity and resulting outcome (266). We could also speculate that stroke can result in elevated oxidative stress both locally and systemically, further stimulating heme oxygenase activity and subsequent bilirubin production.

3) Peripheral arterial disease. Peripheral arterial disease is the building up of fatty deposits and calcium in peripheral arteries, thereby reducing or blocking the blood supply to legs, arms and other organs other than the heart or brain. Perlstein *et al.* (267) reported an inverse relationship between serum bilirubin and the risk of the peripheral arterial disease. They reported a 1.7 μM increase of serum bilirubin was independently associated with a 6% reduction in the odds of peripheral artery disease. Rantner *et al.* found a similar relationship between serum bilirubin and the incidence of peripheral arterial disease (268). Using a cohort of 9,795 type 2 diabetic patients, Chan *et al*. observed an inverse relationship between plasma bilirubin concentration and total lower limb amputation due to peripheral artery diseases. For every 5 μM decrease in plasma bilirubin there was a 1.38-fold increased risk of lower limb amputation (269).

In summary, the above systematic review of available literature strongly suggests an inverse association between plasma bilirubin concentration and the incidence of different types of CVD. With the knowledge that atherosclerosis is the major cause of CVD, combined with the potential anti-atherogenic of bilirubin, it can be surmised that bilirubin and its effects on

atherosclerosis may help explain the observed cardiovascular protection seen with hyperbilirubinemia, especially in Gilbert's syndrome. Bilirubin may attenuate the development and progression of these diseases, therefore improving the quality of human life.

1.6.3 Bilirubin and metabolic diseases

Metabolism refers to all the chemical processes inside our body produce or consume energy. Disruption of the normal metabolism, such as abnormal glucose metabolism in diabetes and abnormal lipid metabolism in dyslipidemia, trigger metabolic diseases. Metabolic diseases encompass a broad range of metabolic syndrome. Metabolic syndrome, including obesity, insulin resistance, hypertension and dyslipidemia, confers risk for developing CVD and metabolic diseases. Metabolic syndrome affects 25% of the adult population in the world (270). Aside from the above potential protective properties of bilirubin in CVD, clinical and experimental evidence indicates that plasma bilirubin concentrations also inversely associate with metabolic disease and its complications.

Numerous clinical studies supporting the association of bilirubin with metabolic disease. One large study involving 16,000 subjects, high serum bilirubin concentrations was associated with a low incidence of diabetes mellitus (271). Specifically, those with bilirubin ≥10 μM had a 20% lower risk of developing diabetes compared to those with bilirubin <10 μM (271). Negative associations have also been reported in a number of populations for serum bilirubin concentrations and abnormal glucose tolerance tests (21), insulin resistance and the prevalence of the metabolic syndrome (272-275). In line with these observations, plasma bilirubin was found to positively associate with circulating IGF-1 concentration, which is negatively correlated with hepatic insulin resistance (276).

Consistent with the clinical studies, experimental evidence suggests that bilirubin improves insulin signaling and glucose metabolism, and that it attenuates insulin resistance. Thus, administration of bilirubin increases insulin sensitivity in the leptin receptor-deficient *db/db* mouse model of spontaneous type 2 diabetes, as well as in diet-induced obese mice via suppression of ER stress and chronic inflammation (207), or the regulation of cholesterol metabolism, adipokines and PPARγ expression (277). Gunn rats, a model of hyperbilirubinemia (278), are characterized by low concentration of fasting blood glucose in streptozotocin-induced diabetes mellitus. Additionally, mice with hyperbilirubinemia due to Gilbert's syndrome polymorphism experience less glucose intolerance induced by high fat (7). It has also been reported that biliverdin, the precursor of bilirubin, protects against the deterioration of glucose tolerance in leptin receptor-deficient *db/db* mice (122).

Insulin resistance influences the initiation and natural progression of CVD via exacerbation of inflammatory, metabolic, or biomechanical processes, and it is an independent risk factor for diabetes, endothelial dysfunction and subsequent CVD. In the setting of insulin

resistance, bilirubin has demonstrated potential protection against CVD. Diabetic patients with Gilbert's syndrome have a lower prevalence of vascular complications compared with normobilirubinemic diabetics (269, 279), while low serum bilirubin is a predictor of CVD in type 2 diabetes patients receiving hemodialysis (22). In addition, partial inhibition of UGT1A1 with the drug atazanavir results in a mild elevation of plasma bilirubin and improved endothelial function in patients with type 2 diabetes (280). Moreover, administration of bilirubin to obese or diabetic mice improves insulin sensitivity and endothelial function, in part via the insulin receptor/PI3K/Akt signaling pathway (207).

Non-alcoholic fatty liver disease (NAFLD) is becoming increasingly common around the world and is associated with many features of metabolic syndrome (281). NAFLD is characterized by hepatic lipid accumulation and progresses from hepatic steatosis (fatty liver). Although the mechanism of NAFLD development remains unclear, the most accepted hypothesis is that NAFLD results from "multiple parallel hits" including insulin resistance, inflammation, lipotoxicity, and oxidative stress (282). It is conceivable that bilirubin may attenuate the development and progression of NAFLD by attenuating these pathogenic processes, thereby preventing liver injury. Bilirubin has recently been reported to decrease hepatic lipid accumulation via activation of PPARα to regulate genes involved in the β-oxidation pathway (7, 8). In parallel with these experimental results, epidemiological studies consistently show that plasma concentrations of bilirubin inversely associate with the risk of hepatic steatosis (283, 284).

Clearly, there is an emerging body of evidence implicating bilirubin in the metabolic disease, insulin signaling and dyslipidemia. However, similar to CVD, a direct causative role of bilirubin in protection against metabolic disease remains to be established.

	In vitro activity	*In vivo* activity	Association
Biliverdin	**Antioxidant:** ↓ lipid[2,3] & protein[108] oxidation ↓ reactive species[108] **Anti-inflammatory:** ↓ IL-2 & T cells via NFAT/NF-κB[112] ↓ TLR4[113] ↑ IL-10 via PI3K[114] **Cytoprotective:** ↑ RBC & hepatocyte survival[110] **Lipid accumulation:** ↓ lipid accumulation via PPARα[8]	**Antioxidant:** ↑ resistance to oxidative injury[111] **Anti-inflammatory:** ↓ endotoxin-induced inflammatory response[113] **Organ injury:** ↓ endotoxin-induced organ damage[113, 115, 116]; ↓ ischemia/reperfusion injury[111, 112, 117-119] **Metabolism:** ↓ β cell apoptosis & glucose tolerance deterioration[122] **Proliferation:** ↓ hyperplasia[120,121]; ↓ neovascularization[66]	
BVRA	**Signaling pathway:** Insulin/IGF-1 & IRK/IRS/MAPK/PI3K[20, 23,135, 136]; PKC[138]; PDK1/Akt/GSK3[137]; IL-10 axis & ↓TLR4[113] **Transcription factor:** ↑ HMOX1 via antioxidant and hypoxia response elements[133,134]	**Insulin resistance:** ↓ β-amyloid & brain insulin resistance in Alzheimer disease models[141,142] **Lipid accumulation:** ↓ hepatic lipid accumulation via PPARα[125]; ↓ renal lipid accumulation via BAD[140]	
BVRB			**Unstable plaque:** ↑ expression reported in intra-plaque hemorrhage[153]
Bilirubin	**Antioxidant:** ↓ lipid & protein oxidation[2, 3, 108, 185, 188, 189]; ↓ reactive species[108, 190] **Cytoprotective:** ↑ RBC, VSMC, cardiomyocyte hepatocyte survival[110, 192, 193] **Anti-inflammatory:** ↓ IL-1β, IL-6, and TNF-α[198]; ↓ LPS-induced inflammation via IL-8[204]; ↓ trans-endothelial leukocyte migration[205, 210] **Proliferation:** ↓VSMC via MAPK & YY1[5, 211] **Endothelial function:** ↓oxLDL-induced EC dysfunction[6]; ↓ glucose-induced EC death[209]; ↑ endothelial progenitor cell activity[210] **Lipid accumulation:** ↓ lipid accumulation via PPARα[8]	**Antioxidant:** ↓ hyperoxia-induced stress[194]; ↓ oxidative stress[126] **Organ injury:** ↓cardiac ischemia/reperfusion injury[195, 196] **Anti-inflammatory:** ↓ T cell proliferation[200]; ↓ VCAM-1, ICAM-1 & WBC in aortic root lesions[4, 198, 199, 205] **VSMC proliferation:** ↓ neo-intimal hyperplasia in balloon injury models[212] **Anti-atherosclerosis:** ↓ atheromatous lesions in *Ldlr*$^{-/-}$ mice[205] **Metabolism:** ↓ HF diet- or streptozotocin-induced glucose intolerance[7, 278]; ↑ insulin sensitivity & endothelial function via PI3K/Akt[207] **Lipid accumulation:** ↑ cholesterol metabolism, adipokines and PPARγ expression[277]; ↓ hepatic lipid accumulation via PPARα[7, 8]	**Antioxidant:** ↓ oxidative stress markers in serum, urine[197] & endarterectomy tissue[224] **Inflammation:** ↓ inflammatory markers (*e.g.*, CRP) in atherosclerosis[206] or metabolic syndrome[208] **Endothelial function:** ↑ endothelial function[231, 232] ↑ flow-mediated vasodilation[233, 234] **Atherosclerosis:** ↓ risk of atherosclerosis[14, 15, 206, 218]; **Unstable plaque:** ↑ plaque stability[219, 227] **Coronary artery disease:** ↓ risk of coronary artery disease[9, 11, 16, 237, 246-248]; ↓ risk of myocardial infarct[238-240]; *UGT1A1*28* ↓ risk of coronary artery disease[10, 249]; **Stroke:** ↓ stroke prevalence[18] and adverse outcomes[17]; **Peripheral arterial disease:** ↓ risk of the peripheral arterial disease[267, 268] & diabetes-related amputation[269] **Metabolic diseases:** ↓ risk of diabetes[271], insulin resistance & metabolic syndrome[21, 272-276] **Fatty liver:** ↓ risk of hepatic steatosis[283, 284]

Figure 1.3 Protective properties of biliverdin, BVRA, BVRB and bilirubin, as well as their associations with cardiovascular and metabolic diseases

1.7 Summary, Hypothesis and Aim of the Study

Plasma bilirubin concentrations inversely associate with the risk of endothelial dysfunction, atherosclerosis, cardiovascular and metabolic diseases. Bilirubin also has potential protective properties, including antioxidant and anti-inflammatory activities, and the ability to inhibit VSMC proliferation, promote endothelial function and regulate lipid metabolism. However, a causative link between bilirubin and these diseases remains to be established.

Hypothesis:

Bilirubin, as an endogenous antioxidant, protects against cardiovascular and metabolic diseases. Biliverdin reductase attenuates endothelial dysfunction and atherosclerotic vascular disease, and this is accentuated in the setting of insulin resistance and dyslipidemia.

Objectives:

The aim of the research program is to examine the role of bilirubin in oxidative stress, atherosclerotic plaque stability and insulin resistance using the *biliverdin reductase a* gene knockout (*Bvra*$^{-/-}$) mouse as model of bilirubin deficiency. The specifics objectives are:

1) To phenotypically characterize *Bvra*$^{-/-}$ mice and assess oxidative stress as a result of *Bvra* deficiency;

2) To investigate the impact of *Bvra* deficiency in an experimental model of atherosclerotic plaque instability; and

3) To investigate the impact of *Bvra* deficiency in two models of diet-induced insulin resistance.

Chapter 2

Materials and Methods

2.1 Animal Study

2.1.1 Generation of *Biliverdin reductase a* gene-deficient mouse

Biliverdin reductase a (Bvra) gene deficient mice were generated by homologous recombination in embryonic stem (ES) cells (Ozgene, Perth, WA, Australia). In this procedure, exon 3 of the *Bvra* gene was replaced via a targeting vector that was created by PCR from C57BL/6J genomic DNA using the plasmid pBR322 as the vector backbone. The targeting vector construct contained a cDNA sequence of exons 2, 4 and 5 of the wild-type mouse *Bvra* gene, with a phosphoglycerine kinase promoter driving a neomycin resistance gene cassette (PKG_*neo*) that was flanked by flippase recognition target (FRT) sites. The targeting vector was electroporated into Bruce4 ES cells derived from a C57BL/6 congenic strain. The antibiotic-resistant heterozygous knockout ES cells were expanded and injected into developing mouse embryos, which were then implanted in pseudo-pregnant females to generate chimeras. The resultant chimeras were mated to Albino BL/6 mice to obtain germ line-transmitting heterozygotes, with ES cell coat color offspring genotyped by Southern blot. To remove the PKG_*neo* cassette, homozygous knockout offspring were mated to a whole body FlpE deleter strain.

After deletion of the PKG_*neo* selection cassette, $Bvra^{+/+}$, $Bvra^{+/-}$ and $Bvra^{-/-}$ littermates were obtained from $Bvra^{+/-}$ x $Bvra^{+/-}$ breeding pairs in the BioCORE facility at the Victor Chang Cardiac Research Institute and used for all experiments described. Male and female mice, 6 to 12 weeks old, were used for experiments. $Bvra^{-/-}$ mice were also crossed with *apolipoprotein E* gene-deficient ($Apoe^{-/-}$) mice on C57BL/6J background to generate $Bvra^{+/-}Apoe^{-/-}$ breeders and $Bvra^{+/+}Apoe^{-/-}$ and $Bvra^{-/-}Apoe^{-/-}$ littermate experimental animals. All mice were housed in a temperature-controlled room (Physical Containment Level 2 certification) on a 12 h light/dark cycle and were allowed access to water and food *ad libitum*. All procedures were carried out according to the Australian National Health & Medical Research Council Guidelines for Animal Research and were approved by the Animal Care and Ethics Committee of the Garvan Institute of Medical Research/St Vincent's Hospital.

Genotyping was performed on genomic DNA isolated from ear punch biopsies via the ISOLATE II Genomic DNA Kit (Bioline, Sydney, NSW, Australia). PCR amplification was performed using the DreamTaq Green PCR Master Mix (Thermo Fisher Scientific, Waltham, MA, USA) with primers purchased from Integrated DNA Technologies. The primers for PCR were designed *de novo* in our laboratory and the detailed information is provided in Table 2.1. The combination of these primers resulted in PCR products of 233 bp in $Bvra^{+/+}$, 233 and 139 bp in $Bvra^{+/-}$, and 139 bp in $Bvra^{-/-}$ mice.

Table 2.1 Sequences and accession numbers of primers used to amplify genomic DNA via RT-PCR

Primer Pair No.	Name	Genbank Accession No.	Oligonucleotide (5'-3')		Product Size (bp)
			Froward	Reverse	
1	$Bvra^{+/+}$	NC_000068.7	CTGGGGTTGCCA GCTTCCCT	CTGGACACATATC CAATCAGGTTTA	233

2	*Bvra*$^{-/-}$	N/A	CTGGGGTTGCCA GCTTCCCT	ATAGGAACTTCGG CGCGCCTGATAT	139

2.1.2 Diets

Mice were fed a standard laboratory chow containing 13% calories from fat, 22% calories from protein, and 65% calories from carbohydrate, 3.1 kcal/g (#27, Gordons Specialty Feeds, Australia) until they were allocated to a study involving high fat (HF), high fat high sucrose (HFHS) diet or Western diet (WD). In the HF diet study, mice were fed for up to 14 weeks a HF diet that was formulated based on D12492 (Research Diet, Inc) containing 60, 20 and 20% calories from fat, protein and carbohydrate, respectively, and 5.2 kcal/g (SF13-092, Specialty Feeds, Australia). The experimental timeline for the HF diet-induced insulin resistance model is shown in Figure 2.1A. In the HFHS diet study, mice were fed for up to 6 weeks a HFHS diet based on D12451 (Research Diets, Inc) containing 47, 21 and 32% calories from fat, protein and carbohydrate, respectively, and 4.7 kcal/g (formulated in-house). The experimental timeline for the HFHS diet-induced insulin resistance model is shown in Figure 2.1B. In the WD study, mice were fed for 13 weeks a WD based on D12079B (Research Diets, Inc) containing 41, 17 and 43% calories from fat, protein and carbohydrate, respectively, and 4.7 kcal/g. WD also contains 1.5 g/kg cholesterol (SF00-219, Specialty Feeds, Australia). The experimental timeline for WD study combined with tandem stenosis surgery is shown in Figure 2.2A.

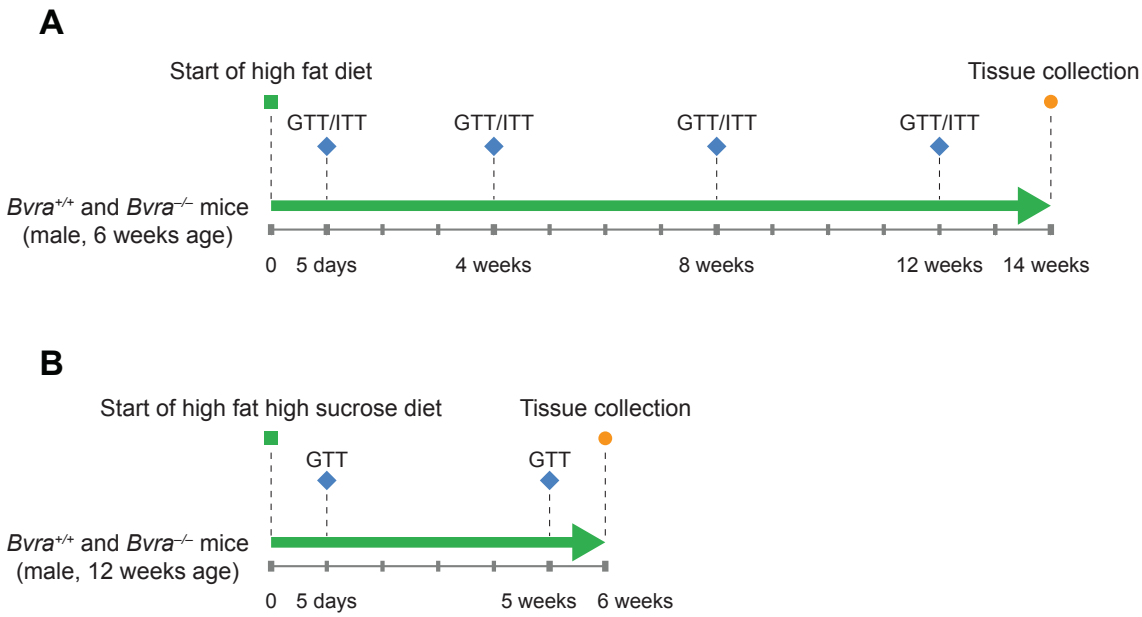

Figure 2.1 Timeline for dietary mouse models. **(A)** Experimental timeline of the high fat (HF) diet-induced insulin resistance model. **(B)** Experimental timeline of the high fat high sucrose (HFHS) diet-induced insulin resistance model. Abbreviations: GTT, intraperitoneal glucose tolerance test; ITT, intraperitoneal insulin tolerance test.

2.1.3 Collection of blood, plasma and tissue samples

Mice were anesthetized by isoflurane inhalation or an overdose of Lethobarb (100 µL of 80 mg/mL, Virbac, Australia) administered via intraperitoneal injection. Blood was collected by cardiac puncture using a 26-gauge needle and transferred into heparin-coated micro tubes (Sarstedt, Nümbrecht, Germany). To obtain plasma, heparinized blood was centrifuged at 2,000 x *g* and 4 °C for 15 min. Immediately following cardiac puncture, mice were gravity-perfused (90 mm Hg) with phosphate buffered saline (PBS). Organs and tissue were collected for biochemical and morphological studies. Tail tips were used to confirm genotype of all experimental mice.

2.2 *In vivo* study

2.2.1 Fasted and non-fasted blood glucose

Blood samples were obtained via tail vein of conscious mice, with or without a prior 8 or 16 h fast. In this procedure a small amount of tissue (~1 mm) was removed from the tail tip via scalpel. At subsequent time points the scab was disrupted to obtain further blood. Blood glucose concentrations were determined using an Accu-Chek Performa Blood Glucose Meter (Roche, Switzerland).

2.2.2 Glucose tolerance and insulin tolerance test

To perform the glucose tolerance test (GTT), mice received 1 or 2 g/kg glucose via intraperitoneal injection of a 10% glucose solution (INJ128, Phebra, Australia) after an 8 or 16 h fast. Blood was collected via tail bleeding at 0, 15, 30, 60, 90 and 120 min for measurement of blood glucose using an Accu-Chek Performa Blood Glucose Meter (Roche, Switzerland) and plasma insulin using an ultra-sensitive mouse insulin ELISA (90080, Crystal Chem, IL, USA). To perform the insulin tolerance test (ITT), mice received insulin (Actrapid, Penfill, Novo Nordisk, Australia) at 0.75 U/kg via intraperitoneal injection after an 8 h fast. Blood samples were obtained via tail bleeding at 0, 15, 30, 60, 90 and 120 min for blood glucose measurement by Accu-Chek Performa Blood Glucose Meter (Roche, Switzerland).

2.2.3 *In vivo* glucose uptake into epididymal adipose tissue

Glucose uptake into epididymal adipose tissue was measured as described previously (285). For [^{3}H] 2-deoxy-D-glucose (2-DOG) uptake, mice were treated for 30 min with 160 µCi/kg 2-DOG (NET238C001MC, Perkin Elmer, MA, USA) and 0.75 U/kg insulin (Actrapid, Penfill, Novo Nordisk, Australia), after an 8 h fast. Blood was collected from the tail tip at 0, 5, 10, 15, 20 and 30 min. Clearance of the 2-DOG tracer from the blood was assessed at each time point to allow calculation of tracer disappearance. At the end of the 30 min time course mice were euthanized with an overdose of Lethobarb (Virbac, Australia) before the adipose tissue was excised immediately. 2-DOG uptake into epididymal adipose tissue and conversion to 2-deoxy-glucose-

6-phosphate was determined. Epididymal adipose tissue (30 mg) was homogenized in 500 µL water via sonication (Bandelin SONOPLUS, Germany) for 150 s. The resulting homogenate was centrifuged for 10 min at 14,000 x *g* and 4 °C, and the aqueous phase was collected. To determine total counts, 150 µL of the aqueous phase was transferred directly into a labeled 5 mL scintillation vial, followed by 850 µL dH_2O and 4 mL of scintillation fluid (Ultima Gold, 6013329, Perkin Elmer, MA, USA). To determine the free counts, 150 µL of the aqueous phase was passed through an anion exchange column (AS 1-X8 resin; Bio-Rad, CA, USA) washed with 3 mL dH_2O, with resulting dripping eluent being collected. 1 mL eluent and 4 mL scintillation fluid were added into a 5 mL scintillation vial and assessed for ^3H radioactivity using the Tri-Carb 4910TR scintillation counter (Perkin Elmer, MA, USA). The uptake of 2-DOG was standardized by the weight of the tissue samples used.

2.2.4 Tandem stenosis (TS) model of plaque instability

The TS model of unstable plaque was used throughout with details of the surgery described previously (286, 287). Male mice at 6 weeks of age were fed a WD containing 22% fat and 0.15% cholesterol (SF00-219, Specialty Feeds, Western Australia) for 13 weeks. 6 weeks after commencement of WD, TS surgery was performed to induce formation of unstable plaques proximal to the proximal suture, as described. All TS surgeries were performed by one operator blinded to genotype. Briefly, *Bvra*$^{+/+}$*Apoe*$^{-/-}$ and *Bvra*$^{-/-}$*Apoe*$^{-/-}$ littermate mice were anaesthetized with 4% isoflurane. An incision was made in the neck and the right common carotid artery dissected from circumferential connective tissues. Two ligatures with 150 µm outer diameter were placed with the distal stenosis 1 mm from the carotid artery bifurcation and the proximal stenosis 3 mm from the distal stenosis. To control for the extent of constriction caused by the stenosis, a 150 µm needle (8-0, W1782, Virgin silk blue, Ethicon) was placed on top of the exposed right common carotid artery before a 6-0 blue-braided polyester fiber suture (0.7 Metric, 3280-11, Ti-Cron) was tied around both the artery and needle, before the needle was removed. Blood flow was measured before and after placement of each ligature using a perivascular flow module (TS420, Transonic, NY, USA) and a 0.7 mm perivascular flow probe (MA0.7PSB, Transonic, NY, USA). Blood flow was reduced to 70% of baseline flow after placement of the distal ligature and to 20% of baseline flow after placement of the proximal ligature (Fig. 2.2).

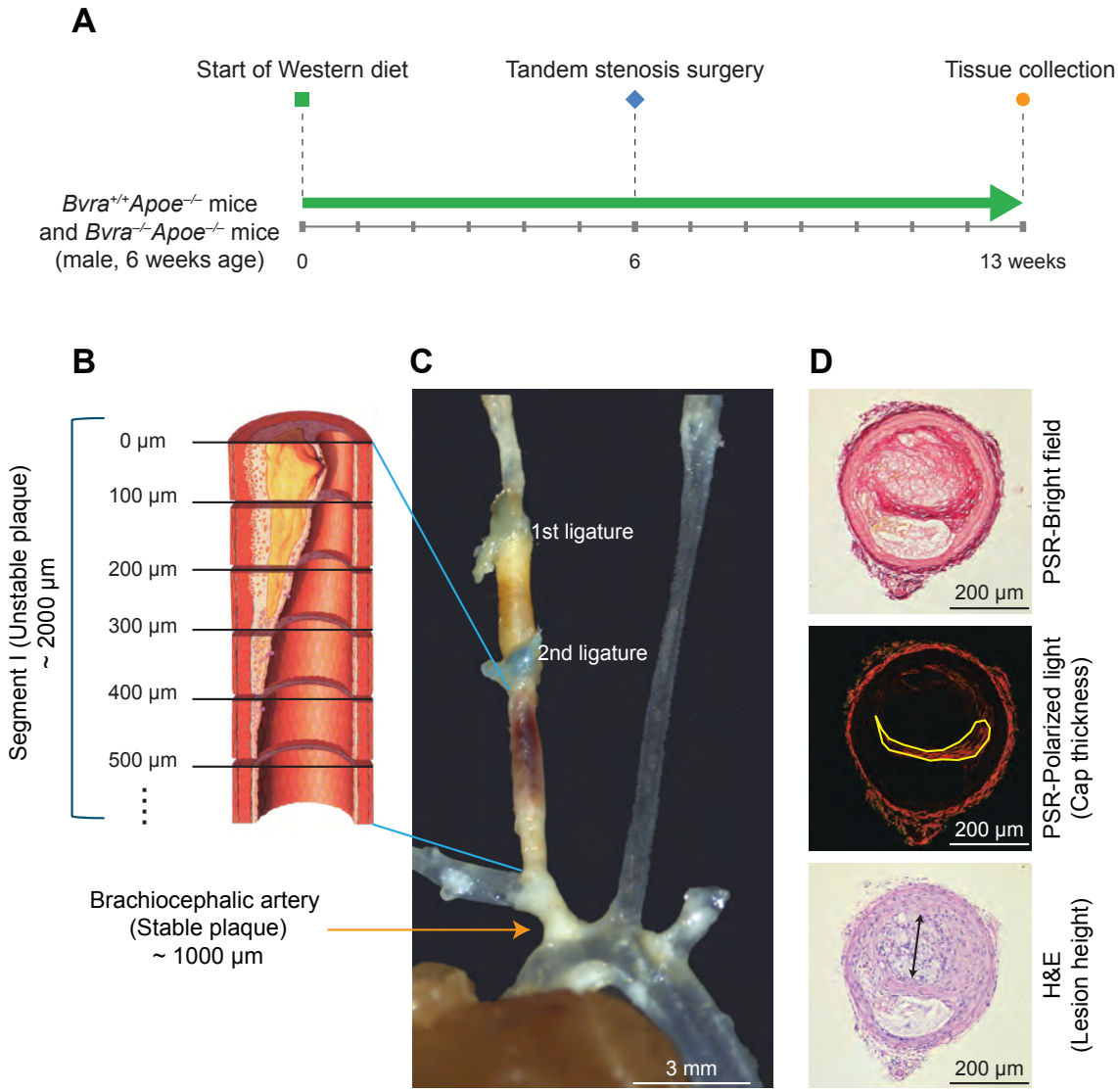

Figure 2.2 Tandem stenosis model of plaque instability. **(A)** Experimental timeline of tandem stenosis (TS) surgery. **(B)** Scheme of the procedure for cross-sectioning the entire Segment I. **(C)** Representative image of right carotid artery 7 weeks after TS surgery, indicating the two ligations, unstable plaque (Segment I) and stable plaque (brachiocephalic artery). **(D)** Picrosirius red (PSR) and hematoxylin and eosin (H&E) staining of plaque with unstable phenotype in the right carotid artery. Cap thickness was determined as the area of PSR-stained cap viewed under polarized light showing the fibrous cap (yellow line). Lesion height was determined from H&E stained sections (arrow).

2.2.5 Collection of tissue samples from TS mice

Seven weeks after TS surgery, mice were anesthetized by isoflurane inhalation and euthanized by exsanguination. Blood was collected by cardiac puncture using a 26-gauge needle and transferred into heparin-coated micro tubes (Sarstedt, Nümbrecht, Germany). Heparinized blood was centrifuged at 2,000 x *g* and 4 °C for 15 min to obtain plasma. Immediately after cardiac puncture, mice were gravity-perfused (90 mm Hg) with phosphate buffered saline (PBS). For biochemical

analyses, tissue samples were used freshly, or after thawing of tissue that was immediately snap-frozen after collection. For morphometric analysis, additional gravity-perfusion with 10% neutral buffered formalin solution was performed before tissue collection. Tissue was fixed overnight in 10% neutral buffered formalin solution and then stored in 80% ethanol. The aortic tree, heart and liver were also collected. Tail tips were collected to confirm genotype of mice.

The segment proximal to the proximal suture in the right common carotid artery (referred to previously as segment I (286)) contains plaque with unstable phenotype, characterized by consistent thinning of the fibrous cap, abundant inflammatory cells and the occasional presence of neovessels, cap disruption, intraplaque hemorrhage, as well as luminal thrombus containing fibrin and platelets. In contrast, the brachiocephalic artery contains lesion with a thick-cap and abundance of collagen in the atheroma area (287). These features are consistent with a stable plaque phenotype, and the brachiocephalic artery is commonly used for atherosclerosis studies in *Apoe*$^{-/-}$ mice, with lesions in this vessel generally being considered stable (288). Computational fluid dynamics have demonstrated no significant reduction in vessel wall shear stress in the brachiocephalic artery following TS surgery (286).

2.2.6 Fluorescence emission computed tomography (FLECT)

In vivo measurement of near infrared autofluorescence (NIRAF) was performed using FLECT-CT (Trifoil InSyTe, CA, US). Seven weeks after TS surgery, mice were anesthetized by isoflurane inhalation. The fur was then removed from behind the eyes and in front of the ears down and around to under the chin, and then from the arms, chest, neck and upper back using small clippers and depilatory cream. Mice were then placed in the imaging chamber for X-ray CT and fluorescence scans. The mouse remained anesthetized throughout the imaging procedure (approximately 65-70 min). X-Ray CT scanning was performed using the following settings: 30 kV for tube voltage, 500 µA for tube current and 150 ms exposure time. The fluorescence scan was performed using a 730 nm excitation laser and 803 nm filter in step-and-shoot scanning mode, 29 source angles per slice and 500 ms exposures. Subsequent fluorescence attenuation scans were performed in continuous mode. A reconstructed 3D image of the X-Ray scan detailing the anatomy of the mouse was overplayed onto the corresponding fluorescence reconstructed image by VivoQuant 3.5 (InviCRO, US).

2.3 *Ex vivo* study

2.3.1 Assessment of MPO activity

Measurement of *ex vivo* MPO activity was carried out largely as described previously (289). In brief, arterial segments were homogenized in 100 µL ice-cold PBS containing protease inhibitor (Roche cOmplete^{TM}, 169749800) and 100 µM DTPA using a Wheaton tissue grinder at 4 °C. Following homogenization, tissue was incubated with glucose (20 mg/mL) and glucose oxidase

(40 μg/mL) in the presence of 20 mM Trolox (238813, Sigma-Aldrich, St Louis, MO, USA) and 50 μM hydroethidine (HE, H12500, Tyger Scientific, Ewing, NJ) for 30 min at 37 °C in the dark. Hydroethidine and its oxidation products were then extracted by the addition of 80% ethanol containing 3 μM 2-chloroethidium-d_5 (prepared in-house) prior to LC-MS/MS analysis as previously described (289).

2.3.2 Odyssey infrared imaging system

Ex vivo measurement of NIRAF was performed using an Odyssey infrared imaging system (CLx, Li-COR, Nebraska, US). Segment I in the right carotid artery (see Figure 2.1), the left carotid artery, and the aortic arch with the brachiocephalic trunk attached (as shown in Figure 2.1) were collected and placed into the imaging system, using a serially diluted fluorescence dye (IRDye800CW, LI-COR, US) as reference. Fluorescence intensity scans were performed using the following settings: 800 nm channel (excitation = 785 nm, emission > 800 nm), intensity level at 5, resolution at 21 μm, image quality at medium. Quantification of fluorescence intensity was performed using Image Studio (LI-COR, US).

2.3.3 Myography

Endothelial function in the abdominal aorta of TS mice was assessed using wire myography as described previously. Briefly, following excision, abdominal aortas were placed in Krebs buffer (Sigma-Aldrich K3753, modified to contain 2.5 mM $CaCl_2$, 10 mM EDTA and 2.1 g/L sodium bicarbonate), cut into 2 mm rings and mounted on a Danish Myo Technology (DMT) multichannel myograph system (DMT 610M, ADInstruments, Bella Vista, Australia) using two 40 μm tungsten wires. Abdominal aortic rings were stretched to an optimal baseline tension of 9 mN 100 mmHg before being stimulated with a high potassium physiological salt solution (60 mM, KPSS; made by equimolar substitution of KCl for NaCl in PSS). Rings were constricted sub-maximally with noradrenaline (1 - 30 μM; A9512, Sigma-Aldrich) to cause 50 - 75% of the maximum response to KPSS response. After stable constriction was achieved, endothelial-dependent relaxation was assessed using acetylcholine (1 - 300 μM; A662, Sigma-Aldrich), and endothelial-independent relaxation was assessed using sodium nitroprusside (1 - 30 μM; Sigma-Aldrich, 22870).

2.3.4 *Ex vivo* glucose uptake into adipose tissue explants

Glucose uptake into epididymal adipose tissue explants was measured as described previously (285). In brief, epididymal fat pads were dissected, transferred immediately to 37 °C Dulbecco's Modified Eagle Medium (DMEM, ThermoFisher, MA, USA) containing 2% (w/v) bovine serum albumin (BSA, Bovostar, Bovogen, Australia) and 20 mM HEPES, pH 7.4, and minced into fine

pieces. Explants were washed twice and incubated in DMEM containing 2% (w/v) BSA and 20 mM HEPES, pH 7.4 for 2 h. The buffer was exchanged with Krebs-Ringer phosphate (KRP) buffer (0.6 mM Na_2HPO_4, 0.4 mM NaH_2PO_4, 120 mM NaCl, 6 mM KCl, 1 mM $CaCl_2$, 1.2 mM $MgSO_4$ and 12.5 mM HEPES, pH 7.4) containing 2% (w/v) BSA by washing with KRP buffer three times. Different concentrations of insulin (0, 0.5, 10 nM, Actrapid, Penfill, Novo Nordisk, Australia) were administrated for 20 min. Glucose transport was initiated by addition of 2-DOG (0.25 μCi, 50 μM, PerkinElmer, MA, USA) for the final 5 min of the assay to measure steady-state rates of 2-DOG uptake. Uptake was terminated by three rapid washes with ice-cold PBS. 100 μL radioimmune precipitation assay buffer (RIPA buffer; 50 mM Tris-HCl, pH 7.5, 150 mM NaCl, 1% (v/v) Triton X-100, 0.5% (w/v) sodium deoxycholate, 0.1% (w/v) SDS, 1 mM EDTA, 10% (v/v) glycerol) supplemented with protease inhibitor cocktail (Roche, Switzerland) was used to lyse the adipose tissue explants. Samples were assessed for ^3H radioactivity using a Tri-Carb 4910TR scintillation counter (PerkinElmer, MA, USA) and the results were normalized to protein concentration determined by the bicinchoninic acid (BCA) assay.

2.4 Biochemical analysis

2.4.1 Analyses of plasma antioxidants, lipids and cholesterylester hydroperoxides

Fresh plasma was processed and analyzed for antioxidants, lipids and oxidized lipids as described (290-292). Plasma (100 μL) was added to 2 mL methanol containing 0.02% (v/v) acetic acid, followed by 10 mL Milli-Q water-washed hexane, mixed vigorously for 30 s and the mixture then centrifuged at 900 x *g* and 4 °C for 5 min. The hexane layer was removed, evaporated under vacuum using a rotary evaporator (vacuum released under argon for ubiquinol measurement), and the residue re-dissolved in 180 μL of argon-flushed mobile phase A (73.4% (v/v) ethanol, 22.5% (v/v) methanol, 3.8% (v/v) isopropyl alcohol, 0.3% (v/v) MilliQ water and 5 mM $LiClO_4 \cdot 3H_2O$). α-Tocopherol (α-TOH), cholesterol, cholesterylesters (CE) and triglycerides (TG) were detected by $UV_{214\,nm}$ (785A, Perkin Elmer, Waltham, MA, USA), whereas cholesterylester hydroperoxides (CE-OOH) were determined by post-column chemiluminescence detection (model CLA1 100, Tohoku Electronics, Tokyo, Japan) as described previously (290, 291). Briefly, isocratic HPLC analysis was performed using a C18 column (250 x 4.6 mm; 5 μm, Supelco, Sigma-Aldrich) with guard column eluted with above mobile phase at 1 mL/min. Following detection at 214 nm, the eluent was combined with the chemiluminescence mobile phase B (50% (v/v) methanol, 50% (v/v) MilliQ water, 40 mM NaOH, 50 mM $Na_2B_4O_7 \cdot 10H_2O$, 1 mM isoluminol, 4 mg/L microperoxidase (MP-11, M6756, Sigma-Aldrich), pH = 10) at 1.5 mL/min for detection of CE-OOH. Ubiquinone-9 and ubiquinol-9 were determined by HPLC with coulometric multi-electrode electrochemical detection (CoulArray, Thermo Fisher Scientific). Isocratic HPLC was performed using a C18 column (250 x 4.6 mm; 5 μm, Supelco, Sigma-Aldrich) with guard column eluted

with 65% (v/v) ethanol, 30% (v/v) methanol, 3% (v/v) isopropyl alcohol and 2% (w/v) ammonium acetate (1 M, pH 4.4) at 1 mL/min. The oxidation and reduction potentials were set at +700 and -700 mV, respectively, with the gain range set at 100 nC. Ascorbic acid was analyzed by HPLC with amperometric electrochemical detection (model LC-4C, Bioanalytical Systems, West Lafayette, IN, USA) (292). One volume of plasma was added to one volume of 10% (w/v) meta-phosphoric acid containing 0.54 mM Na_2EDTA. The mixture was mixed vigorously for 30 s and centrifuged at 735 x *g* and 4 °C for 5 min. The resulting supernate was used to measure ascorbic acid. Isocratic HPLC was performed using a C18 column with guard column (250 x 4.6 mm; 5 µm, Supelco, Sigma-Aldrich) eluted with 92.5% (v/v) MilliQ water, 7.5% (v/v) methanol, 40 mM sodium acetate, 0.45 mM EDTA, 1.5 mM Q12 and pH 4.75 at 0.9 mL/min. The oxidation potential was set at +500 mV, with the gain range set at 50 nA. The concentrations of all analytes were determined from calibration curves generated using authentic standards of ascorbic acid (255564), cholesterol (C8667), C18:2 (C0289), C20:4 (C8753), α-TOH (T3251), TG18:1 (T7140), TG18:2 (T9517) and ubiquinone-9 (27597) purchased from Sigma-Aldrich, and C18:2-OOH (48001) purchased from Cayman Chemical (Ann Arbor, MI, USA). C20:4-OOH was prepared by peroxyl radical-mediated oxidation of C20:4 using 2,2'-azo*bis* (4-methoxy-2,4-dimethylvaleronitrile) (AMVN, V-65, Wako, Tokyo, Japan) in methanol at 50 °C for 5 h (291). C20:4-OOH was purified on a semi-preparative C18 column (250 x 10 mm; 5 µm, Supelco, Sigma-Aldrich) eluted with 73.4% (v/v) ethanol, 22.5% (v/v) methanol, 3.8% (v/v) iso-propanol, 0.3% (v/v) MilliQ water at a flow rate of 3 mL/min with detection at 234 nm. The concentration of C18:2-OOH and C20:4-OOH were determined by 234 nm absorption using a molar extinction coefficient $\varepsilon = 23{,}000\ M^{-1}cm^{-1}$. Ubiquinol-9 was prepared from ubiquinone-9 as described (293).

2.4.2 Reduction with sodium borohydride

The residue derived from evaporation of the 9 mL hexane phase of extracted plasma was re-dissolved in 180 µL of mobile phase A described in **2.4.1**. Re-dissolved lipids (135 µL) were added into 5 µL 1% (w/v) sodium borohydride (452882, Sigma-Aldrich), mixed vigorously and then incubated for 10 min at room temperature protected from light. Following this incubation, acetic acid (10 µL) was added to stop the reaction, and 100 µL of the resulting solution was subjected to HPLC-CL analysis as described above. Control incubations were performed in the absence of sodium borohydride.

2.4.3 Determination of bile pigments

Bile pigments were extracted as described previously (294). Briefly, gall bladders from 5 mice with the same genotype were pooled to give 50 µL bile. Bile was then added to 2 mL 0.4 M glycine/HCl buffer, pH 1.8 followed by consecutive addition of 0.5 mL 10% (w/v) ascorbic acid

dissolved in saturated saline and additional 0.5 g NaCl. The mixture was cooled on ice and extracted with 1.25 mL of chloroform/ethanol (1:1, vol/vol). The absorption spectra of the resulting organic extracts were recorded from 350 - 800 nm against a reference sample using a Cary 100 Spectrophotometer (Agilent Technologies, Santa Clara, CA, USA). The reference sample was generated by subjecting 50 µL PBS to the same extraction procedure as bile pigments, with the resultant organic phase used for the spectrophotometric reference.

2.4.4 LC-MS/MS determination of bilirubin and biliverdin in artery, liver and plasma

Bilirubin and biliverdin in arterial tissue, liver and plasma were analyzed by LC-MS/MS using a 6490 Triple Quadrupole LC-MS/MS (Agilent Technologies), equipped with an electrospray ionization (ESI) source and connected to an Agilent 1290 UHPLC. Arterial segments (1 mg) were homogenized at 4 °C in 100 µL ice-cold PBS containing protease inhibitor (Roche, Switzerland) and 100 µM diethylenetriaminepentaacetic acid (DTPA) and using a Wheaton tissue grinder. The resulting homogenate was bubbled with CO gas for 3 min to displace oxygen from heme proteins and thereby prevent formation of superoxide and secondary reactive oxygen species during subsequent sample work-up. Liver tissue (30 mg) was homogenized at 4 °C in 600 µL ice-cold PBS containing protease inhibitor and 100 µM DTPA and using a Wheaton tissue grinder. The resulting homogenate was centrifuged at 400 x *g* and 4 °C for 5 min, 100 µL supernate was added into 900 µL PBS, mixed vigorously and bubbled with CO for 3 min.

To 50 µL of either CO-bubbled arterial or liver homogenate, or plasma was added 5 µL PBS (containing 5 mM DTPA and 5 mM desferrioxamine), 5 µL 3.75 µM meso-bilirubin (M14136, Frontier Scientific, Logan UT, USA) and 5 µL 0.5 µM meso-biliverdin (M588-9, Frontier Scientific) was added. The solution was mixed for 30 s, before addition of 180 µL ice-cold methanol containing 100 µM DTPA, vigorous mixing and centrifugation (10 min, 13,000 x *g*, 4 °C). The resulting methanolic supernate (5 µL) was injected onto a ZORBAX Eclipse Plus C18 column (50 x 2.1 mm, 1.8 µm, Agilent Technologies, CA, USA) and eluted at 0.2 mL/min. The column was maintained at 25 °C and a gradient elution was used, employing solvents A (59.7% water, 39.8% methanol and 0.5% acetic acid) and B (7.0% water, 92.5% methanol and 0.5% acetic acid): 100% solvent A changed to 100% solvent B over 8 min, then held at 100% solvent B for 8 min, before returning to 100% solvent A over 1 min and holding at 100% solvent A for 3 min. The mass spectrometer was operated in positive electrospray ion mode and quantification of biliverdin and bilirubin was by multiple reaction monitoring (MRM) using the largest fragment ion generated by collision-induced dissociation of the $[M+H]^+$ ion. For biliverdin and bilirubin, respectively, the following mass spectrometer settings were used: m/z 583.3→297.7 with collision energy = 33 V and m/z 585.3→299.2 with collision energy = 17 V. Concentrations were calculated from calibration curves generated using authentic standards of

biliverdin (B584-9, Frontier Scientific) and bilirubin (B655-9, Frontier Scientific), and corrected for recovery of internal standards, and normalized to protein concentration.

2.4.5 HPLC analysis of lipids in artery and liver

Arterial segments and liver tissue were processed and analyzed for lipids by HPLC-UV. The supernate of arterial segments prepared for LC-MS/MS analysis as described above (see **2.4.2**) was used to determine arterial lipids by HPLC with UV detection. For liver, 30 mg tissue was pulverized on dry ice and then homogenized at 4 °C in 300 µL lysis buffer (1% SDS and protease inhibitor cocktail (Roche, Switzerland)) using a Wheaton tissue grinder. Protein concentration of the homogenate was determined by the BCA assay. For lipid extraction, arterial supernate (180 µL) or liver homogenate corresponding to 200 µg protein was added to 2 mL methanol containing 0.02% (v/v) acetic acid, followed by 10 mL Milli-Q water-washed hexane. The mixture was mixed vigorously for 30 s and then centrifuged at 1,000 x *g* and 4 °C for 5 min. The upper hexane layer was removed, evaporated using a rotary evaporator, and the residue re-dissolved in 180 µL of HPLC mobile phase (73.4% (v/v) ethanol, 22.5% (v/v) methanol, 3.8% (v/v) isopropyl alcohol and 0.3% (v/v) MilliQ water). 50 µL of this re-dissolved hexane extract was subjected to isocratic HPLC analysis using a C18 column (250 x 4.6 mm; 5 µm, Supelco, Sigma-Aldrich, St. Louis, USA) with guard column eluted with above mobile phase at 1 mL/min. Cholesterol, CE and TG were detected at 214 nm using a 1100 Variable Wavelengths Detector G1314 (Agilent, CA, USA). Lipids were quantified by comparison of the peak area with that of the corresponding standard curves generated using authentic standards of cholesterol (C8667), C18:2 (C0289), C20:4 (C8753), TG18:1 (T7140), TG18:2 (T9517) purchased from Sigma-Aldrich.

2.4.6 Hematology and clinical biochemistry

Hematological and clinical biochemical analyses were performed at the Veterinary Pathology Diagnostic Services, The University of Sydney. Red blood cells, hemoglobin, hematocrit, mean corpuscular volume, platelets, white blood cells, neutrophil, lymphocyte, monocyte, eosinophil and basophil were determined in EDTA blood with the XT-2000i Hematology Analyzer (Sysmex, Kobe, Japan) by fluorescence flow cytometry technology. Standard clinical biochemistry analyses were performed on heparinized-plasma samples using the Konelab 20i Chemistry Analyzer (Thermo Fisher Scientific) to determine the concentrations of alkaline phosphatase, alanine aminotransferase, aspartate aminotransferase, urea, creatinine, albumin and iron.

2.5 Molecular biology

2.5.1 RNA extraction and analysis

RNA expression was analyzed by semi-quantitative RT-PCR. Animal tissue (30 mg) was homogenized with 1 mL TRIzol (Thermo Fisher Scientific) and RNA isolated following the manufacturer's instructions. RNA pellets were re-suspended in nuclease-free water and the RNA concentrations determined using a NanoDrop 1000 spectrophotometer (Thermo Fisher Scientific). Complementary DNA was prepared using the Superscript III First Strand Synthesis kit (Thermo Fisher Scientific) following the manufacturer's instruction. Real-time semi-quantitative PCR was performed using a LightCycler 480 System (Roche, Basel, Switzerland) and the SensiFAST Probe No-ROX Kit (Bioline). The amount of mRNA was normalized to *β-actin* or *Gapdh* mRNA and presented relative to the corresponding wild-type control using the comparative CT method (295). PCR products were verified by melt curve analysis. The qualified PCR primers (Integrated DNA Technologies, Coralville, IA, USA) used were as described in Table 2.2. The sequences of the qualified primers for *β-actin*, *Bvra*, *Bvrb*, *Gapdh, Hmox1*, *Hmox2*, *Ttpa*, *Txn1*and *Nqo1* mRNA were obtained via PrimerBank (296). The sequences of the qualified primers for *Acaca, Fasn*, *Srebf1*, *Cd36*, *Cpt1a*, *Cyp2j6*, *Cyp4a12*, *Fgf21* and *G6pase* were kindly provided by Dr. Terry Hinds (University of Toledo College of Medicine, Toledo).

Table 2.2 Sequences and Genbank accession numbers of primers used to amplify gene transcripts via RT-PCR

Primer Pair No.	Name	Genbank Accession No.	Oligonucleotide (5'-3')		Product Size (bp)
			Froward	Reverse	
1	*β-actin*	NM_007393	GGATGCAGAAGGAGATTACTG	CGATCCACACAGAGTACTTG	90
2	*Bvra*	NM_026678	AGCCGCTGGTAAGCTCC	ACCAACCACTACCACACCAAA	174
3	*Bvrb*	NM_144923	TTCTCAGCTTTTCCGGCCCT	CCTCATAACCTGCTTGCACCG	120
4	*Hmox1*	NM_010442	AGGTACACATCCAAGCCGAGA	CATCACCAGCTTAAAGCCTTCT	86
5	*Hmox2*	NM_001357050	AGCACATGACCGAGCAGAAAA	GCTCCGTGGGGAAATATAAGGG	179
6	*Ttpa*	NM_015767	TCTACAGAGAACACTAATGAGCAATGTG	TGGTGAAGCCATGTGGAAAGT	83
7	*Txn1*	NM_011660	CATGCCGACCTTCCAGTTTTA	TTTCCTTGTTAGCACCGGAGA	68
8	*Nqo1*	NM_008706	AGGATGGGAGGTACTCGAATC	AGGCGTCCTTCCTTATATGCTA	144
9	*Acaca*	NM_133360	GAATCTCCTGGTGACAATGCTTATT	GGTCTTGCTGAGTTGGGTTAGCT	106
10	*Fasn*	NM_007988	GCTGCTGTTGGAAGTCAGC	AGTGTTCGTTCCTCGGAGTG	76
11	*Srebf1*	NM_001358315	CACCAGCATAGGCGAAGGA	AGTGTGCGGCCTGTGGAT	127
12	*Cd36*	NM_001159558	TCTTGGCTACAGCAAGGCCAGATA	AGCTATGCAGCATGGAACATGACG	173

13	*Cpt1a*	NM_013 495	GGCCTCTGTGGTACA CGACAA	CTCAGTGGGAGCGA CTCTTCA	105
14	*Cyp2j6*	NM_010 008	TGTCACTTCCTGCGA GAGCCCA	AACCGGTCCCCTCA GTCCCTC	95
15	*Cyp4a12*	NM_177 406	GCCTTATACGGAAAT CATGGC	TGGAATCCTGGCCA ACAATC	77
16	*Fgf21*	NM_020 013	CCTCTAGGTTTCTTT GCCAACAG	AAGCTGCAGGCCTC AGGAT	76
17	*G6pase*	NM_008 061	TGCAAGGGAGAACT CAGCAA	GGACCAAGGAAGCC ACAATG	64
18	*Gapdh*	NM_001 289726	AGGTCGGTGTGAAC GGATTTG	TGTAGACCATGTAG TTGAGGTCA	123

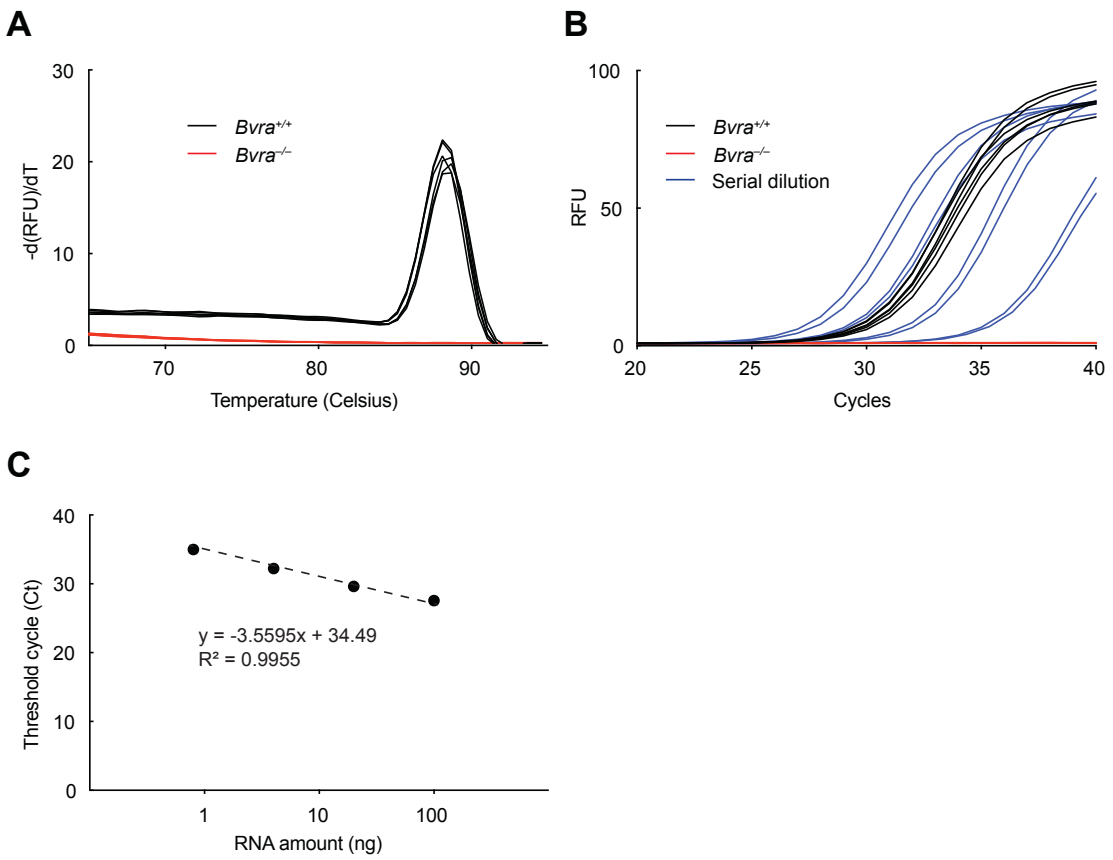

Figure 2.3 The melting curves, amplification plots and standard curve of real-time PCR for detection of *Bvra* mRNA in mouse liver. **(A)** Representative melting curves for detection of *Bvra* mRNA in liver of *Bvra*$^{+/+}$ and *Bvra*$^{-/-}$ naïve mice. **(B)** Representative amplification plots for detection of *Bvra* mRNA in liver of *Bvra*$^{+/+}$ and *Bvra*$^{-/-}$ naïve mice, and 5-fold serial dilution of RNA sample pool of three *Bvra*$^{+/+}$ livers. **(C)** Standard curve derived from the 5-fold serially diluted RNA from a sample pool of three *Bvra*$^{+/+}$ livers. Abbreviation: RFU, relative fluorescence units; T, temperature; -d(RFU)/dT, the change in fluorescence with temperature.

2.5.2 SDS-PAGE and immunoblotting

Tissues were homogenized in SDS-urea lysis buffer (6.7 M urea, 10% (v/v) glycerol, 10 mM Tris pH 6.8, 1% (w/v) SDS, 1 mM DTT, 1 mM PMSF) or RIPA buffer supplemented with protease inhibitor cocktail (Roche, Switzerland) using Wheaton tissue grinder or sonication (Bandelin SONOPLUS, Germany) on ice.

Proteins from cell/tissue lysates were resolved by SDS-PAGE using 10% SDS-polyacrylamide gels (NuPage, Invitrogen). 25 µg protein was electrophoresed at 100 V for 90 min and transferred to nitrocellulose membranes using an iBlot2 Dry Blotting System (Invitrogen, USA). Membranes were blocked with 5% (w/v) BSA at room temperature for 1 h and incubated with primary antibody (BVRA antibody, 1:1,000, v/v, ADI-OSA-450, Enzo Life, NY, USA; β-actin antibody, 1:5,000, v/v, 691001, MP Biomedicals, CA, USA; GLUT4 antibody, 1:500, v/v, in-house (285); pSer473 Akt antibody, 1:1,000, v/v, 4060S, Cell Signaling, MA, USA; pThr308 Akt antibody, 1:1,000, v/v, 9275S, Cell Signaling; Akt antibody, 1:2,000, v/v, 9272S, Cell Signaling; pSer9 GSK-3β antibody, 1:500, v/v, 9336S, Cell Signaling; GSK-3β antibody, 1:2,000 v/v, 9832S, Cell Signaling; pThr642 AS160 antibody, 1:1,000 v/v, 4288S, Cell Signaling; AS160 antibody, 1:1,000, v/v, 2670S, Cell Signaling; α-Tubulin antibody, 1:2,000 v/v, T9026, Sigma Aldrich, MO, USA; 14-3-3 antibody, 1:2,000 v/v, sc-629, Santa Cruz, CA, USA; pSer73 PPARα antibody, 1:500, v/v, ABE2888, Millipore, Merck, NJ, USA; PPARα antibody, 1:1,000, v/v, ab191226, Abcam, Cambridge, UK) in TBST at 4 °C overnight. Membranes were then washed and incubated with IRDye 800CW goat-anti-rabbit IgG or IRDye 680RD goat anti-mouse IgG secondary antibody (LI-COR Biosciences, NE, USA). Proteins were visualized using Odyssey Model 9120 Gel Documentation System and analyzed by densitometry using the Image Studio Lite software (LI-COR Biosciences).

2.5.3 Redox state of peroxiredoxin 2

The redox state of peroxiredoxin 2 (Prx2) was determined as described previously (297). Briefly, one volume of freshly collected mouse blood was added to one volume of 200 mM *N*-ethylmaleimide in EDTA tubes and the mixture incubated at room temperature for 1 h. Samples were then added to non-reducing loading buffer in a 1:1000 ratio (v/v) and 5 µg proteins loaded onto 12% SDS-polyacrylamide gels (NuPage, Thermo Fisher Scientific) or immediately frozen at -80 °C prior to thawing and SDS-polyacrylamide gel electrophoresis. Following separation under non-reducing conditions, proteins were transferred to nitrocellulose membranes (iBlot-2 Transfer Stacks, Thermo Fisher Scientific), blocked with 5% (w/v) BSA in TBS and then incubated with anti-Prx2 antibody (R8656, 1:1000 (v/v), Sigma-Aldrich, St Louis, MO, USA) in TBST for 1 h at room temperature. Proteins were detected using IRDye 800CW goat-anti-rabbit IgG (1:10000 (v/v), LI-COR Biosciences), visualized using Odyssey Model 9120 Gel

Documentation System, and analyzed by densitometry using the Image Studio Lite software.

2.6 Morphometric analysis

2.6.1 Histology for general organ

For hematoxylin and eosin staining (H&E), animal tissues were fixed overnight in 10% (v/v) neutral buffered formalin solution, and then stored in 80% (v/v) ethanol. Stored tissue was embedded in paraffin, sectioned at 5 μm thickness and placed on a labeled glass slide. Sections were deparaffinized by immersion into xylene for 30 min and hydrated in descending alcohol solutions from 100 to 75% (v/v), then immersed in dH_2O. The slides were immersed in filtered Mayer's hematoxylin (H3136, Sigma Aldrich, St. Louis, USA) for 5 min, followed by rinsing with tap water for 1 min. Slides were transferred to 95% (v/v) ethanol for 30 s and then immersed in eosin (HT110132, Sigma Aldrich, St. Louis, US) and stained for 1 min, followed by rinsing in 95% (v/v) ethanol for 2 min. Sections were dehydrated with 100% ethanol, cleared with xylene for 15 min, then mounted with DPX (1.00579, Merck, Sigma Aldrich, St. Louis, USA) and cover-slipped.

For Oil Red O staining, frozen animal tissue was embedded in optimal cutting temperature compound (OCT, #4583, Tissue-Tek, ProSciTech, Australia), sectioned at 5 μm thickness on a cryostat (CM950, Leica Biosystems, Germany), and sections were then placed on a labeled glass slide. Cryosections were fixed in 60% (v/v) isopropyl alcohol for 10 min and stained with 0.3% (w/v) Oil Red O (01391, Sigma Aldrich, St. Louis, USA) in 60% (v/v) isopropyl alcohol for 30 min. Hematoxylin was used to counterstain nuclei, before slides were mounted with aqueous solution and then coverslipped. Sections were visualized using a Leica Digital Microscope DM4000B-M equipped with a Leica MC170 HD microscope camera. Images were obtained at 200X magnification and using Leica Application Suite software V4.4. Twenty independent fields per section were evaluated. Oil Red O stained areas were quantified by Image J (Version 1.49u, NIH, USA).

2.6.2 Histology for arteries

Histologic analysis of atherosclerotic lesion was carried out largely as described previously (287, 288, 298). The hearts, unstable (segment I) and stable plaque (brachiocephalic artery) of TS mice were excised, placed in 10% (v/v) neutral buffered formalin overnight, then stored in 80% (v/v) ethanol. Fixed tissue was dehydrated by xylene, then embedded in paraffin block and used for lesion assessment, which was performed in a blinded fashion by two operators. Specimens were sectioned at 5 μm thickness throughout the entire arterial segment using a vertical microtome (RM 2255, Leica Biosystems, Germany) and placed on labeled glass slides. Sections were deparaffinized by immersion into xylene for 30 min and hydration in descending alcohol solutions from 100 to 75% (v/v), followed by immersion in dH_2O before staining. For hematoxylin and

eosin (H&E) staining, the rehydrated slides were immersed in filtered Mayer's hematoxylin (H3136, Sigma Aldrich, St. Louis, USA) for 5 min, followed by rinsing with water for 5 min. Slides were transferred to 95% (v/v) ethanol for 30 s, and then immersed in eosin and stained for 1 min, followed by rinsing with 95% (v/v) ethanol for 2 min. Sections were dehydrated with 100% ethanol, cleared with xylene for 15 min, then mounted with DPX (1.00579, Merck, Sigma Aldrich) and cover-slipped.

To visualize collagen, the rehydrated sections were stained for 1 h in picrosirius red (PSR) solution (0.6% w/v of direct red (365548, Sigma Aldrich) in saturated picric acid), differentiated in 0.01 M HCl, dehydrated with serial solutions of ethanol and xylene, then mounted with DPX and cover-slipped. To visualize fibrin, the rehydrated slides were immersed in freshly made Weigert's hematoxylin solution (HT109 and HT107, Sigma Aldrich) for 5 min, then differentiated in running trap water for 5 min. Slides were immersed in 0.5% (w/v) Martius yellow (287814, Sigma Aldrich) for 10 min, then immersed in 1% (w/v) Brilliant crystal scarlet (C0644, Sigma Aldrich) for 10 min, followed by differentiation in 1% (w/v) phosphotungstic acid. Sections were counterstained with 0.5% (w/v) aniline blue for 2 min and dehydrated with 100% ethanol, cleared with xylene for 15 min, then mounted with DPX and cover-slipped (299). For hemosiderin staining with Prussian blue, the rehydrated slides were immersed in 2% (v/v) HCl-2% (w/v) ferrocyanide mixture (03899, Sigma Aldrich) for 30 min, counterstained with neutral fast red (N6264, Sigma Aldrich) for 5 min, followed by washing with distilled water for 10 s. Sections were dehydrated with 100% ethanol, cleared with xylene for 15 min, then mounted with DPX and cover-slipped (299). Sections were visualized using a Leica Digital Microscopy DM4000B-M, Leica MC170 HD microscopic camera. Images were obtained by using LAS V4.4, Leica and all histological data analyses were performed by an operator blinded to animal genotype with using Image J software (Version 1.49u, NIH, US).

Assessment of stability of plaques formed in Segment I was carried out as described previously (287). Briefly, unstable plaque (Segment I) was sectioned from the proximal suture to the bifurcation of right subclavian. Sections were taken at 100 μm intervals throughout the entire arterial segments and stained with H&E. Fibrous cap thickness was defined by calculating the positive birefringence area under polarized light in PSR-stained tissue sections. Lesion height was defined by the maximal distance from the lesion to the luminal circumference of the vessel wall (Fig. 2.1) (287).

Atherosclerotic lesion size at the aortic root was quantified by morphometry throughout the entire aortic sinus using H&E stained sections taken in 50 μm intervals and calculated as the average of the cross-sectional lesion areas at 200 and 350 μm distal to the point where the 3 valve leaflets first appeared, as described previously (298).

Atherosclerotic lesion size at the brachiocephalic artery was quantified by morphometry. Brachiocephalic artery was sectioned from the bifurcation of right subclavian to the aortic arch.

Sections were taken at 100 μm intervals throughout the entire arterial segments and stained with H&E.

2.7 Statistical analyses

All the samples and data analyses were performed blinded. Statistical analysis was performed using GraphPrism 8 software. Results are expressed as mean value with error bars representing standard error of the mean (SEM). Numeric data was analyzed for normality using the Shapiro–Wilk normality test, the significance determined using the appropriate parametric or non-parametric test. The Mann-Whitney test, Kruskal-Wallis one-way analysis of variance (ANOVA) and two-way ANOVA analysis of variance were used to determine statistical significance unless indicated otherwise. A P-value of <0.05 was considered as statistically significant.

Chapter 3

Absence of the *biliverdin reductase a* gene is associated with increased endogenous oxidative stress

This chapter contains work published in:

Chen W, Maghzal G, Ayer A, Suarna C, Dunn LL, Stocker R. Absence of the *Bvra* gene is associated with increased endogenous oxidative stress. *Free Radic Biol Med*. 2018; 115: 156-165

Author contributions:

Chen W, Maghzal G, Dunn LL and Stocker R designed the study.

The *Bvra*$^{-/-}$ mice that were generated by OzGene (Perth, Australia), with breeding and experimental procedures performed by Chen W, under guidance from Dunn LL, Newington D and Stocker R. Chen W designed and carried out molecular biology experiments for gene expression related to heme catabolism, as well as hematological and clinical chemistry analyses in naïve *Bvra*$^{-/-}$ mice, with guidance from Dunn LL and Stocker R. Chen W, Maghzal G, Suana C and Stocker R designed and carried out the LC-MS/MS analysis for bile pigment and HPLC analysis to evaluate oxidative stress in the naïve *Bvra*$^{-/-}$ mice.

The specific aims for this chapter are:

1) To phenotypically characterize naïve *biliverdin reductase a* gene-knockout (*Bvra*$^{-/-}$) mice

2) To assess oxidative stress in *Bvra* deficiency by comparing *Bvra*$^{-/-}$ to littermate wild type mice

3.1 Introduction

Bilirubin is the end product of heme catabolism in mammals. Heme is degraded by heme oxygenase to carbon monoxide, ferrous iron and biliverdin, and the latter is then reduced to bilirubin by biliverdin reductase (155). Adult humans produce ~300 mg bilirubin each day (300). The bilirubin formed is essentially insoluble in water and hence tightly bound to albumin for transport in the blood circulation (301). When the binding capacity of albumin for bilirubin is exceeded, this yellow pigment can accumulate in the brain and cause toxicity and neurologic dysfunction. Bilirubin is removed from the circulation by hepatic glucuronyl transferase-mediated conjugation with glucuronic acid. The resulting conjugated bilirubin is secreted into bile, and responsible for the typical yellow appearance of the gall bladder.

Considered originally to be a metabolic waste product, bilirubin in its free, albumin-bound and conjugated forms, has since been recognized to possess potent antioxidant activities *in vitro* (2, 185, 187). These include the efficient inhibition of linoleic acid oxidation by peroxyl radicals (2, 185) and protection of circulating lipids from oxidation via interaction with α-tocopherol (α-TOH) (187). In addition to scavenging lipid peroxyl radicals and α-tocopheroxyl radical (α-TO$^{\bullet}$), bilirubin attenuates oxidative damage to proteins (188, 189); scavenges hypochlorous acid (108), nitric oxide and reactive nitrogen species (190); and inhibits chloramine formation and myeloperoxidase-mediated protein oxidation (191).

Suggestions that bilirubin may be an important antioxidant *in vivo* were initially based on experiments showing protective effects of the pigment in cultured cells. For example, bilirubin formation induced by hemin treatment, protects vascular smooth muscle cells against oxidative stress (192). Bilirubin also attenuates vascular endothelial dysfunction in response to oxidized low-density lipoprotein (6). In human cardiomyocytes, albumin-bound bilirubin is a powerful protector against oxidant toxicity (193). Antioxidant properties of bilirubin have also been reported in several animal models of oxidative stress. For example, bilirubin protected against oxidative stress in hyperbilirubinemic Gunn rats exposed to hyperoxia, as assessed by a decrease in thiobarbituric acid-reactive substances (194). Hemin treatment or exogenously added bilirubin preserved myocardial function in an animal model of cardiac ischemia/reperfusion injury (195). Moreover, *ex vivo* treatment of perfused rat hearts with conjugated bilirubin improved post-ischemic functional outcomes and decreased myocardial oxidative damage (196).

Several human studies indirectly suggest bilirubin to provide benefit *in vivo*. For example, plasma bilirubin concentrations inversely associate with risk of cardiovascular disease (CVD), including atherosclerosis (302), coronary artery disease (9) and stroke (267). Individuals with Gilbert syndrome, who have moderately increased plasma bilirubin as a result of decreased activity of bilirubin uridine diphosphate glucuronosyltransferase have lower risk of CVD (303). In these individuals, markers of oxidative stress, such as serum malonyldialdehyde and urinary 8-hydroxy-2'-deoxyguanosine, are also decreased compared with the normal population (197).

Despite this association between bilirubin and cellular protection, evidence that bilirubin at physiological concentrations directly protects against oxidative stress *in vivo* remains limited. Therefore, we generated a *biliverdin reductase a* gene-deficient (*Bvra*$^{-/-}$) mouse to more directly assess the contribution of bilirubin as an endogenous antioxidant *in vivo*. Herein, we report that *Bvra*$^{-/-}$ mice which lack circulating bilirubin, have higher oxidative stress. Our findings support the notion that normal concentrations of bilirubin contribute to the endogenous antioxidant defense *in vivo*.

3.2 Materials and methods

3.2.1 Animals

Biliverdin reductase a (Bvra) gene deficient mice were generated by homologous recombination in embryonic stem (ES) cells (Ozgene, Perth, WA, Australia) (Fig. 3.1A). The procedures for generation and genotyping of the *Bvra*$^{-/-}$ mice have been described in detail in **Section 2.1.1** of Chapter 2. Male and female mice, 8 to 12 weeks old, were used for experiments. All procedures were carried out according to the Australian NHMRC Guidelines for Animal Research and were approved by the Animal Care and Ethics Committee of the Garvan Institute of Medical Research/St Vincent's Hospital.

3.2.2 Collection of blood, plasma and tissue samples

Mice were anesthetized by isoflurane inhalation. Blood was collected by cardiac puncture using a 26-gauge needle and transferred into heparin-coated micro tubes (Sarstedt, Nümbrecht, Germany). To obtain plasma, heparinized blood was centrifuged at 2,000 x *g* and 4 °C for 15 min. Immediately following cardiac puncture, mice were gravity-perfused (90 mm Hg) with phosphate buffered saline (PBS). Brain, heart, lung, liver, spleen, pancreas and kidneys were collected for organ weight, Western blot and mRNA analyses. Tail tips were collected to confirm genotype of mice.

3.2.3 RNA extraction and analysis

Detailed procedures of RNA extraction, complementary DNA (cDNA) synthesis, real-time quantitative PCR have been described in **Section 2.5.1**. The amount of mRNA was normalized to *β-actin* mRNA and presented relative to the corresponding wild-type control using the comparative CT method (295). PCR products were verified by melt curve analysis.

3.2.4 SDS-PAGE and immunoblotting

Tissues (30 mg) were homogenized in 600 μL SDS-urea lysis buffer (6.7 M urea, 10% (v/v) glycerol, 10 mM Tris pH 6.8, 1% (v/v) SDS, 1 mM DTT, 1 mM PMSF, 1 mM protease inhibitor cocktail) (Roche). Protein concentration of the homogenate was determined by BCA assay.

Detailed procedures of SDS-PAGE and immunoblotting have been described in **Section 2.5.2** of Chapter 2.

3.2.5 Hematology and clinical biochemistry

Hematological and clinical biochemical analyses were performed as described in **Section 2.4.6** of Chapter 2.

3.2.6 Redox state of peroxiredoxin 2

The peroxiredoxin 2 (Prx2) redox state was determined as described in **Section 2.5.3** of Chapter 2.

3.2.7 Determination of bile pigments

Bile pigments in gall bladder were extracted and analyzed as described in **Section 2.4.3** of Chapter 2.

3.2.8 Analyses of antioxidants, lipids and cholesterylester hydroperoxides

Fresh plasma was processed and analyzed for antioxidants, lipids and oxidized lipids as described in **Section 2.4.1** of Chapter 2.

3.2.9 Reduction with sodium borohydride

Reduction of lipid hydroperoxide with sodium borohydride and the subsequent HPLC analysis have been described at in **Section 2.4.2** of Chapter 2.

3.2.10 LC-MS/MS

Plasma biliverdin and bilirubin were analyzed by LC-MS/MS using a 6490 Triple Quadrupole LC-MS/MS (Agilent Technologies) as described in **Section 2.4.4** of Chapter 2. Methanolic phase (5μL) of the plasma lipid extraction in **Section 3.2.8** of Chapter 3 was injected onto the LC-MS/MS.

3.2.11 Statistical analyses

All the samples and data analyses were performed blinded. Statistical analysis was performed using GraphPrism 8 software. Results are expressed as mean ± standard error of the mean (SEM). The Mann-Whitney test, Kruskal-Wallis one-way analysis of variance (ANOVA) and two-way ANOVA were used to determine statistical significance unless indicated otherwise. $P < 0.05$ was considered as statistically significant.

3.3 Results

3.3.1 Generation of *biliverdin reductase a* gene-deficient mouse

Bvra gene deficient (*Bvra*$^{-/-}$) mice were generated by homologous recombination (Fig. 3.1A). In this procedure, exon 3 of the *Bvra* gene, which encodes the binding domain for the catalytic cofactor NAD(P)H of BVRA (304), was removed. This targeting strategy further introduced a translational frameshift that rendered downstream exons non-functional, resulting in no detectable *Bvra* gene products. Genomic DNA obtained from mice tails were used for genotyping. Using a *Brva* universal forward primer, and reverse primers specific for wild-type and *Bvra* knockout alleles, PCR amplification detected a fragment of 233 bp in *Bvra*$^{+/+}$, a fragment of 139 bp in *Bvra*$^{-/-}$, and fragments of 233 and 139 bp in the *Bvra*$^{+/-}$ mice (Fig. 3.1B). Absence of *Bvra* mRNA expression in *Bvra*$^{-/-}$ mice was confirmed in brain, heart, liver and spleen tissues by semi-quantitative RT-PCR (Fig. 3.1C).

Mice also possess a *Bvrb* gene encoding an enzyme that reduces biliverdin IXβ to bilirubin IXβ. Semi-quantitative RT-PCR revealed the absence of compensatory up-regulation of *Bvrb* mRNA in *Bvra*$^{-/-}$ mice (Fig. 3.1C). We next confirmed the lack of BVRA protein expression in *Bvra*$^{-/-}$ mice by Western blot. The 33 kDa BVRA protein detected in *Bvra*$^{+/+}$ and *Bvra*$^{+/-}$ mice was absent in *Bvra*$^{-/-}$ animals (Fig. 3.1D). Notably, protein expression in heterozygote mice was approximately half that seen in wild-type across all tissues examined. Taken together, these data confirmed the successful ablation of BVRA protein in *Bvra*$^{-/-}$ mice.

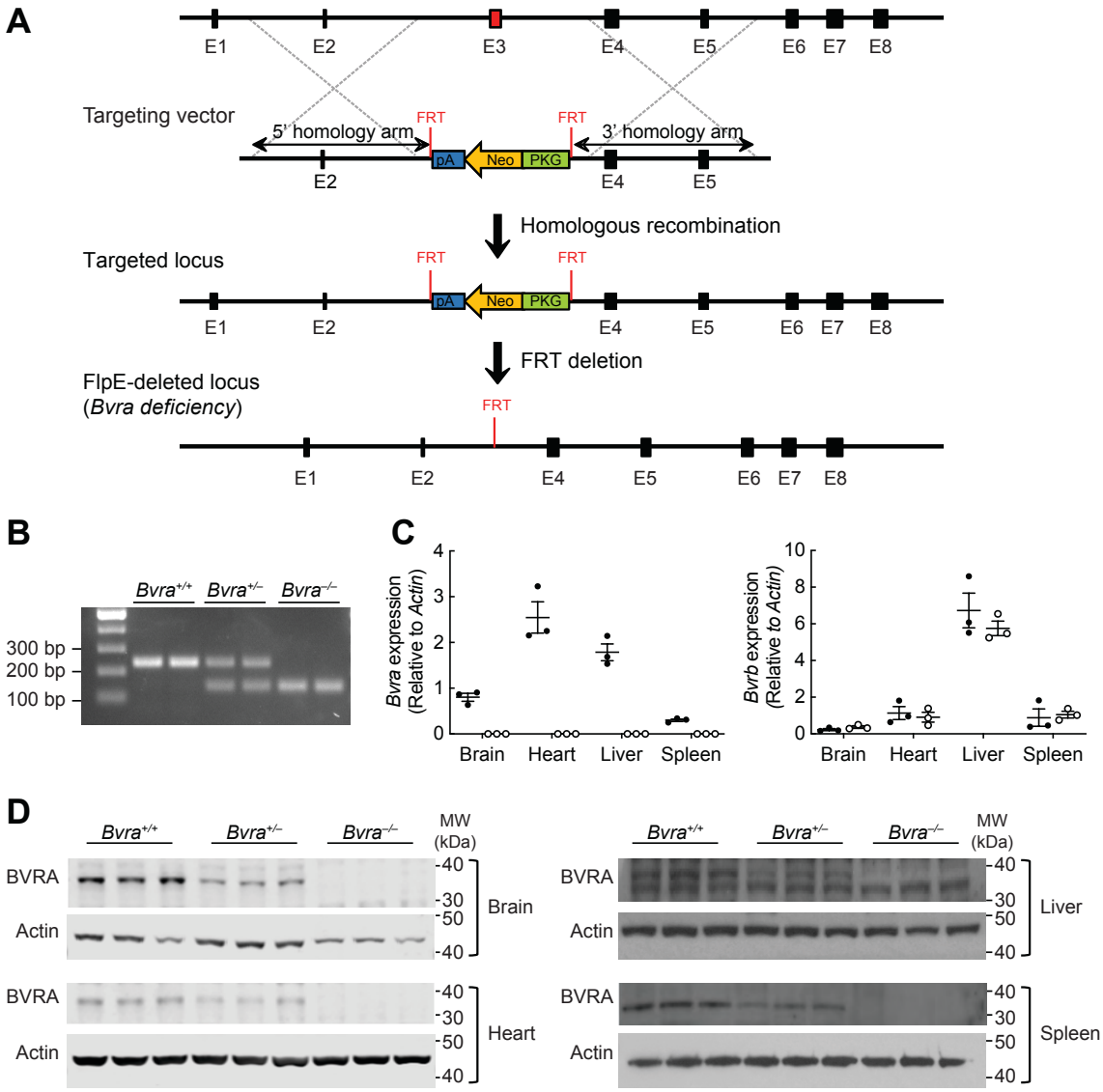

Figure 3.1 Targeted disruption of the mouse *biliverdin reductase a* (*Bvra*) gene. **(A)** Targeting strategy used for deletion of mouse *Bvra* exon 3. The genomic structure of the wild-type *Bvra* allele is shown at the top depicting the promoter region, 8 exons, and intervening introns. The targeting vector was constructed to replace exon 3 with a neomycin (PGK_*neo*) selection cassette, flanked by two FRT sites to allow generation of the targeted locus via homologous recombination. The *neo* cassette was then deleted from the genome by mating of *Bvra*$^{+/-}$ males to FRT-deleter females. **(B)** Genotype identification by PCR analysis of DNA extracted from the tail of mice after deletion of the PKG_*neo* selection cassette. *Brva* universal forward primer and *Bvra* wild-type reverse primer detect a fragment of 233 bp in *Bvra*$^{+/+}$ mice. *Brva* universal forward primer and *Bvra* knockout reverse primer detect a fragment of 139 bp in *Bvra*$^{-/-}$ and fragments of 233 and 139 bp in the *Bvra*$^{+/-}$ mice. **(C)** Semi-quantitative RT-PCR of *Bvra* and *Bvrb* mRNA transcripts in brain, heart, liver and spleen from *Bvra*$^{+/+}$and *Bvra*$^{-/-}$ mice. Results in **(C)** are expressed as mean ± SEM; n = 3 *Bvra*$^{+/+}$ (filled circles) and n = 3 *Bvra*$^{-/-}$ (open circles) mice. **(D)** Western blots of BVRA in brain, heart, liver and spleen from *Bvra*$^{+/+}$, *Bvra*$^{+/-}$ and *Bvra*$^{-/-}$ mice.

3.3.2 Phenotypic characterization of *Bvra* deficiency

Genotypes of the offspring resulting from *Bvra*$^{+/-}$ x *Bvra*$^{+/-}$ matings were consistent with Mendelian ratios and there were no differences in gender ratios (Table 3.1). At 10 weeks of age, brain, heart, lung, liver, spleen, pancreas and kidneys of *Bvra*$^{+/+}$, *Bvra*$^{+/-}$ and *Bvra*$^{-/-}$ littermates were dissected following perfusion, and the organ weight was measured. Compared with wild-type mice, *Bvra*$^{+/-}$ and *Bvra*$^{-/-}$ mice appeared normal in body weight and organ-to-body weight ratio (Table 3.2).

A panel of hematological indices and plasma clinical chemistry analyses were also assessed in *Bvra*$^{+/+}$, *Bvra*$^{+/-}$ and *Bvra*$^{-/-}$ littermates. All parameters assessed were within the normal physiological range observed in C57BL/6J mice (Tables 3.3 and 3.4). The red blood cell (RBC) number and mean corpuscular hemoglobin concentration (MCHC) were slightly but significantly increased, while mean corpuscular volume (MCV) and mean corpuscular hemoglobin (MCH) were significantly decreased in *Bvra*$^{-/-}$ mice compared with corresponding wild-type littermates (Table 3.3). Plasma concentrations of alkaline phosphatase (ALP), alanine aminotransferase (ALT), aspartate aminotransferase (AST), urea, creatinine, iron, TG and cholesterol were not significantly different between *Bvra*$^{+/+}$ and *Bvra*$^{-/-}$ littermates (Table 3.4), suggesting that *Bvra* deficiency has no gross effect on liver or kidney function.

Table 3.1 Gender and genotype distribution in offsprings derived from *Bvra*$^{+/-}$ x *Bvra*$^{+/-}$ mating

Genotype	Male % (n)	Female % (n)	Total % (n)
Bvra$^{+/+}$	24 (69)	26 (81)	25 (150)
Bvra$^{+/-}$	52 (151)	51 (163)	51 (314)
Bvra$^{-/-}$	24 (70)	23 (73)	24 (143)

Table 3.2 Body weight and organ-to-body weight ratio in *Bvra*$^{+/+}$, *Bvra*$^{+/-}$ and *Bvra*$^{-/-}$ mice at 10 ± 1 weeks of age

	Male			Female		
	Bvra$^{+/+}$	*Bvra*$^{+/-}$	*Bvra*$^{-/-}$	*Bvra*$^{+/+}$	*Bvra*$^{+/-}$	*Bvra*$^{-/-}$
Body weight (g)	28.2 ± 0.5	27.9 ± 0.6	27.4 ± 0.5	21.4 ± 0.9	20.8 ± 0.2	21.2 ± 0.6
Brain (%)	1.7 ± 0.0	1.7 ± 0.0	1.8 ± 0.0	2.1 ± 0.0	2.2 ± 0.0	2.3 ± 0.0
Heart (%)	0.7 ± 0.0	0.6 ± 0.1	0.6 ± 0.0	0.7 ± 0.0	0.8 ± 0.0	0.7 ± 0.0
Lung (%)	0.8 ± 0.1	0.7 ± 0.1	0.7 ± 0.1	0.9 ± 0.0	0.9 ± 0.1	0.9 ± 0.1
Liver (%)	5.1 ± 0.2	4.7 ± 0.2	5.1 ± 0.1	5.4 ± 0.2	5.0 ± 0.2	4.9 ± 0.3
Spleen (%)	0.3 ± 0.0	0.3 ± 0.0	0.3 ± 0.0	0.4 ± 0.0	0.4 ± 0.0	0.5 ± 0.0
Pancreas (%)	1.3 ± 0.1	1.3 ± 0.1	1.2 ± 0.0	1.4 ± 0.1	1.4 ± 0.1	1.5 ± 0.1
Kidneys (%)	1.5 ± 0.1	1.4 ± 0.1	1.4 ± 0.0	1.4 ± 0.0	1.5 ± 0.1	1.5 ± 0.0

Results shown are expressed as mean ± SEM, with n = 6 per group/genotype, except for body weight and pancreas where the n-value is 20.

Table 3.3 Hematology of *Bvra*$^{+/+}$, *Bvra*$^{+/-}$ and *Bvra*$^{-/-}$ mice

	Bvra$^{+/+}$ (n = 16)	*Bvra*$^{+/-}$ (n = 10)	*Bvra*$^{-/-}$ (n = 17)
RBC (10^{12}/L)	9.2 ± 0.1	8.8 ± 0.3*	9.4 ± 0.1*
Hemoglobin (g/L)	140 ± 1	133 ± 6	141 ± 1
Hematocrit (%)	42.8 ± 0.3	41.6 ± 1.0	42.6 ± 0.3
MCV (fL)	46.7 ± 0.2	47.2 ± 0.3	45.2 ± 0.2*
MCH (pg)	15.3 ± 0.1	15.0 ± 0.3	15.0 ± 0.1*
MCHC (g/L)	328 ± 1	319 ± 7	332 ± 1*
Platelet (10^9/L)	1324 ± 49	1214 ± 69	1331 ± 54
WBC (10^9/L)	1.2 ± 0.2	1.1 ± 0.1	1.4 ± 0.1
Neutrophil (%)	12.0 ± 2.1	9.7 ± 1.4	9.4 ± 0.8
Lymphocyte (%)	85.9 ± 2.1	88.5 ± 1.2	88.3 ± 0.8
Monocyte (%)	0.7 ± 0.2	0.5 ± 0.2	0.9 ± 0.2
Eosinophil (%)	1.5 ± 0.3	1.3 ± 0.4	1.4 ± 0.2
Basophil (%)	ND	ND	ND

Results show mean ± SEM.

Abbreviations: RBC, red blood cells; MCV, mean corpuscular volume; MCH, mean corpuscular hemoglobin; MCHC, mean corpuscular hemoglobin concentration, WBC, white blood cells; ND, not detected.

Concentrations of neutrophil, lymphocyte, monocyte, eosinophil and basophil were presented as a proportion of total WBC, respectively.

*P<0.05 compared to *Bvra*$^{+/+}$ mice by Kruskal-Wallis test with Dunn's multiple comparison.

Table 3.4 Clinical chemistry of *Bvra*$^{+/+}$ and *Bvra*$^{-/-}$ mice

	Bvra$^{+/+}$ (n = 12)	*Bvra*$^{-/-}$ (n = 15)
ALP (U/L)	192 ± 10	185 ± 9
ALT (U/L)	23.9 ± 5.9	25.3 ± 2.5
AST (U/L)	76.1 ± 8.1	74.1 ± 4.7
Urea (mM)	9.2 ± 0.6	9.7 ± 0.5
Creatinine (μM)	19.8 ± 0.4	19.0 ± 0.3
Albumin (g/L)	26.4 ± 0.4	26.1 ± 0.3
Iron (mM)	33.2 ± 2.0	29.3 ± 1.7
Triglycerides (μM)	390 ± 32	384 ± 37
Cholesterol (μM)	686 ± 24	660 ± 33

Results show mean ± SEM.

Abbreviations: ALP, alkaline phosphatase; ALT, alanine aminotransferase; AST, aspartate aminotransferase.

3.3.3 *Bvra* deficiency eliminates most of the bilirubin in plasma and bile

Gall bladders of *Bvra*$^{-/-}$ mice appeared notably green instead of the typical yellow color seen in *Bvra*$^{+/+}$ and *Bvra*$^{+/-}$ mice (Fig. 3.2A). Similarly, fresh bile samples from *Bvra*$^{-/-}$ mice varied in hue from light to dark green, while bile samples of *Bvra*$^{+/+}$ and *Bvra*$^{+/-}$ had a bright yellow color. These observations indicated that most of the biliary pigment in *Bvra*$^{-/-}$ mice was biliverdin rather than bilirubin. Indeed, spectrophotometric analysis of bile samples from *Bvra*$^{-/-}$ mice displayed a spectrum that closely resembled that of authentic biliverdin, with an absorbance maxima at 380 and 690 nm (Fig. 3.2B). In contrast, spectra of *Bvra*$^{+/+}$ and *Bvra*$^{+/-}$ bile showed maximum absorption at 450 nm, similar to the spectra of bilirubin.

Finally, LC-MS/MS analysis was utilized to measure plasma concentrations of bilirubin and biliverdin. *Bvra*$^{-/-}$ mice had very low concentrations of plasma bilirubin (9 ± 2 nM) compared with littermate *Bvra*$^{+/+}$ and *Bvra*$^{+/-}$ mice, *i.e.*, 1175 ± 181 and 826 ± 132 nM, respectively (Fig. 3.3B). Instead, *Bvra*$^{-/-}$ mice had somewhat elevated plasma biliverdin; *i.e.*, 100 ± 30 nM compared with 4 ± 1 and 3 ± 1 nM for *Bvra*$^{+/+}$ and *Bvra*$^{+/-}$ animals. These results show that biliverdin is the major bile pigment in *Bvra*$^{-/-}$ mice and that bilirubin is only present in the plasma at very low concentrations, ~100-times lower than in corresponding wild-type mice.

We next examined whether the altered concentrations of circulating biliverdin and bilirubin associated with *Bvra* deficiency disturb heme oxygenase expression. We performed semi-quantitative RT-PCR to measure *Hmox1* and *Hmox2* mRNA, the two isoforms of heme oxygenases that initiate heme degradation. We observed no difference in hepatic *Hmox1* and *Hmox2* mRNA between *Bvra*$^{+/+}$ and *Bvra*$^{-/-}$ mice (Fig. 3.3C), indicating that *Bvra* deficiency does not affect heme oxygenase expression. Together, these findings show that the *Bvra*$^{-/-}$ mouse represents a suitable novel model to examine the role of bilirubin as an endogenous antioxidant.

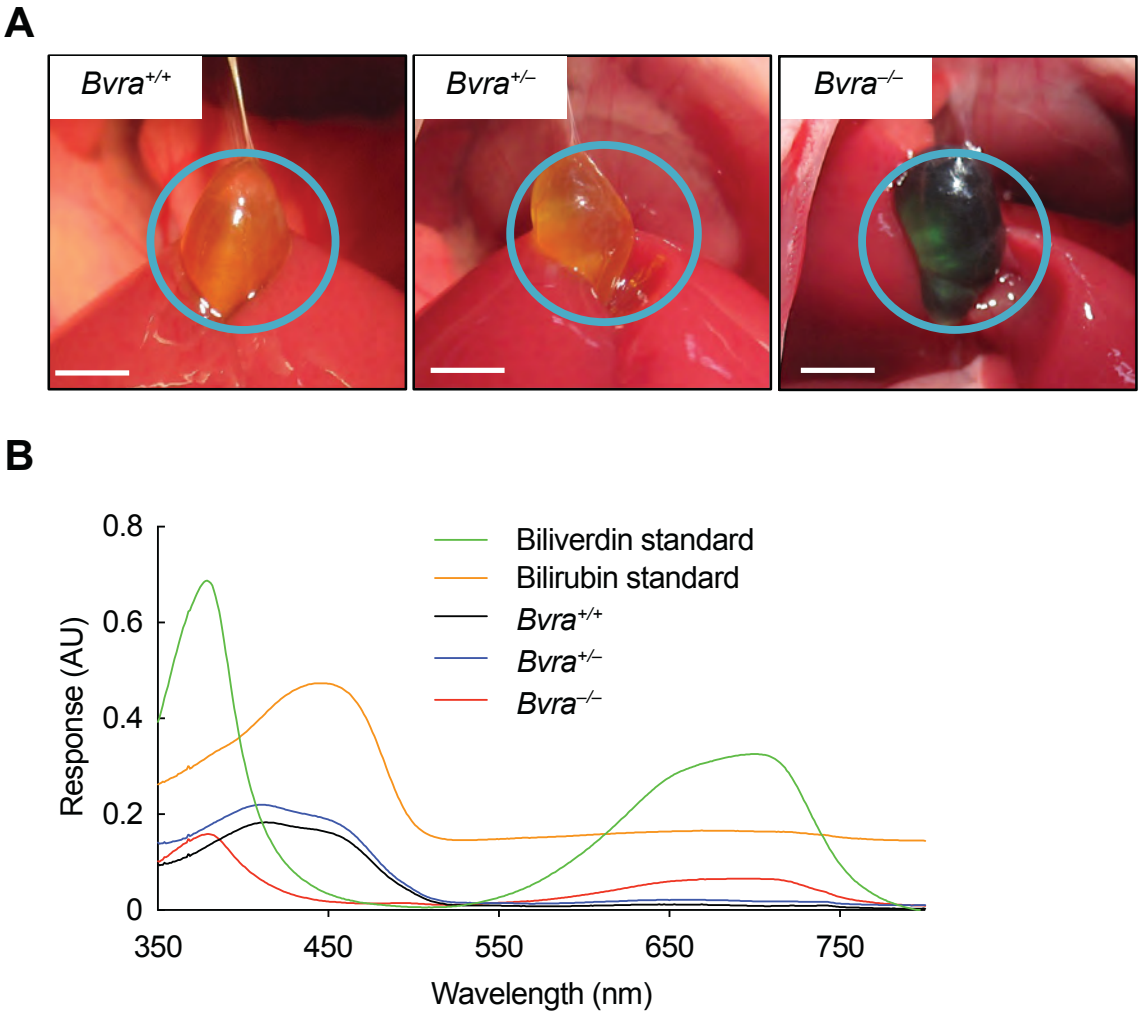

Figure 3.2 Analysis of bile pigments in gall bladder. **(A)** Photos of representative gall bladders of *Bvra*$^{+/+}$, *Bvra*$^{+/-}$ and *Bvra*$^{-/-}$ littermate mice. Scale bar represents 2 mm. **(B)** Typical UV/Vis spectra of biliary pigments in *Bvra*$^{+/+}$, *Bvra*$^{+/-}$ and *Bvra*$^{-/-}$ mice. Spectra were measured in 1 cm path length cuvettes with the reference sample as described in Materials and Methods.

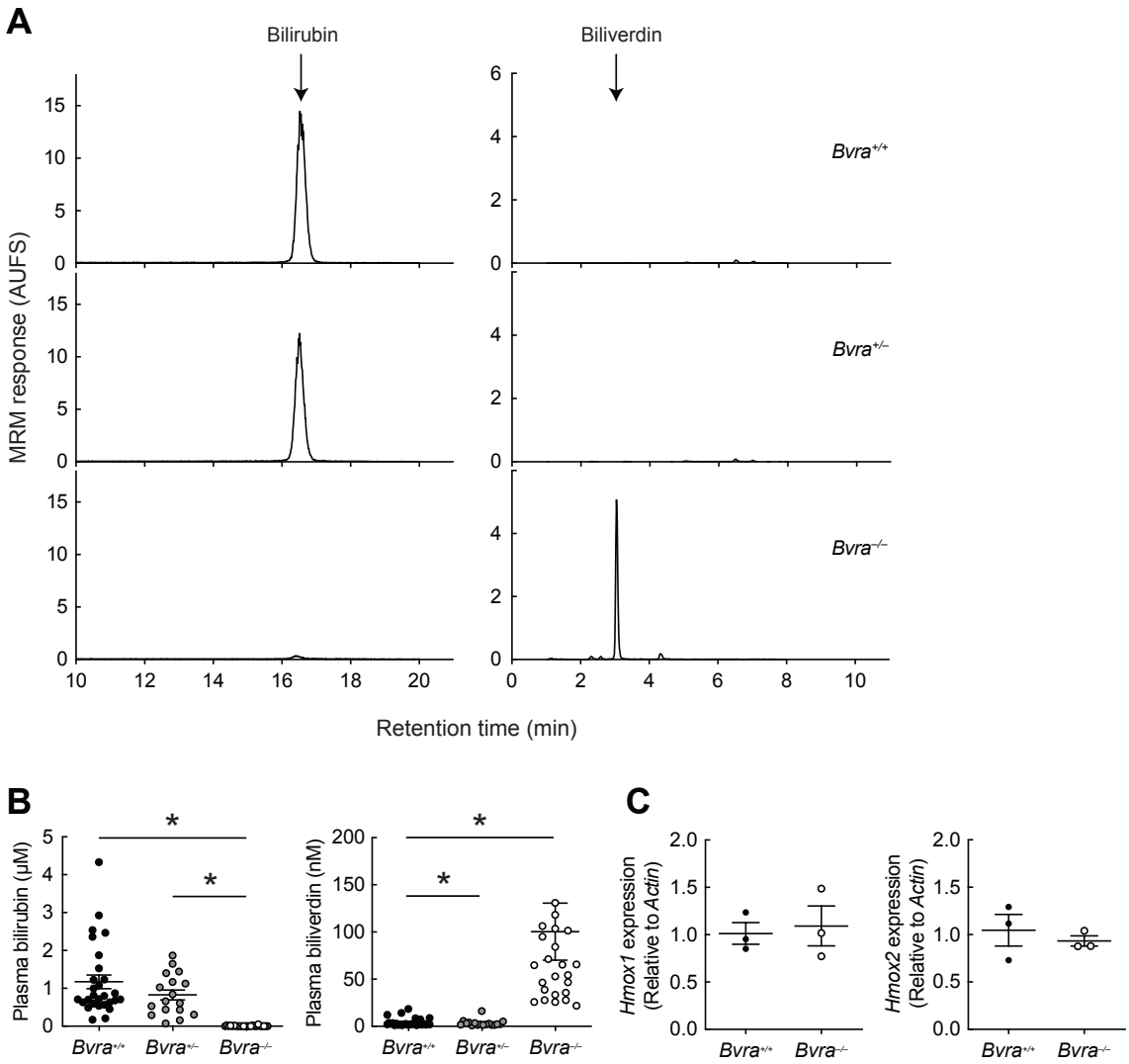

Figure 3.3 Analysis of bile pigments in plasma. **(A)** Typical LC-MS/MS chromatogram of bilirubin and biliverdin in plasma of *Bvra*$^{+/+}$, *Bvra*$^{+/-}$ and *Bvra*$^{-/-}$ mice. **(B)** Quantification of plasma bile pigments in *Bvra*$^{+/+}$, *Bvra*$^{+/-}$ and *Bvra*$^{-/-}$ mice. Results in (**B**) are expressed as mean ± SEM; n = 29 *Bvra*$^{+/+}$ (black filled circles), n = 17 *Bvra*$^{+/-}$ (grey filled circles) and n = 26 *Bvra*$^{-/-}$ mice (open circles). Data was analyzed by the Kruskal-Wallis test with Dunn's multiple comparison. *P<0.05. **(C)** Semi-quantitative RT-PCR of *Hmox1* and *Hmox2* mRNA transcripts in liver from *Bvra*$^{+/+}$ and *Bvra*$^{-/-}$ mice. Results in **(C)** are expressed as mean ± SEM; n = 3 *Bvra*$^{+/+}$ (black filled circles) and n = 3 *Bvra*$^{-/-}$ (open circles) mice.

3.3.4 *Bvra* deficiency increases endogenous oxidative stress

Compared with wild-type littermates, plasma of *Bvra*$^{-/-}$ mice contained significantly higher concentrations of CE-OOH, the major form of reactive oxidized lipids in plasma (Fig. 3.4B). The nature of CE-OOH, eluting with retention times of 8-9 min (Fig. 3.4B arrow) was confirmed by sodium borohydride treatment of the organic phase, which eliminated these chemiluminescence positive peaks (Fig. 3.4C). CE-OOH eluted as two peaks, with the earlier and later peak co-eluting with standards of C20:4-OOH and C18:2-OOH, respectively (Fig. 3.4C). When normalized to CE, the difference in plasma CE-OOH content between *Bvra*$^{-/-}$ and *Bvra*$^{+/+}$ mice became even more apparent, with the former having a 2-fold higher ratio compared with wild-type littermates (Table 3.5). The observed increase in both α-TOH/CE and CE-OOH/CE could be explained by α-TOH-mediated peroxidation (TMP), as reported previously (305, 306) and elaborated upon further in the Discussion. The above parameters were also measured in *Bvra*$^{+/-}$ mice, but no significant differences were observed between *Bvra*$^{+/-}$ and *Bvra*$^{+/+}$ littermates. Phosphatidylcholine hydroperoxides (PC-OOH) are another form of reactive oxidized lipids indicative of oxidative stress. We therefore also analyzed the aqueous methanol phase of the plasma extracts for the presence of PC-OOH by HPLC with post-column chemiluminescence as described previously (290, 291). Using this method, and a detection limit for PC-OOH of 0.8 pmol, we were unable to detect PC-OOH in plasma of either *Bvra*$^{+/+}$ or *Bvra*$^{-/-}$ mice (data not shown). This could be explained by PC-OOH being readily reduced by plasma glutathione peroxidase and lecithin–cholesterol acyltransferase (307).

The ratio of ubiquinol to ubiquinone in plasma has been suggested to be an index of oxidative stress (308). To determine the ratio of ubiquinol to ubiquinone (also known as the coenzyme Q redox ratio), we used coulometric multi-electrode electrochemical detection. We specifically assessed plasma ubiquinone-9 and ubiquinol-9 that are the major forms of coenzyme Q in mouse. We observed no difference in the redox ratio or absolute concentrations of ubiquinone-9 and ubiquinol-9 between *Bvra*$^{+/+}$ and *Bvra*$^{-/-}$ mice (Table 3.5). Approximately 86% of the coenzyme Q was present as ubiquinol-9 and the coenzyme Q redox ratio was unaffected by increased oxidized lipids and α-TOH, indicating that the redox state of coenzyme Q is tightly controlled in the circulation, which matches previous observations in humans (308, 309). While ubiquinol-10 is the first-line antioxidant in the lipid phase of human plasma (310), ascorbic acid is the first-line antioxidant in the aqueous phase (293, 311). Ascorbic acid has been shown to effectively synergize with α-TOH and to inhibit TMP (305, 312). However, we observed no significant difference in plasma ascorbic acid concentrations between *Bvra*$^{+/+}$ and *Bvra*$^{-/-}$ mice (Table 3.5).

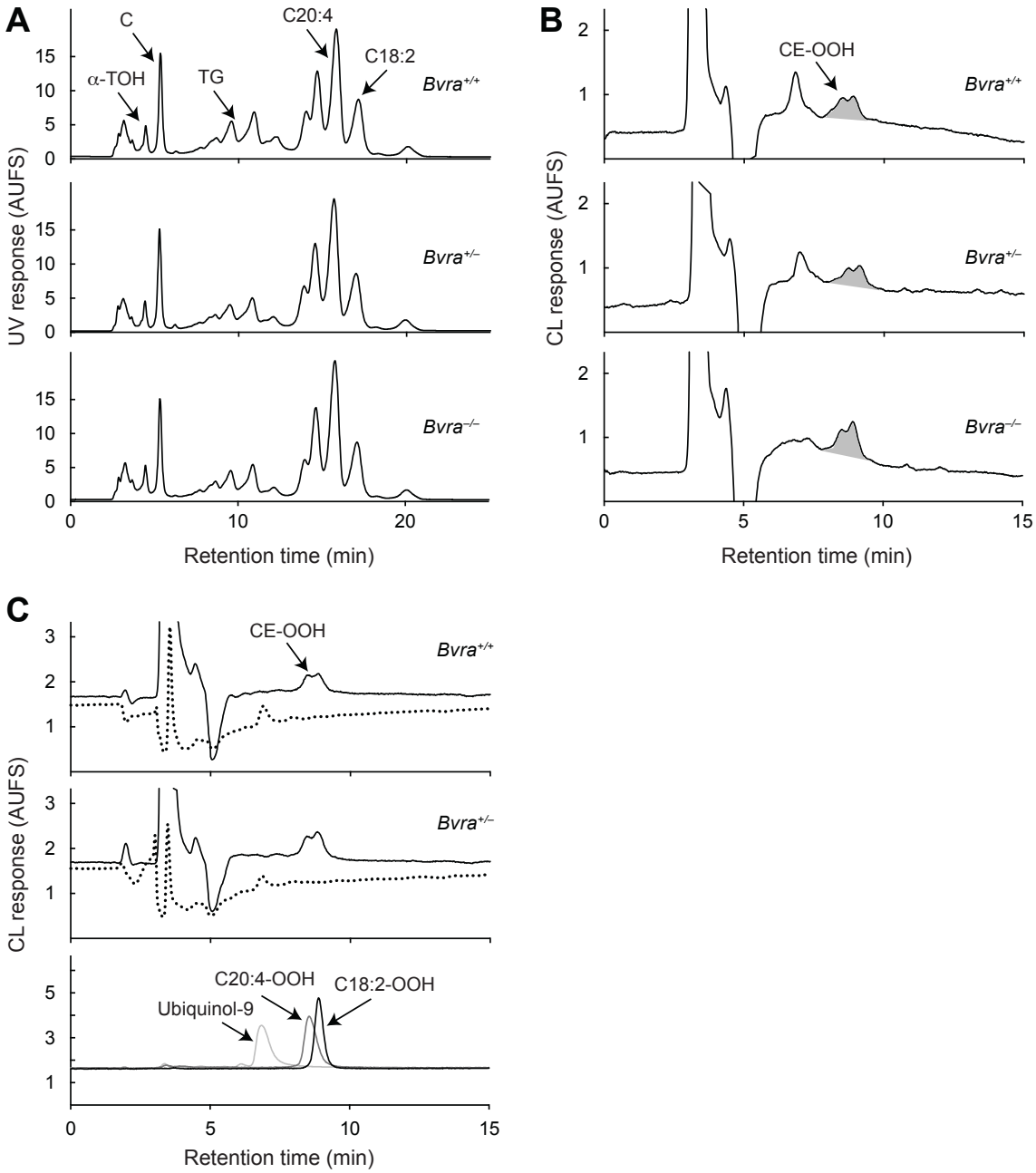

Figure 3.4 Plasma cholesterylester hydroperoxides (CE-OOH) in *Bvra*$^{+/+}$, *Bvra*$^{+/-}$ and *Bvra*$^{-/-}$ mice. **(A)** Chromatographic separation of plasma lipids from *Bvra*$^{+/+}$, *Bvra*$^{+/-}$ and *Bvra*$^{-/-}$ mice detected at 214 nm. Peak assignments: α-TOH, α-tocopherol; C, cholesterol; TG, triglycerides; C20:4, cholesterylarachidonate; C18:2, cholesteryllinoleate. **(B)** HPLC post-column chemiluminescence chromatogram of plasma extracts prepared from *Bvra*$^{+/+}$, *Bvra*$^{+/-}$ and *Bvra*$^{-/-}$ mice. **(C)** Chemiluminescence chromatograms of organic extracts prepared from plasma of *Bvra*$^{+/+}$ and *Bvra*$^{-/-}$ mice with (broken line) and without (solid line) prior sodium borohydride treatment (top, middle); and standards of ubiquinol-9, C20:4-OOH and C18:2-OOH (bottom). Chemiluminescence was recorded at 0.2 μA.

Table 3.5 Concentrations of selected lipids, oxidized lipids and antioxidants in plasma of *Bvra*$^{+/+}$, *Bvra*$^{+/-}$ and *Bvra*$^{-/-}$ mice

	Bvra$^{+/+}$	*Bvra*$^{+/-}$	*Bvra*$^{-/-}$
C18:2 (μM)	517 ± 28	544 ± 30	481 ± 30
C20:4 (μM)	245 ± 17	234 ± 19	209 ± 16
CE (μM)	762 ± 41	777 ± 45	690 ± 42
CE-OOH (nM)[a]	3.5 ± 0.4	5.5 ± 0.8	6.2 ± 0.8*
CE-OOH/CE (μmol/mol)[a]	4.8 ± 0.6	7.4 ± 1.1	9.3 ± 1.3*
α-TOH (μM)	6.4 ± 0.4	6.8 ± 0.4	6.9 ± 0.4
α-TOH/CE (mmol/mol)	8.8 ± 0.5	9.1 ± 0.6	10.2 ± 0.5*
CoQ_9H_2 (nM)[b]	204 ± 14	ND	199 ± 13
CoQ_9 (nM)[b]	34.0 ± 3.9	ND	31.8 ± 4.4
Total coenzyme Q_9 (nM)[b]	238 ± 16	ND	231 ± 14
Coenzyme Q_9 redox ratio (%)[b]	85.9 ± 1.1	ND	86.0 ± 1.7
Ascorbic acid (μM)[c]	81.3 ± 3.9	ND	78.5 ± 5.4

Results show mean ± SEM, with n = 31 *Bvra*$^{+/+}$, n = 19 *Bvra*$^{+/-}$ and n = 28 *Bvra*$^{-/-}$ except where indicated otherwise.

[a]Outliers, defined >2 standard deviations from the mean, have been excluded in the measurement of CE-OOH and CE-OOH/CE ratio (n = 2 *Bvra*$^{+/+}$ and n = 1 *Bvra*$^{-/-}$).

[b]Coenzyme Q_9 redox ratio (n = 9 *Bvra*$^{+/+}$ and n = 11 *Bvra*$^{-/-}$);

[c]Ascorbic acid concentration (n = 12 *Bvra*$^{+/+}$ and n = 12 *Bvra*$^{-/-}$);

Abbreviations: C18:2, cholesteryllinoleate; C20:4, cholesterylarachidonate; CE represents C18:2 plus C20:4; CE-OOH, cholesterylester hydroperoxides; α-TOH, α-tocopherol; CoQ_9H_2, ubiquinol-9; CoQ_9, ubiquinone-9; ND, not determined.

*P<0.05 compared with *Bvra*$^{-/-}$ mice, using Kruskal-Wallis test with Dunn's multiple comparison.

3.3.5 *Bvra* deficiency alters Prx2 redox state

Endogenous oxidative stress was also examined in freshly isolated erythrocytes, using oxidized peroxiredoxin 2 (Prx2) as a marker. Peroxiredoxins are thiol-dependent peroxidases that play a key role in cellular antioxidant defense. Prx2 is the third most abundant protein in erythrocytes. Upon reaction with peroxides, Prx2 monomers are oxidized to dimers that are easily detected by Western blotting. As such, an increase in the Prx2 dimer-to-monomer ratio reflects increased oxidative stress (313, 314). We found that freshly isolated erythrocytes from *Bvra*$^{-/-}$ mice contained a higher proportion of Prx2 as dimer compared with erythrocytes from *Bvra*$^{+/-}$ and *Bvra*$^{-/-}$ littermate mice (Figs 3.5A and 3.5B). This indicated that in *Bvra* deficiency RBC experience increased endogenous oxidative stress.

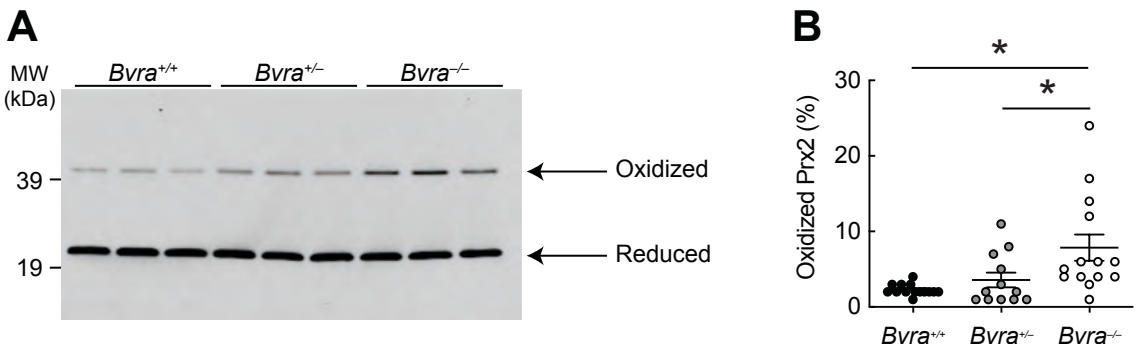

Figure 3.5 Oxidative stress in red blood cells of naïve *Bvra*$^{+/+}$, *Bvra*$^{+/-}$ and *Bvra*$^{-/-}$ mice. The peroxiredoxin-2 (Prx2) dimer to total Prx2 ratio in red blood cells (RBC) was assessed as a measure of oxidative stress. Prx2 cysteine residues were alkylated by addition of 200 mM *N*-ethylmaleimide to blood and incubation for one hour. **(A)** Representative Western blot showing the dimeric (oxidized) and monomeric (reduced) Prx2 in RBC of *Bvra*$^{+/+}$, *Bvra*$^{+/-}$ and *Bvra*$^{-/-}$ mice. **(B)** Densitometric analysis of Prx2 Western blots obtained from RBC of littermate *Bvra*$^{-/-}$ and *Bvra*$^{+/+}$ mice. Results in **(B)** are expressed as mean ± SEM; n = 16 *Bvra*$^{+/+}$ (black filled circles), n = 13 *Bvra*$^{+/-}$ (grey filled circles) and n = 15 *Bvra*$^{-/-}$ (open circles) mice. Data was analyzed by the Kruskal-Wallis test with Dunn's multiple comparison. *P<0.05.

3.4 Discussion

In this study, we generated and characterized a *Bvra* gene deficient mouse. *Bvra*$^{-/-}$ mice had very low concentrations of plasma bilirubin accompanied by modestly elevated plasma biliverdin. Consistent with these changes, and most strikingly, bile of *Bvra*$^{-/-}$ mice appeared green reflecting the presence of biliverdin as the major bile pigment in these animals. The almost complete absence of bilirubin from plasma makes *Bvra*$^{-/-}$ mice a useful and novel tool to address the physiological roles of bilirubin. Focusing on the role of circulating bilirubin as an endogenous antioxidant, we show that *Bvra* deficiency heightened systemic endogenous oxidative stress, as indicated by increases in plasma CE-OOH, CE-OOH/CE and oxidized erythrocyte Prx2.

In C57BL/6J mice, high-density lipoproteins (HDL) are the major lipoproteins and carrier of readily oxidizable lipids. Among lipoprotein-associated lipids, C18:2 and C20:4 represent the major targets for peroxidation because they contain bisallylic hydrogen atoms that are sensitive to hydrogen abstraction. Expressing antioxidants and CE-OOH per CE (C18:2 + C20:4) is therefore a relevant measure for assessing antioxidant sufficiency and oxidative stress (315). While a variety of oxidants may give rise to lipid hydroperoxides, the observed parallel increase in plasma CE-OOH, CE-OOH-to-CE ratio and α-TOH-to-CE ratio in *Bvra*$^{-/-}$ compared with *Bvra*$^{+/+}$ mice in our study can be explained readily by TMP (316). Accordingly, lipoprotein-associated α-TOH can display neutral, anti-, or pro-oxidant activity under different conditions (317). TMP is prevented by co-antioxidants, *i.e.*, compounds that reduce α-TO$^{\bullet}$ to α-TOH and therefore prevent α-TO$^{\bullet}$ from initiating lipid peroxidation (312). The major endogenous co-antioxidants in plasma are ubiquinol, ascorbate and albumin-bound bilirubin (187). The present results suggest that the absence of albumin-bound bilirubin is responsible for the increased concentration of CE-OOH observed in *Bvra*$^{-/-}$ mice. This is because *Bvra*$^{-/-}$ mice essentially lack albumin-bound bilirubin, while plasma concentrations of ubiquinol and ascorbate were comparable in *Bvra*$^{-/-}$ and *Bvra*$^{+/+}$ mice. In particular, mouse plasma contains only low concentrations of lipoprotein-associated ubiquinol, around 25% of that in human plasma, so that the majority of lipoprotein particles including HDL are devoid of ubiquinol. Thus, unlike the situation in humans and low density lipoprotein (312), ubiquinol may not play a major role as endogenous co-antioxidant in mouse plasma/lipoproteins. Similarly, we observed no change in plasma ascorbate between *Bvra*$^{-/-}$ and *Bvra*$^{+/+}$ mice, but increased CE-OOH. This is consistent with our previous observation that bilirubin is consumed despite the presence of ascorbate when human plasma is exposed to controlled oxidation (187). The results suggest that, at least under some conditions, plasma ascorbate does not fully outcompete albumin-bound bilirubin for reaction with α-TOH radical. Additionally, intracellular ascorbate of RBC, which is immersed in plasma, is able to donate electrons to the ascorbate radical in plasma via a plasma membrane redox system (318). Such a redox system enables the RBC to effectively counteract oxidative processes, and thereby preventing depletion of ascorbate in plasma.

A second line of evidence for bilirubin deficiency being associated with increased oxidative stress comes from our observation that RBC Prx2 was more oxidized in *Bvra*$^{-/-}$ compared with littermate *Bvra*$^{+/+}$ mice, as indicated by the increase in the Prx2 dimer-to-monomer ratio. Prx2 is the third most abundant protein in RBC and plays a key role in reducing H_2O_2 and other hydroperoxides. In RBC, Prx2 highly interacts with enzymatic antioxidants (*e.g.,* superoxide dismutase, catalase and glutathione peroxidase) and non-enzymatic antioxidants (*e.g.,* ascorbate and α-TOH) to balance intracellular or extracellular oxidative stress via a plasma membrane redox system (319). Therefore the redox state of Prx2 in RBC is a sensitive readout for lipid peroxidation and oxidative stress in blood (297, 320). In the case of *Bvra*$^{-/-}$ mice, the increase of oxidized Prx2 in RBC indicates intracellular antioxidants have been consumed to donate electrons to protect against extracellular oxidative stress induced by TMP, in some way, explains that antioxidants, *e.g.,* ascorbate, remain similar in plasma of *Bvra*$^{+/+}$ and *Bvra*$^{-/-}$ mice.

Bilirubin is now recognized as an antioxidant (2, 185). In particular, albumin-bound bilirubin protects circulating lipoprotein-associated lipids from oxidation and it effectively prevents TMP of CE via reduction of lipoprotein-associated α-TO$^{\bullet}$ *in vitro* (187). Consistent with these earlier reports, our findings suggest that bilirubin contributes significantly to this antioxidant defense *in vivo*. Our studies do not directly establish whether such antioxidant activity results from the pigment itself or involves BVRA. Indeed, a BVRA-mediated redox cycle has been proposed to explain the antioxidant activity of bilirubin (143, 144). However, such action appears unlikely to explain our observations, for two reasons. First, the BVRA-dependent redox cycle has been proposed for cellular bilirubin/BVRA whereas circulating CE-OOH are formed in the extracellular space, and the increase in RBC Prx2 dimer cannot be explained by differences in cellular BVRA content because RBC do not contain BVRA. Second, the relevance of the proposed BVRA-mediated 'redox cycle' has been questioned (145), in part due to the fact that bilirubin oxidation does not yield stoichiometric amounts of biliverdin for re-reduction to bilirubin (146). Therefore, we interpret our current findings as evidence for bilirubin to directly contribute to the *in vivo* antioxidant defense under physiological (non-stressed) conditions.

Previous studies employing a rat model of Gilbert syndrome have shown elevated concentrations of plasma bilirubin to protect against oxidative stress induced by exposure to hyperoxia (194). In that model, an inverse association between serum bilirubin and serum vitamin E (representing α-, β- and γ-tocopherols) was reported, consistent with the increase in the α-TOH-to-CE ratio observed in *Bvra*$^{-/-}$ mice in the present study. To assess whether the observed changes in the α-TOH-to-CE ratio was caused by differences in the 'retention' of α-TOH, we examined the expression of hepatic α-tocopherol transfer protein (TTP), which plays a key role in determining the plasma concentration of α-TOH (321). We observed no significant difference in *Ttpa* mRNA between *Bvra*$^{+/+}$ and *Bvra*$^{-/-}$ littermate mice (data not shown). Additional studies are

required to examine possible differences in the tissue protein content of TTP between *Bvra*$^{+/+}$ and *Bvra*$^{-/-}$ mice.

The extent of antioxidant protection implied by the increase in oxidative stress observed in *Bvra*$^{-/-}$ versus *Bvra*$^{+/+}$ mice is modest. This is not surprising, given that the plasma concentration of bilirubin in *Bvra*$^{+/+}$ mice is only ~1 μM, while plasma α-TOH, ubiquinol-9 and ascorbate are around 6.5, 0.2 and 80 μM, respectively. A comparatively greater effect would be expected in humans, given that plasma from healthy adults contains ~10 μM bilirubin (322), 40 μM α-TOH, 1 μM ubiquinol-10 and 60 μM ascorbate (310, 323).

Bvra$^{-/-}$ mice showed signs of several modest hematological aberrations, including a mild microcytic anemia characterized by an increase of RBC numbers and MCHC, and a decrease in MCV and MCH. These differences were far less severe than those observed in *Hmox1*$^{-/-}$ mice (324). It remains unknown whether the observed minor alterations of RBC number, MCV, MCH and MCHC in *Bvra* deficiency are the cause or result of oxidative stress. A previously described model of conditional *Bvra*$^{-/-}$ deficiency did not report any hematological changes (125). Despite these differences, *Bvra*$^{-/-}$ mice appeared otherwise healthy compared with littermate *Bvra*$^{+/+}$ animals. Similarly, homozygous mutations resulting in the complete absence of BVRA activity in adult humans are not associated with any apparent signs of an abnormal phenotype other than the appearance of 'green jaundice' in association with cholestasis (127).

In our experiments we compared *Bvra*$^{-/-}$ mice also with their *Bvra*$^{+/-}$ littermates. Despite BVRA protein expression in *Bvra*$^{+/-}$ mice being approximately 50% of that in *Bvra*$^{+/+}$ littermates, no significant differences in plasma biliverdin and bilirubin concentrations were detected. This result indicates that BVRA is highly efficient in reducing biliverdin to bilirubin, consistent with a previous kinetic study of BVRA enzymatic activity (123). Notwithstanding the complete absence of *Bvra* mRNA and BVRA protein in *Bvra*$^{-/-}$ mice, extremely low concentrations of bilirubin were detectable in the plasma. The residual bilirubin detected in *Bvra*$^{-/-}$ mice could conceivably be derived from BVRB. Both biliverdin IX and bilirubin IX exists as four isomers: IXα, IXβ, IXγ and IXδ, of the α-isomer is the predominant form produced from biliverdin IXα in most adult mammals (97). BVRB catalyzes the reduction of only the IXβ, IXγ and IXδ (98), while BVRA can reduce all four biliverdin isomers. To ascertain a potential role of BVRB in the formation of the residual bilirubin detected in *Bvra*$^{-/-}$ mice would require an analytical method capable of distinguishing the different bilirubin isomers which, unfortunately, was not the case with the LC-MS/MS method employed in the present study.

In conclusion, we report a phenotypic characterization of naïve mice deficient in *Bvra*. *Bvra*$^{-/-}$ mice are characterized by elevated levels of biliverdin in plasma and bile, reminiscent of the 'green jaundice' described for *BVRA*-deficient humans subjects with loss of BVRA enzyme activity (127). *Bvra*$^{-/-}$ mice appear healthy under normal physiological conditions despite the

almost complete absence of bilirubin. Closer examination of biochemical parameters indicates that *Bvra*$^{-/-}$ mice have increased endogenous oxidative stress as evidenced by elevated plasma CE-OOH and increased oxidation of Prx2 in RBC. Future investigations will utilize this mouse strain to establish whether there is a direct link between bilirubin and protection against atherosclerosis and related CVD.

Chapter 4

Bvra deficiency renders mice susceptible to hepatic steatosis in the absence of insulin resistance

This chapter contains work with:

Chen W, Dunn LL, Fazakerley D, Cantley J, Tumanov S, Suarna C, Stocker R. *Bvra* deficiency renders mice susceptible to hepatic steatosis in the absence of insulin resistance. Unpublished

Author contributions:

Chen W, Fazakerley D, Cantley J, Dunn LL and Stocker R designed the studies.

Chen W carried out the characterization of the metabolic phenotype in *Bvra*$^{-/-}$ mice. Dunn LL taught Chen W intraperitoneal injection, GTT, ITT, tissue collection, histology and molecular biology/gene expression. Cantley J assisted with preparing HFHS diet and the design of the study. Fazakerly D assisted with the design of the HF diet, and initial glucose uptake and insulin signaling studies. Suarna C and Stocker R designed and initially helped out with the HLPC analysis of lipids. Tumanov S and Suarna C initially helped with the LC-MS/MS analysis of bile pigments

The specific aims for this chapter are:

1) To investigate the impact of *Bvra* deficiency in glucose metabolism and insulin sensitivity using two animal models of diet-induced insulin resistance

2) To study the role of BVRA and/or bilirubin in hepatic lipid accumulation in the setting of insulin resistance.

4.1 Introduction

Metabolic syndrome, including obesity, insulin resistance, hypertension and dyslipidemia, confers an increased risk of cardiovascular and metabolic diseases (325, 326). Non-alcoholic fatty liver disease (NAFLD) is becoming increasingly common around the world and is associated with many features of metabolic syndrome (281). NAFLD is characterized by hepatic lipid accumulation and progresses from hepatic steatosis (fatty liver), through non-alcoholic steatohepatitis to fibrosis and eventually cirrhosis and liver injury (282, 327). Although the mechanism of NAFLD development remains unclear, the most accepted hypothesis is that NAFLD progresses by the "multiple parallel hits" including insulin resistance, inflammation, lipotoxicity, and oxidative stress (282). It is conceivable that modifying these factors may attenuate the development and progression of NAFLD, thereby preventing liver injury.

Bilirubin, a product of heme catabolism, has several potential protective properties against NAFLD progression, involving antioxidant properties (2, 3), anti-inflammatory activities (4), and the ability to regulate lipid metabolism (8). The antioxidant activity of bilirubin protects against systematic oxidative stress (126), which is linked to the development of hepatocyte injury and progression. The anti-inflammatory properties of bilirubin are proposed to regulate acute and chronic hepatic inflammation in animal models (207, 328). Bilirubin also reduces hepatic lipid accumulation via activation of peroxisome proliferator-activated receptor-α (PPARα) to regulate genes involved in the β-oxidation pathway (7, 8). Equally important, biliverdin reductase A (BVRA), an enzyme that generates bilirubin, has the ability to attenuate hepatic steatosis via inhibition of glycogen synthase kinase (GSK)/PPARα signaling pathway (125). In parallel with these experimental results, epidemiological studies consistently show that plasma concentrations of bilirubin inversely associate with the risk of hepatic steatosis (283, 284).

An additional key factor in the pathogenesis of NAFLD and metabolic syndrome is insulin resistance. Bilirubin has been postulated to modulate glucose metabolism and insulin signaling (19, 20). Administration of bilirubin improves insulin sensitivity in obese and diabetic mice via the insulin receptor/PI3K/Akt signaling pathway (207). A mouse model of humanized hyperbilirubinemia protected against high-fat (HF)-fed induced insulin insensitivity and glucose intolerance (7). Moreover, BVRA is proposed to be a regulator of glucose metabolism and a transcription factor to modulate insulin signaling (23). BVRA may serve as a unique serine/threonine/tyrosine kinase, modulating phosphorylation of the insulin receptor substrate (IRS)-1 and other targets of the insulin/insulin-like growth factor (IGF)-1 signaling pathway (16). Correspondingly, a liver specific *Bvra*-deficient mouse exhibited impaired phosphorylation of hepatic Akt, higher glucose and insulin concentrations in plasma, as well as peripheral glucose intolerance. In agreement with these experimental results, a large human study of 16,000 human participants showed that high concentration of serum bilirubin is associated with a low incidence of type 2 diabetes mellitus (a disease that starts with insulin resistance) (271). Individuals with

serum total bilirubin >10 μM had a 20% lower risk of developing diabetes compared to those with lower bilirubin. Likewise, a number of studies have shown that people with Gilbert syndrome (moderately elevated plasma bilirubin due to a mutation in UGT1A1, the enzyme that conjugates bilirubin for biliary excretion) have a decreased risk of abnormal glucose tolerance and insulin resistance, and decreased prevalence of metabolic syndrome (272-275).

Based on the above studies, we hypothesized that bilirubin and/or BVRA protect(s) against metabolic diseases via the modulation of hepatic lipid accumulation and insulin resistance. To test this hypothesis, we fed global *Bvra*-deficient (*Bvra*$^{-/-}$) mice, a mouse model of bilirubin deficiency, a HF diet or a high fat high sucrose (HFHS) diet to induce hepatic steatosis and insulin resistance, respectively. We observed that *Bvra*-deficient mice exhibited enhanced hepatic steatosis as assessed by increased hepatic lipids. In contrast, plasma lipids, fasted plasma glucose, glucose and insulin tolerance, as well as insulin signaling were not altered in *Bvra*$^{-/-}$ compared with littermate *Bvra*$^{+/+}$ mice. These results indicate that bilirubin and/or BVRA render(s) mice susceptible to hepatic steatosis in the absence of insulin resistance.

4.2 Materials and Methods

4.2.1 Animals

The *biliverdin reductase a* gene-deficient (*Bvra*$^{-/-}$) mice have been previously described in Chapter 3. *Bvra*$^{+/+}$ and *Bvra*$^{-/-}$ littermates were obtained from *Bvra*$^{+/-}$ x *Bvra*$^{+/-}$ breeding in the BioCORE facility at the Victor Chang Cardiac Research Institute and used for all experiments described. Male mice at 7 ± 1 weeks of age were used for the experiments. All mice were housed in a temperature-controlled room on a 12 h light/dark cycle and were allowed access to water and food *ad libitum*. All procedures were carried out according to the Australian National Health & Medical Research Council Guidelines for Animal Research and were approved by the Animal Care and Ethics Committee of the Garvan Institute of Medical Research/St Vincent's Hospital.

4.2.2 Collection of tissue samples

Mice were euthanized with an overdose of Lethobarb (100 μL of 80 mg/mL, Virbac, Australia) via intraperitoneal injection. Blood samples were collected by cardiac puncture using a 26-gauge needle and transferred into heparin-coated microtubes (Sarstedt, Germany). To obtain plasma, heparinized blood was centrifuged at 2,000 x *g* and 4 °C for 15 min. Epididymal fat pads and liver were collected and weighed and processed for further analysis, or snap frozen and stored at -80 °C until analysis. Tail tips were collected to confirm the genotype of all experimental mice.

4.2.3 Diets

Animals were fed a standard chow diet containing 13% calories from fat, 22% calories from protein, and 65% calories from carbohydrate, 3.1 kcal/g (#27, Gordons Specialty Feeds,

Australia) until they were allocated to a study involving high fat (HF) or high fat high sucrose (HFHS) diet. In the HF diet study, mice were fed for up to 14 weeks a HF diet that was formulated based on D12492 (Research Diet, Inc) containing 60, 20 and 20% calories from fat, protein and carbohydrate, respectively, and 5.2 kcal/g (SF13-092, Specialty Feeds, Australia). In the HFHS diet study, mice were maintained for up to 6 weeks a HFHS diet based on D12451 (Research Diets, Inc) containing 47, 21 and 32% calories from fat, protein and carbohydrate, respectively, and 4.7 kcal/g (in-house).

4.2.4 *Ex vivo* glucose uptake into adipose tissue explants

Glucose uptake into epididymal adipose tissue explants was measured as described previously in **Section 2.3.4** of Chapter 2 (285).

4.2.5 Fasted and non-fasted blood glucose

Blood samples were obtained via tail vein of conscious mice, with or without a prior 8 or 16 h fast. Blood glucose concentrations were determined using an Accu-Chek Performa Blood Glucose Meter (Roche, Switzerland).

4.2.6 Glucose tolerance and insulin tolerance test

To perform the glucose tolerance test (GTT), mice received 1 or 2 g/kg glucose via intraperitoneal injection of a 10% glucose solution (INJ128, Phebra, Australia) after an 8 or 16 h fast. Blood was collected via tail bleeding at 0, 15, 30, 60, 90 and 120 min for measurement of blood glucose using an Accu-Chek Performa Blood Glucose Meter (Roche, Switzerland) and plasma insulin using an ultra-sensitive mouse insulin ELISA (90080, Crystal Chem, IL, USA). To perform the insulin tolerance test (ITT), mice received insulin (Actrapid, Penfill, Novo Nordisk, Australia) at 0.75 U/kg via intraperitoneal injection after an 8 h fast. Blood samples were obtained via tail bleeding at 0, 15, 30, 60, 90 and 120 min for blood glucose measurement by Accu-Chek Performa Blood Glucose Meter.

4.2.7 Histology

Histological analysis of liver and epididymal fat pads has been described in **Section 2.6.1** of Chapter 2.

4.2.8 HPLC analysis of hepatic and plasma lipids

Lipid analysis of liver and plasma by HPLC detection has been described in **Section 2.4.5** of Chapter 2.

4.2.9 *In vivo* glucose uptake into epididymal adipose tissue

Glucose uptake into epididymal adipose tissue was measured as described previously in **Section 2.2.3** of Chapter 2.

4.2.10 LC-MS/MS detection for bilirubin and biliverdin in liver and plasma

Bilirubin and biliverdin in liver and plasma were determined by LC-MS/MS using a 6490 Triple Quadrupole LC-MS/MS (Agilent Technologies, CA, USA) and described in detail in **Section 2.4.4** of Chapter 2.

4.2.11 RNA extraction and analysis

Detailed procedures of RNA extraction, complementary DNA (cDNA) synthesis, real-time quantitative PCR have been described in **Section 2.5.1**. The amount of mRNA was normalized to *Gapdh* mRNA and presented relative to the corresponding wild-type control using the comparative CT method (295). PCR products were verified by melt curve analysis.

4.2.12 Western blot

Tissues (30 mg) were homogenized in 600 μL RIPA buffer (50 mM Tris-HCl, pH 7.5, 150 mM NaCl, 1% (v/v) Triton X-100, 0.5% (w/v) sodium deoxycholate, 0.1% (w/v) SDS, 1 mM EDTA, 10% (v/v) glycerol) supplemented with protease inhibitor cocktail (Roche, Switzerland). Protein concentration of the homogenate was determined by BCA assay. Detailed procedures of SDS-PAGE and immunoblotting have been described in **Section 2.5.2** of Chapter 2.

4.2.13 Statistical analyses

Unless indicated otherwise, statistical analysis was performed using GraphPrism 8 software. Results are expressed as mean values with error bars representing standard error of the mean (SEM). The Mann-Whitney rank-sum test or two-way ANOVA analysis of variance was used to determine statistical significance, as appropriate. A P-value of <0.05 was considered as statistically significant.

4.3 Results

4.3.1 Hepatic lipids, glucose and insulin tolerance, as well as insulin sensitivity are normal in naïve global BVRA-deficient mice

To assess the role of BVRA in metabolic syndrome, we generated global *Bvra* gene knockout (*Bvra*$^{-/-}$) mice (126) that also serve as a mouse model of bilirubin deficiency. Consistent with their concentrations of plasma bile pigments (126), *Bvra*$^{-/-}$ mice had very low concentrations of hepatic bilirubin (0.32 ± 0.05 pmol/mgp) compared with littermate *Bvra*$^{+/+}$ mice, *i.e.*, 2.91 ± 0.28 pmol/mgp (Fig. 4.1A), as determined by LC-MS/MS analysis. Instead, livers of *Bvra*$^{-/-}$ mice had

elevated biliverdin; *i.e.*, 2.64 ± 0.11 pmol/mgp compared with 0.89 ± 0.05 pmol/mgp for *Bvra*$^{+/+}$ animals (Fig. 4.1B). Overall, the total concentration of bile pigments in the livers of *Bvra*$^{+/+}$ and *Bvra*$^{-/-}$ mice were comparable, *i.e.,* 3.8 ± 0.3 and 3.0 ± 0.1 pmol/mgp, respectively. Fed standard chow diet, *Bvra*$^{+/+}$ and *Bvra*$^{-/-}$ mice exhibited comparable body weight at the age of 7 ± 1 weeks (Fig. 4.1C). Also, hepatic triglycerides (TG), cholesterol and cholesterylesters (CE) were comparable between *Bvra*$^{-/-}$ and wild-type littermates (Figs. 4.1D to 4.1F).

Bvra$^{+/+}$ and *Bvra*$^{-/-}$ littermate mice showed no significant difference in non-fasted blood glucose concentrations (Fig. 4.1G). To determine whether *Bvra* deficiency alters glucose utilization and/or glucose catabolism, GTT and ITT were performed. Following intraperitoneal injection of glucose (1g/kg), blood glucose and plasma insulin concentrations were similar in *Bvra*$^{-/-}$ and *Bvra*$^{+/+}$ littermates (Figs. 4.1H to 4.1J). Likewise, compared to *Bvra*$^{+/+}$ mice, the *Bvra*$^{-/-}$ littermates had comparable insulin tolerance evident by blood glucose concentrations during ITT (Fig. 4.1K and 4.1L).

Since insulin resistance appears in adipose tissue before skeletal muscle and liver, and insulin resistance in the adipose can influence whole body insulin sensitivity (329, 330), we assessed glucose uptake and insulin sensitivity in adipose tissue using [^{3}H] 2-deoxy-D-glucose (2-DOG) and different doses of insulin. We observed no significant difference in glucose uptake between the two genotypes (Fig. 4.1M). Consistent with this, we observed no significant difference in the expression of glucose transporter type 4 (GLUT4, the major regulator of glucose uptake in adipose tissue) between *Bvra*$^{+/+}$ and *Bvra*$^{-/-}$ mice (Fig. 4.1N). Moreover, BVRA did not affect insulin signaling, as indicated by the comparable extent of phosphorylation of Akt and AS160 (which regulate glucose storage and GLUT4 translocation), in the adipose explants treated with different doses of insulin (Fig. 4.1O and 4.1P). Together, these results indicate that global *Bvra* deficiency does not affect hepatic lipids, glucose and insulin tolerance, as well as insulin sensitivity of mice fed standard chow diet.

Figure 4.1

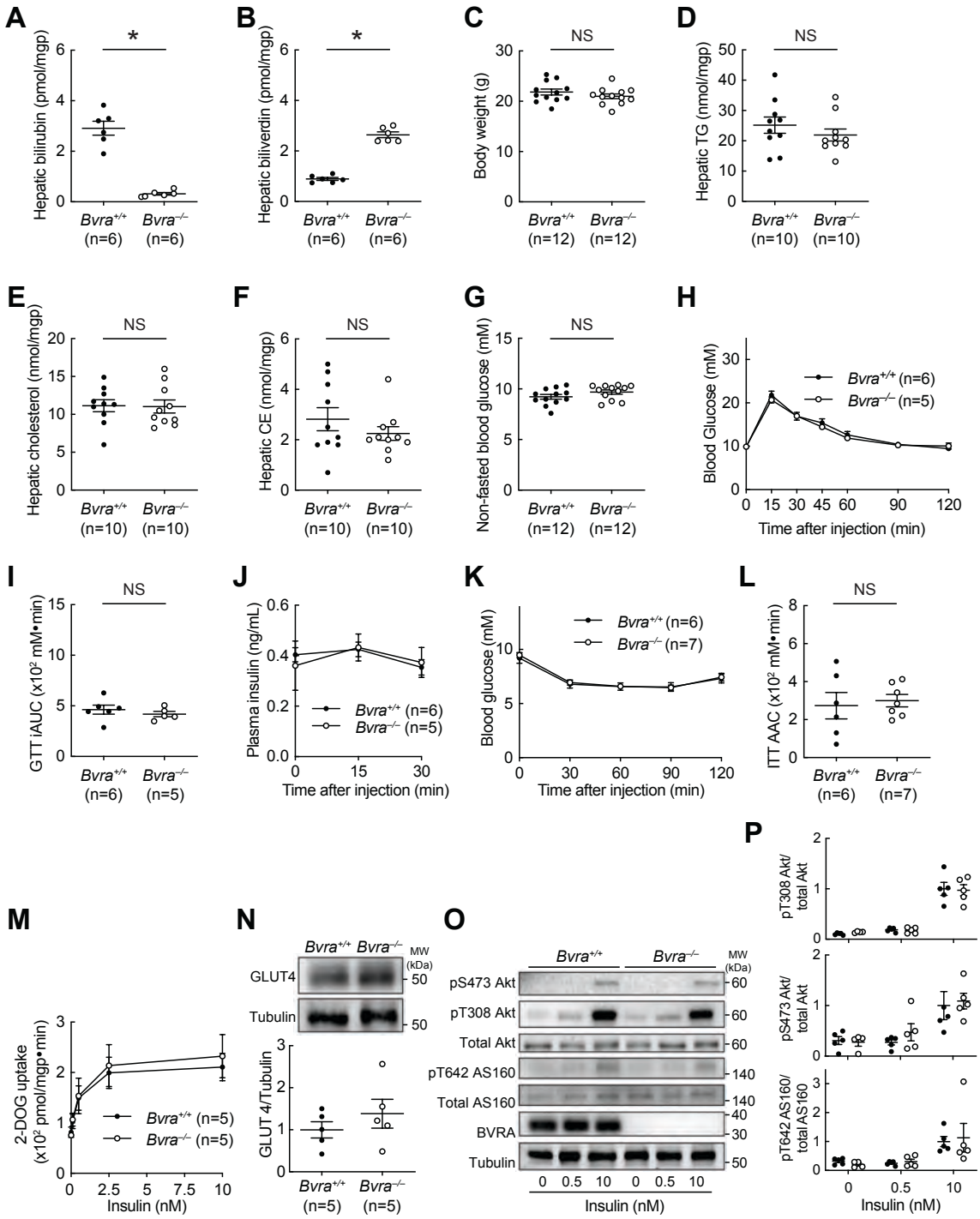
A
Hepatic bilirubin (pmol/mgp)
*
Bvra+/+ (n=6)
Bvra−/− (n=6)
B
Hepatic biliverdin (pmol/mgp)
*
Bvra+/+ (n=6)
Bvra−/− (n=6)
C
Body weight (g)
NS
Bvra+/+ (n=12)
Bvra−/− (n=12)
D
Hepatic TG (nmol/mgp)
NS
Bvra+/+ (n=10)
Bvra−/− (n=10)
E
Hepatic cholesterol (nmol/mgp)
NS
Bvra+/+ (n=10)
Bvra−/− (n=10)
F
Hepatic CE (nmol/mgp)
NS
Bvra+/+ (n=10)
Bvra−/− (n=10)
G
Non-fasted blood glucose (mM)
NS
Bvra+/+ (n=12)
Bvra−/− (n=12)
H
Blood Glucose (mM)
Bvra+/+ (n=6)
Bvra−/− (n=5)
Time after injection (min)
I
GTT iAUC (x10² mM•min)
NS
Bvra+/+ (n=6)
Bvra−/− (n=5)
J
Plasma insulin (ng/mL)
Bvra+/+ (n=6)
Bvra−/− (n=5)
Time after injection (min)
K
Blood glucose (mM)
Bvra+/+ (n=6)
Bvra−/− (n=7)
Time after injection (min)
L
ITT AAC (x10² mM•min)
NS
Bvra+/+ (n=6)
Bvra−/− (n=7)
M
2-DOG uptake (x10² pmol/mgp•min)
Bvra+/+ (n=5)
Bvra−/− (n=5)
Insulin (nM)
N
Bvra+/+ Bvra−/−
MW (kDa)
GLUT4
Tubulin
GLUT 4/Tubulin
Bvra+/+ (n=5)
Bvra−/− (n=5)
O
Bvra+/+
Bvra−/−
MW (kDa)
pS473 Akt
pT308 Akt
Total Akt
pT642 AS160
Total AS160
BVRA
Tubulin
Insulin (nM)
P
pT308 Akt/ total Akt
pS473 Akt/ total Akt
pT642 AS160/ total AS160
Insulin (nM)

Figure 4.1 Hepatic lipids, glucose tolerance, insulin sensitivity and insulin signaling are normal in naïve global *Bvra*$^{-/-}$ mice. **(A**, **B)** Concentration of hepatic biliverdin and bilirubin in naïve *Bvra*$^{+/+}$ and *Bvra*$^{-/-}$ mice. Bile pigments were measured by LC-MS/MS, with results normalized to protein content (mgp). Data was analyzed by the Mann-Whitney test. **P*<0.05. **(C)** Body weight of *Bvra*$^{+/+}$ and *Bvra*$^{-/-}$ mice fed standard chow diet at 7±1 weeks age. **(D-F)** Concentrations of hepatic triglycerides (TG), cholesterol and cholesterylesters (CE) in naïve *Bvra*$^{+/+}$ and *Bvra*$^{-/-}$ mice. Hepatic lipids were analyzed by HPLC-UV, with results normalized to protein content (mgp). **(G)** Blood glucose concentrations of non-fasted *Bvra*$^{+/+}$ and *Bvra*$^{-/-}$ mice fed standard chow diet. **(H)** Blood glucose concentrations following intraperitoneal glucose tolerance test (GTT, 1 g/kg glucose) to fasted (8 hours) *Bvra*$^{+/+}$ (n = 6) and *Bvra*$^{-/-}$ (n = 5) mice fed standard chow diet. **(I)** Incremental area under curve (iAUC) for blood glucose concentrations following GTT in Fig. 4.1H. **(J)** Plasma insulin concentrations following GTT (1 g/kg glucose) to fasted (8 hours) *Bvra*$^{+/+}$ (n = 6) and *Bvra*$^{-/-}$ mice (n = 5) previously fed standard chow diet. **(K)** Blood glucose concentrations following insulin tolerance test (ITT, 0.75 U/kg insulin) to fasted (8 hours) *Bvra*$^{+/+}$ (n = 6) and *Bvra*$^{-/-}$ (n = 7) mice fed standard chow diet. **(L)** Area above curve (AAC) for blood glucose concentrations following ITT in **K**. **(M)** Protein standardized [^{3}H] 2-Deoxy-D-glucose (2-DOG) uptake into adipose tissue explants derived from the epididymal fat pads of *Bvra*$^{+/+}$ (n = 5) and *Bvra*$^{-/-}$ (n = 5) mice after treatment with different concentrations of insulin. The results were normalized to protein content (mgp). **(N)** Representative Western blot of glucose transporter type 4 (GLUT4) in adipose tissue of *Bvra*$^{+/+}$ and *Bvra*$^{-/-}$ mice. Protein expression of GLUT4 in adipose tissue of littermate *Bvra*$^{-/-}$ and *Bvra*$^{+/+}$ mice was quantified by densitometry and normalized to loading control (α-tubulin) and to the expression in the *Bvra*$^{+/+}$ group. **(O)** Representative Western blots of BVRA, Akt and AS160 phosphorylation in adipose tissue of *Bvra*$^{+/+}$ and *Bvra*$^{-/-}$ mice after treatment with different concentrations of insulin. **(P)** Phosphorylation of Ser473 and Thr308 of Akt, and Thr642 of AS160 as assessed by densitometry, and normalized to corresponding total protein content and expressed relative to the 10 nM insulin treatment of *Bvra*$^{+/+}$ group, respectively. n = 5 *Bvra*$^{+/+}$ mice (filled circles) and n = 5 *Bvra*$^{-/-}$ mice (open circles). Numerical results show individual data as well as mean ± SEM.

4.3.2 Deficiency of *Bvra* enhances HF diet-induced hepatic lipid accumulation

As deficiency of *Bvra* does not alter hepatic lipid, glucose tolerance and insulin sensitivity in mice fed standard chow diet, *Bvra*$^{-/-}$ mice were fed HF diet (60% calories from fat) that induces hepatic steatosis and insulin resistance, to investigate the role of BVRA in metabolic syndrome. After 14 weeks HF diet, *Bvra*$^{+/+}$ and *Bvra*$^{-/-}$ littermate mice showed no significant difference in body weight (Fig. 4.2A) and the ratio of liver to bodyweight (Fig. 4.2B), although the mass of epididymal fat pads normalized to body weight, was significantly decreased in *Bvra*$^{-/-}$ compared with wild-type mice (Fig. 4.2C). Compared with *Bvra*$^{+/+}$ animals, *Bvra*$^{-/-}$ mice fed a HF diet showed evidence of hepatic lipid accumulation, indicated by increased Oil Red O-positive staining and the presence of lipid droplets and vacuoles (Figs. 4.2D to 4.2F). Development and progression of hepatic steatosis is linked to *de novo* synthesis of lipid. In agreement with enhanced lipid accumulation in *Bvra*$^{-/-}$ mice fed HF diet, mRNA expression of enzymes involved in lipid synthesis, *i.e.,* acetyl-CoA carboxylase (*Acaca*) and fatty acid synthase (*Fasn*), but not sterol regulatory element-binding transcription factor 1 (*Srebf1*), was increased, compared to the corresponding control littermate mice (Figs. 4.2I to 4.2K). However, we did not observe *Bvra* deficiency to influence the adipose cell size of epididymal fat pads (Figs. 4.2G and 4.2H).

To confirm hepatic lipid accumulation in *Bvra*$^{-/-}$ mice, we used HPLC with UV detection to analyze the content of TG, cholesterol and CE in the livers. Representative UV chromatograms (Fig. 4.3A) indicated differences in the lipid profile between *Bvra*$^{-/-}$ and *Bvra*$^{+/+}$ mice. Specifically, the concentrations of TG and cholesterol were significantly increased in *Bvra*$^{-/-}$ mice compared to wild type littermate mice (551 ± 134 and 38 ± 5 nmol/mgp compared with 237 ± 34 and 25 ± 3 nmol/mgp, respectively (Figs. 4.3B and 4.3C). However, hepatic CE remained were similar (Fig. 4.3D) and we observed no significant difference in plasma cholesterol, CE and TG between the two genotypes fed HF diet (Figs. 4.3E to 4.3G).

Figure 4.2

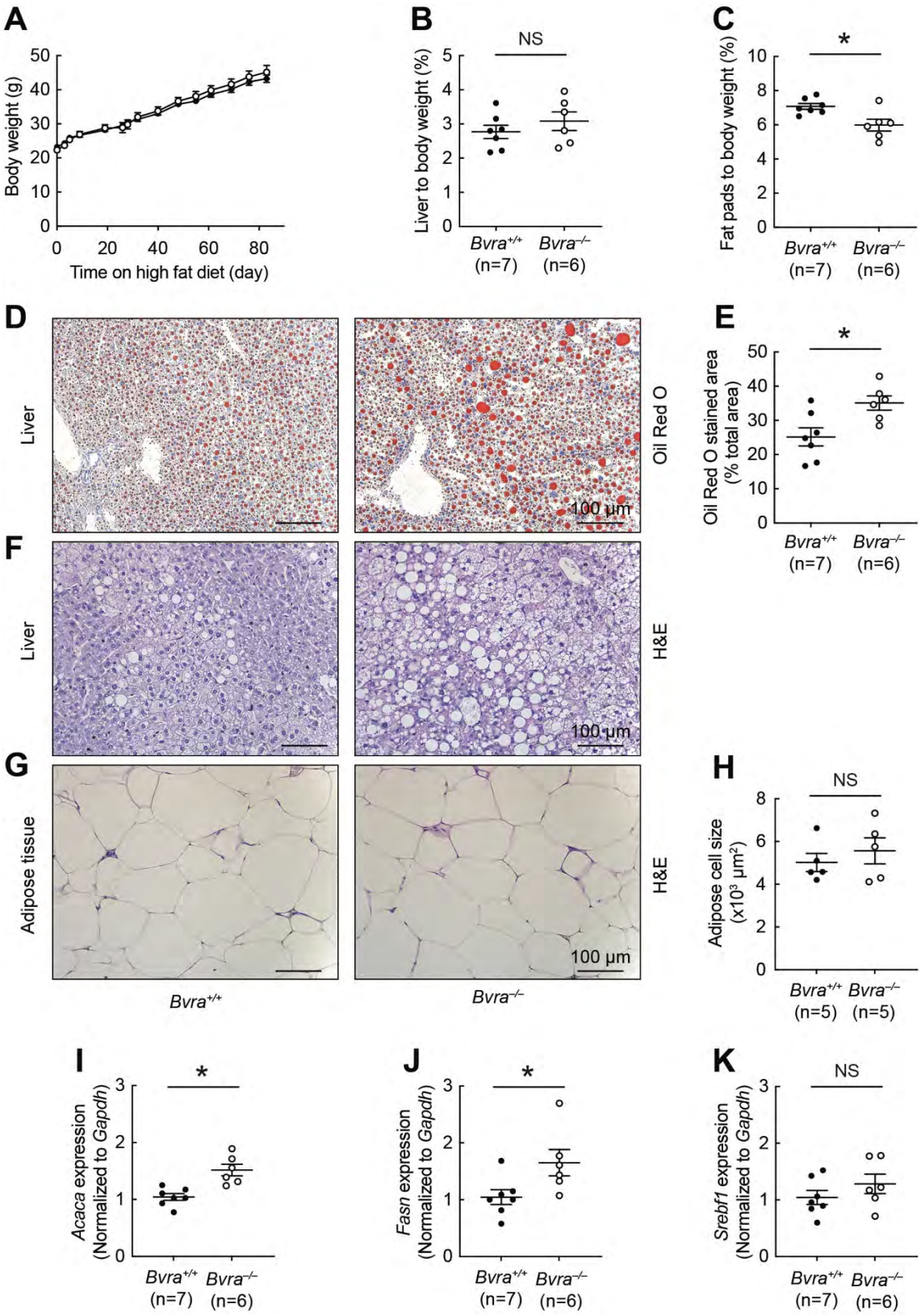
A
Body weight (g)
Time on high fat diet (day)
B
NS
Liver to body weight (%)
Bvra+/+ (n=7)
Bvra−/− (n=6)
C
*
Fat pads to body weight (%)
Bvra+/+ (n=7)
Bvra−/− (n=6)
D
Liver
Oil Red O
100 µm
E
*
Oil Red O stained area (% total area)
Bvra+/+ (n=7)
Bvra−/− (n=6)
F
Liver
H&E
100 µm
G
Adipose tissue
H&E
100 µm
Bvra+/+
Bvra−/−
H
NS
Adipose cell size (x10³ µm²)
Bvra+/+ (n=5)
Bvra−/− (n=5)
I
*
Acaca expression (Normalized to Gapdh)
Bvra+/+ (n=7)
Bvra−/− (n=6)
J
*
Fasn expression (Normalized to Gapdh)
Bvra+/+ (n=7)
Bvra−/− (n=6)
K
NS
Srebf1 expression (Normalized to Gapdh)
Bvra+/+ (n=7)
Bvra−/− (n=6)

Figure 4.2 Deficiency of *Bvra* enhances high-fat (HF) diet induced hepatic lipid accumulation. **(A)** Weekly body mass of *Bvra*$^{+/+}$ and *Bvra*$^{-/-}$ mice fed a HF diet over 12 weeks. n = 12 *Bvra*$^{+/+}$ mice (filled circles) and n = 12 *Bvra*$^{-/-}$ mice (open circles). **(B**, **C)** Mass of liver and epididymal adipose fat pads in male *Bvra*$^{+/+}$ and *Bvra*$^{-/-}$ mice fed HF diet. **(D)** Representative micrographs of Oil Red O stained liver sections of *Bvra*$^{+/+}$ and *Bvra*$^{-/-}$ mice fed HF diet. Scale bar = 100 µm. **(E)** Quantification of Oil Red O stained area of liver sections of *Bvra*$^{+/+}$ and *Bvra*$^{-/-}$ mice fed HF diet. **(F**, **G)** Representative micrographs liver and epididymal adipose fat pad sections stained with H&E from *Bvra*$^{+/+}$ and *Bvra*$^{-/-}$ mice on 14 weeks HF diet. Scale bar = 100 µm. (**H)** Cell size of the adipocyte in epididymal adipose fat pads. **(I-K)** Semi-quantitative RT-PCR of *Acaca, Fasn* and *Srebf1* mRNA transcripts in liver of *Bvra*$^{+/+}$ and *Bvra*$^{-/-}$ mice. Data was analyzed for statistical differences by the Mann-Whitney test. *P<0.05 compared to *Bvra*$^{+/+}$ mice. NS, not significant. All the results in this figure were expressed as mean ± SEM.

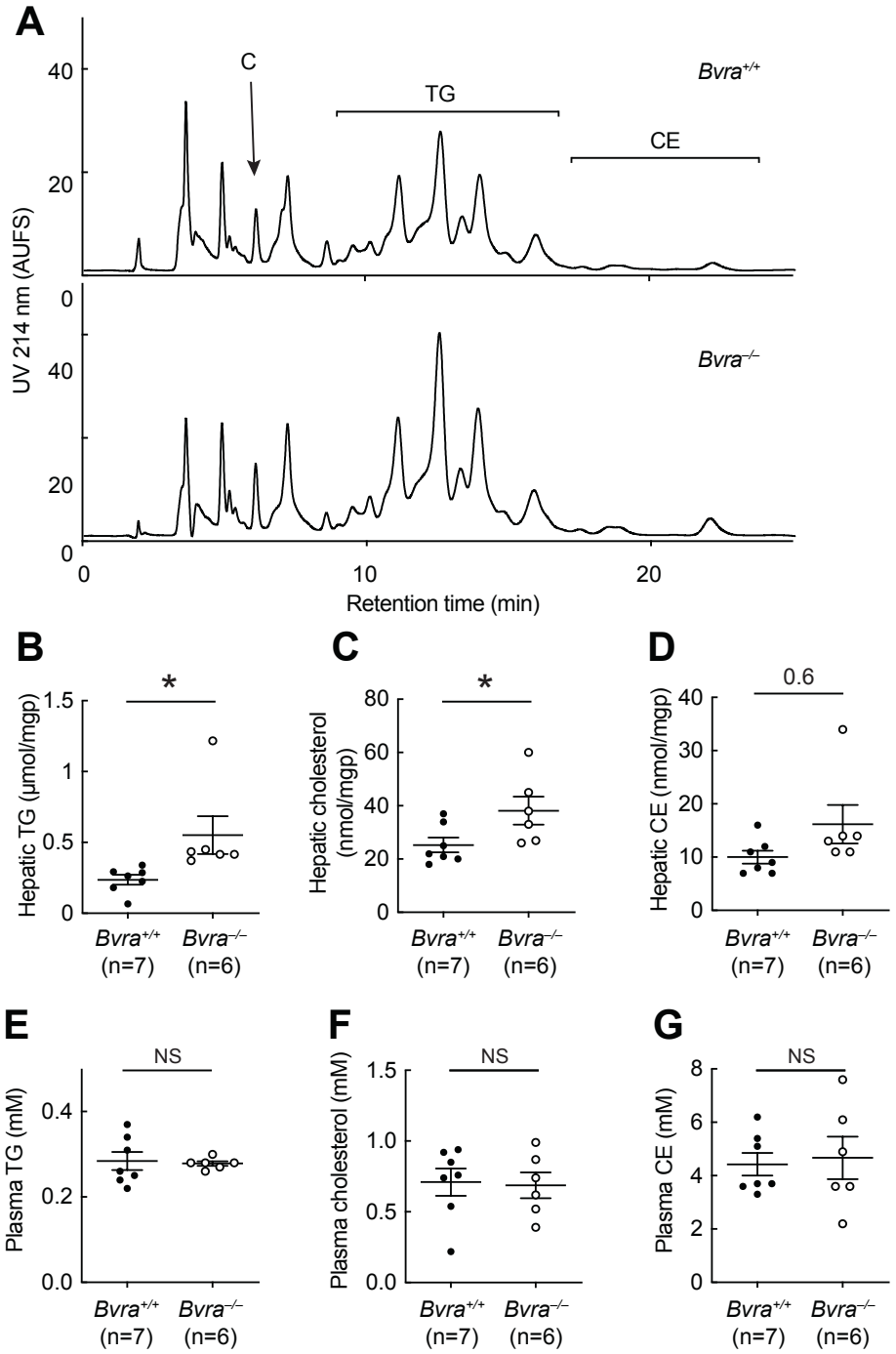

Figure 4.3 Lipid profile of liver and plasma in *Bvra*$^{+/+}$ and *Bvra*$^{-/-}$ mice fed a HF diet. **(A)** Chromatographic separation of hepatic lipids from *Bvra*$^{+/+}$ and *Bvra*$^{-/-}$ mice fed 14 weeks HF diet detected at 214 nm. Peak assignments: C, cholesterol; TG, triglycerides; CE, cholesterylesters. **(B-D)** Hepatic concentrations of TG, cholesterol and CE in *Bvra*$^{+/+}$ and *Bvra*$^{-/-}$ mice fed HF diet. Hepatic lipids were analyzed by HPLC-UV, with results normalized to protein content (mgp). Data was analyzed by the Mann-Whitney test. *P<0.05. **(E-G)** Concentrations of plasma TG, cholesterol and CE in *Bvra*$^{+/+}$ and *Bvra*$^{-/-}$ mice fed HF diet for 14 weeks. Plasma lipids were analyzed by HPLC-UV. Numerical results show individual data as well as mean ± SEM.

4.3.3 Deficiency of bilirubin alters hepatic PPARα expression and activity

We next confirmed the absence of bilirubin in the liver of *Bvra*$^{-/-}$ mice fed HF diet by LC-MS/MS analysis. Compared with corresponding wild-type littermate mice, *Bvra*$^{-/-}$ mice had very low concentrations of hepatic bilirubin (0.2 ± 0.02 versus 3.1 ± 0.5 pmol/mgp for *Bvra*$^{-/-}$ and *Bvra*$^{+/+}$, respectively) while biliverdin was elevated (4.4 ± 0.3 versus 1.3 ± 0.3 pmol/mgp for *Bvra*$^{-/-}$ and *Bvra*$^{+/+}$, respectively) (Figs. 4.4A and 4.4B). Consistently, bilirubin was barely detectable in plasma of *Bvra*$^{-/-}$ mice fed a HF diet, compared with *Bvra*$^{+/+}$mice (Fig. 4.4C). This essential absence of bilirubin in *Bvra*$^{-/-}$ mice was accompanied by an increase in plasma biliverdin (Fig. 4.4D). Bilirubin has recently been reported to regulate lipid metabolism via activation of PPARα (8), just as BVRA regulates PPARα via GSK3β (125). We next examined whether the altered concentrations of hepatic bile pigments associated with *Bvra* deficiency disturbed PPARα expression and activity. Using Western blotting, we observed increased PPARα phosphorylation in livers of *Bvra*$^{-/-}$ mice fed HF diet compared with wild-type controls, while hepatic expression of PPARα were not different (Figs. 4.4E to 4G). This increase in PPARα phosphorylation was associated with decreased mRNA levels of genes targeted by PPARα, including carnitine palmitoyltransferase 1A (*Cpt1a*), cytochrome P450, family 2 (*Cyp2j6*) and cytochrome P450 family 4 (*Cyp4a12*). These results suggest that bilirubin deficiency may affect hepatic PPARα activity in *Bvra*$^{-/-}$ mice, although the mRNA levels of other PPARα targeted genes, such as cluster of differentiation 36 (*Cd36*) and glucose 6-phosphatase (*G6pase*) remained similar in the two genotypes (Fig. 4.4H).

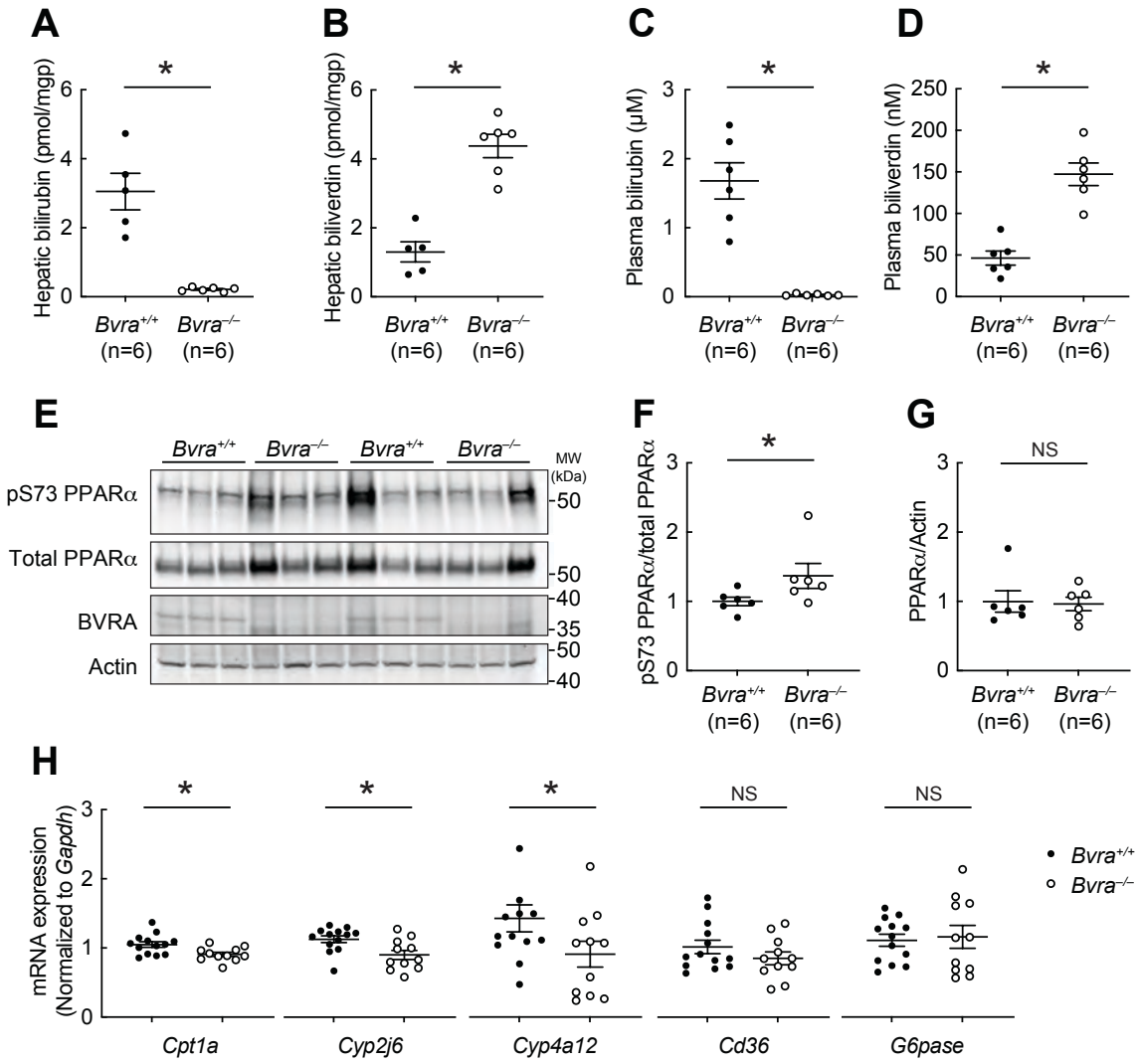

Figure 4.4 Deficiency of *Bvra* and bilirubin regulates PPARα expression and activity in the liver. **(A**, **B)** Hepatic concentrations of biliverdin and bilirubin in *Bvra*$^{+/+}$ and *Bvra*$^{-/-}$ mice fed HF diet for 14 weeks. Bile pigments were measured by LC-MS/MS, with results normalized to protein content (mgp). **(C**, **D)** Plasma concentrations of biliverdin and bilirubin in *Bvra*$^{+/+}$ and *Bvra*$^{-/-}$ mice fed HF diet. **(E)** Western blots of phosphorylation of PPARα in livers of *Bvra*$^{+/+}$ and *Bvra*$^{-/-}$ mice fed HF diet for 14 weeks. **(F**, **G)** Densitometry analysis of expression of PPARα and phosphorylation status of Ser73 in liver. Data was normalized to corresponding total protein content or loading control (actin). **(H)** Semi-quantitative RT-PCR of *Cpt1a*, *Cyp2j6*, *Cyp4a12*, *Cd36* and *G6pase* mRNA transcripts in livers of *Bvra*$^{+/+}$ and *Bvra*$^{-/-}$ mice fed HF diet for 14 weeks. n = 13 *Bvra*$^{+/+}$ mice (filled circles) and n = 11 *Bvra*$^{-/-}$ mice (open circles). Data was analyzed by the Mann-Whitney test. *P<0.05 compared with *Bvra*$^{+/+}$ mice. NS, not significant. Numerical results show individual data as well as mean ± SEM.

4.3.4 *Bvra* deficiency does not alter HF diet-induced glucose intolerance and insulin sensitivity

Insulin resistance has been observed in mice on short- or long-term HF diet as reported in a large number of publications (331-333). After 9 to 10 days of HF diet, mice had an impaired tolerance to glucose and insulin as determined by GTT and ITT (331). Therefore, we next investigated whether BVRA deficiency regulates glucose intolerance and insulin sensitivity in the setting of insulin resistance. Following HF diet, wild-type *Bvra*$^{+/+}$ mice showed impaired tolerance to glucose and insulin (Figs. 4.1I, 4.1L, 4.5C and 4.5F), as reported previously. Littermate *Bvra*$^{-/-}$ mice had fasting blood glucose concentrations comparable to those in *Bvra*$^{+/+}$ mice (Fig. 4.5A). Similar to the naïve mice fed standard chow, there were also no significant differences in glucose or insulin tolerance between *Bvra*$^{-/-}$ and *Bvra*$^{+/+}$ mice fed HF diet (Figs. 4.5B to 4.5F). In GTT (1 g/kg glucose), *Bvra*$^{+/+}$ and *Bvra*$^{-/-}$ mice showed comparable blood glucose and plasma insulin responses (Figs. 4.5B and 4.5D). Similarly, there were also no significant differences in blood glucose concentration in ITT (Figs. 4.5E and 4.5F).

In a direct measurement of insulin sensitivity *in vivo*, BVRA deficiency did not alter responsiveness of mice fed HF diet to insulin as measured by 2-DOG uptake into epididymal fat pads (Fig. 4.5G). Equally, insulin signaling responses including phosphorylation of Akt, AS160, as well as GLUT4 expression in epididymal fat pads were not changed in *Bvra*$^{-/-}$ mice compared with wild-type littermate mice (Figs. 4.5H and 4.5I). These results reflect similar insulin sensitivity in adipose tissues of *Bvra*$^{+/+}$ and *Bvra*$^{-/-}$ mice. Moreover, hepatic phosphorylation of Akt and GSK3β in *Bvra*$^{+/+}$ and *Bvra*$^{-/-}$ mice was comparable (Figs. 4.5J and 4.5K) further demonstrating that deficiency of BVRA did also not alter insulin sensitivity in the liver.

Figure 4.5

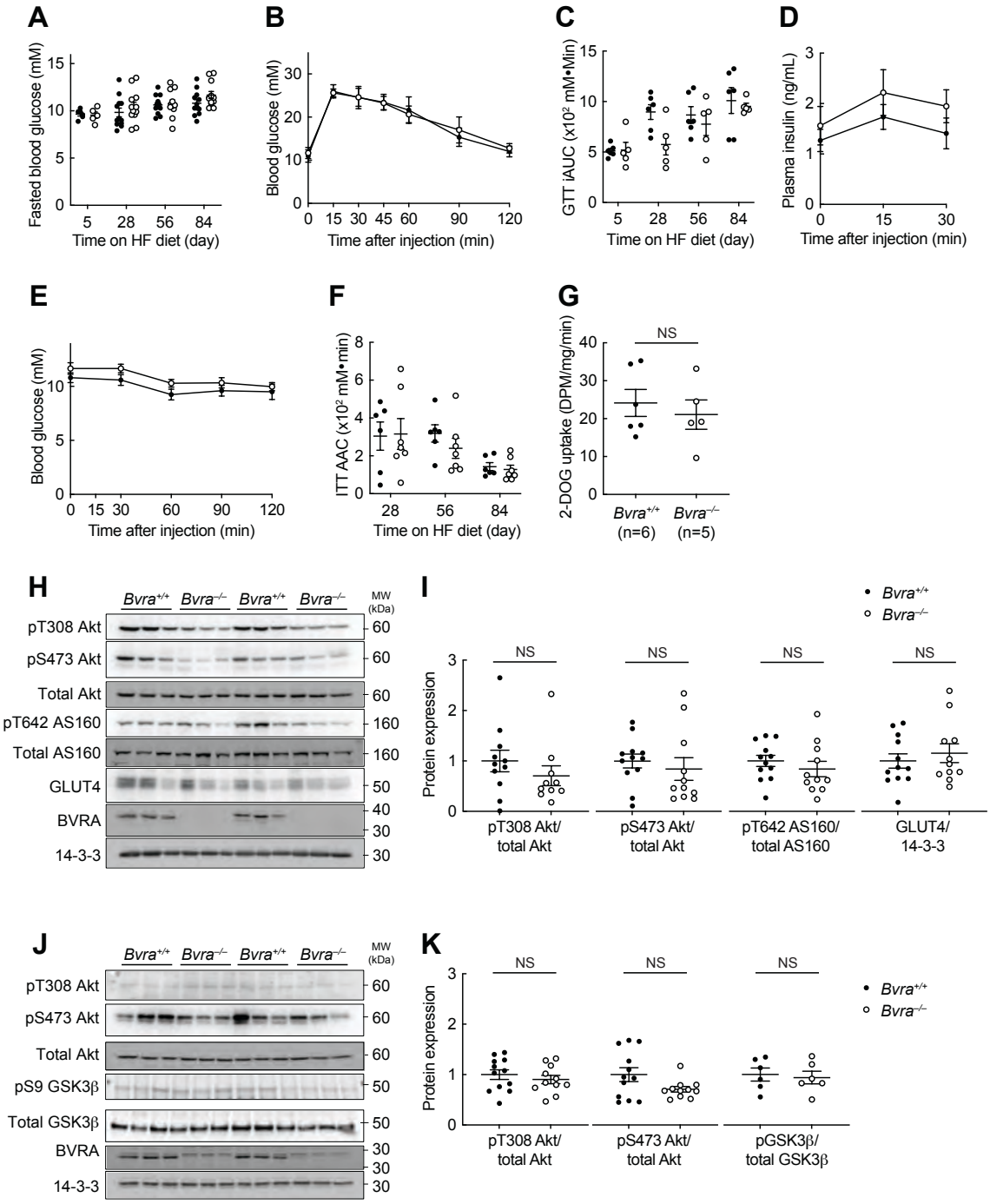
A
Fasted blood glucose (mM)
Time on HF diet (day)
B
Blood glucose (mM)
Time after injection (min)
C
GTT iAUC (x10² mM•Min)
Time on HF diet (day)
D
Plasma insulin (ng/mL)
Time after injection (min)
E
Blood glucose (mM)
Time after injection (min)
F
ITT AAC (x10² mM•min)
Time on HF diet (day)
G
2-DOG uptake (DPM/mg/min)
NS
Bvra+/+ (n=6)
Bvra−/− (n=5)
H
Bvra+/+ Bvra−/− Bvra+/+ Bvra−/−
MW (kDa)
pT308 Akt
pS473 Akt
Total Akt
pT642 AS160
Total AS160
GLUT4
BVRA
14-3-3
I
Bvra+/+
Bvra−/−
Protein expression
NS
pT308 Akt/ total Akt
pS473 Akt/ total Akt
pT642 AS160/ total AS160
GLUT4/ 14-3-3
J
Bvra+/+ Bvra−/− Bvra+/+ Bvra−/−
MW (kDa)
pT308 Akt
pS473 Akt
Total Akt
pS9 GSK3β
Total GSK3β
BVRA
14-3-3
K
Protein expression
NS
pT308 Akt/ total Akt
pS473 Akt/ total Akt
pGSK3β/ total GSK3β
Bvra+/+
Bvra−/−

Figure 4.5 *Bvra* deficiency does not alleviate HF diet-induced glucose intolerance, insulin resistance and insulin signaling. **(A)** Blood glucose concentrations in fasted (8 hours) *Bvra*$^{+/+}$ (n = 12) and *Bvra*$^{-/-}$ mice (n = 12) fed HF diet for 5, 28, 56 and 84 days. **(B)** Blood glucose concentrations following GTT (1 g/kg glucose) in fasted (8 hours) *Bvra*$^{+/+}$ (n = 6) and *Bvra*$^{-/-}$ mice (n = 5) fed HF diet for 84 days. **(C)** iAUC for blood glucose concentrations following GTT (1 g/kg glucose) in fasted (8 hours) *Bvra*$^{+/+}$ (n = 6) and *Bvra*$^{-/-}$ mice (n = 5) fed HF diet for 5, 28, 56 and 84 days. **(D)** Plasma insulin concentrations following GTT (1 g/kg glucose) in fasted (8 hours) *Bvra*$^{+/+}$ (n = 6) and *Bvra*$^{-/-}$ mice (n = 5) fed HF diet for 84 days. **(E)** Blood glucose concentrations following ITT (0.75 U/kg insulin) in fasted (8 hours) *Bvra*$^{+/+}$ (n = 6) and *Bvra*$^{-/-}$ (n = 7) mice fed HF diet for 84 days. **(F)** AAC for blood glucose concentrations following ITT (0.75 U/kg insulin) in fasted (8 hours) *Bvra*$^{+/+}$ (n = 6) and *Bvra*$^{-/-}$ mice (n = 7) fed HF diet for 5, 28, 56 and 84 days. **(G)** Insulin induced 2-DOG uptake into epididymal adipose tissue of *Bvra*$^{+/+}$ and *Bvra*$^{-/-}$ mice fed HF diet for 14 weeks. **(H)** Representative Western blots of BVRA, GLUT4, as well as Akt and AS160 phosphorylation in epididymal adipose tissue of *Bvra*$^{+/+}$ and *Bvra*$^{-/-}$ mice fed HF diet for 14 weeks (two independent experiments). **(I)** Densitometry analysis of expression of GLUT4, phosphorylation of Ser473 and Thr308 of Akt, and Thr642 of AS160 in adipose tissue of *Bvra*$^{+/+}$ (n = 12) and *Bvra*$^{-/-}$ (n = 11) mice. Data was normalized to total protein content or loading control (14-3-3), respectively. **(J)** Representative Western blots of BVRA, phosphorylation of Akt and GSK3β in livers of *Bvra*$^{+/+}$ and *Bvra*$^{-/-}$ mice fed HF diet for 14 weeks (two independent experiments). **(K)** Densitometry analysis of phosphorylation of Ser473 and Thr308 of Akt, and Ser9 of GSK3β in livers of *Bvra*$^{+/+}$ (n = 12) and *Bvra*$^{-/-}$ (n = 11) mice. Data was normalized to total protein content. Numerical results show individual data as well as mean ± SEM. Open and filled circles correspond to *Bvra*$^{-/-}$ and *Bvra*$^{+/+}$ mice, respectively.

4.3.5 *Bvra* deficiency does not affect high fat high sucrose (HFHS) diet-induced glucose intolerance

The HFHS diet represents a more commonly used model of insulin resistance in diabetes studies. Adipose tissue insulin resistance was observed as early as 5 days on the HFHS diet, and this degree of resistance was maintained at 42 days of HFHS diet feeding (285). Fed on HFHS diet, *Bvra*$^{+/+}$ and *Bvra*$^{-/-}$ mice showed similar body weight (Figs. 4.6A). However, hepatic TG in *Bvra*$^{-/-}$ mice was increased in response to 6 weeks HFHS diet (Fig. 4.6B), while no significant difference was observed in hepatic cholesterol and CE between the two genotypes (Figs. 4.6C and 4.6D). *Bvra*$^{-/-}$ and *Bvra*$^{+/+}$ mice had comparable concentrations of fasted blood glucose (Fig. 4.6E). GTT (2 g/kg glucose) was also performed on *Bvra*$^{+/+}$ and *Bvra*$^{-/-}$ mice fed HFHS diet for 5 and 35 days. Again, no significant difference was found in blood glucose and plasma insulin during GTT between *Bvra*$^{+/+}$ and *Bvra*$^{-/-}$ mice fed HFHS diet (Figs. 4.6F to 4.6H).

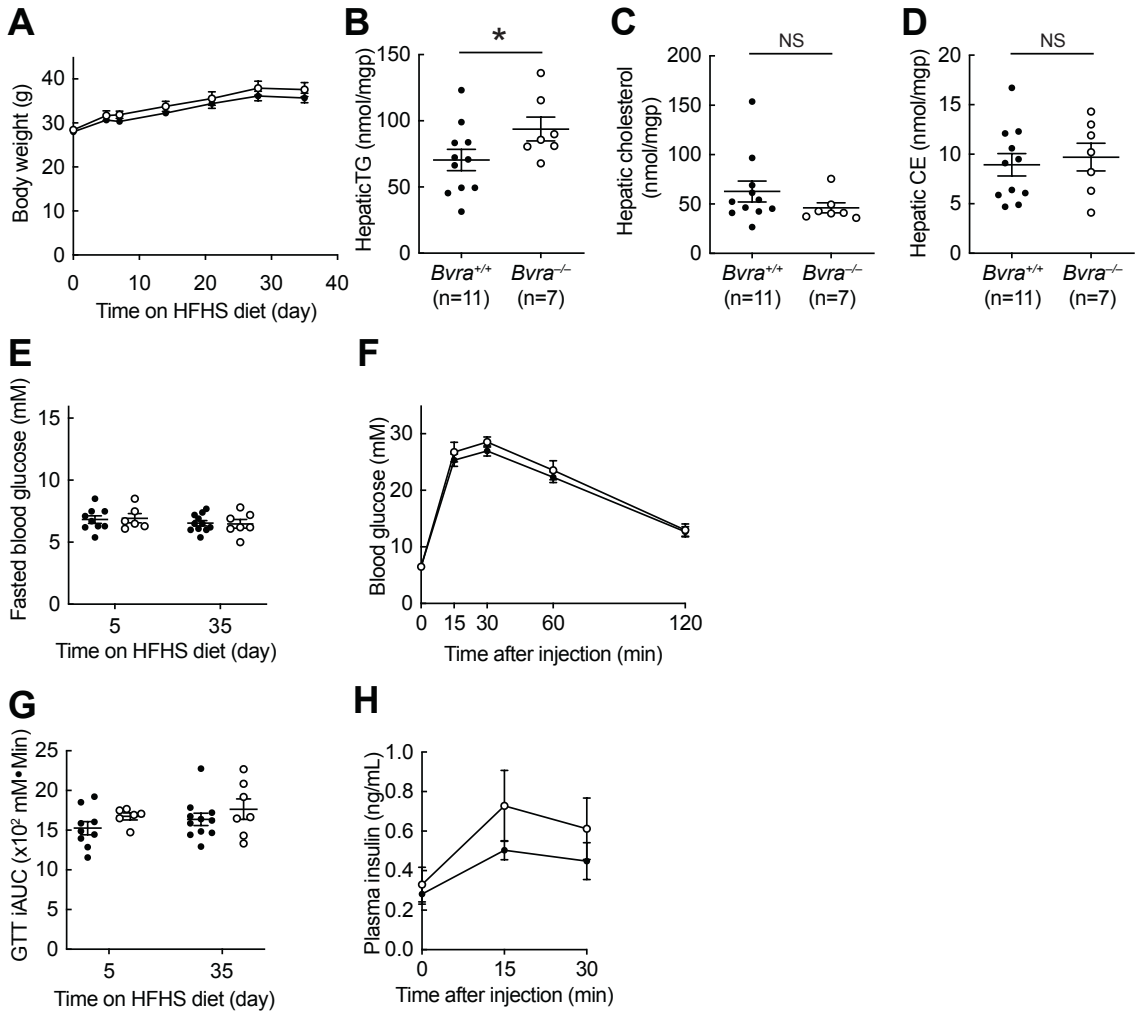

Figure 4.6 *Bvra* deficiency does not affect high fat high sucrose (HFHS) diet-induced glucose intolerance and hepatic lipid accumulation. **(A)** Weekly body mass of *Bvra*$^{+/+}$ (n = 11) and *Bvra*$^{-/-}$ (n = 7) mice fed on a HFHS diet for 5 weeks. **(B-D)** Hepatic concentrations of TG, cholesterol and CE in *Bvra*$^{+/+}$ and *Bvra*$^{-/-}$ mice fed HFHS diet. Hepatic lipids were analyzed by HPLC-UV, with results normalized to protein content (mgp). Data was analyzed by the Mann-Whitney test (one tail). *P<0.05. **(E)** Blood glucose concentrations in fasted (16 hours) *Bvra*$^{+/+}$ (n = 11) and *Bvra*$^{-/-}$ mice (n = 7) fed HFHS diet for 5 and 35 days. **(F)** Blood glucose concentrations following GTT (2 g/kg glucose) in fasted (16 hours) *Bvra*$^{+/+}$ (n = 11) and *Bvra*$^{-/-}$ mice (n = 7) fed HFHS diet for 35 days. **(G)** iAUC for blood glucose concentrations following GTT (2 g/kg glucose) to fasted (16 hours) *Bvra*$^{+/+}$ (n = 11) and *Bvra*$^{-/-}$ mice (n = 7) fed HFHS diet for 5 and 35 days. **(H)** Plasma insulin concentrations following GTT (2 g/kg glucose) in fasted (16 hours) *Bvra*$^{+/+}$ (n = 11) and *Bvra*$^{-/-}$ mice (n = 7) fed HFHS diet for 35 days. Numerical results show individual data as well as mean ± SEM. Open and filled circles correspond to *Bvra*$^{-/-}$ and *Bvra*$^{+/+}$ mice, respectively.

4.4 Discussion

In this study, we characterized the metabolic phenotype of the *Bvra* gene deficient mice by using three different dietary models, namely standard laboratory chow, HF and HFHS diet. Specifically, in the HF diet model, *Bvra*$^{-/-}$ mice exhibited enhanced hepatic steatosis as assessed by increased hepatic mRNA expression of lipogenesis genes, hepatic TG and cholesterol, and Oil-Red-O staining. We also found that the activity of PPARα, which regulates lipid metabolism, was attenuated in the *Bvra*$^{-/-}$ mice fed HF diet. However, compared with littermate wild-type animals, *Bvra*$^{-/-}$ mice fed any of these three diets consistently showed no significant difference in blood glucose and plasma insulin, glucose and insulin tolerance, glucose uptake, and insulin signaling. Together, these results suggest that *Bvra* deficiency renders mice susceptible to hepatic steatosis in the absence of insulin resistance.

Our observation that global BVRA deficiency combined with a HF diet for 14 weeks enhances hepatic steatosis characterized by increases in hepatic TG and cholesterol is consistent with a recent study by Hinds *et al.* reporting that liver-specific knockout of BVRA to cause hepatic steatosis (125). An increase in hepatic TG (but not cholesterol) was also observed in global *Bvra*$^{-/-}$ mice fed HFHS diet for 6 weeks, but not in mice fed standard chow. The duration and the fat ratio of the diet could be the reasons of the modest increase of hepatic lipids in *Bvra*$^{-/-}$ mice fed HFHS diet, compared with the more obvious lipid accumulation in the livers of *Bvra*$^{-/-}$ mice fed HF diet. TG accumulation in the liver occurs when the rate of synthesis exceeds the rate of catabolism of this class of lipids. Enhanced hepatic triglyceride synthesis is the result of increased hepatic *de novo* lipogenesis and/or fatty acid uptake. *De novo* lipogenesis enables the liver to synthesize new fatty acids from acetyl-CoA. Initially, acetyl-CoA is converted to malonyl-CoA by acetyl-CoA carboxylase (encoded by *Acaca*) and malonyl-CoA is then converted to palmitate by fatty acid synthase (encodes by *Fasn*). Fatty acids then undergo a range of desaturation, elongation, and esterification steps before ultimately being stored as TG (334). In agreement with the enhancement of hepatic lipid accumulation, especially hepatic TG, increased hepatic mRNA expression of *Acaca* and *Fasn* was observed in *Bvra*$^{-/-}$ mice. This links that hepatic lipid accumulation in *Bvra*$^{-/-}$ mice to *de novo* lipogenesis. However, hepatic CD36 mRNA, which enhances fatty acid uptake by increasing the rate of intracellular esterification (335), was not changed in *Bvra*$^{-/-}$ mice, compared to the *Bvra*$^{+/+}$ mice, indicating that hepatic lipid accumulation in *Bvra* deficiency may not be due to the hepatic uptake of fatty acids.

Suppression of TG catabolism depends upon fatty acid oxidation and exportation of TG as very low-density lipoproteins. Carnitine palmitoyl transferase 1A mRNA (*Cpt1a*), an essential factor to trigger β-oxidation of long chain fatty acids in mitochondria, was decreased in the *Bvra*$^{-/-}$ mice fed HF diet. Similarly, mRNA expression of family 2 (*Cyp2j6*) and family 4 (*Cyp4a12*) of cytochrome P450 was decreased in *Bvra*$^{-/-}$ mice in response to HF diet. As cytochrome P450 species are involved in the hydroxylation reactions, the first step in fatty acid ω-oxidation, an

alternative pathway to β-oxidation (336), our findings suggest that in addition to enhancing fatty acid synthesis, bilirubin deficiency also decreases fatty acid catabolism.

Hinds *et al.* reported BVRA to attenuate hepatic steatosis via the PPARα signaling pathway (125). Similarly, the product of BVRA enzymatic activity, bilirubin, has also been reported to promote β-oxidation of fatty acids via activation of PPARα (8), and hyperbilirubinemia decreases HF diet induced hepatic lipid accumulation by increasing the activity of PPARα (7). These previous studies provide a feasible explanation for the enhanced hepatic lipid accumulation observed in our global BVRA deficient mice that show substantially lower concentration of hepatic bilirubin compared with their littermate wild-type controls. PPARα is a transcription factor that promotes fatty acid oxidation. Phosphorylation of Ser73 in PPARα, which attenuates PPARα activity (125), was increased in the livers of *Bvra*$^{-/-}$ mice fed HF diet (125). Consistent with this paradigm, mRNA expression of the target genes of PPARα, *e.g., Cpt1a*, *Cyp2j6* and *Cyp4a12* was decreased in *Bvra*$^{-/-}$ mice, thereby indicating that a decrease in the activity of PPARα was a likely explanation for the observed lipid accumulation in the livers of *Bvra*$^{-/-}$ mice fed HF diet. As plasma concentrations of TG, cholesterol and CE were not affected in *Bvra*$^{-/-}$ mice fed HF diet, global deficiency of *Bvra* does not appear to affect hepatic secretion of lipoprotein lipids under these conditions. Therefore, our results overall indicate that global deficiency of *Bvra* enhances hepatic steatosis by promotion of *de novo* lipogenesis and suppression of lipid oxidation during lipid metabolism, rather than via increasing hepatic fatty acid uptake or TG secretion.

Previous studies suggested BVRA to regulate glucose metabolism and to act as a transcription factor that modulates insulin signaling (20, 23, 135, 136). In apparent contrast to these earlier studies, the present investigation documents that BVRA is not required for normal glucose metabolism and insulin signaling in naïve mice. Thus, global deficiency of *Bvra* did not lead to insulin resistance in naïve *Bvra*$^{-/-}$ mice, as they are characterized by normal blood glucose and glucose uptake, glucose and insulin tolerance, plasma insulin concentrations, insulin sensitivity by adipose explant tissue, and insulin signaling including GLUT4 expression and phosphorylation of Akt and AS160. Given the unexpected nature of these results, we further examined glucose metabolism and insulin resistance in metabolically stressed *Bvra*$^{-/-}$ mice by feeding these animals a HF or HFHS diet, which are commonly used to induce insulin resistance *in vivo* (285, 331-333). For both diets, deficiency of *Bvra* did not alter glucose intolerance and related metabolic changes. These results suggest that BVRA may not play a significant role for *in vivo* glucose and insulin metabolism. We speculate that the duality of BVRA in insulin signaling (135) is a reason for this surprising result we obtained.

Using liver-specific BVRA knockout mice fed a similar HF diet for the same duration used in the present work, Hinds *et al.* (125) reported hepatic steatosis to cause impaired hepatic

insulin signaling (as indicated by suppression of Akt phosphorylation, but not insulin receptor β and its precursor) that manifests into peripheral insulin resistance (increased fasted blood glucose and plasma insulin, and enhanced glucose intolerance), without a change in insulin tolerance. Although hepatic steatosis is widely believed to result in insulin resistance (327, 337, 338), there is also evidence indicating that hepatic lipid accumulation is insufficient to cause, and can occur independent of, insulin resistance (339-341), especially hepatic insulin resistance (342). However, in the present study, we have not observed insulin resistance in liver or other tissue by assessing phosphorylation of Akt, AS160 and GSK3β, expression of GLUT4 and glucose uptake in *Bvra*$^{-/-}$ mice fed HF diet with a relative high n value for each experiment. To assess hepatic insulin resistance directly euglycemic-hyperinsulinemic and hyperglycemic clamps would be needed (343, 344). As the present studies as well as Hinds *et al.* (125) did not conduct such studies, the potential role of BVRA deficiency on hepatic insulin resistance requires to be investigated in the future.

Determining hepatic bile pigments in *Bvra*$^{-/-}$ and *Bvra*$^{+/+}$ littermate mice, the present study confirms that global deficiency of *Bvra* substantially lowers hepatic bilirubin in addition to that in plasma and bile (126). However, different to the situation in plasma, where the total concentration of bile pigments (biliverdin plus bilirubin) is 10-fold lower in *Bvra*$^{-/-}$ than *Bvra*$^{+/+}$ mice (126), the concentrations of total bile pigments in the livers remain similar between the two genotypes, due to the corresponding increase of hepatic biliverdin in *Bvra*$^{-/-}$ mice. The reason for this increase of hepatic biliverdin in *Bvra*$^{-/-}$ mice remains unclear, just as it is not clear whether maintaining the overall hepatic bile pigment concentration affords a biological activity. This green bile pigment is water-soluble, and hence may be readily secreted into bile. Additionally, the kinetic efficiency of BVRA is high so that once formed by heme oxygenase, biliverdin is thought to be reduced rapidly to bilirubin by BVRA. It is difficult to explain why biliverdin accounts for ~25% of hepatic bile pigments in *Bvra*$^{+/+}$ mice. A possible explanation for the relatively high hepatic concentrations of biliverdin in *Bvra*$^{+/+}$ mice and its compensatory increase in *Bvra*$^{-/-}$ mice is that biliverdin may protect the liver against pathological conditions. For example, biliverdin has been reported to suppress hepatic oxidative stress induced by bile acid (345) and to initiate liver regeneration after immune-mediated injury or ischemia/reperfusion injury (119, 346). More relative to our case is that biliverdin was found to regulate lipid metabolism and attenuate lipid accumulation *in vitro* via regulation of PPARα (8).

In conclusion, we provide a metabolic characterization of mice with global BVRA deficiency in three different dietary models. Naïve *Bvra*$^{-/-}$ mice fed standard chow show normal glucose metabolism and insulin sensitivity, demonstrating that BVRA is not required for glucose metabolism and insulin signaling. When stressed by a HF diet, *Bvra*$^{-/-}$ mice develop a fatty liver phenotype, likely as a result of suppressed of PPARα activity. Despite this however, *Bvra*$^{-/-}$ mice retain glucose metabolism and insulin sensitivity comparable to that of wild-type animals, just as

in the HFHS dietary model. Therefore, *Bvra* deficiency renders mice susceptible to hepatic steatosis in the absence of insulin resistance.

Chapter 5

Bvra deficiency enhances atherosclerosis and destabilizes atherosclerotic plaque

This chapter contains work with:

Chen W, Dunn LL, Stanley C, Newington D, Suarna C, Tumanov S, Talib J, Cheng D, Stocker R. *Bvra* deficiency enhances atherosclerosis and destabilizes atherosclerotic plaque. Unpublished.

Author contributions:

Chen W, Dunn LL and Stocker R designed the study.

Chen W, Dunn LL and Newington D carried out the experiments generating the *Bvra*$^{-/-}$*Apoe*$^{-/-}$ TS mice, and morphological experiments to evaluate the development of atherosclerosis and stability of atherosclerotic plaque with guidance from Stocker R. Cheng D assisted with measurement of hemosiderin. Chen W, Suarna C and Stocker R designed and carried out HLPC analysis for antioxidants and lipid profile in plasma and tissue, with assistance from Tumanov S and Talib J for LC-MS/MS analysis of bile pigment. Chen W, Stanley C and Stocker R designed and carried out the myography experiments for vessel function. Chen W, Dunn LL and Stocker R designed and carried out experiments to detect near infrared auto fluorescence.

The specific aims for this chapter are:

1) To investigate the impact of *Bvra* deficiency on atherosclerosis;

2) To study the role of bilirubin in atherosclerotic plaque instability using the tandem stenosis mouse model of unstable plaque;

5.1 Introduction

Atherosclerosis is the major cause of cardiovascular disease (CVD) and rupture of atherosclerotic plaque contributes to CVD death. Atherosclerosis is a lipid- and inflammation-driven disease that leads to plaque formation at specific sites of the arterial tree through intimal lipid-accumulation, inflammation, necrosis, fibrosis, and calcification. Thin-cap fibroatheroma (TCFA) characterized by a thin fibrous cap, large lipid-rich necrotic core, and a high inflammatory cell content represents a high-risk or unstable plaque (hereafter referred to as unstable plaque), prone to rupture (347). Notably, epidemiological studies consistently show that low plasma concentrations of bilirubin are associated with increased risk of atherosclerosis (14, 15), coronary artery disease (9, 16) and myocardial infarction (238-240). Conversely, individuals with moderate hyperbilirubinemia have a decrease risk of CVD, and this is particularly the case for subjects with Gilbert's syndrome, a mild liver disorder where a mutation in uridine diphosphate glucuronyl transferase (UGT1A1) attenuates hepatic conjugation of bilirubin for biliary excretion, and therefore increases circulating bilirubin (10, 348).

There are a number of mechanisms by which bilirubin may exert protection against CVD. In its free, albumin-bound and conjugated forms, bilirubin has potent antioxidant activities *in vitro*, *ex vivo* and *in vivo* (2, 185, 196). The pigment also acts synergistically with α-tocopherol (α-TOH) to protect circulating lipids from becoming oxidized (187). In addition, bilirubin has anti-inflammatory properties, as it attenuates the chemotactic activity of monocytes, the adhesion of leukocytes to blood vessels, and the production of pro-inflammatory cytokines (205, 207, 328). Moreover, bilirubin is able to attenuate vascular endothelial activation and dysfunction (231). As an agonist of peroxisome proliferator-activated receptor-α (PPARα), bilirubin also suppresses lipid accumulation and protects from adiposity (8).

However, despite the well-established association of plasma bilirubin with the outcome of CVD and related diseases, a causative link between bilirubin and CVD remains to be established. Until recently, it has been difficult to study unstable plaque largely due to the absence of such plaques in standard experimental murine models of atherosclerosis, including the *low-density lipoprotein receptor*-deficient (*Ldlr*$^{-/-}$) and *apolipoptrotein E* gene-deficient (*Apoe*$^{-/-}$) mice (288, 349). The recent development of the tandem stenosis (TS) mouse model of plaque instability has provided a useful tool to assess mechanisms contributing to the development of unstable atherosclerotic plaque. In this model, a TS is surgically introduced in the right carotid artery of *Apoe*$^{-/-}$ mice fed a Western diet to induce low shear and high tensile stress, resulting in plaques with unstable phenotype that share many features of culprit lesions in humans (286).

Another difficulty is the absence of mouse models with altered concentrations of plasma bilirubin. Long-term daily-treatment of mice with bilirubin is not feasible, due to the low solubility of the pigment in physiological buffers, and the highly efficient excretion of bilirubin in mice via UGT1A1. Also, *Ugta1a1* gene-deficient mice develop severe hyperbilirubinemia

upon birth and do not survive past one week due to kernicterus (350, 351). As bilirubin is formed from biliverdin by biliverdin reductase, we generated a global *biliverdin reductase a* gene knockout (*Bvra*$^{-/-}$) mouse, characterized by very low concentrations of plasma bilirubin and slightly increased plasma biliverdin (126). We crossed these *Bvra*$^{-/-}$ mice with *Apoe*$^{-/-}$ animals (*Bvra*$^{-/-}$*Apoe*$^{-/-}$) and subjected them to TS surgery as a tool to assess the role of bilirubin in atherogenesis and atherosclerotic plaque stability.

Herein, it is shown that compared with littermate *Bvra*$^{+/+}$*Apoe*$^{-/-}$ TS animals, *Bvra*$^{-/-}$ *Apoe*$^{-/-}$ TS mice have larger atherosclerotic lesions and increased plaque instability, as assessed by a decrease in fibrous cap thickness. *Bvra*$^{-/-}$*Apoe*$^{-/-}$ TS mice also have increased positive arterial remodeling at the sites where unstable plaques form compared with littermate *Bvra*$^{+/+}$*Apoe*$^{-/-}$ TS animals. Further, *Bvra*$^{-/-}$*Apoe*$^{-/-}$ TS mice show signs of increased systemic oxidative stress, have enhanced endothelial dysfunction and increased plasma and hepatic lipids. Our data suggest that the absence of BVRA and bilirubin generates a hyperlipidemic pro-atherogenic phenotype, characterized by increased endothelial dysfunction, atherosclerosis, as well as plaque destabilization, compensatory arterial remodeling and hepatic steatosis. These findings are consistent with previous epidemiological literature and support a causative role for bilirubin in decreasing CVD risk.

5.2 Materials and Methods

5.2.1 Animals

The *biliverdin reductase a (Bvra)* gene deficient mouse on C57BL/6J background has been described previously in **Section 2.1.1** of Chapter 2. *Bvra*$^{-/-}$ mice were crossed with *Apoe*$^{-/-}$ mice on C57BL/6J background in the BioCORE facility at the Victor Chang Cardiac Research Institute to generate *Bvra*$^{+/-}$*Apoe*$^{-/-}$ breeders and *Bvra*$^{+/+}$*Apoe*$^{-/-}$ and *Bvra*$^{-/-}$*Apoe*$^{-/-}$ littermate experimental animals. All mice were housed in a temperature-controlled room on a 12 h light/dark cycle and were allowed access to water and food *ad libitum*. All procedures were carried out according to the Australian NHMRC Guidelines for Animal Research and were approved by the Animal Care and Ethics Committee of the Garvan Institute of Medical Research/St Vincent's Hospital.

5.2.2 Tandem Stenosis (TS) model of plaque instability

The TS model of unstable plaque was used throughout with details of the surgery described previously in **Section 2.2.4** of Chapter 2.

5.2.3 Collection of tissue samples

Seven weeks after TS surgery, mice were anesthetized by isoflurane inhalation and euthanized by exsanguination for tissue collection. The detailed procedure for tissue collection has been described in **Section 2.2.5** in Chapter 2.

5.2.4 LC-MS/MS analysis of bilirubin and biliverdin in artery, liver and plasma

Bilirubin and biliverdin in arterial tissue, liver and plasma were analyzed by LC-MS/MS using a 6490 Triple Quadrupole LC-MS/MS (Agilent Technologies) as described in **Section 2.4.4** of Chapter 2.

5.2.5 HPLC analysis of lipids in artery and liver

Measurement of lipids in artery and liver by HPLC analysis has been described in detail in **Section 2.4.5** of Chapter 2.

5.2.6 Analyses of plasma antioxidants, lipids and cholesterylester hydroperoxides

Fresh plasma was processed and analyzed for antioxidants, lipids and oxidized lipids as described in **Section 2.4.1** of Chapter 2.

5.2.7 Histology

Histologic analysis of atherosclerotic lesion was carried out largely as described in **Section 2.6.2** of Chapter 2.

5.2.8 Redox state of peroxiredoxin 2

The analysis of peroxiredoxin 2 (Prx2) redox state was performed as described in **Section 2.5.3** of Chapter 2.

5.2.9 SDS-PAGE and immunoblotting for BVRA

Arterial segments (1 mg) were homogenized at 4 °C in 100 µL ice-cold PBS containing protease inhibitor (Roche, Switzerland) and 100 µM diethylenetriaminepentaacetic acid (DTPA) and using a Wheaton tissue grinder. Protein concentration of the homogenate was determined by BCA assay. One volume of homogenate was added into one volume of SDS-urea lysis buffer (6.7 M urea, 10% glycerol, 10 mM Tris pH 6.8, 1% SDS, 1 mM DTT, 1 mM PMSF). Proteins of homogenates were resolved by SDS-PAGE using 10% SDS-polyacrylamide gels (NuPage, Invitrogen). 30 µg protein was electrophoresed at 100 V for 90 min and transferred to nitrocellulose membranes using an iBlot2 Dry Blotting System (Invitrogen, USA). Membranes were blocked with 5% BSA at room temperature for 1 h and incubated with primary antibody (BVRA antibody, 1:1000, ADI-OSA-450, Enzo Life, NY, USA; β-actin antibody, 1:5000, 691001, MP Biomedicals, CA, USA) at 4 °C overnight. Membranes were then washed and incubated with IRDye 800CW goat-anti-rabbit IgG or IRDye 680RD goat anti-mouse IgG secondary antibody (LI-COR Biosciences, NE, USA). Proteins were visualized using Odyssey infrared imaging system (model CLx) and analyzed by densitometry using the Image Studio Lite software (LI-COR Biosciences).

5.2.10 Assessment of MPO activity

Measurement of *ex vivo* MPO activity was carried out largely as described in **Section 2.3.1** of Chapter 2.

5.2.11 Fluorescence emission computed tomography (FLECT)

In vivo measurement of near infrared autofluorescence (NIRAF) was performed using FLECT-CT (Trifoil InSyTe, CA, US) as described in **Section 2.2.6** of Chapter 2.

5.2.12 Odyssey infrared imaging system

Ex vivo measurement of NIRAF was performed using an Odyssey infrared imaging system (CLx, Li-COR, Nebraska, US) as described in **Section 2.3.2** of Chapter 2.

5.2.13 Myography

Endothelial function in the abdominal aorta of TS mice was assessed using wire myography as described in **Section 2.3.3** of Chapter 2.

5.2.14 Statistical analyses

Unless indicated otherwise, statistical analysis was performed using GraphPrism 8 software. Results are expressed as mean values with error bars representing standard error of the mean. Numeric data was analyzed for normality using the Shapiro-Wilk normality test, the significance determined using the appropriate parametric or non-parametric test. The Mann-Whitney rank-sum test or two-way ANOVA analysis of variance was used to determine statistical significance. A P value of <0.05 was considered as statistically significant.

5.3 Results

5.3.1 Genetic deletion of *Bvra* eliminates most of the plasma bilirubin

Littermate *Bvra*$^{+/+}$*Apoe*$^{-/-}$ and *Bvra*$^{-/-}$*Apoe*$^{-/-}$ mice fed WD for 13 weeks and subjected to TS surgery at the sixth week after the commencement of WD had comparable body weight (Fig. 5.1A). Consistent with previous findings in naïve *Bvra*$^{+/+}$ and *Bvra*$^{-/-}$ mice (126), bilirubin was barely detectable (12 ± 1 nM) in plasma of *Bvra*$^{-/-}$*Apoe*$^{-/-}$ TS mice compared with *Bvra*$^{+/+}$*Apoe*$^{-/-}$ TS animals (1,902 ± 308 nM) (Fig. 5.1B). This essential absence of bilirubin was accompanied by an increase in plasma biliverdin, *i.e.*, 117 ± 10 versus 7 ± 1 nM for *Bvra*$^{-/-}$*Apoe*$^{-/-}$ and *Bvra*$^{+/+}$*Apoe*$^{-/-}$ mice, respectively (Fig. 5.2C).

5.3.2 *Bvra* deficiency enhances endothelial dysfunction

Endothelial dysfunction precedes atherosclerosis (6), and recent work indicates that TS surgery in the carotid artery is associated with increased systemic endothelial dysfunction in remote sites

such as the abdominal aorta (352). Therefore, we first assessed endothelial function in the abdominal aorta of *Bvra*$^{-/-}$*Apoe*$^{-/-}$ and *Bvra*$^{+/+}$*Apoe*$^{-/-}$ TS mice using wire myography. BVRA deficiency significantly decreased acetylcholine (ACh)-induced, endothelium-dependent relaxation, whereas it had no material effect on sodium nitroprusside (SNP)-induced, endothelium-independent relaxation (Fig. 5.1D to G). These results suggest that *Bvra* deficiency and the essential absence of bilirubin enhances systemic endothelial dysfunction that may contribute to atherogenesis.

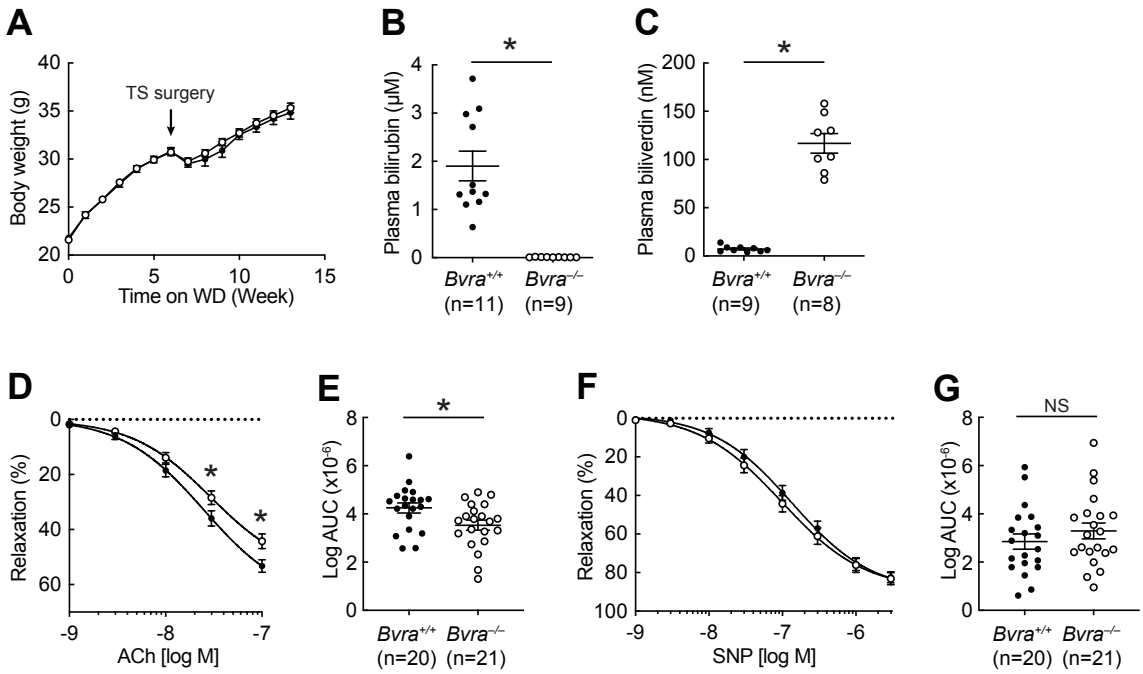

Figure 5.1 *Bvra* gene deletion eliminates plasma bilirubin and enhances endothelial dysfunction. **(A)** Body weight of *Bvra*$^{+/+}$*Apoe*$^{-/-}$ (n = 51) and *Bvra*$^{-/-}$*Apoe*$^{-/-}$ (n = 49) mice fed a Western diet (WD) for 13 weeks, with TS surgery performed at the sixth week after the commencement of WD. **(B**, **C**) Concentrations of plasma bilirubin and biliverdin in *Bvra*$^{+/+}$*Apoe*$^{-/-}$ and *Bvra*$^{-/-}$*Apoe*$^{-/-}$ TS mice. Bilirubin and biliverdin were measured by LC-MS/MS. (**D-G**) Relaxation of abdominal arteries isolated from *Bvra*$^{+/+}$*Apoe*$^{-/-}$ TS and *Bvra*$^{-/-}$*Apoe*$^{-/-}$ TS mice. Abdominal arterial rings were pre-constricted with norepinephrine and relaxation responses to **(D**, **E)** acetylcholine (ACh) and **(F**, **G)** sodium nitroprusside (SNP) were determined using wire myography. Relaxation responses to ACh **(D)** and SNP **(F)**. n = 20 *Bvra*$^{+/+}$*Apoe*$^{-/-}$ TS mice and n = 21 *Bvra*$^{-/-}$*Apoe*$^{-/-}$ TS mice. (**E**, **G**) Area under curve (AUC) for relaxation responses shown in **D** and **F**, respectively. Numerical results show individual data as well as mean ± SEM, with data in **B**, **C**, **E** and **G** analyzed by the Mann-Whitney test, and data in **D** and **F** analyzed by two-way ANOVA. *P<0.05 compared to *Bvra*$^{+/+}$*Apoe*$^{-/-}$ mice. Not significant (NS). Open and filled circles correspond to *Bvra*$^{-/-}$*Apoe*$^{-/-}$ TS and *Bvra*$^{+/+}$*Apoe*$^{-/-}$ TS mice, respectively.

5.3.3 *Bvra* deficiency increases atherosclerosis

We therefore next assessed the influence of global BVRA deficiency on atherosclerotic lesion size in *Apoe*$^{-/-}$ TS mice by morphometry, as described previously (353) and recommended by Daugherty *et al.* (288). BVRA deficiency significantly increased lesion size in the aortic root (Fig. 5.2A to C) and brachiocephalic artery (Fig. 5.2D to F) of *Apoe*$^{-/-}$ TS mice. The observed increase in plaque size at the brachiocephalic artery by BVRA deficiency was confirmed by increases in plaque triglycerides (TG), cholesterol and cholesterylester (CE) (Fig. 5.2G to I). These data show that BVRA deficiency enhances atherogenesis. Our findings are consistent with a previous study reporting a decrease in atherosclerotic lesion size at the aortic root of *LdLr*$^{-/-}$ mice, where by intraperitoneal administration of 30 mg/kg bilirubin resulted in plasma bilirubin concentrations of ~25 μM (205).

As hyperlipidemia promotes atherosclerosis (354) and plasma bilirubin concentrations inversely associate with hyperlipidemia (*e.g.,* familial hypercholesterolemia) (355, 356), we next assessed whether BVRA deficiency affected plasma lipids, as determined by HPLC analysis. Plasma concentrations of cholesterol and CE were significantly increased in *Bvra*$^{-/-}$*Apoe*$^{-/-}$ compared with *Bvra*$^{+/+}$*Apoe*$^{-/-}$ TS mice (Table 5.1). The concentrations of TG were too small to reliably determine by the HPLC method used (data not shown). These results indicate that BVRA deficiency increases hyperlipidemia, and this could help explain the observed increase in atherogenesis.

Figure 5.2

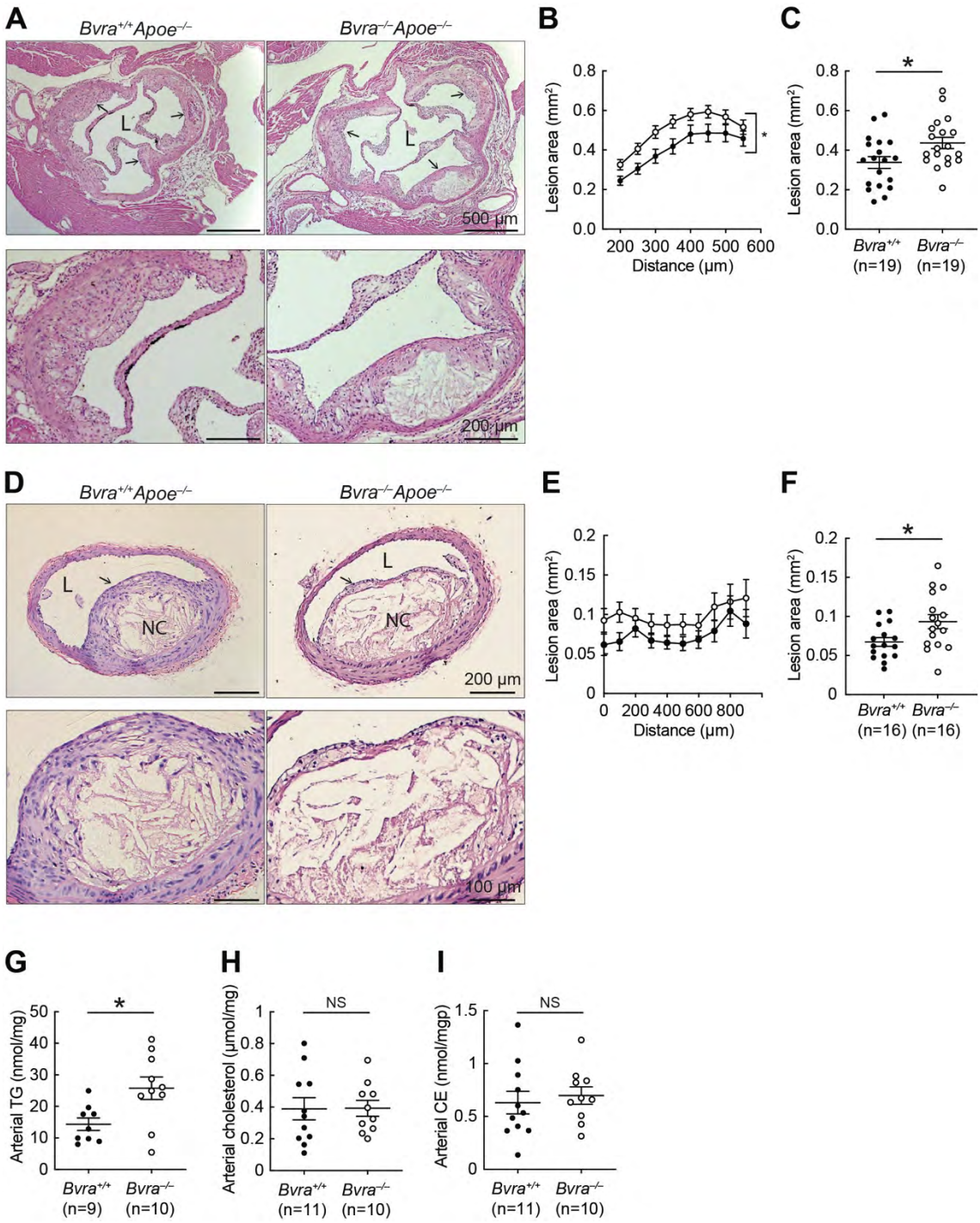
A
Bvra+/+Apoe−/−
Bvra−/−Apoe−/−
L
500 µm
200 µm
B
Lesion area (mm²)
Distance (µm)
C
Bvra+/+ (n=19)
Bvra−/− (n=19)
D
NC
200 µm
100 µm
E
F
Bvra+/+ (n=16)
Bvra−/− (n=16)
G
Arterial TG (nmol/mg)
Bvra+/+ (n=9)
Bvra−/− (n=10)
H
Arterial cholesterol (µmol/mg)
NS
Bvra+/+ (n=11)
Bvra−/− (n=10)
I
Arterial CE (nmol/mgp)

Figure 5.2 *Bvra* gene deletion enhances atherosclerosis**. (A-C)** Atherosclerotic lesion size was determined from serial cross-sections at the aortic root and assessed by morphometry. (**A**) Representative H&E stained sections of the aortic root taken at 300 µm distance from the aortic origin where all three aortic valve leaflets appear first. Higher magnifications of lesion are provided in the lower panels. (**B**) Morphometric assessment of lesion area within the ascending aorta quantified from serial sections taken 200 to 550 µm distance from the aortic origin. n = 19 *Bvra*$^{+/+}$*Apoe*$^{-/-}$ TS mice and n = 19 *Bvra*$^{-/-}$*Apoe*$^{-/-}$ TS mice. **(C)** Average lesion area in the aortic root at 200 and 350 µm distance from the aortic origin. **(D-F)** Atherosclerotic lesions in the brachiocephalic artery of *Bvra*$^{+/+}$*Apoe*$^{-/-}$ and *Bvra*$^{-/-}$*Apoe*$^{-/-}$ TS mice. **(D)** Representative H&E stained sections of brachiocephalic artery at 500 µm distance from the bifurcation of the right subclavian and carotid artery. Higher magnification of the necrotic core (NC) are provided at the lower panel. **(E)** Lesion area within the brachiocephalic artery and assessed by morphometry of serial cross-sections taken at different distances from the bifurcation of the right subclavian and carotid artery. n = 16 *Bvra*$^{+/+}$*Apoe*$^{-/-}$ TS mice and n = 16 *Bvra*$^{-/-}$*Apoe*$^{-/-}$ TS mice. **(F)** Average lesion area in the brachiocephalic artery at 0 to 900 µm distance from the bifurcation. **(G-I)** Concentrations of triglycerides (TG), cholesterol and cholesterylester (CE) in the brachiocephalic artery of *Bvra*$^{+/+}$*Apoe*$^{-/-}$ TS and *Bvra*$^{-/-}$*Apoe*$^{-/-}$ TS mice. Arterial lipids were analyzed by HPLC-UV. Results are standardized to protein concentration. Data shown are mean ± SEM, with data in **C**, **F**, **G**, **H** and **I** analyzed by the Mann-Whitney test, and data in **B** and **E** by two-way ANOVA. $^{*}P<0.05$ compared to *Bvra*$^{+/+}$*Apoe*$^{-/-}$ mice. Not significant (NS). The arrows indicate the presence of atherosclerotic lesion; L represents the lumen. Open and filled circles correspond to *Bvra*$^{-/-}$ *Apoe*$^{-/-}$ TS and *Bvra*$^{+/+}$*Apoe*$^{-/-}$ TS mice respectively.

Table 5.1 Concentrations of selected lipids, oxidized lipids and antioxidants in plasma of *Bvra*$^{+/+}$*Apoe*$^{-/-}$ and *Bvra*$^{-/-}$*Apoe*$^{-/-}$ TS mice.

	Bvra$^{+/+}$*Apoe*$^{-/-}$ (n)	*Bvra*$^{-/-}$*Apoe*$^{-/-}$ (n)
Cholesterol (μM)	7884 ± 497 (24)	9431 ± 318 (22)*
C18:2 (μM)	7261 ± 544 (24)	9294 ± 678 (22)*
C20:4 (μM)	1009 ± 138 (24)	1207 ± 114 (22)
CE (μM)	8215 ± 626 (24)	10501 ± 750 (22)*
CE-OOH (nM)	54.1 ± 5.9 (24)	80.2 ± 10.6 (22)*
CE-OOH/CE (μmol/mol)	7.5 ± 0.9 (24)	7.9 ± 0.8 (22)
CoQ_9H_2 (nM)	1607 ± 169 (11)	1384 ± 133 (10)
CoQ_9 (nM)	497 ± 65 (11)	459 ± 31 (10)
CoQ_9 redox ratio (%)	77 ± 1 (11)	75 ± 1 (10)
Total CoQ_9/CE (μmol/mol)	330 ± 65 (11)	247 ± 26 (10)
α-TOH (μM)	37.2 ± 5.2 (23)	47.8 ± 5.4 (20)
α-TOH/CE (mmol/mol)	5.3 ± 0.7 (23)	5.4 ± 0.7 (20)

Result shown are mean ± SEM with the number of separate animals indicated in parenthesis. Abbreviations: α-TOH, α-tocopherol; C18:2, cholesteryllinoleate; C20:4, cholesterylarachidonate; CE, cholesterylesters (C18:2 + C20:4); CE-OOH, cholesterylester hydroperoxides; CoQ_9, ubiquinone-9; CoQ_9H_2, ubiquinol-9.

*P<0.05 compared with *Bvra*$^{+/+}$*Apoe*$^{-/-}$ TS mice by Mann-Whitney test.

5.3.4 *Bvra* deficiency destabilizes atherosclerotic plaque

Serum total bilirubin concentrations have been reported to inversely associate with human coronary plaque stability, as assessed by plaque fibrosis, plaque and lipid burden, as well as arterial remodeling determined by coronary angiography and intravascular ultrasound in patients with acute coronary syndrome versus stable angina pectoris and age-matched controls (227). We determined fibrous cap thickness as primary discriminator of plaque vulnerability (357) in *Bvra*$^{+/+}$*Apoe*$^{-/-}$ TS and *Bvra*$^{-/-}$*Apoe*$^{-/-}$ TS mice to test more directly a role for BVRA and its enzymatic product bilirubin in plaque stabilization. Thickness of the cap was assessed by the quantification of its collagen content using picrosirius red (PSR) staining under polarized light (Fig. 5.3A). Irrespective of whether 'cap thickness' was determined as thickness (Fig. 5.3C), area (Fig. 5.3E) or volume (Fig. 5.3F), BVRA deficiency significantly decreased 'cap thickness'. Such cap thinning was observed throughout the entire region where unstable plaques form in *Apoe*$^{-/-}$ TS mice, *i.e.,* from the proximal suture to the bifurcation of the right subclavian artery (Figs. 5.3B, D and G). Similarly, BVRA deficiency significantly decreased the cap-to-lesion height ratio by 57 % (Fig. 5.3H).

As secondary endpoints of plaque stability, we assessed the content of lipids, hemosiderin and fibrin. BVRA deficiency increased the lipid burden in unstable plaque, as determined by HPLC measurement of TG, cholesterol and CE (Fig. 5.4A to C). However, preliminary data showed that BVRA deficiency did not significantly increase the content of hemosiderin (Fig. 5.4D and E), a marker of long-term storage of iron derived from erythrocytes/hemoglobin and hence intra-plaque hemorrhage (358, 359). Moreover, fibrin deposition only showed a trend of increase in unstable plaque of *Bvra*$^{-/-}$*Apoe*$^{-/-}$ compared with *Bvra*$^{+/+}$*Apoe*$^{-/-}$ TS mice, as assessed by Martian scarlet blue staining (Fig. 5.4F and G). Further analysis of hemosiderin and fibrin, as well as other marker for intra-plaque hemorrhage will be performed to confirm these initial results. Together, these findings indicate that the absence of BVRA destabilizes atherosclerotic plaque in the *Apoe*$^{-/-}$ TS mouse model.

Figure 5.3

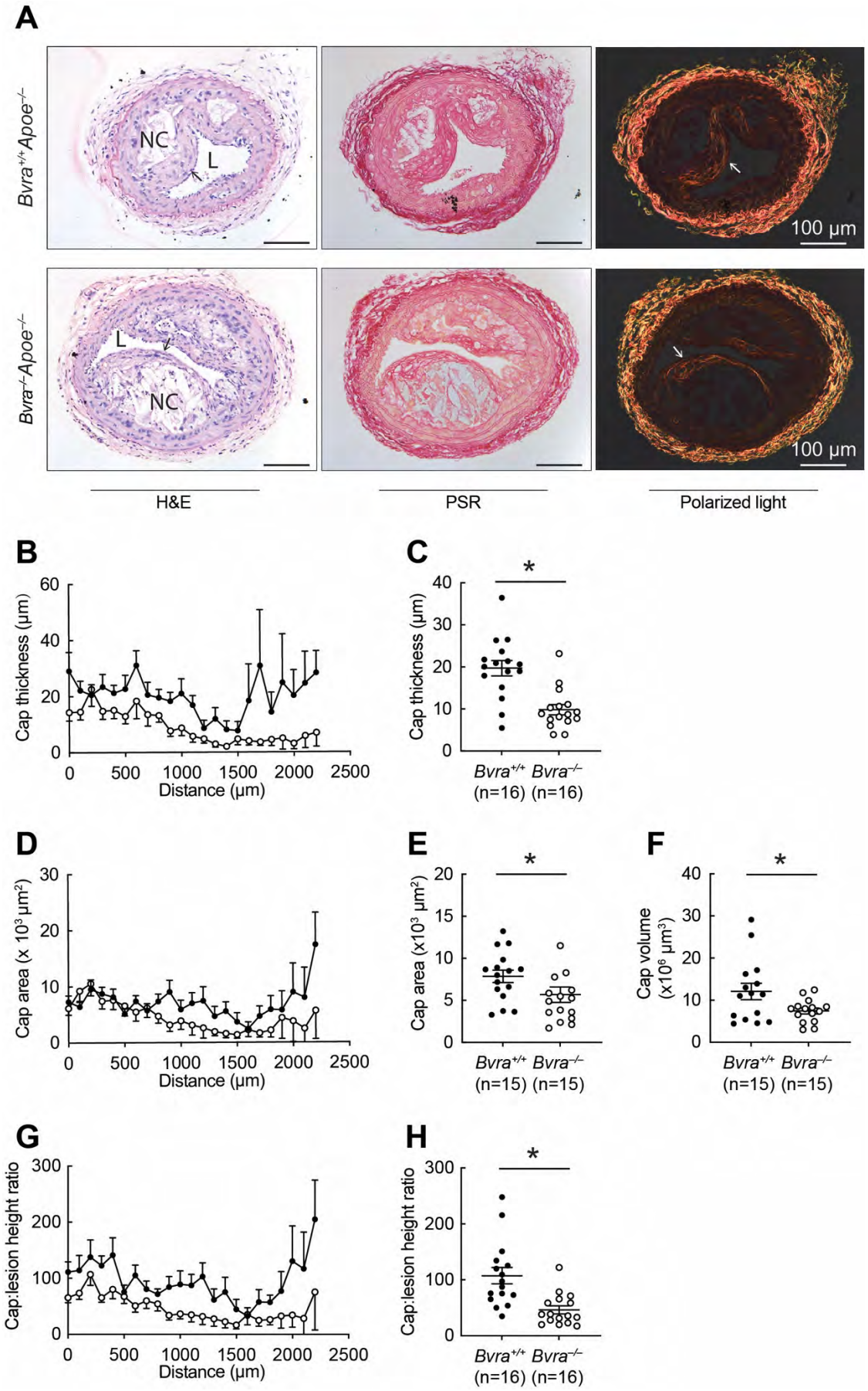
A
Bvra+/+Apoe−/−
Bvra−/−Apoe−/−
NC
L
100 µm
H&E
PSR
Polarized light
B
Cap thickness (µm)
Distance (µm)
C
Cap thickness (µm)
Bvra+/+ Bvra−/−
(n=16) (n=16)
D
Cap area (x 10³ µm²)
Distance (µm)
E
Cap area (x10³ µm²)
Bvra+/+ Bvra−/−
(n=15) (n=15)
F
Cap volume (x10⁶ µm³)
Bvra+/+ Bvra−/−
(n=15) (n=15)
G
Cap:lesion height ratio
Distance (µm)
H
Cap:lesion height ratio
Bvra+/+ Bvra−/−
(n=16) (n=16)

Figure 5.3 *Bvra* gene deletion destabilizes atherosclerotic plaque. Stability of atherosclerotic plaque was determined at the end of the 13 weeks study from serial cross-sections of unstable plaque by assessment of fibrous cap thickness. **(A)** Representative H&E-stained and picrosirius red (PSR)-stained sections of unstable plaque at 500 µm distance from the proximal suture, viewed under bight field and polarized light. **(B)** Cumulative data of fibrous cap thickness determined at 100 µm intervals from the proximal suture and throughout the entire arterial segment of unstable plaque in the right carotid artery. **(C)** Average fibrous cap thickness in unstable plaque of *Bvra*$^{+/+}$*Apoe*$^{-/-}$ and *Bvra*$^{-/-}$*Apoe*$^{-/-}$ TS mice. **(D)** Cumulative data of fibrous cap area determined at 100 µm intervals from the proximal suture and throughout the entire arterial segment of unstable plaque. **(E, F)** Average fibrous cap area and accumulative fibrous cap volume in unstable plaque of *Bvra*$^{+/+}$*Apoe*$^{-/-}$ and *Bvra*$^{-/-}$*Apoe*$^{-/-}$ TS mice. **(G)** Cumulative data of cap: lesion height determined at 100 µm intervals from the proximal suture and throughout the entire arterial segment of unstable plaque. **(H)** Average cap: lesion height ratio in *Bvra*$^{+/+}$*Apoe*$^{-/-}$ and *Bvra*$^{-/-}$*Apoe*$^{-/-}$ TS mice. Result shown represent individual results or mean ± SEM, with significance evaluated using the Mann-Whitney test. *$P<0.05$ compared to *Bvra*$^{+/+}$*Apoe*$^{-/-}$ mice. The arrow indicates the fibrous cap; L represents the lumen; NC represents the necrotic core. Open and filled circles correspond to *Bvra*$^{-/-}$*Apoe*$^{-/-}$ TS and *Bvra*$^{+/+}$*Apoe*$^{-/-}$ TS mice, respectively.

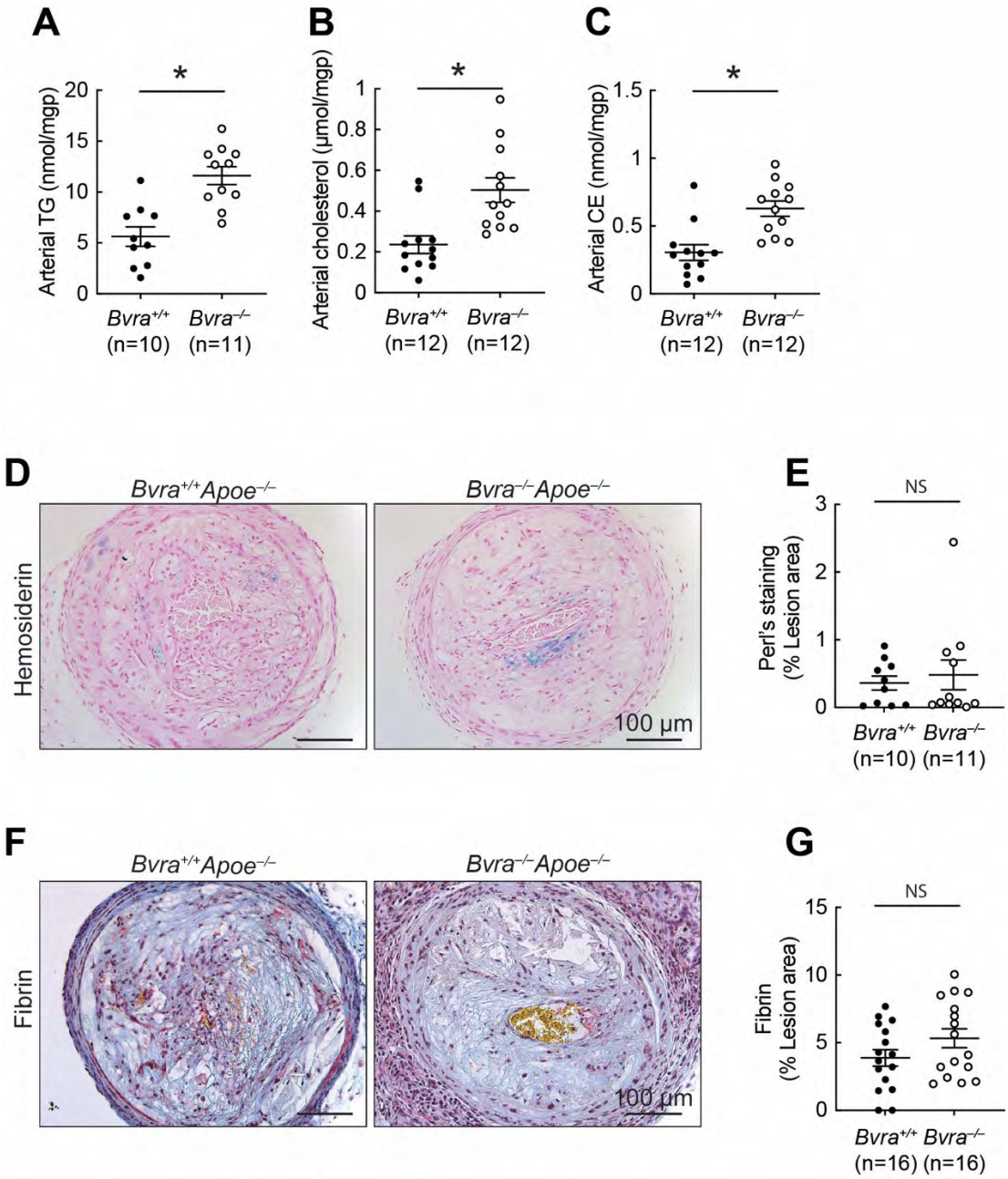

Figure 5.4 *Bvra* gene deletion increases the content of lipids, hemosiderin and fibrin in unstable plaque. **(A-C)** Concentrations of TG, cholesterol and CE in unstable plaque of *Bvra*$^{+/+}$*Apoe*$^{-/-}$and *Bvra*$^{-/-}$*Apoe*$^{-/-}$ TS mice. Arterial lipids were analyzed by HPLC-UV, and results are standardized to protein content (mgp). **(D)** Representative images of Perl's stained sections of unstable plaque, with hemosiderin positive region appearing in blue. **(E)** Quantification of hemosiderin positive area, expressed as percentage of total lesion area, in unstable plaque for *Bvra*$^{+/+}$*Apoe*$^{-/-}$ and *Bvra*$^{-/-}$*Apoe*$^{-/-}$ TS mice. **(F)** Representative images of MSB stained sections of unstable plaque. Fibrin appears bright red, collagen blue, red blood cell yellow, and nuclei brown. **(G)** Quantification of fibrin-positive area expressed as percentage of total lesion area. Quantitative results show individual data as well as mean ± SEM. *P<0.05 compared to *Bvra*$^{+/+}$*Apoe*$^{-/-}$ TS mice, as assessed by Mann-Whitney test.

5.3.5 Mechanistic studies addressing potential mechanisms by which BVRA deficiency destabilizes plaque

To begin to address potential mechanism(s) by which a deficiency in BVRA may destabilize atherosclerotic plaques, we first determined the expression of BVRA and the content of bile pigments in unstable plaque of TS *Apoe*$^{-/-}$ mice. BVRA protein was detected in unstable plaque of *Bvra*$^{+/+}$*Apoe*$^{-/-}$ but not *Bvra*$^{-/-}$*Apoe*$^{-/-}$ TS mice using Western blotting (Fig. 5.5A). To assess whether the observed expression of BVRA in unstable plaque translated into increased enzyme activity, we determined plaque concentrations of biliverdin and bilirubin by LC-MS/MS. As expected, BVRA deficiency significantly increased plaque biliverdin (Fig. 5.5B), while it decreased bilirubin (Fig. 5.5C). These results confirm the presence of active BVRA in unstable plaque and suggest that the local absence of BVRA enzymatic activity and/or bilirubin destabilizes plaque.

As plasma bilirubin concentrations inversely associate with positive (or compensatory) arterial remodeling in human (227), and positive remodeling is associated with increased susceptibility to plaque rupture (360), we next examined the effect of BVRA deficiency on arterial remodeling in unstable versus stable plaque in the *Apoe*$^{-/-}$ TS model. We observed that positive remodeling was increased in unstable (Fig. 5.5D) but not stable plaque (Fig. 5.5E) of *Bvra*$^{-/-}$*Apoe*$^{-/-}$ compared with *Bvra*$^{+/+}$*Apoe*$^{-/-}$mice, suggesting that processes contributing to positive remodeling are enhanced in the absence of BVRA/bilirubin.

Proteases are well-known contributors to compensatory remodeling (361-363), and their activities are regulated by the pro-inflammatory enzyme myeloperoxidase (MPO) via activation of metalloproteinases and inactivation of metalloproteinase inhibitor (364). Moreover, MPO causes systemic endothelial dysfunction (352) and plaque destabilization in the *Apoe*$^{-/-}$ TS mouse model (287), as observed in *Bvra*$^{-/-}$ TS mice, while administration of bilirubin to *Ldlr*$^{-/-}$ mice decreases the biomarker of MPO activity, chlorotyrosine, in stable plaque (365) as assessed by immunofluorescence (205). We therefore assessed MPO activity *ex vivo* in unstable atherosclerotic plaque of *Bvra*$^{+/+}$*Apoe*$^{-/-}$and *Bvra*$^{-/-}$*Apoe*$^{-/-}$ TS mice by quantifying arterial 2-choroethidium 30 min after addition of hydroethidine and glucose/glucose oxidase (289). We observed no difference in *ex vivo* MPO activity in unstable plaque between *Bvra*$^{+/+}$*Apoe*$^{-/-}$ and *Bvra*$^{-/-}$*Apoe*$^{-/-}$ TS mice (Fig. 5.5F).

Figure 5.5

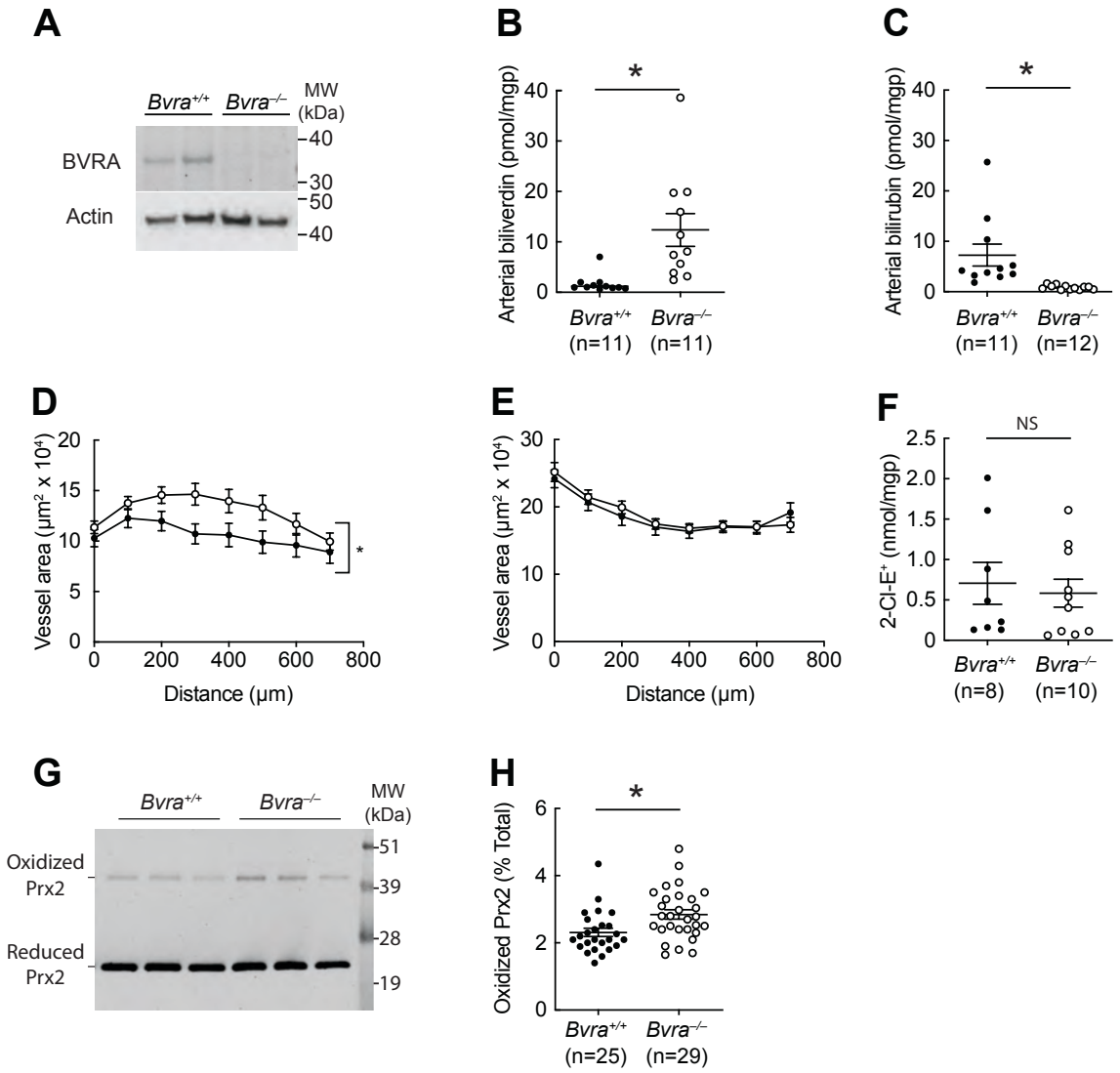
A
Bvra+/+
Bvra−/−
MW (kDa)
BVRA
Actin
40
30
50
40
B
Arterial biliverdin (pmol/mgp)
*
Bvra+/+ (n=11)
Bvra−/− (n=11)
C
Arterial bilirubin (pmol/mgp)
*
Bvra+/+ (n=11)
Bvra−/− (n=12)
D
Vessel area (μm² x 10⁴)
Distance (μm)
*
E
Vessel area (μm² x 10⁴)
Distance (μm)
F
NS
2-Cl-E⁺ (nmol/mgp)
Bvra+/+ (n=8)
Bvra−/− (n=10)
G
Bvra+/+
Bvra−/−
MW (kDa)
Oxidized Prx2
Reduced Prx2
51
39
28
19
H
Oxidized Prx2 (% Total)
*
Bvra+/+ (n=25)
Bvra−/− (n=29)

Figure 5.5 BVRA expression and bile pigment concentrations in unstable atherosclerotic plaque. **(A)** BVRA expression in unstable atherosclerotic plaque as determined by Western blotting. Two pools of unstable plaque from n = 6 mice each obtained from *Bvra*$^{+/+}$*Apoe*$^{-/-}$ and *Bvra*$^{-/-}$*Apoe*$^{-/-}$ TS mice were subjected to electrophoresis followed by transfer and Western blotting using a commercial polyclonal anti-BVRA antibody, with β-actin acting as loading control. **(B**, **C)** Concentrations of biliverdin and bilirubin in unstable atherosclerotic plaque of *Bvra*$^{+/+}$*Apoe*$^{-/-}$ and *Bvra*$^{-/-}$*Apoe*$^{-/-}$ TS mice. Bile pigments were determined by LC-MS/MS, with results normalized to protein content (mgp). (**D, E**) Assessment of arterial remodeling by morphometry. **(D)** Vessel area of the artery containing unstable plaque was quantified from serial sections 0 to 700 µm distance from the proximal ligature. n = 16 *Bvra*$^{+/+}$*Apoe*$^{-/-}$ TS mice and n = 16 *Bvra*$^{-/-}$*Apoe*$^{-/-}$ TS. **(E)** Vessel area of the artery containing stable plaque (brachiocephalic artery) was quantified from serial sections 0 to 700 distance form the bifurcation of the right subclavian and carotid artery. n = 16 *Bvra*$^{+/+}$*Apoe*$^{-/-}$ TS mice and n = 16 *Bvra*$^{-/-}$*Apoe*$^{-/-}$ TS mice. **(F)** Chlorinating activity in unstable plaque of *Bvra*$^{+/+}$*Apoe*$^{-/-}$ and *Bvra*$^{-/-}$*Apoe*$^{-/-}$ TS mice. Unstable plaque homogenate was analyzed for *ex vivo* MPO activity be assessing the conversion of hydroethidine to 2-chloroethidium (2-Cl-E^{+}) 30 min after addition of glucose and glucose oxidase as a source of H_2O_2. **(G)** Representative Western blot showing the peroxiredoxin 2 (Prx2) dimer (oxidized) and monomer (reduced) in blood cells of *Bvra*$^{+/+}$*Apoe*$^{-/-}$ and *Bvra*$^{-/-}$*Apoe*$^{-/-}$ TS mice. **(H)** Densitometric analysis of Prx2 Western blots obtained from blood cells of littermate *Bvra*$^{+/+}$*Apoe*$^{-/-}$ and *Bvra*$^{-/-}$*Apoe*$^{-/-}$ TS mice. Quantitative results show mean ± SEM, with data in **B**, **C**, **F** and **H** analyzed by the Mann-Whitney test, and data in **D** and **E** analyzed by two-way ANOVA. *P<0.05 compared to *Bvra*$^{+/+}$*Apoe*$^{-/-}$ mice; NS, not significant. Open and filled circles correspond to *Bvra*$^{-/-}$*Apoe*$^{-/-}$ TS and *Bvra*$^{+/+}$*Apoe*$^{-/-}$ TS mice, respectively.

5.3.6 Influence of *Bvra* deficiency on oxidative stress of *Apoe*$^{-/-}$ TS mice

Atherosclerotic plaque progression and vulnerability to rupture have been linked to dysregulation of oxidative stress (366). Bilirubin has potent antioxidant activity (2, 126), which could conceivably regulate the progress of atherosclerotic plaque rupture. Therefore, we next examined potential changes in oxidative stress in response to *Bvra* deficiency and the associated low plasma bilirubin concentrations. HPLC with post-column chemiluminescence detection was used for the determination of lipid hydroperoxide (CE-OOH), the major form of oxidized lipids in plasma. Compared with *Bvra*$^{+/+}$*Apoe*$^{-/-}$ TS mice, plasma of *Bvra*$^{-/-}$*Apoe*$^{-/-}$ TS mice contained significantly higher concentrations of CE-OOH (Table 5.1). Normalizing the concentration of CE-OOH to readily oxidizable CE (*i.e.*, C20:4 + C18:2), abolished this statistical difference, indicating that while the total concentration of circulating CE-OOH was elevated in *Bvra*$^{-/-}$*Apoe*$^{-/-}$ TS mice, the 'oxidizability' of plasma CE was not different between the two mouse lines. Consistent with this interpretation, there was no difference in the plasma concentration of α-TOH and the plasma ubiquinol-9 to ubiquinone-9 redox ratio between *Bvra*$^{+/+}$*Apoe*$^{-/-}$ and *Bvra*$^{-/-}$*Apoe*$^{-/-}$ TS mice (Table 1). Endogenous oxidative stress was also examined in freshly isolated erythrocytes, using oxidized peroxiredoxin 2 (Prx2) as a marker (313, 314). We found that freshly isolated erythrocytes from *Bvra*$^{-/-}$*Apoe*$^{-/-}$ TS mice contained a small but statistically significant higher proportion of oxidized Prx2 compared with *Bvra*$^{+/+}$*Apoe*$^{-/-}$ TS mice (Fig. 5.5G and H). Together, these findings suggest that *Bvra* deficiency resulted in a modest increase in red blood cell but not systematic oxidative stress in this mouse model of unstable plaque.

5.3.7 Deletion of *Bvra* gene increases hepatic lipids

Similar to *Bvra*$^{-/-}$ mice on high fat diet (Chapter 4), *Bvra*$^{-/-}$*Apoe*$^{-/-}$ TS mice caused the essential absence of bilirubin in liver (Fig. 5.6A and B) and this was associated with increased hepatic lipid content. Thus, compared with *Bvra*$^{+/+}$*Apoe*$^{-/-}$ TS mice, *Bvra*$^{-/-}$*Apoe*$^{-/-}$ TS mice had higher mean concentrations of hepatic TG, cholesterol and CE, although this reached statistical significance for only hepatic TG (Fig. 5.6C to E).

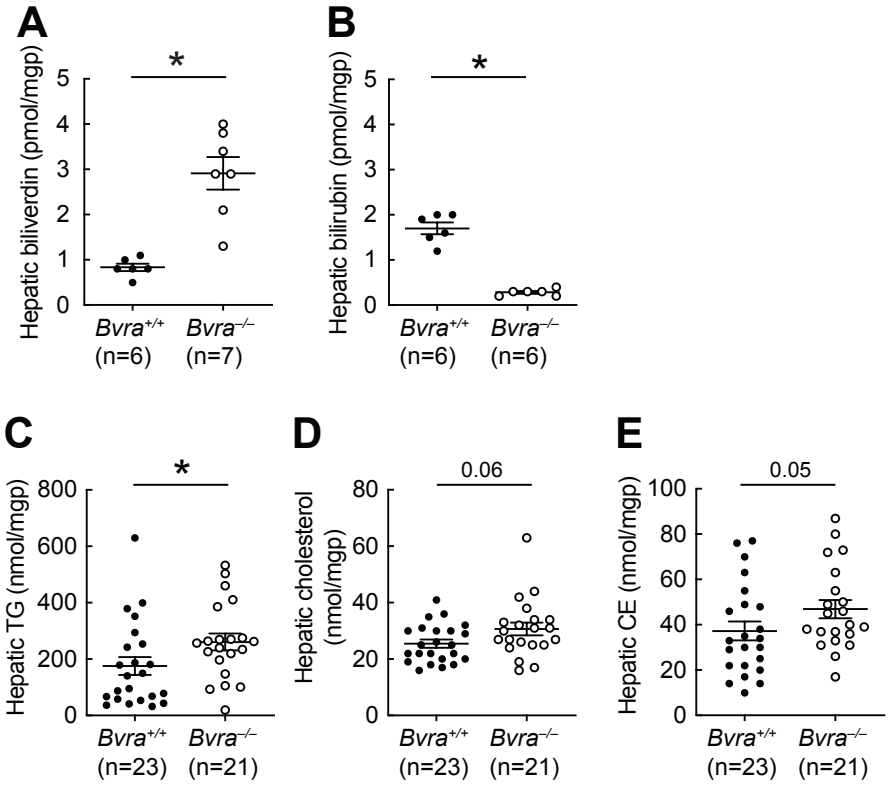

Figure 5.6 Deficiency in *Bvra* enhances hepatic steatosis in *Apoe*$^{-/-}$ TS mice**. (A**, **B)** Hepatic biliverdin and bilirubin in *Bvra*$^{+/+}$*Apoe*$^{-/-}$ TS and *Bvra*$^{-/-}$*Apoe*$^{-/-}$ TS mice, as determined by LC-MS/MS and with results normalized to protein concentration. **(C-E)** Hepatic cholesterol, TG and CE in *Bvra*$^{+/+}$*Apoe*$^{-/-}$ and *Bvra*$^{-/-}$*Apoe*$^{-/-}$ TS mice, as determined by HPLC-UV, and with results normalized to protein content (mgp). Individual results as well as mean ± SEM are shown, with data analyzed by the Mann-Whitney test. *P<0.05 compared to *Bvra*$^{+/+}$*Apoe*$^{-/-}$ mice.

5.3.8 Bilirubin does not support a broad range of NIRAF in intraplaque hemorrhage

It was reported previously that intra-plaque hemorrhage in human carotid endarterectomy specimen and unstable plaque in the TS mouse model was associated with increased infrared autofluorescence (NIRAF) (45). The associated increase in bilirubin content in unstable plaque was suggested as the source of NIRAF in that study (45). As unstable plaque of *Bvra*$^{-/-}$*Apoe*$^{-/-}$ TS mice lacks bilirubin (see above), we tested the proposed role for bilirubin as the source of NIRAF by subjecting *Bvra*$^{+/+}$*Apoe*$^{-/-}$and *Bvra*$^{-/-}$*Apoe*$^{-/-}$ TS mice to non-invasive fluorescence emission computed tomography (FLECT-CT) and excised carotid arteries to *ex vivo* Odyssey infrared imaging. We failed to observe NIRAF by FLECT-CT in *Bvra*$^{+/+}$*Apoe*$^{-/-}$ and *Bvra*$^{-/-}$*Apoe*$^{-/-}$ TS mice (Fig. 5.7A), despite these animals exhibiting intra-plaque hemorrhage in the unstable plaque. Using Odyssey infrared imaging of excised, intra-plaque hemorrhage-containing plaque from *Bvra*$^{+/+}$*Apoe*$^{-/-}$ TS mice showed detectable NIRAF that was undistinguishable in intensity compared with that seen with *Bvra*$^{-/-}$*Apoe*$^{-/-}$ TS mice (Fig. 5.7B). Importantly, quantification of fluorescence intensity using the Odyssey infrared imaging system demonstrated higher NIRAF in unstable plaque compared with the disease-free left carotid artery for both *Bvra*$^{+/+}$*Apoe*$^{-/-}$ and *Bvra*$^{-/-}$*Apoe*$^{-/-}$ TS mice (Fig. 5.7C). These findings confirm that plaque with intra-plaque hemorrhage emits NIRAF, and hence that NIRAF is a potential marker of unstable plaque, although bilirubin is not a likely source of this NIRAF.

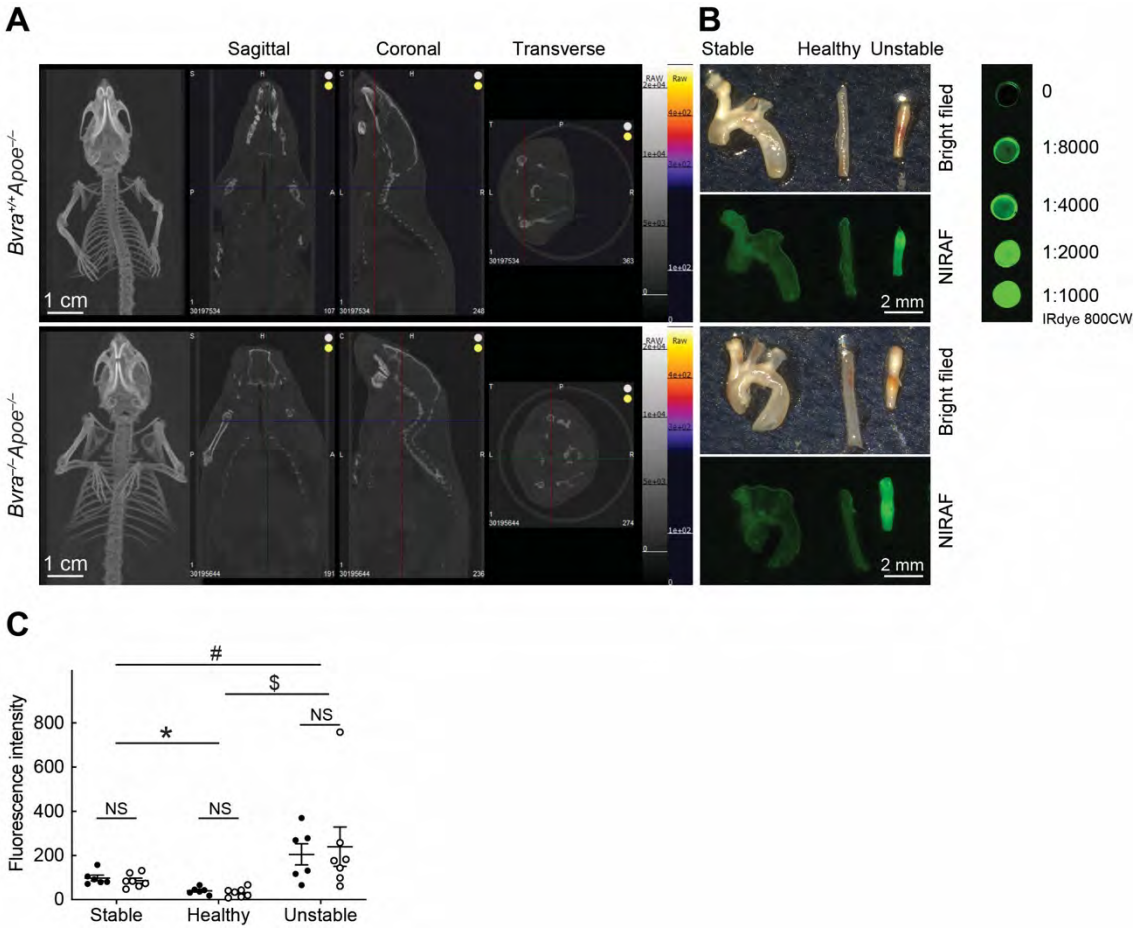

Figure 5.7 Autofluorescence in unstable and stable plaque of *Bvra*$^{+/+}$*Apoe*$^{-/-}$ and *Bvra*$^{-/-}$*Apoe*$^{-/-}$ TS mice. Near infrared autofluorescence (NIRAF) in unstable carotid artery plaque with visible intra-plaque hemorrhage was assessed by a fluorescence emission computer tomography (FLECT-CT) *in vivo* and Odyssey infrared imaging *ex vivo*. **(A)** Representative reconstructed FLECT-CT images showing the absence of NIRAF in the carotid artery. 730 nm excitation laser, 803 nm filter and scale bar = 1 cm. (**B**) Representative bright field and Odyssey NIRAF images of stable plaque, healthy artery and unstable plaque with visible intra-plaque hemorrhage from *Bvra*$^{+/+}$*Apoe*$^{-/-}$ (top two panels) and *Bvra*$^{-/-}$*Apoe*$^{-/-}$ TS mice (bottom two panels) in comparison with a serial dilution of IRDye800CW (excitation = 785 nm, emission > 800 nm) used for quantification of the results. Scale bar = 2 mm. **(C)** Quantification of NIRAF intensity of stable plaque, healthy artery and unstable plaque determined by Odyssey infrared imaging system. Results show individual data as well as mean ± SEM from n = 6 *Bvra*$^{+/+}$*Apoe*$^{-/-}$ TS mice (filled circles) and n = 7 *Bvra*$^{-/-}$*Apoe*$^{-/-}$ TS mice (open circles), with data analyzed by the Mann-Whitney test. Not significant (NS), *Bvra*$^{-/-}$*Apoe*$^{-/-}$ TS mice compared to *Bvra*$^{+/+}$*Apoe*$^{-/-}$ TS mice. $$P<0.05$ unstable plaque compared to healthy artery. *$P<0.05$ stable plaque compared with healthy artery. #$P<0.05$ unstable plaque compared with stable plaque.

5.4 Discussion

In this study, we investigated the role of BVRA in the *Apoe*$^{-/-}$ TS mouse model of atherosclerotic plaque instability. Our data show that BVRA activity is increased in unstable plaque in this model and that BVRA deficiency decreases plaque bilirubin and markedly exacerbates plaque instability as evidenced by a decrease in fibrous cap thickness and increase in lipid content. *Bvra*$^{-/-}$*Apoe*$^{-/-}$ TS mice have negligible bilirubin in blood plasma. This is associated with a modest enhancement of systematic oxidative stress and endothelial dysfunction, as well as an increase in circulating lipids and the size of stable atherosclerotic lesions examined at two separate anatomical sites. Our data show that the absence of *Bvra* and bilirubin in *Apoe*$^{-/-}$ TS mice generates a pro-atherogenic phenotype and destabilizes plaque, suggesting a causal relationship between bilirubin and a decreased atherosclerosis and hence CVD risk.

The experimental approach chosen in the present study does not directly allow conclusions to be drawn about whether the plaque destabilizing effect observed with BVRA deficiency is due to the absence of BVRA and/or bilirubin. BVRA is best known for its role of converting biliverdin to bilirubin. Existing literature indicates that the expression of heme oxygenase-1 (Hmox1), the enzyme responsible for formation of biliverdin, is increased in human and mouse unstable plaque compared with stable plaque (46, 153). In the *Apoe*$^{-/-}$ TS model, the majority (~98%) of the biliverdin formed becomes reduced to bilirubin, as judged by the arterial ratio of the two pigments (45), suggesting that these bile pigments are formed locally as a result of increased activities of Hmox1 and BVRA in the unstable plaque rather than derived from the circulation. This interpretation is supported by the fact that the concentration of biliverdin plus bilirubin in unstable plaque was comparable in *Bvra*$^{+/+}$*Apoe*$^{-/-}$ and *Bvra*$^{-/-}$*Apoe*$^{-/-}$ TS mice, whereas this was not the case for plasma. Importantly, increasing Hmox1 activity by either intravascular adenoviral transfection (46) or pharmacological induction (45) inhibits the development of unstable plaque. In light of these findings, the simplest interpretation of the observed decrease in plaque stability associated with BVRA deficiency is that the decrease in plaque bilirubin resulting from the absence of BVRA, rather than a change in Hmox1 activity or an activity of BVRA unrelated to bilirubin formation is responsible for plaque destabilization. Clearly, additional and separate experimental approaches, such as using models of hyperbilirubinemia, are required to unambiguously address this question.

The observation that deficiency of BVRA destabilizes plaque by thinning the fibrous cap by more than 50% is consistent with a human study reporting that serum concentrations of total bilirubin to be both: lower in patients experiencing an acute coronary syndrome than patients with stable angina pectoris or control subject; and positively associated with fibrous content in the culprit/target plaque, as assessed using intravascular ultrasound (227). Fibrous cap is composed predominantly of vascular smooth muscle cells (VSMC) and extracellular matrix proteins including collagen produced by these cells (367, 368). The underlying mechanisms linking BVRA

deficiency and loss of bilirubin with a decrease in fibrous cap thickness have not been fully elucidated, although it is commonly proposed that bilirubin prevents plaque progression via its antioxidant property. Bilirubin inhibits free radical chain reactions and as such protects lipids and proteins from oxidation (126, 187, 188). Bilirubin-mediated inhibition of lipoprotein lipid peroxidation in the lesion could conceivably attenuate VSMC apoptosis induced by oxidized lipoproteins (369). Unfortunately, HPLC with UV detection did not provide sufficient sensitivity to detect cholesterylester hydroxides, the single major form of oxidized lipid in atherosclerotic lesion (315), in the small amounts of lesion material available from unstable plaque of *Bvra*$^{+/+}$*Apoe*$^{-/-}$ and *Bvra*$^{-/-}$*Apoe*$^{-/-}$ TS mice (data not shown). However, lipoprotein lipid hydroperoxides could be detected in plasma of these animals, and the results obtained show that BVRA deficiency is associated with increased lipid peroxidation. It will be important to determine the extent of lipid oxidation in unstable plaque, using more sensitive methods, such as the recently described UHPLC ion mobility QTOF method for the profiling of oxidized lipids (370). Similarly, it will be important to determine the content and phenotype of VSMC in unstable plaque of *Bvra*$^{+/+}$*Apoe*$^{-/-}$ and *Bvra*$^{-/-}$*Apoe*$^{-/-}$ TS mice to more directly test whether BVRA/bilirubin regulates the content of VSMC, and hence potentially collagen synthesis. What has been reported is that intraperitoneal administration of bilirubin decreases VSMC and collagen content in stable lesions in *Ldlr*$^{-/-}$ mice beyond the observed decrease in lesion size (205), although this study lacked detailed description of the immunohistochemical method used to detect and quantify collagen, and it is currently not know whether and if so to what extent, data from stable plaque can be extrapolated to unstable plaque.

In addition to modulating the formation of extracellular matrix/collagen, *Bvra* deficiency may also promote cap thinning by increasing the degradation of extracellular matrix/collagen via regulation of metalloproteinase and/or collagenase activity. For example, products derived from lipid peroxidation enhance the production of metalloproteinase-9 in macrophages (371) and metalloproteinase-2 in VSMC (372), that can lead to increased collagen degradation. Indirect support for the notion that BVRA deficiency decreases plaque stability by increasing extracellular matrix degradation comes from our finding that compensatory (positive) remodeling is specifically enhanced in unstable compared with stable plaque in *Bvra*$^{-/-}$*Apoe*$^{-/-}$ TS mice. Pharmacological induction of Hmox1 has been reported to inhibit compensatory remodeling by decreasing the production and activity of metalloproteinase-2 and -9 (361). As the pro-inflammatory enzyme MPO causes plaque destabilization in the *Apoe*$^{-/-}$ TS mouse model (287, 373) and can activate metalloproteinase directly or indirectly via inhibition of tissue inhibitor of metalloproteinase (364, 374), we examined MPO *ex vivo* activity in unstable atherosclerotic plaque of *Bvra*$^{+/+}$*Apoe*$^{-/-}$ and *Bvra*$^{-/-}$*Apoe*$^{-/-}$ TS mice by measuring the extent of chlorination of hydroethidine to 2-chloroethidium, determined by LC-MS/MS. We observed no difference in MPO activity determined at a single time point. Additional, time-dependent MPO activity

measurements are required to exclude the possibility that BVRA deficiency increases MPO activity in unstable plaque. This is because bilirubin could conceivably act as both an inhibitor and substrate of MPO. In the latter case, bilirubin may enhance MPO activity by facilitating reduction of MPO compound II back to the native state, as described for tyrosine (375). In addition, it is possible that BVRA/bilirubin deficiency modulates the activity of peroxidasin, an enzyme with MPO-related activity, involved in the formation of collagen IV cross-links (376). This possibility could be tested by determining the content of collagen IV dimers in unstable plaque of *Bvra*$^{+/+}$*Apoe*$^{-/-}$ and *Bvra*$^{-/-}$*Apoe*$^{-/-}$ TS mice.

In humans, lower serum total bilirubin concentration correlate with higher lipid content in plaques (227), and plaque lipid content and distribution influence fibrous cap thinning and the propensity of human atherosclerotic plaques to disrupt (377). For example, esterified cholesterol (CE) accumulates at the edge of disrupted plaques (377). We observed that unstable plaque of *Bvra*$^{-/-}$*Apoe*$^{-/-}$ TS mice contained approximately twice as much cholesterol, CE and TG compared with *Bvra*$^{+/+}$*Apoe*$^{-/-}$ TS mice, as assessed by HPLC analysis of plaque homogenates. Unfortunately, this method does not allow assignment of altered lipid to specific plaque regions, so that it is not possible to conclude whether the increased lipid content in BVRA deficiency contributed to plaque destabilization.

Similar to phenotype of *Bvra*$^{-/-}$ mice on high fat diet (Chapter 4), the apparent absence of bilirubin in the livers of *Bvra*$^{-/-}$*Apoe*$^{-/-}$ TS mice was associated with hepatic lipid accumulation. Different to *Bvra*$^{-/-}$ mice, where lipid accumulation was limited to the liver, *Bvra*$^{-/-}$*Apoe*$^{-/-}$ TS mice showed signs of systemic hyperlipidemia, with significant increases in circulating cholesterol and CE. This could help explain the observed increase in endothelial dysfunction and atherogenesis in *Bvra*$^{-/-}$*Apoe*$^{-/-}$ compared with *Bvra*$^{+/+}$*Apoe*$^{-/-}$ TS mice. This hyperlipidemic phenotype is consistent with the human and animal data documenting an inverse relationship between plasma bilirubin concentration and endothelial dysfunction and risk of atherosclerosis (14, 15, 205).

It has been suggested recently that accumulation of bilirubin is the main source of NIRAF in unstable plaque with intra-plaque hemorrhage (45). As *Bvra*$^{-/-}$*Apoe*$^{-/-}$ TS mice effectively lack bilirubin, yet develop intra-plaque hemorrhage, we sought to confirm bilirubin as the source of NIRAF, using both non-invasive FLECT-CT and *ex vivo* NIRAF detection by Odyssey Imaging system. Our results confirm the presence of NIRAF in unstable plaque with intraplaque hemorrhage, as determined by the Odyssey Imaging system. Intriguingly, there was no material difference in such NIRAF between *Bvra*$^{+/+}$*Apoe*$^{-/-}$ and *Bvra*$^{-/-}$*Apoe*$^{-/-}$ TS mice. We were unable to detect NIRAF in unstable plaque by FLECT-CT, despite imaging more than 10 TS mice containing visible hemorrhage, for reasons not clear at present. Despite this, our results obtained with the Odyssey Imaging system argue against bilirubin being responsible for NIRAF in hemorrhage-containing plaque, even though our results confirm that unstable plaque contains

more bilirubin than stable plaque (45). There is separate evidence in support of the conclusion that bilirubin is not the source of NIRAF. Thus, maximal excitation and fluorescence emission of the natural form of bilirubin in mammals, bilirubin IXα, is at 460 and 530 nm, respectively, independent of whether the pigment exists in its free or protein-bound form (378), whereas the NIRAF detected in unstable plaque used excitation and emission wavelengths of 730 and 803 nm, respectively. Also, while bilirubin fluorescence can be affected by its environment, the pigment is essentially non-fluorescent in most solvents. Together, these findings do not support the notion that bilirubin is the source of NIRAF in unstable plaque with hemorrhage, although they do not negate the potential utility of NIRAF as a non-invasive marker of intra-plaque hemorrhage and hence plaque instability.

In conclusion, our data suggests that BVRA deficiency and the associated absence of bilirubin in *Apoe*$^{-/-}$ mice generates a pro-atherogenic phenotype characterized by systemic hyperlipidemia, and steatosis, increased endothelial dysfunction and atherosclerosis, as well as plaque destabilization. Indirect evidence suggests that these phenotypic alterations may be caused by the absence of bilirubin, consistent with epidemiological data that overwhelmingly documents an inverse association of plasma bilirubin with cardiovascular disease. Therefore, measures aimed at increasing plasma bilirubin modestly may represent a novel strategy to lower the risk of CVD.

Chapter 6

General Discussion

6.1 Summary of principal findings

The central scientific interest of this PhD project is to aid our understanding of the role of bilirubin in cardiovascular and metabolic diseases. The research undertaken has focused on utilizing a novel experimental mouse model of bilirubin deficiency to empirically assess the role of bilirubin in cardiometabolic pathologies. To this end I have: 1) phenotypically characterized *biliverdin reductase a* gene-knockout (*Bvra*$^{-/-}$) mice; *Bvra*$^{-/-}$ mice are characterized by the essential absence of bilirubin associated with a modest elevation of biliverdin in blood plasma, bile and liver, reminiscent of the 'green jaundice' described for humans with loss of BVRA enzyme activity (127). Importantly, *Bvra*$^{-/-}$ mice appear healthy under normal physiological conditions, inconsistent with the proposed essential role of BVRA in the activation of ERK1/2 kinases (379), as *Erk2*$^{-/-}$ mice are embryonically lethal (380). 2) Assessed oxidative stress resulting from *Bvra* deficiency; in response to *Bvra* deficiency and the associated very low plasma bilirubin concentrations, *Bvra*$^{-/-}$ mice have heightened systemic endogenous oxidative stress demonstrated by increases in plasma CE-OOH, CE-OOH/CE and oxidized Prx2 in erythrocytes. 3) Investigated the impact of *Bvra* deficiency on hepatic steatosis and insulin resistance in three different dietary models; naïve *Bvra*$^{-/-}$ mice on standard chow diet show normal glucose metabolism and insulin sensitivity, demonstrating that BVRA is not required for glucose metabolism and insulin signaling. When stressed by a HF diet, *Bvra*$^{-/-}$ mice develop a fatty liver phenotype, likely as a result of suppressed PPARα activity. Despite this, however, *Bvra*$^{-/-}$ mice retain glucose metabolism and insulin sensitivity comparable to that of wild-type animals, just as in the HFHS dietary model. Therefore, *Bvra* deficiency renders mice susceptible to HF-induced hepatic steatosis in the absence of insulin resistance. 4) Examined the impact of BVRA deficiency on atherosclerotic plaque stability. Using the *Apoe*$^{-/-}$ TS mouse model of plaque instability, our data demonstrates that the absence of BVRA generates a hyperlipidemic pro-atherogenic phenotype that is characterized by increased endothelial dysfunction, atherosclerosis and plaque destabilization, consistent with bilirubin directly decreasing atherosclerosis and risk of CVD.

Taken together, these results suggest a causal relationship between bilirubin and CVD and steatosis, beyond the well-established inverse association between the pigment and CVD. By implication, biliverdin reductase attenuates endothelial dysfunction and atherosclerotic vascular disease, and this is accentuated in the setting of insulin resistance and dyslipidemia. The knowledge gained will be helpful in devising future investigations aimed at unraveling the detailed mechanisms underlying these protective effects, as well as strategies aimed at developing novel protective strategies against cardiovascular and metabolic diseases.

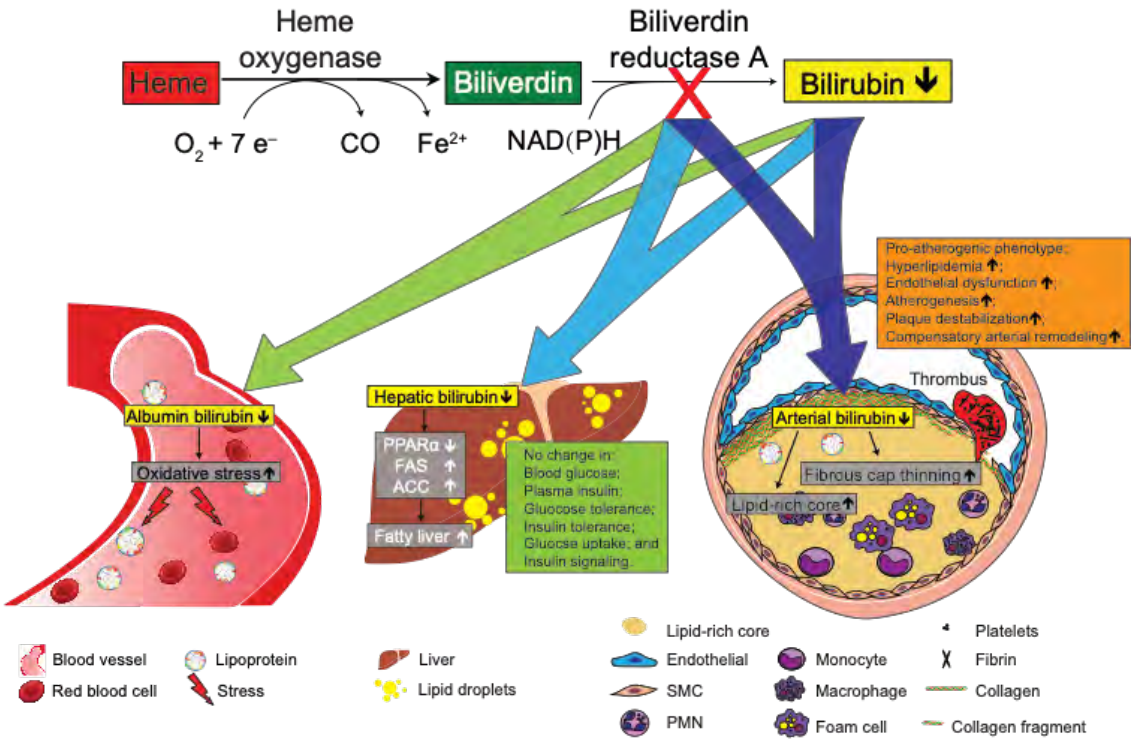

Figure 6.1 Summary diagram. Absence of biliverdin reductase A and the resulting deficiency of bilirubin increase systemic oxidative stress in naïve mice, demonstrating that physiological concentrations of bilirubin in plasma attenuate endogenous oxidative stress. In combination with a fat-rich diet, the absence of BVRA and bilirubin renders mice susceptible to hepatic steatosis in the absence of insulin resistance. Furthermore, in the mouse model of atherosclerotic plaque instability, the absence of BVRA and bilirubin causes a pro-atherogenic phenotype, characterized by increased hyperlipidemia, endothelial dysfunction and atherogenesis, as well as plaque destabilization and compensatory arterial remodeling.

6.2 Limitation of current animal model for *in vivo* investigation of bilirubin

The almost complete absence of bilirubin from plasma makes *Bvra*$^{-/-}$ mice a useful and novel tool to address the physiological roles of bilirubin (126). However, these mice have elevated concentrations of biliverdin in plasma, bile and other tissues, including liver and arteries. Since the physiological role of biliverdin in mammals is less well understood, there remains a limitation in solely summarizing the *in vivo* properties of bilirubin based on the phenotype of *Bvra*$^{-/-}$ mice. An additional potential limitation of the model relates to the proposed redox amplification cycle, whereby bilirubin is oxidized to biliverdin that is then recycled back to bilirubin by biliverdin reductase (143). However, the biological relevance of this 'redox cycle' has been challenged by our laboratory and others, essentially based on the fact that biliverdin is not a major oxidation product of bilirubin under most conditions of oxidative stress (145, 146). BVRA is also proposed to be a regulator of glucose metabolism and a transcription factor to regulate insulin signaling (20, 23, 135, 136), although our results, showing normal insulin sensitivity and glucose

metabolism in the complete absence of BVRA, are inconsistent with such a proposed role of the reductase. Nevertheless, the deficiency of BVRA combined with the comparatively (to bilirubin) small increase in tissue concentrations of biliverdin does not allow unambiguous interpretation of the results presented as demonstrating that bilirubin protects against cardiovascular and metabolic diseases.

An alternative experimental approach to investigate the properties of bilirubin *in vivo* would be to increase bilirubin concentrations. Provision of exogenous bilirubin does not appear to be a readily feasible approach, given that the pigment is scarcely soluble in physiological buffer. Therefore, supplementing experimental animals with bilirubin requires either administering bilirubin dissolved in alkaline buffer, using conjugated bilirubin (*e.g.,* bilirubin ditaurate) to enhance water solubility (277, 381), or administering biliverdin as precursor of bilirubin (111, 115, 118, 119, 122). Although these modifications can increase serum bilirubin in animals (277, 381), the following issues have to be considered and represent potential limitations: i) how does this exogenous bilirubin relate to endogenous bilirubin? ii) what is the mechanism of uptake of exogenous bilirubin into circulation? iii) how can a moderate increase in bilirubin concentration be maintained using exogenous bilirubin in light of the highly efficient conversion of bilirubin via UGT1A1? and (iv) does administration of biliverdin exert a biologically noticeable oxidative stress, given that conversion to bilirubin will result in oxidation of reduced pyridine nucleotides?

In light of the above questions, genetically modified animals with elevated endogenous bilirubin concentrations may be a better choice. For instance, the Gunn rat is a well-known model of hyperbilirubinemia as this animal has plasma bilirubin concentrations of 80~120 μM due to a deficiency of hepatic glucuronyl transferase (382). However, such high bilirubin concentrations more closely resemble the Crigler–Najjar rather than the Gilbert syndrome, and they cause neurotoxicity and lead to brain damage (174, 175). Also, using a rat model for this PhD project has obvious limitations, including that the rat is not a commonly used species to study cardiovascular and metabolic diseases, as relevant genetically modified animals are not readily available (288).

A mouse model with *Ugt1a1* deficiency could be an alternative choice. The initially generated global *Ugt1a1* gene knock-out mouse is characterized by severe hyperbilirubinemia, the development of kernicterus, and resulting lethality in the first weeks of life (350, 351). More recently, a *Ugta1a* humanized mouse with inactivated endogenous *Ugt1a1* gene and transgenic expression of the human *UGT1A1*28* gene has been generated. *UGT1A1*28* refers to a polymorphism with an ATATATATATATATATAA sequence in the promoter region of the gene replacing the ATATATATATATATAA sequence of the normal allele *UGT1A1*1*. The *UGT1A1*28* polymorphism results in a slight decrease in *UGT1A1* transcription and this impairs enzymatic function and causes moderate hyperbilirubinemia resembling Gilbert's syndrome (350, 351). While humanized *UGT1A1**28 mice exhibit neonatal hyperbilirubinemia, only ~10% of the

mice experience kernicterus followed by death, and plasma bilirubin concentrations eventually return to moderate levels of around 35 μM in adulthood (7, 350). Unfortunately, these animals were not available at the beginning of my PhD project. In light of the interesting results observed in the current thesis with BVRA-deficient mice, repeating some of the experiments with *Ugta1a* humanized mice is warranted. Such experiments have the potential to unambiguously establish, or otherwise, the role of non-toxic concentrations of bilirubin resembling those observed in humans with Gilbert's syndrome in the prevention of experimental systematic oxidative stress, atherogenesis and atherosclerotic plaque destabilization, and hepatic steatosis, as suggested by the results presented in this thesis.

6.3 Knowledge gap of elevated biliverdin

At the start of my candidature, evidence for accumulation of biliverdin during normal heme metabolism in mice was not available. In fact, biliverdin was thought to be essentially undetectable *in vivo*, due to its rapid reduction to bilirubin of biliverdin reductase. However, we demonstrated that biliverdin accounts for ~25% of hepatic bile pigments in wild-type mice under both stress and non-stress conditions. This is different to the situation in plasma, where biliverdin accounts for only ~1% of bile pigments. Bile pigments were detected by LC-MS/MS-based methods, providing improved specificity and sensitivity compared to previously used methods (185, 383). The relatively large amounts of biliverdin that accumulate in liver under physiological conditions indicates that either some of the pigment 'escapes' reduction by active BVRA, or the available BVRA activity is insufficient to 'deal with' the amounts of biliverdin formed/present in the liver. Our finding also suggests a potential limitation to the perceived role of BVRA in 'releasing' biliverdin from heme oxygenase, and as such accelerating the rate-limiting step in the three-step degradation process of heme by the oxygenase (384). A possible biological explanation for the relatively high hepatic concentration of biliverdin in wild-type mice may be that biliverdin protects the liver against pathological conditions. For example, biliverdin has antioxidant property *in vitro* (300), suppresses hepatic oxidative stress induced by bile acid (345), initiates liver regeneration after immune-mediated injury or ischemia/reperfusion injury (119, 346), and regulates lipid accumulation (8). It would be interesting to examine whether significant amounts of biliverdin are also present in tissues other than liver, utilizing the LC-MS/MS method employed in the present studies.

6.4 Knowledge gap of biliverdin reductase

Deficiency of biliverdin reductase was once thought to be lethal (385), since release of biliverdin from heme oxygenase, and hence heme metabolism, was thought to be driven by biliverdin reductase (see above). Therefore, it was thought that in the absence of functional biliverdin reductase, activity of heme oxygenase could conceivably decrease, with heme accumulating to

high toxic concentrations.

However, the absence of BVRA unlikely altered heme oxygenase activity as hepatic expression of *Hmox1* and *Homx2* mRNA as well as biliverdin and bilirubin concentrations were comparable in *Bvra*$^{+/+}$ and *Bvra*$^{-/-}$ mice. Furthermore, plasma iron, one of the heme catabolism products, was not different between *Bvra*$^{+/+}$ and *Bvra*$^{-/-}$ mice. We are yet to measure CO concentration, another product of heme oxygenase activity.

In addition to the results presented in this thesis, two recent reports describing three patients with a homozygous mutation in *BLVRA* resulting in inactive reductase argue against the notion that BVRA is essential for survival of mammals and humans (127, 386). While the mutation reported results in the complete absence of biliverdin reductase activity, the phenotype of the affected subjects is the appearance of green jaundice in association with cholestasis (127). Unfortunately, tissue concentrations of heme were not reported in the human cases. In any case, a lethal condition associated with heme accumulation was not observed.

Consistently, the global BVRA-deficient mouse generated for this thesis (126) (Chapter 3) shows no signs of substantive heme accumulation, is healthy and fecund, and is characterized by a green gall bladder (126). Moreover, Dr. Wadie Bahou (Stony Brook University, New York) revealed (personal communication) that mice with global deficiency of BVRB are also healthy and do not show an obvious phenotype. Together, these findings strongly suggest that the absence of BVRA (and possibly also BVRB) is not lethal and does not alter heme degradation. It would be interesting to test whether there is redundancy in the function of BVRA and BVRB, by generating *Bvra*$^{-/-}$*Bvrb*$^{-/-}$ mice.

6.5 Evolutionary advantage of biliverdin reductase

The evolutionary reason for the introduction of biliverdin reductase and associated formation of bilirubin, the product of its enzymatic activity, is poorly understood. Birds, amphibians and reptiles secrete biliverdin as the degradation product of heme. Therefore, enzymatic conversion of biliverdin to bilirubin via biliverdin reductase for excretion of metabolic waste appears unnecessary. Moreover, bilirubin has to go through a further energetically expensive glucuronidation reaction catalyzed by UGT1A1 to become water-soluble for excretion. As indicated previously, biliverdin has potential cytoprotective properties and can act as a hydrophilic antioxidant. Stocker *et al*. has also shown that biliverdin in different forms has a stronger antioxidant activity than bilirubin *in vitro* (2, 3, 109). However, biliverdin may not accumulate in sufficient concentration in the blood to provide such protection and eliminate harmful oxidants in mammals, as it is rapidly removed from the circulation (126, 387). Biliverdin reductase, therefore, may have evolved to convert biliverdin (a water-soluble antioxidant) to bilirubin (a water-insoluble antioxidant), thus maintaining sufficient bile pigment in the body, as the body seeks to retain this tetrapyrrole for its antioxidant protective effects.

6.6 Overall results

The alterations of oxidative stress, endothelial function and atherosclerosis in *Bvra*-deficient *versus* wild-type mice are statistically significant, but modest. Such modest effects are perhaps not surprising, however, given that the plasma concentration of bilirubin in wild-type mice is only ~1-2 μM, and the observed increase in biliverdin concentration in *Bvra*$^{-/-}$ mice may represent a compensatory response. Interestingly, BVRA deficiency caused a comparatively more substantial difference in atherosclerotic plaque stability, comparable to the effect reported for deficiency in the pro-inflammatory enzyme myeloperoxidase (287), warranting further mechanistic studies. In any case, a comparatively greater effect would be expected in humans, with bilirubin concentrations of 3-14 μM (normal range) (322) and 20-50 μM for individuals with Gilbert's syndrome who are protected from CVD.

Chapter 7

References

1. WHO (2017) Cardiovascular diseases, fact sheet, reviewed September 2016.
2. Stocker R, Yamamoto Y, McDonagh AF, Glazer AN, & Ames BN (1987) Bilirubin is an antioxidant of possible physiological importance. *Science* 235:1043-1046.
3. Stocker R & Ames BN (1987) Potential role of conjugated bilirubin and copper in the metabolism of lipid peroxides in bile. *Proc Natl Acad Sci U S A* 84:8130-8134.
4. Hayashi S, Takamiya R, Yamaguchi T, Matsumoto K, Tojo SJ, Tamatani T, Kitajima M, Makino N, Ishimura Y, & Suematsu M (1999) Induction of heme oxygenase-1 suppresses venular leukocyte adhesion elicited by oxidative stress: role of bilirubin generated by the enzyme. *Circ Res* 85:663-671.
5. Ollinger R, Bilban M, Erat A, Froio A, McDaid J, Tyagi S, Csizmadia E, Graca-Souza AV, Liloia A, Soares MP, Otterbein LE, Usheva A, Yamashita K, & Bach FH (2005) Bilirubin: a natural inhibitor of vascular smooth muscle cell proliferation. *Circulation* 112:1030-1039.
6. Kawamura K, Ishikawa K, Wada Y, Kimura S, Matsumoto H, Kohro T, Itabe H, Kodama T, & Maruyama Y (2005) Bilirubin from heme oxygenase-1 attenuates vascular endothelial activation and dysfunction. *Arterioscler Thromb Vasc Biol* 25:155-160.
7. Hinds TD, Jr., Hosick PA, Chen S, Tukey RH, Hankins MW, Nestor-Kalinoski A, & Stec DE (2017) Mice with hyperbilirubinemia due to Gilbert's syndrome polymorphism are resistant to hepatic steatosis by decreased serine 73 phosphorylation of PPARα. *Am J Physiol Endocrinol Metab* 312:244-252.
8. Stec DE, John K, Trabbic CJ, Luniwal A, Hankins MW, Baum J, & Hinds TD, Jr. (2016) Bilirubin binding to PPARα inhibits lipid accumulation. *PLoS One* 11:e0153427.
9. Schwertner HA, Jackson WG, & Tolan G (1994) Association of low serum concentration of bilirubin with increased risk of coronary artery disease. *Clin Chem* 40:18-23.
10. Lin JP, O'Donnell CJ, Schwaiger JP, Cupples LA, Lingenhel A, Hunt SC, Yang S, & Kronenberg F (2006) Association between the UGT1A1*28 allele, bilirubin levels, and coronary heart disease in the Framingham Heart Study. *Circulation* 114:1476-1481.
11. Hopkins PN, Wu LL, Hunt SC, James BC, Vincent GM, & Williams RR (1996) Higher serum bilirubin is associated with decreased risk for early familial coronary artery disease. *Arterioscler Thromb Vasc Biol* 16:250-255.
12. Lin JP, Cupples LA, Wilson PW, Heard-Costa N, & O'Donnell CJ (2003) Evidence for a gene influencing serum bilirubin on chromosome 2q telomere: a genomewide scan in the Framingham study. *Am J Hum Genet* 72:1029-1034.
13. Tukey RH & Strassburg CP (2000) Human UDP-glucuronosyltransferases: metabolism, expression, and disease. *Annu Rev Pharmacol Toxicol* 40:581-616.

14. Ishizaka N, Ishizaka Y, Takahashi E, Yamakado M, & Hashimoto H (2001) High serum bilirubin level is inversely associated with the presence of carotid plaque. *Stroke* 32:580-583.
15. Yang XF, Chen YZ, Su JL, Wang FY, & Wang LX (2009) Relationship between serum bilirubin and carotid atherosclerosis in hypertensive patients. *Intern Med* 48:1595-1599.
16. Schwertner HA & Fischer JR, Jr. (2000) Comparison of various lipid, lipoprotein, and bilirubin combinations as risk factors for predicting coronary artery disease. *Atherosclerosis* 150:381-387.
17. Perlstein TS, Pande RL, Creager MA, Weuve J, & Beckman JA (2008) Serum total bilirubin level, prevalent stroke, and stroke outcomes: NHANES 1999-2004. *Am J Med* 121:781-788.
18. Oda E & Kawai R (2012) A possible cross-sectional association of serum total bilirubin with coronary heart disease and stroke in a Japanese health screening population. *Heart Vessels* 27:29-36.
19. O'Brien L, Hosick PA, John K, Stec DE, & Hinds TD, Jr. (2015) Biliverdin reductase isozymes in metabolism. *Trends Endocrinol Metab* 26:212-220.
20. Maines MD (2010) Potential application of biliverdin reductase and its fragments to modulate insulin/IGF-1/MAPK/PI3-K signaling pathways in therapeutic settings. *Curr Drug Targets* 11:1586-1594.
21. Ko GT, Chan JC, Woo J, Lau E, Yeung VT, Chow CC, Li JK, So WY, & Cockram CS (1996) Serum bilirubin and cardiovascular risk factors in a Chinese population. *J Cardiovasc Risk* 3:459-463.
22. Fukui M, Tanaka M, Yamazaki M, Hasegawa G, Nishimura M, Iwamoto N, Ono T, Imai S, & Nakamura N (2011) Low serum bilirubin concentration in haemodialysis patients with type 2 diabetes. *Diabet Med* 28:96-99.
23. Kapitulnik J & Maines MD (2009) Pleiotropic functions of biliverdin reductase: cellular signaling and generation of cytoprotective and cytotoxic bilirubin. *Trends Pharmacol Sci* 30:129-137.
24. AIHW (2018) Australian Institute of Health and Welfare reports, Cardiovascular disease snapshot.
25. Rodgers KR (1999) Heme-based sensors in biological systems. *Curr Opin Chem Biol* 3:158-167.
26. Fernandez AZ, Lopez F, Tablante A, Romano E, Hurt-Camejo E, Camejo G, & Apitz-Castro R (2001) Intravascular hemolysis increases atherogenicity of diet-induced hypercholesterolemia in rabbits in spite of heme oxygenase-1 gene and protein induction. *Atherosclerosis* 158:103-111.

27. Wagener FA, Eggert A, Boerman OC, Oyen WJ, Verhofstad A, Abraham NG, Adema G, van Kooyk Y, de Witte T, & Figdor CG (2001) Heme is a potent inducer of inflammation in mice and is counteracted by heme oxygenase. *Blood* 98:1802-1811.
28. Tenhunen R, Marver HS, & Schmid R (1969) Microsomal heme oxygenase. *J Biol Chem* 244:6388-6394.
29. Balla G, Jacob HS, Balla J, Rosenberg M, Nath K, Apple F, Eaton JW, & Vercellotti GM (1992) Ferritin: a cytoprotective antioxidant strategem of endothelium. *J Biol Chem* 267:18148-18153.
30. McDonagh AF (2001) Turning green to gold. *Nat Struct Biol* 8:198-200.
31. Ryter SW, Alam J, & Choi AM (2006) Heme oxygenase-1/carbon monoxide: from basic science to therapeutic applications. *Physiol Rev* 86:583-650.
32. Lee BS, Heo J, Kim YM, Shim SM, Pae HO, Kim YM, & Chung HT (2006) Carbon monoxide mediates heme oxygenase 1 induction via Nrf2 activation in hepatoma cells. *Biochem Biophys Res Commun* 343:965-972.
33. Ma Q (2013) Role of nrf2 in oxidative stress and toxicity. *Annu Rev Pharmacol Toxicol* 53:401-426.
34. Ayer A, Zarjou A, Agarwal A, & Stocker R (2016) Heme oxygenases in cardiovascular health and disease. *Physiol Rev* 96:1449-1508.
35. Reichard JF, Motz GT, & Puga A (2007) Heme oxygenase-1 induction by NRF2 requires inactivation of the transcriptional repressor BACH1. *Nucleic Acids Res* 35:7074-7086.
36. Stocker R & Perrella MA (2006) Heme oxygenase-1: a novel drug target for atherosclerotic diseases? *Circulation* 114:2178-2189.
37. Dunn LL, Midwinter RG, Ni J, Hamid HA, Parish CR, & Stocker R (2014) New insights into intracellular locations and functions of heme oxygenase-1. *Antioxid Redox Signal* 20:1723-1742.
38. Wu BJ, Midwinter RG, Cassano C, Beck K, Wang Y, Changsiri D, Gamble JR, & Stocker R (2009) Heme oxygenase-1 increases endothelial progenitor cells. *Arterioscler Thromb Vasc Biol* 29:1537-1542.
39. Brouard S, Otterbein LE, Anrather J, Tobiasch E, Bach FH, Choi AM, & Soares MP (2000) Carbon monoxide generated by heme oxygenase 1 suppresses endothelial cell apoptosis. *J Exp Med* 192:1015-1026.
40. Morita T, Perrella MA, Lee ME, & Kourembanas S (1995) Smooth muscle cell-derived carbon monoxide is a regulator of vascular cGMP. *Proc Natl Acad Sci U S A* 92:1475-1479.
41. Chan KH, Ng MK, & Stocker R (2011) Haem oxygenase-1 and cardiovascular disease: mechanisms and therapeutic potential. *Clin Sci (Lond)* 120:493-504.

42. Wang LJ, Lee TS, Lee FY, Pai RC, & Chau LY (1998) Expression of heme oxygenase-1 in atherosclerotic lesions. *Am J Pathol* 152:711-720.

43. Ishikawa K, Sugawara D, Wang X, Suzuki K, Itabe H, Maruyama Y, & Lusis AJ (2001) Heme oxygenase-1 inhibits atherosclerotic lesion formation in Ldl-receptor knockout mice. *Circ Res* 88:506-512.

44. Yet SF, Layne MD, Liu X, Chen YH, Ith B, Sibinga NE, & Perrella MA (2003) Absence of heme oxygenase-1 exacerbates atherosclerotic lesion formation and vascular remodeling. *FASEB J* 17:1759-1761.

45. Htun NM, Chen YC, Lim B, Schiller T, Maghzal GJ, Huang AL, Elgass KD, Rivera J, Schneider HG, Wood BR, Stocker R, & Peter K (2017) Near-infrared autofluorescence induced by intraplaque hemorrhage and heme degradation as marker for high-risk atherosclerotic plaques. *Nat Commun* 8:75.

46. Cheng C, Noordeloos AM, Jeney V, Soares MP, Moll F, Pasterkamp G, Serruys PW, & Duckers HJ (2009) Heme oxygenase 1 determines atherosclerotic lesion progression into a vulnerable plaque. *Circulation* 119:3017-3027.

47. Wu BJ, Kathir K, Witting PK, Beck K, Choy K, Li C, Croft KD, Mori TA, Tanous D, Adams MR, Lau AK, & Stocker R (2006) Antioxidants protect from atherosclerosis by a heme oxygenase-1 pathway that is independent of free radical scavenging. *J Exp Med* 203:1117-1127.

48. Lau AK, Leichtweis SB, Hume P, Mashima R, Hou JY, Chaufour X, Wilkinson B, Hunt NH, Celermajer DS, & Stocker R (2003) Probucol promotes functional reendothelialization in balloon-injured rabbit aortas. *Circulation* 107:2031-2036.

49. Beck K, Wu BJ, Ni J, Santiago FS, Malabanan KP, Li C, Wang Y, Khachigian LM, & Stocker R (2010) Interplay between heme oxygenase-1 and the multifunctional transcription factor yin yang 1 in the inhibition of intimal hyperplasia. *Circ Res* 107:1490-1497.

50. Collinson EJ, Wimmer-Kleikamp S, Gerega SK, Yang YH, Parish CR, Dawes IW, & Stocker R (2011) The yeast homolog of heme oxygenase-1 affords cellular antioxidant protection via the transcriptional regulation of known antioxidant genes. *J Biol Chem* 286:2205-2214.

51. Nicolai A, Li M, Kim DH, Peterson SJ, Vanella L, Positano V, Gastaldelli A, Rezzani R, Rodella LF, Drummond G, Kusmic C, L'Abbate A, Kappas A, & Abraham NG (2009) Heme oxygenase-1 induction remodels adipose tissue and improves insulin sensitivity in obesity-induced diabetic rats. *Hypertension* 53:508-515.

52. Ndisang JF, Lane N, & Jadhav A (2009) The heme oxygenase system abates hyperglycemia in Zucker diabetic fatty rats by potentiating insulin-sensitizing pathways. *Endocrinology* 150:2098-2108.

53. Ndisang JF & Jadhav A (2009) Up-regulating the hemeoxygenase system enhances insulin sensitivity and improves glucose metabolism in insulin-resistant diabetes in Goto-Kakizaki rats. *Endocrinology* 150:2627-2636.

54. Burgess A, Li M, Vanella L, Kim DH, Rezzani R, Rodella L, Sodhi K, Canestraro M, Martasek P, Peterson SJ, Kappas A, & Abraham NG (2010) Adipocyte heme oxygenase-1 induction attenuates metabolic syndrome in both male and female obese mice. *Hypertension* 56:1124-1130.

55. Chen YH, Lin SJ, Lin MW, Tsai HL, Kuo SS, Chen JW, Charng MJ, Wu TC, Chen LC, Ding YA, Pan WH, Jou YS, & Chau LY (2002) Microsatellite polymorphism in promoter of heme oxygenase-1 gene is associated with susceptibility to coronary artery disease in type 2 diabetic patients. *Hum Genet* 111:1-8.

56. Arredondo M, Jorquera D, Carrasco E, Albala C, & Hertrampf E (2007) Microsatellite polymorphism in the heme oxygenase-1 gene promoter is associated with iron status in persons with type 2 diabetes mellitus. *Am J Clin Nutr* 86:1347-1353.

57. Shakeri-Manesch S, Zeyda M, Huber J, Ludvik B, Prager G, & Stulnig TM (2009) Diminished upregulation of visceral adipose heme oxygenase-1 correlates with waist-to-hip ratio and insulin resistance. *Int J Obes (Lond)* 33:1257-1264.

58. Qiao H, Sai X, Gai L, Huang G, Chen X, Tu X, & Ding Z (2014) Association between heme oxygenase 1 gene promoter polymorphisms and susceptibility to coronary artery disease: a HuGE review and meta-analysis. *Am J Epidemiol* 179:1039-1048.

59. Jais A, Einwallner E, Sharif O, Gossens K, Lu TT, Soyal SM, Medgyesi D, Neureiter D, Paier-Pourani J, Dalgaard K, Duvigneau JC, Lindroos-Christensen J, Zapf TC, Amann S, Saluzzo S, Jantscher F, Stiedl P, Todoric J, Martins R, Oberkofler H, Muller S, Hauser-Kronberger C, Kenner L, Casanova E, Sutterluty-Fall H, Bilban M, Miller K, Kozlov AV, Krempler F, Knapp S, Lumeng CN, Patsch W, Wagner O, Pospisilik JA, & Esterbauer H (2014) Heme oxygenase-1 drives metaflammation and insulin resistance in mouse and man. *Cell* 158:25-40.

60. Raju VS, McCoubrey WK, Jr., & Maines MD (1997) Regulation of heme oxygenase-2 by glucocorticoids in neonatal rat brain: characterization of a functional glucocorticoid response element. *Biochim Biophys Acta* 1351:89-104.

61. Williams SE, Wootton P, Mason HS, Bould J, Iles DE, Riccardi D, Peers C, & Kemp PJ (2004) Heme oxygenase-2 is an oxygen sensor for a calcium-sensitive potassium channel. *Science* 306:2093-2097.

62. Ortega-Saenz P, Pascual A, Gomez-Diaz R, & Lopez-Barneo J (2006) Acute oxygen sensing in heme oxygenase-2 null mice. *J Gen Physiol* 128:405-411.

63. Bellner L, Martinelli L, Halilovic A, Patil K, Puri N, Dunn MW, Regan RF, & Schwartzman ML (2009) Heme oxygenase-2 deletion causes endothelial cell activation

marked by oxidative stress, inflammation, and angiogenesis. *J Pharmacol Exp Ther* 331:925-932.

64. He JZ, Ho JJ, Gingerich S, Courtman DW, Marsden PA, & Ward ME (2010) Enhanced translation of heme oxygenase-2 preserves human endothelial cell viability during hypoxia. *J Biol Chem* 285:9452-9461.
65. Seta F, Bellner L, Rezzani R, Regan RF, Dunn MW, Abraham NG, Gronert K, & Laniado-Schwartzman M (2006) Heme oxygenase-2 is a critical determinant for execution of an acute inflammatory and reparative response. *Am J Pathol* 169:1612-1623.
66. Bellner L, Vitto M, Patil KA, Dunn MW, Regan R, & Laniado-Schwartzman M (2008) Exacerbated corneal inflammation and neovascularization in the HO-2 null mice is ameliorated by biliverdin. *Exp Eye Res* 87:268-278.
67. Otterbein LE, Bach FH, Alam J, Soares M, Tao Lu H, Wysk M, Davis RJ, Flavell RA, & Choi AM (2000) Carbon monoxide has anti-inflammatory effects involving the mitogen-activated protein kinase pathway. *Nat Med* 6:422-428.
68. Otterbein LE, Foresti R, & Motterlini R (2016) Heme oxygenase-1 and carbon monoxide in the heart: the balancing act between danger signaling and pro-survival. *Circ Res* 118:1940-1959.
69. Almeida AS, Queiroga CS, Sousa MF, Alves PM, & Vieira HL (2012) Carbon monoxide modulates apoptosis by reinforcing oxidative metabolism in astrocytes: role of Bcl-2. *J Biol Chem* 287:10761-10770.
70. Berne JP, Lauzier B, Rochette L, & Vergely C (2012) Carbon monoxide protects against ischemia-reperfusion injury in vitro via antioxidant properties. *Cell Physiol Biochem* 29:475-484.
71. Lee TS & Chau LY (2002) Heme oxygenase-1 mediates the anti-inflammatory effect of interleukin-10 in mice. *Nat Med* 8:240-246.
72. Thorup C, Jones CL, Gross SS, Moore LC, & Goligorsky MS (1999) Carbon monoxide induces vasodilation and nitric oxide release but suppresses endothelial NOS. *Am J Physiol* 277:882-889.
73. Otterbein LE, Zuckerbraun BS, Haga M, Liu F, Song R, Usheva A, Stachulak C, Bodyak N, Smith RN, Csizmadia E, Tyagi S, Akamatsu Y, Flavell RJ, Billiar TR, Tzeng E, Bach FH, Choi AM, & Soares MP (2003) Carbon monoxide suppresses arteriosclerotic lesions associated with chronic graft rejection and with balloon injury. *Nat Med* 9:183-190.
74. Chlopicki S, Olszanecki R, Marcinkiewicz E, Lomnicka M, & Motterlini R (2006) Carbon monoxide released by CORM-3 inhibits human platelets by a mechanism independent of soluble guanylate cyclase. *Cardiovasc Res* 71:393-401.
75. Sato K, Balla J, Otterbein L, Smith RN, Brouard S, Lin Y, Csizmadia E, Sevigny J, Robson SC, Vercellotti G, Choi AM, Bach FH, & Soares MP (2001) Carbon monoxide

generated by heme oxygenase-1 suppresses the rejection of mouse-to-rat cardiac transplants. *J Immunol* 166:4185-4194.

76. Kim KM, Pae HO, Zheng M, Park R, Kim YM, & Chung HT (2007) Carbon monoxide induces heme oxygenase-1 via activation of protein kinase R-like endoplasmic reticulum kinase and inhibits endothelial cell apoptosis triggered by endoplasmic reticulum stress. *Circ Res* 101:919-927.
77. Hopper CP, Meinel L, Steiger C, & Otterbein LE (2018) Where is the clinical breakthrough of heme oxygenase-1/carbon monoxide therapeutics? *Curr Pharm Des* 24:2264-2282.
78. Sawicki KT, Chang HC, & Ardehali H (2015) Role of heme in cardiovascular physiology and disease. *J Am Heart Assoc* 4:e001138.
79. Poss KD & Tonegawa S (1997) Heme oxygenase 1 is required for mammalian iron reutilization. *Proc Natl Acad Sci U S A* 94:10919-10924.
80. Delaby C, Pilard N, Puy H, & Canonne-Hergaux F (2008) Sequential regulation of ferroportin expression after erythrophagocytosis in murine macrophages: early mRNA induction by haem, followed by iron-dependent protein expression. *Biochem J* 411:123-131.
81. Eisenstein RS, Garcia-Mayol D, Pettingell W, & Munro HN (1991) Regulation of ferritin and heme oxygenase synthesis in rat fibroblasts by different forms of iron. *Proc Natl Acad Sci U S A* 88:688-692.
82. Ponka P, Beaumont C, & Richardson DR (1998) Function and regulation of transferrin and ferritin. *Semin Hematol* 35:35-54.
83. Hentze MW, Muckenthaler MU, Galy B, & Camaschella C (2010) Two to tango: regulation of Mammalian iron metabolism. *Cell* 142:24-38.
84. Dunn LL, Suryo Rahmanto Y, & Richardson DR (2007) Iron uptake and metabolism in the new millennium. *Trends Cell Biol* 17:93-100.
85. Petrat F, de Groot H, & Rauen U (2000) Determination of the chelatable iron pool of single intact cells by laser scanning microscopy. *Arch Biochem Biophys* 376:74-81.
86. Sullivan JL (2009) Iron in arterial plaque: modifiable risk factor for atherosclerosis. *Biochim Biophys Acta* 1790:718-723.
87. Sullivan JL (1981) Iron and the sex difference in heart disease risk. *Lancet* 1:1293-1294.
88. Stocker R & Keaney JF, Jr. (2004) Role of oxidative modifications in atherosclerosis. *Physiol Rev* 84:1381-1478.
89. Satchell L & Leake DS (2012) Oxidation of low-density lipoprotein by iron at lysosomal pH: implications for atherosclerosis. *Biochemistry* 51:3767-3775.

90. Li L & Frei B (2006) Iron chelation inhibits NF-κB-mediated adhesion molecule expression by inhibiting p22(phox) protein expression and NADPH oxidase activity. *Arterioscler Thromb Vasc Biol* 26:2638-2643.

91. DeBoer DA & Clark RE (1992) Iron chelation in myocardial preservation after ischemia-reperfusion injury: the importance of pretreatment and toxicity. *Ann Thorac Surg* 53:412-418.

92. Hedlund BE & Hallaway PE (1993) High-dose systemic iron chelation attenuates reperfusion injury. *Biochem Soc Trans* 21:340-343.

93. Simcox JA & McClain DA (2013) Iron and diabetes risk. *Cell Metab* 17:329-341.

94. Cooksey RC, Jones D, Gabrielsen S, Huang J, Simcox JA, Luo B, Soesanto Y, Rienhoff H, Abel ED, & McClain DA (2010) Dietary iron restriction or iron chelation protects from diabetes and loss of β-cell function in the obese mouse. *Am J Physiol Endocrinol Metab* 298:1236-1243.

95. Miller M & Hutchins GM (1994) Hemochromatosis, multiorgan hemosiderosis, and coronary artery disease. *JAMA* 272:231-233.

96. Beutler E, Felitti VJ, Koziol JA, Ho NJ, & Gelbart T (2002) Penetrance of 845G->A (C282Y) HFE hereditary haemochromatosis mutation in the USA. *Lancet* 359:211-218.

97. Gray CH, Nicholson DC, & Tipton G (1972) Degradation of haem compounds to bile pigments. *Nat New Biol* 239:5-8.

98. Franklin EM, Browne S, Horan AM, Inomata K, Hammam MA, Kinoshita H, Lamparter T, Golfis G, & Mantle TJ (2009) The use of synthetic linear tetrapyrroles to probe the verdin sites of human biliverdin-IXα reductase and human biliverdin-IXβ reductase. *FEBS J* 276:4405-4413.

99. Yamaguchi T & Nakajima H (1995) Changes in the composition of bilirubin-IX isomers during human prenatal development. *Eur J Biochem* 233:467-472.

100. O'Carra P & Colleran E (1970) Methine-bridge specificity of the coupled oxidation of myoglobin and haemoglobin with ascorbate. *Biochem J* 119:42-43.

101. Rockwell NC & Lagarias JC (2006) The structure of phytochrome: a picture is worth a thousand spectra. *Plant Cell* 18:4-14.

102. Hongo Y, Yasuda N, & Naga IS (2017) Identification of genes for synthesis of the blue pigment, biliverdin IXα, in the blue coral *heliopora coerulea*. *Biol Bull* 232:71-81.

103. Hargitai R, Boross N, Hamori S, Neuberger E, & Nyiri Z (2017) Eggshell biliverdin and protoporphyrin pigments in a songbird: are they derived from erythrocytes, blood plasma, or the shell gland? *Physiol Biochem Zool* 90:613-626.

104. Ishikawa S, Suzuki K, Fukuda E, Arihara K, Yamamoto Y, Mukai T, & Itoh M (2010) Photodynamic antimicrobial activity of avian eggshell pigments. *FEBS Lett* 584:770-774.

105. Zhang T, Liu H, Wang J, Li L, Han C, Mustafa A, & Xiong X (2019) Evidences in duck (Anas platyrhynchos) by transcriptome data for supporting the biliverdin was mainly synthesized by shell gland. *Poult Sci* 98:2260-2271.

106. García-Navas V, Sanz JJ, Merino S, Martínez–de la Puente J, Lobato E, del Cerro S, Rivero J, Ruiz de Castañeda R, & Moreno J (2011) Experimental evidence for the role of calcium in eggshell pigmentation pattern and breeding performance in Blue Tits *Cyanistes caeruleus*. *J Ornithol* 152:71-82.

107. Wiemann J, Yang T-R, Sander PN, Schneider M, Engeser M, Kath-Schorr S, Müller CE, & Sander PM (2017) Dinosaur origin of egg color: oviraptors laid blue-green eggs. *PeerJ* 5:e3706.

108. Stocker R & Peterhans E (1989) Antioxidant properties of conjugated bilirubin and biliverdin: biologically relevant scavenging of hypochlorous acid. *Free Radic Res Commun* 6:57-66.

109. Stocker R & Peterhans E (1989) Synergistic interaction between vitamin E and the bile pigments bilirubin and biliverdin. *Biochim Biophys Acta* 1002:238-244.

110. Wu TW, Carey D, Wu J, & Sugiyama H (1991) The cytoprotective effects of bilirubin and biliverdin on rat hepatocytes and human erythrocytes and the impact of albumin. *Biochem Cell Biol* 69:828-834.

111. Deguchi K, Hayashi T, Nagotani S, Sehara Y, Zhang H, Tsuchiya A, Ohta Y, Tomiyama K, Morimoto N, Miyazaki M, Huh NH, Nakao A, Kamiya T, & Abe K (2008) Reduction of cerebral infarction in rats by biliverdin associated with amelioration of oxidative stress. *Brain Res* 1188:1-8.

112. Yamashita K, McDaid J, Ollinger R, Tsui TY, Berberat PO, Usheva A, Csizmadia E, Smith RN, Soares MP, & Bach FH (2004) Biliverdin, a natural product of heme catabolism, induces tolerance to cardiac allografts. *FASEB J* 18:765-767.

113. Wegiel B, Gallo D, Csizmadia E, Roger T, Kaczmarek E, Harris C, Zuckerbraun BS, & Otterbein LE (2011) Biliverdin inhibits Toll-like receptor-4 (TLR4) expression through nitric oxide-dependent nuclear translocation of biliverdin reductase. *Proc Natl Acad Sci U S A* 108:18849-18854.

114. Wegiel B, Baty CJ, Gallo D, Csizmadia E, Scott JR, Akhavan A, Chin BY, Kaczmarek E, Alam J, Bach FH, Zuckerbraun BS, & Otterbein LE (2009) Cell surface biliverdin reductase mediates biliverdin-induced anti-inflammatory effects via phosphatidylinositol 3-kinase and Akt. *J Biol Chem* 284:21369-21378.

115. Sarady-Andrews JK, Liu F, Gallo D, Nakao A, Overhaus M, Ollinger R, Choi AM, & Otterbein LE (2005) Biliverdin administration protects against endotoxin-induced acute lung injury in rats. *Am J Physiol Lung Cell Mol Physiol* 289:1131-1137.

116. Overhaus M, Moore BA, Barbato JE, Behrendt FF, Doering JG, & Bauer AJ (2006) Biliverdin protects against polymicrobial sepsis by modulating inflammatory mediators. *Am J Physiol Gastrointest Liver Physiol* 290:695-703.

117. Sugimoto R, Tanaka Y, Noda K, Kawamura T, Toyoda Y, Billiar TR, McCurry KR, & Nakao A (2012) Preservation solution supplemented with biliverdin prevents lung cold ischaemia/reperfusion injury. *Eur J Cardiothorac Surg* 42:1035-1041.

118. Ollinger R, Wang H, Yamashita K, Wegiel B, Thomas M, Margreiter R, & Bach FH (2007) Therapeutic applications of bilirubin and biliverdin in transplantation. *Antioxid Redox Signal* 9:2175-2185.

119. Fondevila C, Katori M, Lassman C, Carmody I, Busuttil RW, Bach FH, & Kupiec-Weglinski JW (2003) Biliverdin protects rat livers from ischemia/reperfusion injury. *Transplant Proc* 35:1798-1799.

120. Ollinger R, Yamashita K, Bilban M, Erat A, Kogler P, Thomas M, Csizmadia E, Usheva A, Margreiter R, & Bach FH (2007) Bilirubin and biliverdin treatment of atherosclerotic diseases. *Cell Cycle* 6:39-43.

121. Nakao A, Murase N, Ho C, Toyokawa H, Billiar TR, & Kanno S (2005) Biliverdin administration prevents the formation of intimal hyperplasia induced by vascular injury. *Circulation* 112:587-591.

122. Ikeda N, Inoguchi T, Sonoda N, Fujii M, Takei R, Hirata E, Yokomizo H, Zheng J, Maeda Y, Kobayashi K, & Takayanagi R (2011) Biliverdin protects against the deterioration of glucose tolerance in *db/db* mice. *Diabetologia* 54:2183-2191.

123. Yamaguchi T, Komoda Y, & Nakajima H (1994) Biliverdin-IXα reductase and biliverdin-IXβ reductase from human liver. Purification and characterization. *J Biol Chem* 269:24343-24349.

124. Sakai T & Endo M (1990) Changes in the composition of bile pigments in the bile of yellowtail with phenylhydrazine-induced hemolytic anemia. *Agric Biol Chem* 54:3339-3340.

125. Hinds TD, Jr., Burns KA, Hosick PA, McBeth L, Nestor-Kalinoski A, Drummond HA, AlAmodi AA, Hankins MW, Vanden Heuvel JP, & Stec DE (2016) Biliverdin reductase a attenuates hepatic steatosis by inhibition of glycogen synthase kinase (GSK) 3β phosphorylation of serine 73 of peroxisome proliferator-activated receptor (PPAR) α. *J Biol Chem* 291:25179-25191.

126. Chen W, Maghzal GJ, Ayer A, Suarna C, Dunn LL, & Stocker R (2018) Absence of the biliverdin reductase-a gene is associated with increased endogenous oxidative stress. *Free Radic Biol Med* 115:156-165.

127. Nytofte NS, Serrano MA, Monte MJ, Gonzalez-Sanchez E, Tumer Z, Ladefoged K, Briz O, & Marin JJ (2011) A homozygous nonsense mutation (c.214C->A) in the biliverdin

reductase a gene (BLVRA) results in accumulation of biliverdin during episodes of cholestasis. *J Med Genet* 48:219-225.

128. McDonagh AF, Palma LA, & Schmid R (1981) Reduction of biliverdin and placental transfer of bilirubin and biliverdin in the pregnant guinea pig. *Biochem J* 194:273-282.
129. UniProt Consortium T (2018) UniProt: the universal protein knowledgebase. *Nucleic Acids Res* 46:2699-2699.
130. Maines MD & Trakshel GM (1993) Purification and characterization of human biliverdin reductase. *Arch Biochem Biophys* 300:320-326.
131. Kutty RK & Maines MD (1981) Purification and characterization of biliverdin reductase from rat liver. *J Biol Chem* 256:3956-3962.
132. Chu W-T, Nesbitt NM, Gnatenko DV, Li Z, Zhang B, Seeliger MA, Browne S, Mantle TJ, Bahou WF, & Wang J (2017) Enzymatic activity and thermodynamic stability of biliverdin IXβ reductase are maintained by an active site serine. *Chemistry* 23:1891-1900.
133. Ahmad Z, Salim M, & Maines MD (2002) Human biliverdin reductase is a leucine zipper-like DNA-binding protein and functions in transcriptional activation of heme oxygenase-1 by oxidative stress. *J Biol Chem* 277:9226-9232.
134. Tudor C, Lerner-Marmarosh N, Engelborghs Y, Gibbs PE, & Maines MD (2008) Biliverdin reductase is a transporter of haem into the nucleus and is essential for regulation of HO-1 gene expression by haematin. *Biochem J* 413:405-416.
135. Gibbs PE, Lerner-Marmarosh N, Poulin A, Farah E, & Maines MD (2014) Human biliverdin reductase-based peptides activate and inhibit glucose uptake through direct interaction with the kinase domain of insulin receptor. *FASEB J* 28:2478-2491.
136. Lerner-Marmarosh N, Miralem T, Gibbs PE, & Maines MD (2008) Human biliverdin reductase is an ERK activator; hBVR is an ERK nuclear transporter and is required for MAPK signaling. *Proc Natl Acad Sci U S A* 105:6870-6875.
137. Miralem T, Lerner-Marmarosh N, Gibbs PE, Jenkins JL, Heimiller C, & Maines MD (2016) Interaction of human biliverdin reductase with Akt/protein kinase B and phosphatidylinositol-dependent kinase 1 regulates glycogen synthase kinase 3 activity: a novel mechanism of Akt activation. *FASEB J* 30:2926-2944.
138. Maines MD (2007) Biliverdin reductase: PKC interaction at the cross-talk of MAPK and PI3K signaling pathways. *Antioxid Redox Signal* 9:2187-2195.
139. Lerner-Marmarosh N, Shen J, Torno MD, Kravets A, Hu Z, & Maines MD (2005) Human biliverdin reductase: a member of the insulin receptor substrate family with serine/threonine/tyrosine kinase activity. *Proc Natl Acad Sci U S A* 102:7109-7114.
140. Adeosun SO, Gordon DM, Weeks MF, Moore KH, Hall JE, Hinds TD, Jr., & Stec DE (2018) Loss of biliverdin reductase-A promotes lipid accumulation and lipotoxicity in mouse proximal tubule cells. *Am J Physiol Renal Physiol* 315:323.

141. Triani F, Tramutola A, Di Domenico F, Sharma N, Butterfield DA, Head E, Perluigi M, & Barone E (2018) Biliverdin reductase-A impairment links brain insulin resistance with increased Aβ production in an animal model of aging: Implications for Alzheimer disease. *Biochim Biophys Acta Mol Basis Dis* 1864:3181-3194.

142. Barone E, Tramutola A, Triani F, Calcagnini S, Di Domenico F, Ripoli C, Gaetani S, Grassi C, Butterfield DA, Cassano T, & Perluigi M (2018) Biliverdin reductase A mediates the beneficial effects of intranasal insulin in Alzheimer disease. *Mol Neurobiol* 56:2922-2943.

143. Baranano DE, Rao M, Ferris CD, & Snyder SH (2002) Biliverdin reductase: a major physiologic cytoprotectant. *Proc Natl Acad Sci U S A* 99:16093-16098.

144. Sedlak TW & Snyder SH (2004) Bilirubin benefits: cellular protection by a biliverdin reductase antioxidant cycle. *Pediatrics* 113:1776-1782.

145. Maghzal GJ, Leck MC, Collinson E, Li C, & Stocker R (2009) Limited role for the bilirubin-biliverdin redox amplification cycle in the cellular antioxidant protection by biliverdin reductase. *J Biol Chem* 284:29251-29259.

146. McDonagh AF (2010) The biliverdin-bilirubin antioxidant cycle of cellular protection: Missing a wheel? *Free Radic Biol Med* 49:814-820.

147. Jansen T & Daiber A (2012) Direct antioxidant properties of bilirubin and biliverdin. Is there a role for biliverdin reductase? *Front Pharmacol* 3:1-10.

148. Paukovich N, Xue M, Elder JR, Redzic JS, Blue A, Pike H, Miller BG, Pitts TM, Pollock DD, Hansen K, D'Alessandro A, & Eisenmesser EZ (2018) Biliverdin reductase B dynamics are coupled to coenzyme binding. *J Mol Biol* 430:3234-3250.

149. Wu S, Li Z, Gnatenko DV, Zhang B, Zhao L, Malone LE, Markova N, Mantle TJ, Nesbitt NM, & Bahou WF (2016) BLVRB redox mutation defines heme degradation in a metabolic pathway of enhanced thrombopoiesis in humans. *Blood* 128:699-709.

150. Nakajima H, Takemura T, Nakajima O, & Yamaoka K (1963) Studies on heme α-methenyl oxygenase. *J Biol Chem* 238:3784-3796.

151. Cunningham O, Dunne A, Sabido P, Lightner D, & Mantle TJ (2000) Studies on the specificity of the tetrapyrrole substrate for human biliverdin-IXα reductase and biliverdin-IXβ reductase. Structure-activity relationships define models for both active sites. *J Biol Chem* 275:19009-19017.

152. Shalloe F, Elliott G, Ennis O, & Mantle TJ (1996) Evidence that biliverdin-IXβ reductase and flavin reductase are identical. *Biochem J* 316:385-387.

153. Matic LP, Jesus Iglesias M, Vesterlund M, Lengquist M, Hong MG, Saieed S, Sanchez-Rivera L, Berg M, Razuvaev A, Kronqvist M, Lund K, Caidahl K, Gillgren P, Ponten F, Uhlen M, Schwenk JM, Hansson GK, Paulsson-Berne G, Fagman E, Roy J, Hultgren R, Bergstrom G, Lehtio J, Odeberg J, & Hedin U (2018) Novel multiomics profiling of

human carotid atherosclerotic plaques and plasma reveals biliverdin reductase b as a marker of intraplaque hemorrhage. *JACC Basic Transl Sci* 3:464-480.

154. Robinson SH (1968) The origins of bilirubin. *N Engl J Med* 279:143-149.
155. Schmid R & McDonagh AF (1975) The enzymatic formation of bilirubin. *Ann N Y Acad Sci* 244:533-552.
156. Hallgren R, Karlsson FA, Roxin LE, & Venge P (1978) Myoglobin turnover-influence of renal and extrarenal factors. *J Lab Clin Med* 91:246-254.
157. Ziberna L, Martelanc M, Franko M, & Passamonti S (2016) Bilirubin is an endogenous antioxidant in human vascular endothelial cells. *Sci Rep* 6:29240.
158. Lightner DA & McDonagh AF (2001) Structure and metabolism of natural and synthetic bilirubins. *J Perinatol* 21:13-16.
159. Fevery J, Van de Vijver M, Michiels R, & Heirwegh KP (1977) Comparison in different species of biliary bilirubin-IXα conjugates with the activities of hepatic and renal bilirubin-IXα-uridine diphosphate glycosyltransferases. *Biochem J* 164:737-746.
160. Cui Y, Konig J, Leier I, Buchholz U, & Keppler D (2001) Hepatic uptake of bilirubin and its conjugates by the human organic anion transporter SLC21A6. *J Biol Chem* 276:9626-9630.
161. Stollman YR, Gartner U, Theilmann L, Ohmi N, & Wolkoff AW (1983) Hepatic bilirubin uptake in the isolated perfused rat liver is not facilitated by albumin binding. *J Clin Invest* 72:718-723.
162. Bosma PJ, Seppen J, Goldhoorn B, Bakker C, Oude Elferink RP, Chowdhury JR, Chowdhury NR, & Jansen PL (1994) Bilirubin UDP-glucuronosyltransferase 1 is the only relevant bilirubin glucuronidating isoform in man. *J Biol Chem* 269:17960-17964.
163. Kamisako T, Leier I, Cui Y, Konig J, Buchholz U, Hummel-Eisenbeiss J, & Keppler D (1999) Transport of monoglucuronosyl and bisglucuronosyl bilirubin by recombinant human and rat multidrug resistance protein 2. *Hepatology* 30:485-490.
164. Hamoud AR, Weaver L, Stec DE, & Hinds TD, Jr. (2018) Bilirubin in the liver-gut signaling axis. *Trends Endocrinol Metab* 29:140-150.
165. Muraca M, Fevery J, & Blanckaert N (1988) Analytic aspects and clinical interpretation of serum bilirubins. *Semin Liver Dis* 8:137-147.
166. Westwood A (1991) The analysis of bilirubin in serum. *Ann Clin Biochem* 28:119-130.
167. Diamond I & Schmid R (1966) Experimental bilirubin encephalopathy. The mode of entry of bilirubin-14C into the central nervous system. *J Clin Invest* 45:678.
168. Dennery PA, Seidman DS, & Stevenson DK (2001) Neonatal hyperbilirubinemia. *N Engl J Med* 344:581-590.
169. Araujo JA, Meng L, Tward AD, Hancock WW, Zhai Y, Lee A, Ishikawa K, Iyer S, Buelow R, Busuttil RW, Shih DM, Lusis AJ, & Kupiec-Weglinski JW (2003) Systemic

rather than local heme oxygenase-1 overexpression improves cardiac allograft outcomes in a new transgenic mouse. *J Immunol* 171:1572-1580.

170. Subhanova I, Muchova L, Lenicek M, Vreman HJ, Luksan O, Kubickova K, Kreidlova M, Zima T, Vitek L, & Urbanek P (2013) Expression of biliverdin reductase A in peripheral blood leukocytes is associated with treatment response in HCV-infected patients. *PLoS One* 8:e57555.

171. Barone E, Mancuso C, Di Domenico F, Sultana R, Murphy MP, Head E, & Butterfield DA (2012) Biliverdin reductase-A: a novel drug target for atorvastatin in a dog pre-clinical model of Alzheimer disease. *J Neurochem* 120:135-146.

172. Leung AK & Sauve RS (1989) Breastfeeding and breast milk jaundice. *J R Soc Health* 109:213-217.

173. van de Steeg E, Stranecky V, Hartmannova H, Noskova L, Hrebicek M, Wagenaar E, van Esch A, de Waart DR, Oude Elferink RP, Kenworthy KE, Sticova E, al-Edreesi M, Knisely AS, Kmoch S, Jirsa M, & Schinkel AH (2012) Complete OATP1B1 and OATP1B3 deficiency causes human Rotor syndrome by interrupting conjugated bilirubin reuptake into the liver. *J Clin Invest* 122:519-528.

174. Bosma PJ, Chowdhury JR, Bakker C, Gantla S, de Boer A, Oostra BA, Lindhout D, Tytgat GN, Jansen PL, Oude Elferink RP, & et al. (1995) The genetic basis of the reduced expression of bilirubin UDP-glucuronosyltransferase 1 in Gilbert's syndrome. *N Engl J Med* 333:1171-1175.

175. Yamamoto K, Sato H, Fujiyama Y, Doida Y, & Bamba T (1998) Contribution of two missense mutations (G71R and Y486D) of the bilirubin UDP glycosyltransferase (UGT1A1) gene to phenotypes of Gilbert's syndrome and Crigler-Najjar syndrome type II. *Biochim Biophys Acta* 1406:267-273.

176. Maruo Y, Nishizawa K, Sato H, Doida Y, & Shimada M (1999) Association of neonatal hyperbilirubinemia with bilirubin UDP-glucuronosyltransferase polymorphism. *Pediatrics* 103:1224-1227.

177. Wolkoff AW, Cohen LE, & Arias IM (1973) Inheritance of the Dubin-Johnson syndrome. *N Engl J Med* 288:113-117.

178. Kitamura T, Jansen P, Hardenbrook C, Kamimoto Y, Gatmaitan Z, & Arias IM (1990) Defective ATP-dependent bile canalicular transport of organic anions in mutant (TR-) rats with conjugated hyperbilirubinemia. *Proc Natl Acad Sci U S A* 87:3557-3561.

179. McDonagh AF (2007) Movement of bilirubin and bilirubin conjugates across the placenta. *Pediatrics* 119:1032-1033.

180. Blumenthal SG, Stucker T, Rasmussen RD, Ikeda RM, Ruebner BH, Bergstrom DE, & Hanson FW (1980) Changes in bilirubins in human prenatal development. *Biochem J* 186:693-700.

181. McDonagh AF, Palma LA, & Lightner DA (1980) Blue light and bilirubin excretion. *Science* 208:145-151.

182. Fevery J (2008) Bilirubin in clinical practice: a review. *Liver Int* 28:592-605.

183. Tiribelli C & Ostrow JD (1990) New concepts in bilirubin chemistry, transport and metabolism: report of the International Bilirubin Workshop, April 6-8, 1989, Trieste, Italy. *Hepatology* 11:303-313.

184. Schmid R & Hammaker L (1963) Metabolism and disposition of C14-bilirubin in congenital nonhemolytic jaundice. *J Clin Invest* 42:1720-1734.

185. Stocker R, Glazer AN, & Ames BN (1987) Antioxidant activity of albumin-bound bilirubin. *Proc Natl Acad Sci U S A* 84:5918-5922.

186. Stocker R (2004) Antioxidant activities of bile pigments. *Antioxid Redox Signal* 6:841-849.

187. Neuzil J & Stocker R (1994) Free and albumin-bound bilirubin are efficient co-antioxidants for α-tocopherol, inhibiting plasma and low density lipoprotein lipid peroxidation. *J Biol Chem* 269:16712-16719.

188. Neuzil J, Gebicki JM, & Stocker R (1993) Radical-induced chain oxidation of proteins and its inhibition by chain-breaking antioxidants. *Biochem J* 293:601-606.

189. Neuzil J & Stocker R (1993) Bilirubin attenuates radical-mediated damage to serum albumin. *FEBS Lett* 331:281-284.

190. Kaur H, Hughes MN, Green CJ, Naughton P, Foresti R, & Motterlini R (2003) Interaction of bilirubin and biliverdin with reactive nitrogen species. *FEBS Lett* 543:113-119.

191. Boon AC, Hawkins CL, Coombes JS, Wagner KH, & Bulmer AC (2015) Bilirubin scavenges chloramines and inhibits myeloperoxidase-induced protein/lipid oxidation in physiologically relevant hyperbilirubinemic serum. *Free Radic Biol Med* 86:259-268.

192. Clark JE, Foresti R, Green CJ, & Motterlini R (2000) Dynamics of haem oxygenase-1 expression and bilirubin production in cellular protection against oxidative stress. *Biochem J* 348:615-619.

193. Wu TW, Wu J, Li RK, Mickle D, & Carey D (1991) Albumin-bound bilirubins protect human ventricular myocytes against oxyradical damage. *Biochem Cell Biol* 69:683-688.

194. Dennery PA, McDonagh AF, Spitz DR, Rodgers PA, & Stevenson DK (1995) Hyperbilirubinemia results in reduced oxidative injury in neonatal Gunn rats exposed to hyperoxia. *Free Radic Biol Med* 19:395-404.

195. Clark JE, Foresti R, Sarathchandra P, Kaur H, Green CJ, & Motterlini R (2000) Heme oxygenase-1-derived bilirubin ameliorates postischemic myocardial dysfunction. *Am J Physiol Heart Circ Physiol* 278:643-651.

196. Bakrania B, Du Toit EF, Wagner KH, Headrick JP, & Bulmer AC (2016) Pre- or post-ischemic bilirubin ditaurate treatment reduces oxidative tissue damage and improves cardiac function. *Int J Cardiol* 202:27-33.

197. Maruhashi T, Soga J, Fujimura N, Idei N, Mikami S, Iwamoto Y, Kajikawa M, Matsumoto T, Kihara Y, Chayama K, Noma K, Nakashima A, Tomiyama H, Takase B, Yamashina A, & Higashi Y (2012) Hyperbilirubinemia, augmentation of endothelial function, and decrease in oxidative stress in Gilbert syndrome. *Circulation* 126:598-603.

198. Mazzone GL, Rigato I, Ostrow JD, Bossi F, Bortoluzzi A, Sukowati CH, Tedesco F, & Tiribelli C (2009) Bilirubin inhibits the TNFα-related induction of three endothelial adhesion molecules. *Biochem Biophys Res Commun* 386:338-344.

199. Vogel ME & Zucker SD (2016) Bilirubin acts as an endogenous regulator of inflammation by disrupting adhesion molecule-mediated leukocyte migration. *Inflamm Cell Signal* 3:e1178.

200. Liu Y, Li P, Lu J, Xiong W, Oger J, Tetzlaff W, & Cynader M (2008) Bilirubin possesses powerful immunomodulatory activity and suppresses experimental autoimmune encephalomyelitis. *J Immunol* 181:1887-1897.

201. Miler I, Větvicka V, Sima P, & Taborsky L (1985) The effect of bilirubin on the phagocytic activity of mouse peripheral granulocytes and monocytes *in vivo*. *Folia Microbiol (Praha)* 30:267-271.

202. Miler I, Sima P, Větvicka V, Indrova M, & Slavikova M (1988) The potential immunosuppressive effect of bilirubin. *Allerg Immunol (Leipz)* 34:177-184.

203. Větvicka V, Miler I, Sima P, Taborsky L, & Fornusek L (1985) The effect of bilirubin on the Fc receptor expression and phagocytic activity of mouse peritoneal macrophages. *Folia Microbiol (Praha)* 30:373-380.

204. Weinberger B, Archer FE, Kathiravan S, Hirsch DS, Kleinfeld AM, Vetrano AM, & Hegyi T (2013) Effects of bilirubin on neutrophil responses in newborn infants. *Neonatology* 103:105-111.

205. Vogel ME, Idelman G, Konaniah ES, & Zucker SD (2017) Bilirubin prevents atherosclerotic lesion formation in low-density lipoprotein receptor-deficient mice by inhibiting endothelial VCAM-1 and ICAM-1 signaling. *J Am Heart Assoc* 6:e004820.

206. Akboga MK, Canpolat U, Sahinarslan A, Alsancak Y, Nurkoc S, Aras D, Aydogdu S, & Abaci A (2015) Association of serum total bilirubin level with severity of coronary atherosclerosis is linked to systemic inflammation. *Atherosclerosis* 240:110-114.

207. Dong H, Huang H, Yun X, Kim DS, Yue Y, Wu H, Sutter A, Chavin KD, Otterbein LE, Adams DB, Kim YB, & Wang H (2014) Bilirubin increases insulin sensitivity in leptin-receptor deficient and diet-induced obese mice through suppression of ER stress and chronic inflammation. *Endocrinology* 155:818-828.

208. Dullaart RP, Gruppen EG, Connelly MA, & Lefrandt JD (2015) A pro-inflammatory glycoprotein biomarker is associated with lower bilirubin in metabolic syndrome. *Clin Biochem* 48:1045-1047.

209. He M, Nitti M, Piras S, Furfaro AL, Traverso N, Pronzato MA, & Mann GE (2015) Heme oxygenase-1-derived bilirubin protects endothelial cells against high glucose-induced damage. *Free Radic Biol Med* 89:91-98.

210. Jabarpour M, Siavashi V, Asadian S, Babaei H, Jafari SM, & Nassiri SM (2018) Hyperbilirubinemia-induced pro-angiogenic activity of infantile endothelial progenitor cells. *Microvasc Res* 118:49-56.

211. Peyton KJ, Shebib AR, Azam MA, Liu XM, Tulis DA, & Durante W (2012) Bilirubin inhibits neointima formation and vascular smooth muscle cell proliferation and migration. *Front Pharmacol* 3:1-7.

212. Bae I-H, Park DS, Lee S-Y, Jang E-J, Shim J-W, Lim K-S, Park J-K, Kim JH, Sim DS, & Jeong MH (2018) Bilirubin coating attenuates the inflammatory response to everolimus-coated stents. *J Biomed Mater Res B Appl Biomater* 106:1486-1495.

213. Sarwar N, Gao P, Seshasai SR, Gobin R, Kaptoge S, Di Angelantonio E, Ingelsson E, Lawlor DA, Selvin E, Stampfer M, Stehouwer CD, Lewington S, Pennells L, Thompson A, Sattar N, White IR, Ray KK, & Danesh J (2010) Diabetes mellitus, fasting blood glucose concentration, and risk of vascular disease: a collaborative meta-analysis of 102 prospective studies. *Lancet* 375:2215-2222.

214. DeFronzo RA & Ferrannini E (1991) Insulin resistance: a multifaceted syndrome responsible for NIDDM, obesity, hypertension, dyslipidemia, and atherosclerotic cardiovascular disease. *Diabetes Care* 14:173-194.

215. van der Wal AC & Becker AE (1999) Atherosclerotic plaque rupture-pathologic basis of plaque stability and instability. *Cardiovasc Res* 41:334-344.

216. Burke AP, Farb A, Malcom GT, Liang YH, Smialek J, & Virmani R (1997) Coronary risk factors and plaque morphology in men with coronary disease who died suddenly. *N Engl J Med* 336:1276-1282.

217. Virmani R, Kolodgie FD, Burke AP, Farb A, & Schwartz SM (2000) Lessons from sudden coronary death: a comprehensive morphological classification scheme for atherosclerotic lesions. *Arterioscler Thromb Vasc Biol* 20:1262-1275.

218. Kang SJ, Kim D, Park HE, Chung GE, Choi SH, Choi SY, Lee W, Kim JS, & Cho SH (2013) Elevated serum bilirubin levels are inversely associated with coronary artery atherosclerosis. *Atherosclerosis* 230:242-248.

219. Canpolat U, Aytemir K, Yorgun H, Hazirolan T, Kaya EB, Sahiner L, Sunman H, Tokgozoglu L, Kabakci G, & Oto A (2013) Association of serum total bilirubin levels

with the severity, extent and subtypes of coronary atherosclerotic plaques detected by coronary CT angiography. *Int J Cardiovasc Imaging* 29:1371-1379.

220. Lönn ME, Dennis JM, & Stocker R (2012) Actions of "antioxidants" in the protection against atherosclerosis. *Free Radic Biol Med* 53:863-884.
221. Libby P (2012) Inflammation in atherosclerosis. *Arterioscler Thromb Vasc Biol* 32:2045-2051.
222. Gimbrone MA, Jr. & Garcia-Cardena G (2016) Endothelial cell dysfunction and the pathobiology of atherosclerosis. *Circ Res* 118:620-636.
223. Libby P, Bornfeldt KE, & Tall AR (2016) Atherosclerosis: successes, surprises, and future challenges. *Circ Res* 118:531-534.
224. Lapenna D, Ciofani G, Pierdomenico SD, Giamberardino MA, Ucchino S, & Davi G (2018) Association of serum bilirubin with oxidant damage of human atherosclerotic plaques and the severity of atherosclerosis. *Clin Exp Med* 18:119-124.
225. Moore K & Roberts LJ, 2nd (1998) Measurement of lipid peroxidation. *Free Radic Res* 28:659-671.
226. Amor AJ, Ortega E, Perea V, Cofan M, Sala-Vila A, Nunez I, Gilabert R, & Ros E (2017) Relationship between total serum bilirubin levels and carotid and femoral atherosclerosis in familial dyslipidemia. *Arterioscler Thromb Vasc Biol* 37:2356-2363.
227. Zhu KF, Wang YM, Wang YQ, & Wang NF (2016) The relationship between serum levels of total bilirubin and coronary plaque vulnerability. *Coron Artery Dis* 27:52-58.
228. Abbate R, Cioni G, Ricci I, Miranda M, & Gori AM (2012) Thrombosis and acute coronary syndrome. *Thromb Res* 129:235-240.
229. Kundur AR, Santhakumar AB, Bulmer AC, & Singh I (2017) Mildly elevated unconjugated bilirubin is associated with reduced platelet activation-related thrombogenesis and inflammation in Gilbert's syndrome. *Platelets* 28:779-785.
230. Kundur AR, Bulmer AC, & Singh I (2014) Unconjugated bilirubin inhibits collagen induced platelet activation. *Platelets* 25:45-50.
231. Yoshino S, Hamasaki S, Ishida S, Kataoka T, Yoshikawa A, Oketani N, Saihara K, Okui H, Shinsato T, Ichiki H, Kubozono T, Kuwahata S, Fujita S, Kanda D, Nakazaki M, Miyata M, & Tei C (2011) Relationship between bilirubin concentration, coronary endothelial function, and inflammatory stress in overweight patients. *J Atheroscler Thromb* 18:403-412.
232. Dekker D, Dorresteijn MJ, Pijnenburg M, Heemskerk S, Rasing-Hoogveld A, Burger DM, Wagener FA, & Smits P (2011) The bilirubin-increasing drug atazanavir improves endothelial function in patients with type 2 diabetes mellitus. *Arterioscler Thromb Vasc Biol* 31:458-463.

233. Erdogan D, Gullu H, Yildirim E, Tok D, Kirbas I, Ciftci O, Baycan ST, & Muderrisoglu H (2006) Low serum bilirubin levels are independently and inversely related to impaired flow-mediated vasodilation and increased carotid intima-media thickness in both men and women. *Atherosclerosis* 184:431-437.

234. Gullu H, Erdogan D, Tok D, Topcu S, Caliskan M, Ulus T, & Muderrisoglu H (2005) High serum bilirubin concentrations preserve coronary flow reserve and coronary microvascular functions. *Arterioscler Thromb Vasc Biol* 25:2289-2294.

235. Zhu C, Xiong Z, Zheng Z, Chen Y, Chen X, & Qian X (2012) Association of arterial stiffness with serum bilirubin levels in established coronary artery disease. *Intern Med* 51:2083-2089.

236. Kawamura K, Ishikawa K, Wada Y, Kimura S, Matsumoto H, Kohro T, Itabe H, Kodama T, & Maruyama Y (2005) Bilirubin from heme oxygenase-1 attenuates vascular endothelial activation and dysfunction. *Arterioscler Thromb Vasc Biol* 25:155.

237. Endler G, Hamwi A, Sunder-Plassmann R, Exner M, Vukovich T, Mannhalter C, Wojta J, Huber K, & Wagner O (2003) Is low serum bilirubin an independent risk factor for coronary artery disease in men but not in women? *Clin Chem* 49:1201-1204.

238. Kono S (2011) Letter by Kono regarding article, "Plasma bilirubin and UGT1A1*28 are not protective factors against first-time myocardial infarction in a prospective, nested case-referent setting". *Circ Cardiovasc Genet* 4:1.

239. Ekblom K, Marklund SL, Jansson JH, Osterman P, Hallmans G, Weinehall L, & Hultdin J (2010) Plasma bilirubin and UGT1A1*28 are not protective factors against first-time myocardial infarction in a prospective, nested case-referent setting. *Circ Cardiovasc Genet* 3:340-347.

240. Djousse L, Levy D, Cupples LA, Evans JC, D'Agostino RB, & Ellison RC (2001) Total serum bilirubin and risk of cardiovascular disease in the Framingham offspring study. *Am J Cardiol* 87:1196-1200.

241. Tanaka M, Fukui M, Tomiyasu K, Akabame S, Nakano K, Hasegawa G, Oda Y, & Nakamura N (2009) Low serum bilirubin concentration is associated with coronary artery calcification (CAC). *Atherosclerosis* 206:287-291.

242. Zhang ZY, Bian LQ, Kim SJ, Zhou CC, & Choi YH (2012) Inverse relation of total serum bilirubin to coronary artery calcification score detected by multidetector computed tomography in males. *Clin Cardiol* 35:301-306.

243. Mahabadi AA, Lehmann N, Mohlenkamp S, Kalsch H, Bauer M, Schulz R, Moebus S, Jockel KH, Erbel R, & Heusch G (2014) Association of bilirubin with coronary artery calcification and cardiovascular events in the general population without known liver disease: the Heinz Nixdorf Recall study. *Clin Res Cardiol* 103:647-653.

244. Huang FY, Peng Y, Huang BT, Yang Y, Pu XB, Chen SJ, Gui YY, Xia TL, Chen F, Liu RS, Zhu Y, & Chen M (2017) The correlation between serum total bilirubin and outcomes in patients with different subtypes of coronary artery disease. *Clin Chim Acta* 465:101-105.

245. Tanindi A, Erkan AF, Alhan A, & Tore HF (2015) Arterial stiffness and central arterial wave reflection are associated with serum uric acid, total bilirubin, and neutrophil-to-lymphocyte ratio in patients with coronary artery disease. *Anatol J Cardiol* 15:396-403.

246. Song YS, Koo BK, Cho NH, & Moon MK (2014) Effect of low serum total bilirubin levels (≤0.32 mg/dl) on risk of coronary artery disease in patients with metabolic syndrome. *Am J Cardiol* 114:1695-1700.

247. Leem J, Koh EH, Jang JE, Woo CY, Oh JS, Lee MJ, Kang JW, Lim TH, Jung CH, Lee WJ, Park JY, & Lee KU (2015) Serum total bilirubin levels provide additive risk information over the framingham risk score for identifying asymptomatic diabetic patients at higher risk for coronary artery stenosis. *Diabetes Metab J* 39:414-423.

248. Bosma PJ, van der Meer IM, Bakker CT, Hofman A, Paul-Abrahamse M, & Witteman JC (2003) UGT1A1*28 allele and coronary heart disease: the Rotterdam Study. *Clin Chem* 49:1180-1181.

249. Lin R, Wang Y, Wang Y, Fu W, Zhang D, Zheng H, Yu T, Wang Y, Shen M, Lei R, Wu H, Sun A, Zhang R, Wang X, Xiong M, Huang W, & Jin L (2009) Common variants of four bilirubin metabolism genes and their association with serum bilirubin and coronary artery disease in Chinese Han population. *Pharmacogenet Genomics* 19:310-318.

250. Lingenhel A, Kollerits B, Schwaiger JP, Hunt SC, Gress R, Hopkins PN, Schoenborn V, Heid IM, & Kronenberg F (2008) Serum bilirubin levels, UGT1A1 polymorphisms and risk for coronary artery disease. *Exp Gerontol* 43:1102-1107.

251. Gajdos V, Petit FM, Perret C, Mollet-Boudjemline A, Colin P, Capel L, Nicaud V, Evans A, Arveiler D, Parisot F, Francoual J, Genin E, Cambien F, & Labrune P (2006) Further evidence that the UGT1A1*28 allele is not associated with coronary heart disease: The ECTIM Study. *Clin Chem* 52:2313-2314.

252. Chung SR, Yang TH, Shin HC, Jin HY, Seo JS, Jang JS, Kim DK, Kim DS, Seo GW, Song PS, Kim DK, Kim KH, Seol SH, Kim DI, Cho YK, Yoon HJ, Nam CW, Hur SH, Kim U, Park JS, & Kim YJ (2016) Initial total bilirubin and clinical outcome in patients with ST-segment elevation myocardial infarction undergoing primary percutaneous coronary intervention with drug-eluting stents. *Circ J* 80:1437-1444.

253. Baumann S, Huseynov A, Koepp J, Jabbour C, Behnes M, Becher T, Renker M, Lang S, Borggrefe M, Lehmann R, & Akin I (2016) Comparison of serum uric acid, bilirubin, and c-reactive protein as prognostic biomarkers of in-hospital MACE between women and men with ST-segment elevation myocardial infarction. *Angiology* 67:272-280.

254. Sahin O, Akpek M, Elcik D, Karadavut S, Simsek V, Tulmac M, Orscelik O, Calapkorur B, Ergin A, & Kaya MG (2013) Bilirubin levels and the burden of coronary atherosclerosis in patients with STEMI. *Angiology* 64:200-204.

255. Gul M, Uyarel H, Ergelen M, Akgul O, Karaca G, Turen S, Ugur M, Erturk M, Kul S, Surgit O, Bozbay M, & Uslu N (2013) Prognostic value of total bilirubin in patients with ST-segment elevation acute myocardial infarction undergoing primary coronary intervention. *Am J Cardiol* 111:166-171.

256. Xu C, Dong M, Deng Y, Zhang L, Deng F, Zhou J, & Yuan Z (2019) Relation of direct, indirect, and total bilirubin to adverse long-term outcomes among patients with acute coronary syndrome. *Am J Cardiol* 123:1244-1248.

257. Kimm H, Yun JE, Jo J, & Jee SH (2009) Low serum bilirubin level as an independent predictor of stroke incidence: a prospective study in Korean men and women. *Stroke* 40:3422-3427.

258. Dohi K, Mochizuki Y, Satoh K, Jimbo H, Hayashi M, Toyoda I, Ikeda Y, Abe T, & Aruga T (2003) Transient elevation of serum bilirubin (a heme oxygenase-1 metabolite) level in hemorrhagic stroke: bilirubin is a marker of oxidant stress. *Acta Neurochir Suppl* 86:247-249.

259. Luo Y, Li JW, Lu ZJ, Wang C, Guan DN, & Xu Y (2012) Serum bilirubin after acute ischemic stroke is associated with stroke severity. *Curr Neurovasc Res* 9:128-132.

260. Xu T, Zhang J, Xu T, Liu W, Kong Y, & Zhang Y (2013) Association of serum bilirubin with stroke severity and clinical outcomes. *Can J Neurol Sci* 40:80-84.

261. Luo Y, Li J, Zhang J, & Xu Y (2013) Elevated bilirubin after acute ischemic stroke linked to the stroke severity. *Int J Dev Neurosci* 31:634-638.

262. Zhang B, Zhang W, Li X, Pu S, Yin J, Yang N, Yi Y, Gao Q, & Gao C (2011) Admission markers predict lacunar and non-lacunar stroke in young patients. *Thromb Res* 128:14-17.

263. Lin SP, Lin PY, Jiang HL, Long YM, & Chen XH (2015) Is serum total bilirubin useful to differentiate cardioembolic stroke from other stroke subtypes? *Neurol Res* 37:727-731.

264. Adams HP, Jr., Bendixen BH, Kappelle LJ, Biller J, Love BB, Gordon DL, & Marsh EE, 3rd (1993) Classification of subtype of acute ischemic stroke. Definitions for use in a multicenter clinical trial. TOAST. Trial of Org 10172 in Acute Stroke Treatment. *Stroke* 24:35-41.

265. Mizuno K & Ueno Y (2017) Autonomic nervous system and the liver. *Hepatol Res* 47:160-165.

266. Pineda S, Bang OY, Saver JL, Starkman S, Yun SW, Liebeskind DS, Kim D, Ali LK, Shah SH, & Ovbiagele B (2008) Association of serum bilirubin with ischemic stroke outcomes. *J Stroke Cerebrovasc Dis* 17:147-152.

267. Perlstein TS, Pande RL, Beckman JA, & Creager MA (2008) Serum total bilirubin level and prevalent lower-extremity peripheral arterial disease: National Health and Nutrition Examination Survey (NHANES) 1999 to 2004. *Arterioscler Thromb Vasc Biol* 28:166-172.

268. Rantner B, Kollerits B, Anderwald-Stadler M, Klein-Weigel P, Gruber I, Gehringer A, Haak M, Schnapka-Kopf M, Fraedrich G, & Kronenberg F (2008) Association between the UGT1A1 TA-repeat polymorphism and bilirubin concentration in patients with intermittent claudication: results from the CAVASIC study. *Clin Chem* 54:851-857.

269. Chan KH, O'Connell RL, Sullivan DR, Hoffmann LS, Rajamani K, Whiting M, Donoghoe MW, Vanhala M, Hamer A, Yu B, Stocker R, Ng MK, Keech AC, & Investigators FS (2013) Plasma total bilirubin levels predict amputation events in type 2 diabetes mellitus: the Fenofibrate Intervention and Event Lowering in Diabetes (FIELD) study. *Diabetologia* 56:724-736.

270. O'Neill S & O'Driscoll L (2015) Metabolic syndrome: a closer look at the growing epidemic and its associated pathologies. *Obes Rev* 16:1-12.

271. Cheriyath P, Gorrepati VS, Peters I, Nookala V, Murphy ME, Srouji N, & Fischman D (2010) High total bilirubin as a protective factor for diabetes mellitus: an analysis of NHANES data from 1999 - 2006. *J Clin Med Res* 2:201-206.

272. Lin LY, Kuo HK, Hwang JJ, Lai LP, Chiang FT, Tseng CD, & Lin JL (2009) Serum bilirubin is inversely associated with insulin resistance and metabolic syndrome among children and adolescents. *Atherosclerosis* 203:563-568.

273. Wu Y, Li M, Xu M, Bi Y, Li X, Chen Y, Ning G, & Wang W (2011) Low serum total bilirubin concentrations are associated with increased prevalence of metabolic syndrome in Chinese. *J Diabetes* 3:217-224.

274. Kwon KM, Kam JH, Kim MY, Kim MY, Chung CH, Kim JK, Linton JA, Eom A, Koh SB, & Kang HT (2011) Inverse association between total bilirubin and metabolic syndrome in rural korean women. *J Womens Health (Larchmt)* 20:963-969.

275. Choi SH, Yun KE, & Choi HJ (2013) Relationships between serum total bilirubin levels and metabolic syndrome in Korean adults. *Nutr Metab Cardiovasc Dis* 23:31-37.

276. Matsumoto R, Koga M, Kasayama S, Fukuoka H, Iguchi G, Odake Y, Yoshida K, Bando H, Suda K, Nishizawa H, Takahashi M, Ogawa W, & Takahashi Y (2018) Factors correlated with serum insulin-like growth factor-I levels in health check-up subjects. *Growth Horm IGF Res* 40:55-60.

277. Liu J, Dong H, Zhang Y, Cao M, Song L, Pan Q, Bulmer A, Adams DB, Dong X, & Wang H (2015) Bilirubin increases insulin sensitivity by regulating cholesterol metabolism, adipokines and PPARγ levels. *Sci Rep* 5:9886.

278. Fu YY, Kang KJ, Ahn JM, Kim HR, Na KY, Chae DW, Kim S, & Chin HJ (2010) Hyperbilirubinemia reduces the streptozotocin-induced pancreatic damage through attenuating the oxidative stress in the Gunn rat. *Tohoku J Exp Med* 222:265-273.

279. Inoue T, Sonoda N, Hiramatsu S, Kimura S, Ogawa Y, & Inoguchi T (2018) Serum bilirubin concentration is associated with left ventricular remodeling in patients with type 2 diabetes mellitus: a cohort study. *Diabetes Ther* 9:331-338.

280. Dekker D, Dorresteijn MJ, Pijnenburg M, Heemskerk S, Rasing-Hoogveld A, Burger DM, Wagener FA, & Smits P (2011) The bilirubin-increasing drug atazanavir improves endothelial function in patients with type 2 diabetes mellitus. *Arterioscler Thromb Vasc Biol* 31:458.

281. Bedogni G, Miglioli L, Masutti F, Tiribelli C, Marchesini G, & Bellentani S (2005) Prevalence of and risk factors for nonalcoholic fatty liver disease: the Dionysos nutrition and liver study. *Hepatology* 42:44-52.

282. Tilg H & Moschen AR (2010) Evolution of inflammation in nonalcoholic fatty liver disease: the multiple parallel hits hypothesis. *Hepatology* 52:1836-1846.

283. Kumar R, Rastogi A, Maras JS, & Sarin SK (2012) Unconjugated hyperbilirubinemia in patients with non-alcoholic fatty liver disease: a favorable endogenous response. *Clin Biochem* 45:272-274.

284. Kwak MS, Kim D, Chung GE, Kang SJ, Park MJ, Kim YJ, Yoon JH, & Lee HS (2012) Serum bilirubin levels are inversely associated with nonalcoholic fatty liver disease. *Clin Mol Hepatol* 18:383-390.

285. Fazakerley DJ, Chaudhuri R, Yang P, Maghzal GJ, Thomas KC, Krycer JR, Humphrey SJ, Parker BL, Fisher-Wellman KH, Meoli CC, Hoffman NJ, Diskin C, Burchfield JG, Cowley MJ, Kaplan W, Modrusan Z, Kolumam G, Yang JY, Chen DL, Samocha-Bonet D, Greenfield JR, Hoehn KL, Stocker R, & James DE (2018) Mitochondrial CoQ deficiency is a common driver of mitochondrial oxidants and insulin resistance. *Elife* 7:e32111.

286. Chen YC, Bui AV, Diesch J, Manasseh R, Hausding C, Rivera J, Haviv I, Agrotis A, Htun NM, Jowett J, Hagemeyer CE, Hannan RD, Bobik A, & Peter K (2013) A novel mouse model of atherosclerotic plaque instability for drug testing and mechanistic/therapeutic discoveries using gene and microRNA expression profiling. *Circ Res* 113:252-265.

287. Rashid I, Maghzal GJ, Chen YC, Cheng D, Talib J, Newington D, Ren M, Vajandar SK, Searle A, Maluenda A, Lindstedt EL, Jabbour A, Kettle AJ, Bongers A, Power C, Michaelsson E, Peter K, & Stocker R (2018) Myeloperoxidase is a potential molecular imaging and therapeutic target for the identification and stabilization of high-risk atherosclerotic plaque. *Eur Heart J* 39:3301-3310.

288. Daugherty A, Tall AR, Daemen M, Falk E, Fisher EA, Garcia-Cardena G, Lusis AJ, Owens AP, 3rd, Rosenfeld ME, Virmani R, American Heart Association Council on Arteriosclerosis T, Vascular B, & Council on Basic Cardiovascular S (2017) Recommendation on design, execution, and reporting of animal atherosclerosis studies: a scientific statement from the American Heart Association. *Circ Res* 121:53-79.

289. Talib J, Maghzal GJ, Cheng D, & Stocker R (2016) Detailed protocol to assess *in vivo* and *ex vivo* myeloperoxidase activity in mouse models of vascular inflammation and disease using hydroethidine. *Free Radic Biol Med* 97:124-135.

290. Yamamoto Y, Brodsky MH, Baker JC, & Ames BN (1987) Detection and characterization of lipid hydroperoxides at picomole levels by high-performance liquid chromatography. *Anal Biochem* 160:7-13.

291. Sattler W, Mohr D, & Stocker R (1994) Rapid isolation of lipoproteins and assessment of their peroxidation by high-performance liquid chromatography postcolumn chemiluminescence. *Methods Enzymol* 233:469-489.

292. Behrens WA & Madere R (1987) A highly sensitive high-performance liquid chromatography method for the estimation of ascorbic and dehydroascorbic acid in tissues, biological fluids, and foods. *Anal Biochem* 165:102-107.

293. Frei B, Kim MC, & Ames BN (1990) Ubiquinol-10 is an effective lipid-soluble antioxidant at physiological concentrations. *Proc Natl Acad Sci U S A* 87:4879-4883.

294. McDonagh AF & Palma LA (1982) Heme catabolism in fish. Bile pigments in gallbladder bile of the electric torpedo, Torpedo californicus. *Comp Biochem Physiol B* 73:501-507.

295. Pfaffl MW (2001) A new mathematical model for relative quantification in real-time RT-PCR. *Nucleic Acids Res* 29:2002-2007.

296. Spandidos A, Wang X, Wang H, & Seed B (2010) PrimerBank: a resource of human and mouse PCR primer pairs for gene expression detection and quantification. *Nucleic Acids Res* 38:792-799.

297. Bayer SB, Maghzal G, Stocker R, Hampton MB, & Winterbourn CC (2013) Neutrophil-mediated oxidation of erythrocyte peroxiredoxin 2 as a potential marker of oxidative stress in inflammation. *FASEB J* 27:3315-3322.

298. Martinic G, Hazell L, & Stocker R (2003) Vascular microdissection, perfusion, and excision of the murine arterial tree for use in atherogenic disease investigations. *Contemp Top Lab Anim Sci* 42:47-53.

299. Sluimer JC, Gijbels MJ, & Heeneman S (2015) Detection of intraplaque hemorrhage in mouse atherosclerotic lesions. *Methods Mol Biol* 1339:339-348.

300. Stocker R, McDonagh AF, Glazer AN, & Ames BN (1990) Antioxidant activities of bile pigments: biliverdin and bilirubin. *Methods Enzymol* 186:301-309.

301. Brodersen R (1980) Binding of bilirubin to albumin. *CRC Crit Rev Clin Lab Sci* 11:305-399.

302. Novotny L & Vitek L (2003) Inverse relationship between serum bilirubin and atherosclerosis in men: a meta-analysis of published studies. *Exp Biol Med (Maywood)* 228:568-571.

303. Vitek L, Jirsa M, Brodanova M, Kalab M, Marecek Z, Danzig V, Novotny L, & Kotal P (2002) Gilbert syndrome and ischemic heart disease: a protective effect of elevated bilirubin levels. *Atherosclerosis* 160:449-456.

304. Kikuchi A, Park SY, Miyatake H, Sun D, Sato M, Yoshida T, & Shiro Y (2001) Crystal structure of rat biliverdin reductase. *Nat Struct Biol* 8:221-225.

305. Bowry VW & Stocker R (1993) Tocopherol-mediated peroxidation. The prooxidant effect of vitamin E on the radical-initiated oxidation of human low-density lipoprotein. *J Am Chem Soc* 115:6029-6044.

306. Bowry VW, Ingold KU, & Stocker R (1992) Vitamin E in human low-density lipoprotein. When and how this antioxidant becomes a pro-oxidant. *Biochem J* 288:341-344.

307. Yamamoto Y, Nagata Y, Niki E, Watanabe K, & Yoshimura S (1993) Plasma glutathione peroxidase reduces phosphatidylcholine hydroperoxide. *Biochem Biophys Res Commun* 193:133-138.

308. Mohr D, Bowry VW, & Stocker R (1992) Dietary supplementation with coenzyme Q10 results in increased levels of ubiquinol-10 within circulating lipoproteins and increased resistance of human low-density lipoprotein to the initiation of lipid peroxidation. *Biochim Biophys Acta* 1126:247-254.

309. Yamamoto Y & Yamashita S (1997) Plasma ratio of ubiquinol and ubiquinone as a marker of oxidative stress. *Mol Aspects Med* 18:79-84.

310. Stocker R, Bowry VW, & Frei B (1991) Ubiquinol-10 protects human low density lipoprotein more efficiently against lipid peroxidation than does α-tocopherol. *Proc Natl Acad Sci U S A* 88:1646-1650.

311. Frei B, Stocker R, & Ames BN (1988) Antioxidant defenses and lipid peroxidation in human blood plasma. *Proc Natl Acad Sci U S A* 85:9748-9752.

312. Bowry VW, Mohr D, Cleary J, & Stocker R (1995) Prevention of tocopherol-mediated peroxidation in ubiquinol-10-free human low density lipoprotein. *J Biol Chem* 270:5756-5763.

313. Low FM, Hampton MB, & Winterbourn CC (2008) Peroxiredoxin 2 and peroxide metabolism in the erythrocyte. *Antioxid Redox Signal* 10:1621-1630.

314. Johnson RM, Ho YS, Yu DY, Kuypers FA, Ravindranath Y, & Goyette GW (2010) The effects of disruption of genes for peroxiredoxin-2, glutathione peroxidase-1, and catalase on erythrocyte oxidative metabolism. *Free Radic Biol Med* 48:519-525.

315. Suarna C, Dean RT, May J, & Stocker R (1995) Human atherosclerotic plaque contains both oxidized lipids and relatively large amounts of α-tocopherol and ascorbate. *Arterioscler Thromb Vasc Biol* 15:1616-1624.

316. Upston JM, Terentis AC, & Stocker R (1999) Tocopherol-mediated peroxidation of lipoproteins: implications for vitamin E as a potential antiatherogenic supplement. *FASEB J* 13:977-994.

317. Neuzil J, Thomas SR, & Stocker R (1997) Requirement for, promotion, or inhibition by α-tocopherol of radical-induced initiation of plasma lipoprotein lipid peroxidation. *Free Radic Biol Med* 22:57-71.

318. VanDuijn MM, Tijssen K, VanSteveninck J, Van Den Broek PJ, & Van Der Zee J (2000) Erythrocytes reduce extracellular ascorbate free radicals using intracellular ascorbate as an electron donor. *J Biol Chem* 275:27720.

319. Kuhn V, Diederich L, Keller TCSt, Kramer CM, Luckstadt W, Panknin C, Suvorava T, Isakson BE, Kelm M, & Cortese-Krott MM (2017) Red Blood Cell Function and Dysfunction: Redox Regulation, Nitric Oxide Metabolism, Anemia. *Antioxid Redox Signal* 26:718-742.

320. Low FM, Hampton MB, Peskin AV, & Winterbourn CC (2007) Peroxiredoxin 2 functions as a noncatalytic scavenger of low-level hydrogen peroxide in the erythrocyte. *Blood* 109:2611-2617.

321. Traber MG (1994) Determinants of plasma vitamin E concentrations. *Free Radic Biol Med* 16:229-239.

322. Lentner C ed (1984) *Physical chemistry, composition of blood, hematology, somatometric data* (Ciba Geigy, Basel), eighth Ed, Vol 3, pp 1-359.

323. Polidori MC, Stahl W, Eichler O, Niestroj I, & Sies H (2001) Profiles of antioxidants in human plasma. *Free Radic Biol Med* 30:456-462.

324. Fraser ST, Midwinter RG, Coupland LA, Kong S, Berger BS, Yeo JH, Andrade OC, Cromer D, Suarna C, Lam M, Maghzal GJ, Chong BH, Parish CR, & Stocker R (2015) Heme oxygenase-1 deficiency alters erythroblastic island formation, steady-state erythropoiesis and red blood cell lifespan in mice. *Haematologica* 100:601-610.

325. Perrone-Filardi P, Paolillo S, Costanzo P, Savarese G, Trimarco B, & Bonow RO (2015) The role of metabolic syndrome in heart failure. *Eur Heart J* 36:2630-2634.

326. Bozkurt B, Aguilar D, Deswal A, Dunbar SB, Francis GS, Horwich T, Jessup M, Kosiborod M, Pritchett AM, Ramasubbu K, Rosendorff C, & Yancy C (2016) Contributory risk and management of comorbidities of hypertension, obesity, diabetes mellitus, hyperlipidemia, and metabolic syndrome in chronic heart failure: a scientific statement from the American Heart Association. *Circulation* 134:535-578.

327. Marchesini G, Bugianesi E, Forlani G, Cerrelli F, Lenzi M, Manini R, Natale S, Vanni E, Villanova N, Melchionda N, & Rizzetto M (2003) Nonalcoholic fatty liver, steatohepatitis, and the metabolic syndrome. *Hepatology* 37:917-923.

328. Wang WW, Smith DL, & Zucker SD (2004) Bilirubin inhibits iNOS expression and NO production in response to endotoxin in rats. *Hepatology* 40:424-433.

329. Abel ED, Peroni O, Kim JK, Kim YB, Boss O, Hadro E, Minnemann T, Shulman GI, & Kahn BB (2001) Adipose-selective targeting of the GLUT4 gene impairs insulin action in muscle and liver. *Nature* 409:729-733.

330. Sugii S, Olson P, Sears DD, Saberi M, Atkins AR, Barish GD, Hong SH, Castro GL, Yin YQ, Nelson MC, Hsiao G, Greaves DR, Downes M, Yu RT, Olefsky JM, & Evans RM (2009) PPARγ activation in adipocytes is sufficient for systemic insulin sensitization. *Proc Natl Acad Sci U S A* 106:22504-22509.

331. Raher MJ, Thibault HB, Buys ES, Kuruppu D, Shimizu N, Brownell AL, Blake SL, Rieusset J, Kaneki M, Derumeaux G, Picard MH, Bloch KD, & Scherrer-Crosbie M (2008) A short duration of high-fat diet induces insulin resistance and predisposes to adverse left ventricular remodeling after pressure overload. *Am J Physiol Heart Circ Physiol* 295:2495-2502.

332. Haluzik M, Gavrilova O, & LeRoith D (2004) Peroxisome proliferator-activated receptor-α deficiency does not alter insulin sensitivity in mice maintained on regular or high-fat diet: hyperinsulinemic-euglycemic clamp studies. *Endocrinology* 145:1662-1667.

333. Foley KP, Zlitni S, Denou E, Duggan BM, Chan RW, Stearns JC, & Schertzer JD (2018) Long term but not short term exposure to obesity related microbiota promotes host insulin resistance. *Nat Commun* 9:4681.

334. Ipsen DH, Lykkesfeldt J, & Tveden-Nyborg P (2018) Molecular mechanisms of hepatic lipid accumulation in non-alcoholic fatty liver disease. *Cell Mol Life Sci* 75:3313-3327.

335. Xu S, Jay A, Brunaldi K, Huang N, & Hamilton JA (2013) CD36 enhances fatty acid uptake by increasing the rate of intracellular esterification but not transport across the plasma membrane. *Biochemistry* 52:7254-7261.

336. Wanders RJ, Komen J, & Kemp S (2011) Fatty acid ω-oxidation as a rescue pathway for fatty acid oxidation disorders in humans. *FEBS J* 278:182-194.

337. Marchesini G, Brizi M, Bianchi G, Tomassetti S, Bugianesi E, Lenzi M, McCullough AJ, Natale S, Forlani G, & Melchionda N (2001) Nonalcoholic fatty liver disease: a feature of the metabolic syndrome. *Diabetes* 50:1844-1850.

338. Anstee QM & Goldin RD (2006) Mouse models in non-alcoholic fatty liver disease and steatohepatitis research. *Int J Exp Pathol* 87:1-16.

339. Monetti M, Levin MC, Watt MJ, Sajan MP, Marmor S, Hubbard BK, Stevens RD, Bain JR, Newgard CB, Farese RV, Sr., Hevener AL, & Farese RV, Jr. (2007) Dissociation of hepatic steatosis and insulin resistance in mice overexpressing DGAT in the liver. *Cell Metab* 6:69-78.

340. van der Veen JN, Lingrell S, McCloskey N, LeBlond ND, Galleguillos D, Zhao YY, Curtis JM, Sipione S, Fullerton MD, Vance DE, & Jacobs RL (2019) A role for phosphatidylcholine and phosphatidylethanolamine in hepatic insulin signaling. *FASEB J* 33:5045-5057.

341. Minehira K, Young SG, Villanueva CJ, Yetukuri L, Oresic M, Hellerstein MK, Farese RV, Jr., Horton JD, Preitner F, Thorens B, & Tappy L (2008) Blocking VLDL secretion causes hepatic steatosis but does not affect peripheral lipid stores or insulin sensitivity in mice. *J Lipid Res* 49:2038-2044.

342. Asai A, Chou PM, Bu HF, Wang X, Rao MS, Jiang A, DiDonato CJ, & Tan XD (2014) Dissociation of hepatic insulin resistance from susceptibility of nonalcoholic fatty liver disease induced by a high-fat and high-carbohydrate diet in mice. *Am J Physiol Gastrointest Liver Physiol* 306:496-504.

343. Shen SW, Reaven GM, & Farquhar JW (1970) Comparison of impedance to insulin-mediated glucose uptake in normal subjects and in subjects with latent diabetes. *J Clin Invest* 49:2151-2160.

344. Kim JK (2009) Hyperinsulinemic-euglycemic clamp to assess insulin sensitivity *in vivo*. *Methods Mol Biol* 560:221-238.

345. Gonzalez-Sanchez E, Perez MJ, Nytofte NS, Briz O, Monte MJ, Lozano E, Serrano MA, & Marin JJG (2016) Protective role of biliverdin against bile acid-induced oxidative stress in liver cells. *Free Radic Biol Med* 97:466-477.

346. Sass G, Seyfried S, Parreira Soares M, Yamashita K, Kaczmarek E, Neuhuber WL, & Tiegs G (2004) Cooperative effect of biliverdin and carbon monoxide on survival of mice in immune-mediated liver injury. *Hepatology* 40:1128-1135.

347. Anderson JL & Morrow DA (2017) Acute myocardial infarction. *N Engl J Med* 376:2053-2064.

348. Schwertner HA & Vitek L (2008) Gilbert syndrome, UGT1A1*28 allele, and cardiovascular disease risk: possible protective effects and therapeutic applications of bilirubin. *Atherosclerosis* 198:1-11.

349. Daugherty A (2002) Mouse models of atherosclerosis. *Am J Med Sci* 323:3-10.

350. Fujiwara R, Nguyen N, Chen S, & Tukey RH (2010) Developmental hyperbilirubinemia and CNS toxicity in mice humanized with the UDP glucuronosyltransferase 1 (UGT1) locus. *Proc Natl Acad Sci U S A* 107:5024-5029.

351. Cai H, Nguyen N, Peterkin V, Yang YS, Hotz K, La Placa DB, Chen S, Tukey RH, & Stevens JC (2010) A humanized UGT1 mouse model expressing the UGT1A1*28 allele for assessing drug clearance by UGT1A1-dependent glucuronidation. *Drug Metab Dispos* 38:879-886.

352. Cheng D, Talib J, Stanley CP, Rashid I, Michaelsson E, Lindstedt EL, Croft KD, Kettle AJ, Maghzal GJ, & Stocker R (2019) Inhibition of MPO (Myeloperoxidase) Attenuates Endothelial Dysfunction in Mouse Models of Vascular Inflammation and Atherosclerosis. *Arterioscler Thromb Vasc Biol* 39:1448-1457.

353. Witting PK, Pettersson K, Letters J, & Stocker R (2000) Site-specific antiatherogenic effect of probucol in apolipoprotein E-deficient mice. *Arterioscler Thromb Vasc Biol* 20:26-33.

354. Juonala M, Viikari JS, Ronnemaa T, Marniemi J, Jula A, Loo BM, & Raitakari OT (2008) Associations of dyslipidemias from childhood to adulthood with carotid intima-media thickness, elasticity, and brachial flow-mediated dilatation in adulthood: the Cardiovascular Risk in Young Finns Study. *Arterioscler Thromb Vasc Biol* 28:1012-1017.

355. Bulmer AC, Verkade HJ, & Wagner KH (2013) Bilirubin and beyond: a review of lipid status in Gilbert's syndrome and its relevance to cardiovascular disease protection. *Prog Lipid Res* 52:193-205.

356. de Sauvage Nolting PR, Kusters DM, Hutten BA, Kastelein JJ, & Ex Psg (2011) Serum bilirubin levels in familial hypercholesterolemia: a new risk marker for cardiovascular disease? *J Lipid Res* 52:1755-1759.

357. Narula J, Nakano M, Virmani R, Kolodgie FD, Petersen R, Newcomb R, Malik S, Fuster V, & Finn AV (2013) Histopathologic characteristics of atherosclerotic coronary disease and implications of the findings for the invasive and noninvasive detection of vulnerable plaques. *J Am Coll Cardiol* 61:1041-1051.

358. Kolodgie FD, Gold HK, Burke AP, Fowler DR, Kruth HS, Weber DK, Farb A, Guerrero LJ, Hayase M, Kutys R, Narula J, Finn AV, & Virmani R (2003) Intraplaque hemorrhage and progression of coronary atheroma. *N Engl J Med* 349:2316-2325.

359. Kopriva D, Kisheev A, Meena D, Pelle S, Karnitsky M, Lavoie A, & Buttigieg J (2015) The nature of iron deposits differs between symptomatic and asymptomatic carotid atherosclerotic plaques. *PLoS One* 10:e0143138.

360. Raffel OC, Merchant FM, Tearney GJ, Chia S, Gauthier DD, Pomerantsev E, Mizuno K, Bouma BE, & Jang IK (2008) In vivo association between positive coronary artery remodelling and coronary plaque characteristics assessed by intravascular optical coherence tomography. *Eur Heart J* 29:1721-1728.

361. Wu BJ, Di Girolamo N, Beck K, Hanratty CG, Choy K, Hou JY, Ward MR, & Stocker R (2007) Probucol [4,4'-[(1-methylethylidene)bis(thio)]bis-[2,6-bis(1,1-dimethylethyl)phenol]] inhibits compensatory remodeling and promotes lumen loss associated with atherosclerosis in apolipoprotein E-deficient mice. *J Pharmacol Exp Ther* 321:477-484.

362. Jormsjo S, Wuttge DM, Sirsjo A, Whatling C, Hamsten A, Stemme S, & Eriksson P (2002) Differential expression of cysteine and aspartic proteases during progression of atherosclerosis in apolipoprotein E-deficient mice. *Am J Pathol* 161:939-945.

363. Garcia-Touchard A, Henry TD, Sangiorgi G, Spagnoli LG, Mauriello A, Conover C, & Schwartz RS (2005) Extracellular proteases in atherosclerosis and restenosis. *Arterioscler Thromb Vasc Biol* 25:1119-1127.

364. Fu X, Kassim SY, Parks WC, & Heinecke JW (2001) Hypochlorous acid oxygenates the cysteine switch domain of pro-matrilysin (MMP-7). A mechanism for matrix metalloproteinase activation and atherosclerotic plaque rupture by myeloperoxidase. *J Biol Chem* 276:41279-41287.

365. Hazen SL & Heinecke JW (1997) 3-Chlorotyrosine, a specific marker of myeloperoxidase-catalyzed oxidation, is markedly elevated in low density lipoprotein isolated from human atherosclerotic intima. *J Clin Invest* 99:2075-2080.

366. Gargiulo S, Testa G, Gamba P, Staurenghi E, Poli G, & Leonarduzzi G (2017) Oxysterols and 4-hydroxy-2-nonenal contribute to atherosclerotic plaque destabilization. *Free Radic Biol Med* 111:140-150.

367. Amento EP, Ehsani N, Palmer H, & Libby P (1991) Cytokines and growth factors positively and negatively regulate interstitial collagen gene expression in human vascular smooth muscle cells. *Arterioscler Thromb* 11:1223-1230.

368. Libby P (2013) Mechanisms of acute coronary syndromes and their implications for therapy. *N Engl J Med* 368:2004-2013.

369. Siow RC, Richards JP, Pedley KC, Leake DS, & Mann GE (1999) Vitamin C protects human vascular smooth muscle cells against apoptosis induced by moderately oxidized LDL containing high levels of lipid hydroperoxides. *Arterioscler Thromb Vasc Biol* 19:2387-2394.

370. Hinz C, Liggi S, Mocciaro G, Jung SM, Induruwa I, Pereira M, Bryant CE, Meckelmann SW, O'Donnell VB, Farndale RW, Fjeldsted JC, & Griffin JL (2019) A comprehensive UHPLC ion mobility QTOF method for profiling and quantification of eicosanoids, other oxylipins and fatty acids. *Anal Chem* (91):8025-8035.

371. Lee SJ, Kim CE, Yun MR, Seo KW, Park HM, Yun JW, Shin HK, Bae SS, & Kim CD (2010) 4-Hydroxynonenal enhances MMP-9 production in murine macrophages via 5-

lipoxygenase-mediated activation of ERK and p38 MAPK. *Toxicol Appl Pharmacol* 242:191-198.

372. Lee SJ, Seo KW, Yun MR, Bae SS, Lee WS, Hong KW, & Kim CD (2008) 4-Hydroxynonenal enhances MMP-2 production in vascular smooth muscle cells via mitochondrial ROS-mediated activation of the Akt/NF-κB signaling pathways. *Free Radic Biol Med* 45:1487-1492.
373. Zhang R, Brennan ML, Fu X, Aviles RJ, Pearce GL, Penn MS, Topol EJ, Sprecher DL, & Hazen SL (2001) Association between myeloperoxidase levels and risk of coronary artery disease. *JAMA* 286:2136-2142.
374. Wang Y, Rosen H, Madtes DK, Shao B, Martin TR, Heinecke JW, & Fu X (2007) Myeloperoxidase inactivates TIMP-1 by oxidizing its N-terminal cysteine residue: an oxidative mechanism for regulating proteolysis during inflammation. *J Biol Chem* 282:31826-31834.
375. Vlasova, II, Sokolov AV, & Arnhold J (2012) The free amino acid tyrosine enhances the chlorinating activity of human myeloperoxidase. *J Inorg Biochem* 106:76-83.
376. Bhave G, Cummings CF, Vanacore RM, Kumagai-Cresse C, Ero-Tolliver IA, Rafi M, Kang JS, Pedchenko V, Fessler LI, Fessler JH, & Hudson BG (2012) Peroxidasin forms sulfilimine chemical bonds using hypohalous acids in tissue genesis. *Nat Chem Biol* 8:784-790.
377. Janoudi A, Shamoun FE, Kalavakunta JK, & Abela GS (2016) Cholesterol crystal induced arterial inflammation and destabilization of atherosclerotic plaque. *Eur Heart J* 37:1959-1967.
378. Cu A, Bellah GG, & Lightner DA (1975) Letter: On the fluorescence of bilirubin. *J Am Chem Soc* 97:2579-2580.
379. Gibbs PE, Tudor C, & Maines MD (2012) Biliverdin reductase: more than a namesake - the reductase, its peptide fragments, and biliverdin regulate activity of the three classes of protein kinase C. *Front Pharmacol* 3:1-10.
380. Yao Y, Li W, Wu J, Germann UA, Su MS, Kuida K, & Boucher DM (2003) Extracellular signal-regulated kinase 2 is necessary for mesoderm differentiation. *Proc Natl Acad Sci U S A* 100:12759-12764.
381. Labori KJ, Lyberg T, & Raeder MG (2009) Effects of bilirubin ditaurate overload on canalicular membrane function and ultrastructure of the pig liver. *Injury* 40:868-872.
382. Toietta G, Mane VP, Norona WS, Finegold MJ, Ng P, McDonagh AF, Beaudet AL, & Lee B (2005) Lifelong elimination of hyperbilirubinemia in the Gunn rat with a single injection of helper-dependent adenoviral vector. *Proc Natl Acad Sci U S A* 102:3930-3935.

383. McDonagh AF, Palma LA, Trull FR, & Lightner DA (1982) Phototherapy for neonatal jaundice. Configurational isomers of bilirubin. *J Am Chem Soc* 104:6865-6867.

384. Liu Y & Ortiz de Montellano PR (2000) Reaction intermediates and single turnover rate constants for the oxidation of heme by human heme oxygenase-1. *J Biol Chem* 275:5297-5307.

385. Maines MD (2005) New insights into biliverdin reductase functions: linking heme metabolism to cell signaling. *Physiology* 20:382-389.

386. Gafvels M, Holmstrom P, Somell A, Sjovall F, Svensson JO, Stahle L, Broome U, & Stal P (2009) A novel mutation in the biliverdin reductase-A gene combined with liver cirrhosis results in hyperbiliverdinaemia (green jaundice). *Liver Int* 29:1116-1124.

387. McDonagh AF (2010) Green jaundice revisited. *Am J Med* 123:23.